Flexural Behaviour of Partially Bonded CFRP Strengthened Concrete T-Beams

by

Han Tae Choi

A thesis
presented to the University of Waterloo
in fulfillment of the
thesis requirement for the degree of
Doctor of Philosophy
in
Civil and Environmental Engineering

Waterloo, Ontario, Canada, 2008

AUTHOR'S DECLARATION

I hereby declare that I am the sole author of this thesis. This is a true copy of the thesis, including any required final revisions, as accepted by my examiners.

I understand that my thesis may be made electronically available to the public.

Abstract

Fibre-reinforced-polymer (FRP) composites have been widely used for the flexural strengthening of reinforced concrete (RC) structures. Flexural strengthening methods with FRP include external bonding of FRP composites (EB system) and insertion of FRP strips or bars into grooves cut into the concrete (near-surface-mounted or NSM system). Recently, a prestressed FRP strengthening system has been developed and investigated, whereby the FRP reinforcement is pretensioned prior to attachment to the concrete to maximize the use of the high tensile strength of the FRP reinforcement. Existing studies have shown that the ultimate load carrying capacity and serviceability were greatly improved in FRP flexural strengthened beams. However, the only disadvantage of the FRP strengthening system is the reduction of deformability compared to that of unstrengthened structures due to the limited strain capacity of the FRP reinforcement and premature debonding failure. Structures with low deformability may fail suddenly without warning to evacuate, resulting in catastrophic failure. Therefore, a study on the improvement of deformability is critical for the effective use of FRP strengthening systems.

In this study, a partially bonded concept is introduced and applied to various FRP strengthening methods, with the specific objective of increasing deformability in FRP strengthened beams. The FRP reinforcement is usually completely bonded to the concrete tensile surface, while a portion of the FRP length is intentionally unbonded in the partially bonded system in order to improve deformability while sustaining high load carrying capacity. To investigate the general behaviour of the partially bonded system, a new analytical model has been developed because conventional section analysis used for analysis of the fully bonded system is not applicable due to strain incompatibility at the FRP reinforcement level within the unbonded length. The analysis shows that a partially bonded system has a high potential to improve deformability without the loss of strength capacity.

An extensive experimental program was conducted to verify the analytical model and to investigate the actual behaviour of the partially bonded beams. A total of seventeen, 3.5m long, RC T-beams were constructed and tested. One of them is an unstrengthened control beam, while the other 16 beams consist of four test groups that were strengthened by different strengthening methods: non-prestressed EB, non-prestressed NSM, 40% prestressed NSM, and 60% prestressed NSM. To allow investigation of the effect of partially unbonding, each group has different unbonded lengths and includes a fully bonded beam.

For the non-prestressed EB strengthened beams, the failure mode of all beams was premature FRP debonding failure without regard to the bond condition. The ultimate strength and the ultimate deformability of the partially bonded beams were improved compared to the fully bonded beam. This was because the typical intermediate debonding failure that occurred in the fully bonded beam was avoided due to intentional unbonding in the partially bonded beams. The analytical model predicted the general behaviour of the EB strengthened beams well except at the ultimate response due to the premature debonding failure. A three-dimensional nonlinear finite element (FE) analysis was performed utilizing interfacial elements and contact modeling to investigate the debonding failure of this system. The FE analysis represented the behaviour of the debonding failure and bond stress distributions at FRP-concrete interface of both the fully bonded and partially bonded beams well.

For the non-prestressed NSM strengthened beams, the premature debonding failure that occurred in the EB strengthened beams was not observed, and almost the full capacity of FRP was exhibited. Prominent stiffness reduction was observed in terms of load-deflection diagrams at the post-yielding stage with the increase of the unbonded length. This stiffness reduction increased the deformability of the partially bonded beams for a given applied load after steel yielding in comparison to the fully bonded beam. The FRP started to slip at high load levels and the concrete crushed gradually with a gradual loss of the beam's cross-section, inducing nonlinear behaviour near the ultimate state of the

beams. To address this behaviour, an advanced analytical model utilizing idealized section model and slip model is proposed to consider the FRP slip and concrete gradual failure.

Prestressed NSM strengthened beams were very effective to improve the cracking load, to decrease the deflection at service load, and to increase the ultimate load compared to non-prestressed NSM strengthened beams. This improvement was greater as the prestressing level increased. The partially bonded prestressed beams showed an improvement in deformability compared to the fully bonded prestressed beams while minimizing the reduction of the ultimate load carrying capacity and serviceability. The partially bonded system was more effective to improve the deformability at higher levels of prestressing force.

Based on the model developed, a parametric study was performed varying the main parameters. This showed that the FRP strengthened beam that has an FRP area (A_f) less than the balanced FRP area ($A_{f,b}$) of the beam has a high potential to improve the deformability as the unbonded length increases. The balanced FRP area is increased as the concrete strength and the FRP prestressing force are increased, or as the area of the steel reinforcement decreases. Finally, design recommendations and procedures are proposed for the effective use of the partially bonded system to improve the deformability of FRP strengthened concrete beams.

Acknowledgements

I would like to express my sincere gratitude and appreciation to my supervisors Prof. Jeffrey West and Prof. Khaled Soudki from Civil and Environmental Engineering at the University of Waterloo for their support, guidance, and encouragement during the research program.

I also would like to thank my lab colleagues: Dr. Ahmad, Dr. Moataz, Rania, and Maria for their help and sincere advice during the lab work.

The help of the technical staff: Ken, Doug, and Richard during the experimental program is greatly appreciated and acknowledged.

I also would like to express my gratitude to the Natural Sciences and Engineering Research Council of Canada (NSERC) for its financial support, and to the Ontario Graduate Scholarship Program. The donation of CFRP materials by Sika Canada, Inc., is also appreciated.

Finally but most importantly, I would like to thank my family for their support and continuous encouragement. Special thanks go to my wife Mi Jung for her devotion to me and daughters Eun Seo and Sun Min.

To my mother, my wife, and my kids

Table of Contents

List of Figures

List of Tables

Notations

A = Cross-sectional Area, mm^2

A_1 = Area under concrete strain distribution at FRP level within unbonded region, mm^2

A_2 = Area under FRP strain distribution within unbonded region, mm^2

A_f, A_s = Cross-sectional area of FRP reinforcement and steel reinforcement, respectively, mm^2

$A_{f,b}$ = Cross-sectional area of FRP reinforcement in fully bonded beams at the balanced condition, mm^2

$A'_{f,b}$ = Cross-sectional area of FRP reinforcement in partially bonded beams at the balanced condition, mm^2

b = Width of the rectangular beam cross section, mm

b_f, b_w = Width of the flange and the web of the T-beam cross section, respectively, mm

C = Resultant concrete compression force, N

C_t, C_u, C_y = Resultant concrete compression force at transition section, at ultimate section, and at steel yielding section, respectively, N

c_b, c_t, c_u, c_y = Neutral axis depth at the balanced condition, at transition section, at ultimate section, and at steel yielding section, respectively, mm

c'_b = Neutral axis depth of partially bonded beams at the balanced condition, mm

d_b = Diameter of steel reinforcement, mm

d_s, d_f = Depth of steel reinforcement and FRP reinforcement, respectively, mm

$d\lambda$ = Positive scalar factor of proportionality

E = Modulus of elasticity, MPa

E_b = Slip modulus in the bond stress-slip relationship, MPa/mm

E_{ct} = Initial tangent concrete modulus of elasticity, MPa

E_{el} = Elastic energy accumulated in the system, N-mm

E_f, E_s = Modulus of elasticity of FRP and steel reinforcement, respectively, MPa

E_t = Modulus of elasticity in concrete tension, MPa

E_{tot} = Total energy in the system, N-mm

E_u = Energy accumulated in the system up to ultimate state, N-mm

E_y = Energy accumulated in the system up to steel reinforcement yielding, N-mm

e_f = Eccentricity of the FRP reinforcement from neutral axis of the section, mm

f = Yield function, or loading surface function

f'_c = Concrete compressive strength, MPa

f_c, f_f = Concrete compressive stress and FRP tensile stress, respectively, MPa

f_{frpu} = Ultimate tensile strength of FRP reinforcement, MPa

f_{fu} = Tensile stress of FRP reinforcement at ultimate section, MPa

f_r = Modulus of rupture of Concrete, MPa

f_{pe} = Effective stress of the FRP due to prestressing force, MPa

f_s, f_{sy} = Stress and yield stress of steel reinforcement, respectively, MPa

f_t = Concrete tensile stress, MPa

f'_t = Flexural tensile strength of concrete, MPa

G_F = Fracture energy – area under the bond stress-slip curve, MPa-mm

g = Plastic potential function

h = Height of the beam cross section, mm

I = Moment of inertia of the section, mm^4, or inertia force, N

k_h = Horizontal stiffness of link element, MPa/mm

k_v = Vertical stiffness of link element, MPa/mm

L = Beam span, mm

L_{ub} = Unbonded length from mid-span to transition section, mm

L_{ubb} = Balanced unbonded length, mm

L_p, L_{uby}, L_{ubcr} = Length from mid-span to the loading point, to steel yielding section, and to cracking moment section, respectively, mm

M, M_{cr} = Service moment and cracking moment, respectively, N-mm

M_t, M_u, M_y = Moment at transition section, at ultimate section, and at steel yielding section, respectively, N-mm

n = Number of ply of FRP reinforcement

P = Applied load, N

P_{cr}, P_y, P_u = Applied load at cracking, at steel yielding, and at ultimate state, respectively, N

P_f, P_p = Ultimate load of fully bonded and partially bonded beams, respectively, N

R_p = Strength ratio between partially bonded and fully bonded beams, $R_P = P_p / P_f$

R_Δ = Deflection ratio between partially bonded and fully bonded beams, $R_\Delta = \Delta_p / \Delta_f$

s = Slip of FRP reinforcement, mm

s_{max} = Maximum slip of FRP reinforcement, mm

T_f, T_s = Resultant tension force of FRP reinforcement and steel reinforcement, respectively, N

T_t, T_u, T_y = Sum of Resultant tension forces at transition section ($T_{ts} + T_{tf}$), at ultimate section ($T_{us} + T_{uf}$), and at steel yielding section ($T_{ys} + T_{yf}$), respectively, N

T_{tf}, T_{uf}, T_{yf} = Resultant tension force of FRP reinforcement at transition section, at ultimate section, and at steel yielding section, respectively, N

T_{ts}, T_{us}, T_{ys} = Resultant tension force of steel reinforcement at transition section, at ultimate section, and at steel yielding section, respectively, N

t_f = Thickness of the flange of T-beam cross section, mm

t_{frp} = Thickness of FRP plate or sheet, mm

u = Displacement, mm

α = Concrete mean stress factor

α_1 = Ratio of average stress in rectangular compression block

α_t, α_u, α_y = Concrete mean stress factor at transition section, at ultimate section, and at steel yielding section, respectively

β_1 = Ratio of depth of rectangular compression block to the neutral axis

γ = Concrete stress centroid factor

γ_t, γ_u, γ_y = Concrete stress centroid factor at transition section, at ultimate section, and at steel yielding section, respectively

Δl = Total deformation of the concrete in the unbonded region, mm

Δ_{cr}, Δ_y, Δ_u = Mid-span deflection of the Beam at cracking, at steel yielding, and at ultimate state, respectively, mm

Δ_f, Δ_p = Ultimate deflection of fully bonded and partially bonded beam, respectively, mm

Δ_s = Mid-span deflection at the service load, mm

$\Delta_{u,ACI}$ = Ultimate deflection based on ACI 440.2R (2008) maximum FRP strain limit, mm

ε_{bcr}, ε_{bt}, ε_{bu}, ε_{by} = Concrete strain at FRP level at cracking moment section, at transition section, at ultimate section, and at steel yielding section, respectively, mm/mm

ε_{bi} = Initial concrete bottom strain (prior to FRP installation), mm/mm

ε'_c = Concrete strain corresponding to f'_c, mm/mm

ε_c = Concrete compressive strain, mm/mm

ε_{ct}, ε_{cu}, ε_{cy} = Concrete top fibre strain at transition section, at ultimate section, and at steel yielding section, respectively, mm/mm

ε_f = FRP tensile strain, mm/mm

ε'_f = Strain at FRP location of partially bonded beam at balanced condition, mm/mm

ε_{fcr}, ε_{ft}, ε_{fu} = FRP tensile strain at cracking moment section, at transition section, and at ultimate section, respectively, mm/mm

ε_{fd} = Debonding strain based on ACI 440.2R (2008), mm/mm

$\varepsilon_{f,max}$ = Maximum limited FRP tensile strain based on Concrete Society (2004), mm/mm

ε_{frpu} = FRP ultimate tensile strain, mm/mm

ε_{ij}^{p} = Plastic strain tensor

ε_{pe} = Effective strain of FRP reinforcement due to prestressing, mm/mm

ε_s = Steel reinforcement strain, mm/mm

ε_{su} = Steel reinforcement strain at rupture, mm/mm

ε_{sy} = Steel reinforcement yield strain, mm/mm

ϕ = Beam Curvature, rad/mm, or daimetre of the bar, mm

ϕ_{cr}, ϕ_t, ϕ_u, ϕ_y = Curvature at cracking moment section, at transition section, at ultimate section, and at steel yielding section, respectively, rad/mm

ϕ_{fb}, ϕ_{pb}, ϕ_{ub} = Curvature of the fully bonded beam, the partially bonded beam, and the fully unbonded beam, respectively, rad/mm

ϕ_s = Curvature at the service load, rad/mm

μ = Deformability index

μ_{E1} = Energy ductility index 1

μ_{E2} = Energy ductility index 2 based on Naaman and Jeong (1995)

$\mu_{\Delta 1}$ = Deflection ductility index

$\mu_{\Delta 2}$ = Deflection deformability index based on Tann el al. (2003)

$\mu_{\phi 1}$ = Curvature ductility index

$\mu_{\phi 2}$ = Curvature deformability index based on ISIS Design Manual No. 5 (2008)

ρ = Steel reinforcement ratio (A_s/bd_s), mm^2/mm^2

ρ_{max} = Maximum steel reinforcement ratio, mm^2/mm^2

ρ_{min} = Minimum steel reinforcement ratio, mm^2/mm^2

σ = Normal stress, MPa

σ_{ij} = Stress tensor

σ_{max} = Maximum tensile strength in concrete tension, MPa

τ = Bond stress, MPa

τ_{max} = Maximum bond strength, MPa

ω = Crack width, mm, or uniform load, N/mm

ω_c = Crack opening width, mm

Chapter 1
Introduction

1.1 General

Concrete structures may become deteriorated with time due to external environmental factors and internal material factors. Deteriorated structures should be repaired to ensure proper functioning and to extend their service life. Structures without damage may also need to be strengthened because of design or construction errors, or to accommodate changes in use or increased loads. According to ASCE's Report Card (2005), the overall grade of the condition and capacity of America's infrastructure is “D”, and ASCE estimates that $1.6 trillion is needed over a five-year period to bring the nation’s infrastructure to good condition. Based on the final report of Canada’s Civil Infrastructures Systems (CIS) Technology Road Map (TRM) (2003), some of the infrastructure has already reached the end of its service life and is breaking down, and many of the remaining systems will need renewal or replacement within next 10 years. The estimated cost to rehabilitate just the municipal infrastructure (70% of the total Canadian CIS) would be more than $110 billion in 2027 if left unchecked. Therefore, it is important to develop an effective method for repairing and strengthening deteriorated structures to reduce the future maintenance cost while extending their service life.

One of the promising strengthening methods is the use of fibre-reinforced-polymer (FRP) composites for rehabilitation of reinforced concrete (RC) structures due to their many advantages in comparison to the conventional steel reinforcement: a low weight to volume ratio, a high strength to weight ratio, high fatigue performance and non-corrosive property. Extensive investigations on the behaviour of structures repaired or strengthened with FRP have been performed and shown that a great enhancement on their flexural, shear, and axial capacity in members was achieved (Bank 2006, Teng et al. 2002). Related design guidelines were published for externally bonded FRP strengthening

system (ACI 440.2R 2008, ISIS Design Manual No.4 2008). In addition to the external strengthening, FRP material has also been used for new construction as an alternative of internal steel reinforcement. ACI 440.1R (2006) and ISIS Design Manual No.3 (2007) cover the design of structural concrete reinforced with internal FRP bars. Prestressed FRP internal reinforced beams have also been investigated to maximize the high tensile strength of FRP material, and related guidelines for the use of internal prestressed FRP system are also published (ACI 440.4R 2004, ISIS Design Manual No.5 2008). A study on the application of the prestressed FRP system to the repair and strengthening of deteriorated structures is in progress.

1.2 Problem Statement

Typical load-deflection diagrams in flexural for the unstrengthened beams, FRP strengthened beams, and prestressed FRP strengthened beams, assuming no premature bond failure, are shown in Figure 1-1. The points labeled "x" represent the ultimate response at failure of each beam. The ultimate load carrying capacity of the FRP strengthened beams is greatly improved compared to that of the unstrengthened beam. However, if the deformability is defined by the ratio of the ultimate deflection to the deflection at steel yielding, then the deformability and ultimate deflection in the FRP strengthened beams, especially in the prestressed FRP strengthened beam, is greatly decreased when compared to the unstrengthened beam. Moreover, this lack of deformability becomes even more unfavorable considering the possibility of a premature debonding failure in the FRP strengthened beams.

The improvement of deformability in the FRP strengthening system is critical because structures with low deformability typically fail suddenly without warning to evacuate and repair. Therefore, not only the improvement of load carrying capacity, but also the enhancement of deformability should be obtained in FRP strengthened flexural members. Nevertheless, most of the existing studies on FRP

strengthened beams have focused only on the improvement of ultimate load carrying capacity, and studies on the improvement of deformability are very limited.

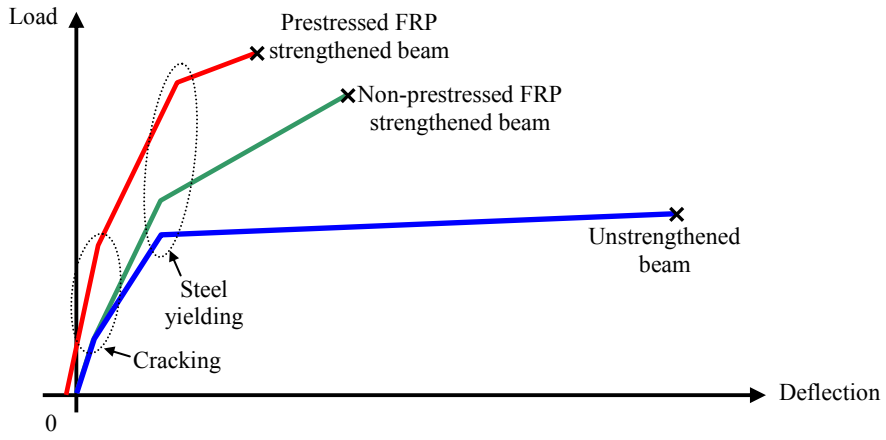

Figure 1-1 Effect of FRP strengthening on load-deflection behaviour

One of the methods to improve the deformability of FRP strengthened beams is to apply a partially bonded system where a portion of FRP is intentionally unbonded from the beam. However, research on this topic is very limited and an appropriate analytical model to describe the general behaviour of the partially bonded system has not been developed due to the analytical complexity.

Therefore, the investigation on the behaviour of partially bonded beams is required including the development of a new analytical model and performance of an experimental program for verifying the model and investigating the actual behaviour of the strengthened beams.

1.3 Research Objectives

The ultimate objective of the study is to achieve a balance between improvement of load carrying capacity and the corresponding reduction of deformability by applying a partially bonded FRP strengthening system to RC beams. To achieve this objective, the research is conducted with two

main parts: analytical and experimental investigations. Specific objectives for each part are summarized as follows.

1.3.1 Analytical investigation

- To develop an analytical model for the investigation of the general behaviour of partially bonded FRP strengthened beams;
- To perform linear elastic finite element (FE) analysis to investigate the bond stress distributions in the elastic stage at the FRP-concrete interface;
- To perform nonlinear finite element analysis up to failure, considering the nonlinear effect of materials, to investigate the premature debonding failure of externally bonded FRP strengthened beams;
- To develop an advanced analytical model for the investigation of the nonlinear behaviour of non-prestressed NSM strengthened beams considering the gradual slip of FRP reinforcement and the concrete progressive failure;
- To perform a parametric study to investigate the effect of main variables of partially bonded FRP strengthened beams on the flexural behaviour; and
- To propose the design recommendations and procedures for the effective use of the partially bonded system.

1.3.2 Experimental investigation

- To investigate the effect of partial unbonding on the behaviour of the beams strengthened with externally bonded (EB) FRP;
- To investigate the behaviour of near-surface-mounted (NSM) FRP strengthened beams with various unbonded lengths and to compare the responses to EB strengthened beams;
- To develop a self anchored prestressing system for the prestressed NSM strengthening system;

- To investigate the behaviour of prestressed NSM FRP strengthened beams with varying unbonded length and to compare the responses between non-prestressed and prestressed NSM beams;
- To investigate the effect of different prestressing levels on the behaviour of the prestressed NSM strengthened beams; and
- To verify the analytical model by comparing the predicted vs. measured load-deflection diagrams and load-strain diagrams of partially bonded FRP strengthened beams.

1.4 Scope of Thesis

This thesis focuses on the flexural behaviour of RC T-beams strengthened with CFRP reinforcement. A partially bonded system is introduced and applied to various flexural strengthening systems, and the test results and discussions are presented with the specific objective of increasing deformability. Deformability is defined as the amount of deformation, so no plastic work is required. Therefore, the concept of deformability is more applicable to FRP strengthened concrete beams than that of ductility (see Section 2.6). Only deformability concept was used in this thesis.

The thesis consists of nine chapters as shown in Figure 1-2. Chapter 1 provides the introduction including the problem statement, objectives, and the scope of the thesis. Literature review on flexural strengthening with FRP and the introduction of the partially bonded system are described in Chapter 2. Chapter 3 introduces a new analytical model developed for the analysis of the partially bonded system, and linear elastic finite element analysis is performed in this chapter. In Chapter 4, an experimental program consisting of four test groups is described. Test results for each group are describes in Chapters 5 to 7. Chapter 5 shows the test results of the EB FRP strengthened beams (Test Group I), and the nonlinear FE analysis is carried out for the analysis of the premature debonding failure in this chapter. Chapter 6 provides the test results and discussions of the NSM FRP strengthened beams (Test Group II), and an advanced analytical model is introduced to address the nonlinear behaviour of

the beams caused by the FRP slip and the gradual concrete failure. In Chapter 7, the test results of the prestressed NSM FRP strengthened beams (Test Group III and IV) are presented and the comparisons between non-prestressed and prestressed beams are discussed. A parametric study is performed and the design recommendations and procedures for the effective use of the partially bonded system are given in Chapter 8. Finally, conclusions and future work are summarized in Chapter 9.

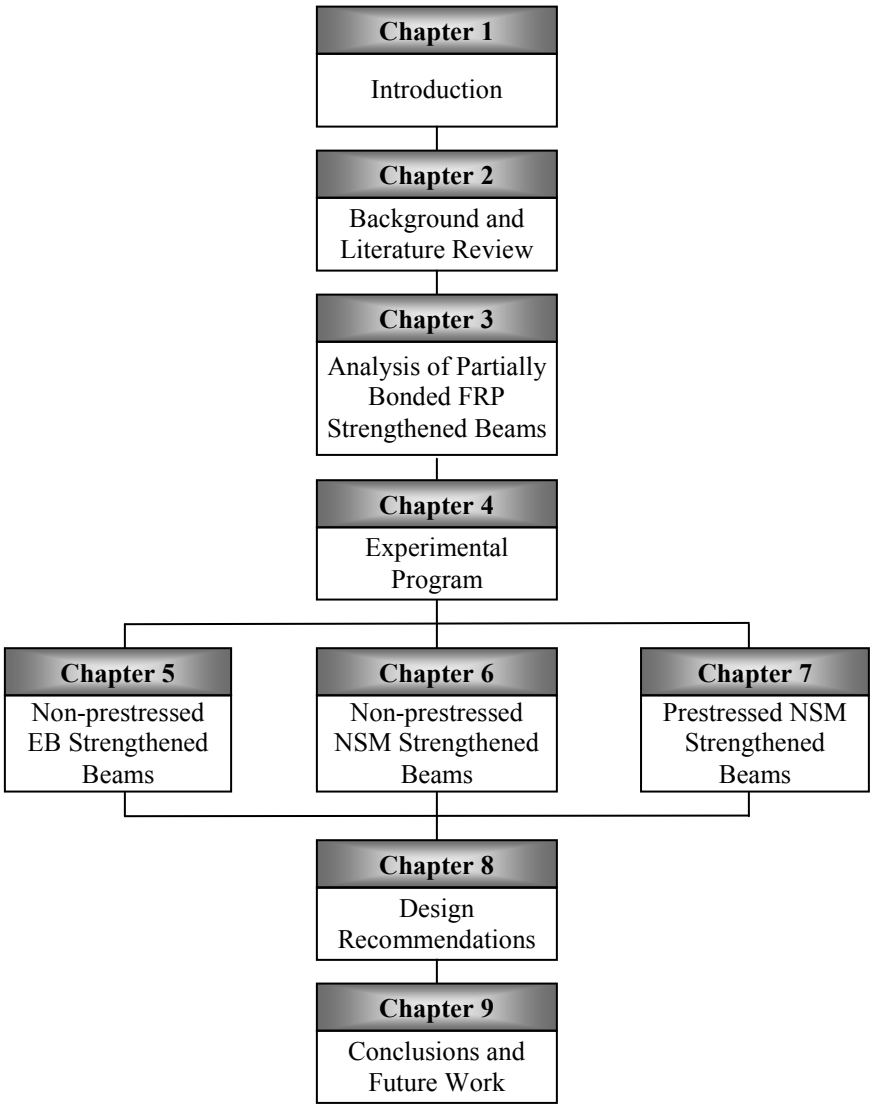

Figure 1-2 Thesis organization

Chapter 2
Background and Literature Review

2.1 General

An appropriate strengthening strategy is needed for deteriorated or damaged structures to recover their strength and serviceability and to extend their service life depending on structural types (flexural, shear, or compression members). In this chapter, background and literature review of FRP strengthened members are discussed focusing on the flexural strengthening of reinforced concrete (RC) members. General flexural strengthening methods are described in Section 2.2. The properties of FRP material as a strengthening reinforcement are described in Section 2.3, and Section 2.4 introduces flexural strengthening methods utilizing FRP material including the description of failure modes and anchor systems. Prestressed FRP strengthening systems are described in Section 2.5 and the basic concept of ductility and deformability is described in Section 2.6. The partially bonded system is introduced in Section 2.7, and Section 2.8 deals with the basics of finite element (FE) modeling of the FRP strengthened members.

2.2 Flexural Strengthening

General methods for the flexural strengthening are summarized in Table 2-1. The basic concept of flexural strengthening is to improve the strength and stiffness of concrete flexural members by adding reinforcement to the concrete tensile surface. Conventionally, steel reinforcement has been widely used as a strengthening material. For example, section enlargement using steel reinforced concrete, steel plate bonding, and external steel post-tensioning technique have been widely applied as shown in Table 2-1(a), (b), and (c). Recently, flexural strengthening utilizing fibre-reinforced-polymer (FRP) material has been investigated and applied because of its many advantages compared to the conventional steel reinforcement (see Table 2-1(d) and (e)). For the maximum use of high tensile

strength of FRP material, a prestressed FRP strengthening system has been recently developed and investigated. Details of prestressed strengthening systems are described in Section 2.5.

Table 2-1 Methods for flexural strengthening

Methods	Illustration	Description
(a) Section enlargement	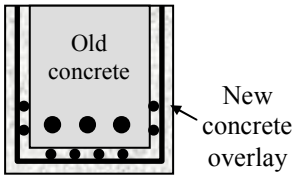	• "Bonded" reinforced concrete is added to an existing structural member in the form of an overlay or a jacket.
(b) Steel plate bonding	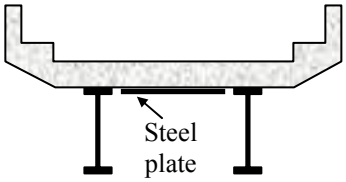	• Steel plates are glued to the concrete surface by epoxy adhesive to create a composite system and improve flexural strength.
(c) External post-tensioning method	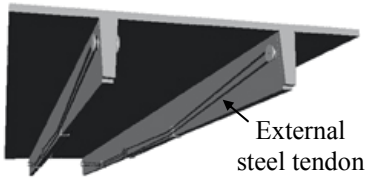	• Active external forces are applied to the structural member using post-tensioned (stressed) cables to improve flexural strength.
(d) Externally bonded (EB) system		• FRP composites are bonded to the concrete surface to improve the flexural strength. FRP material could be in the form of sheets or plates.
(e) Near-surface-mounted (NSM) system	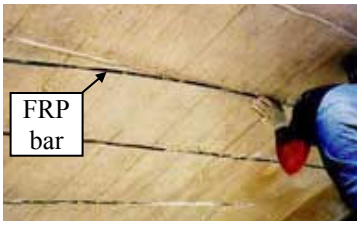	• FRP bars or plates are inserted into a groove on the concrete surface and bonded to the concrete using epoxy adhesive.

2.3 Fibre Reinforced Polymer (FRP)

Fibre reinforced polymer (FRP) composites are formed by embedding continuous fibres in a resin matrix that binds the fibres together. The common fibres are carbon fibres, glass fibres, and aramid

fibres, and epoxy resins, polyester resins and vinylester resins are the common resins. Depending on the fibres used, FRP composites are classified into three types: Glass FRP (GFRP) composites; Carbon FRP (CFRP) composites; and Aramid FRP (AFRP) composites. Table 2-2 shows the typical mechanical properties of FRP composites and steel reinforcement. The weight of FRP is much lighter with higher tensile strength compared to the conventional steel reinforcement as shown in Table 2-2.

Table 2-2 Typical mechanical properties of FRP and steel materials (Teng et al. 2002a)

FRP types	GFRP	CFRP	AFRP	Steel
Fibre content (% by weight)	50~80	65~75	60~70	N/A
Density (kg/m^3)	1600~ 2000	1600~ 1900	1050~ 1250	7850
Tensile modulus(GPa)	20~55	120~ 250	40~ 125	200
Tensile strength(MPa)	400~ 1800	1200~ 2250	1000~ 1800	400

Figure 2-1 shows the typical stress and strain diagrams of FRP and steel materials. One of the typical properties of FRP composites is to exhibit perfect elastic behaviour up to failure without yielding, as shown in Figure 2-1.

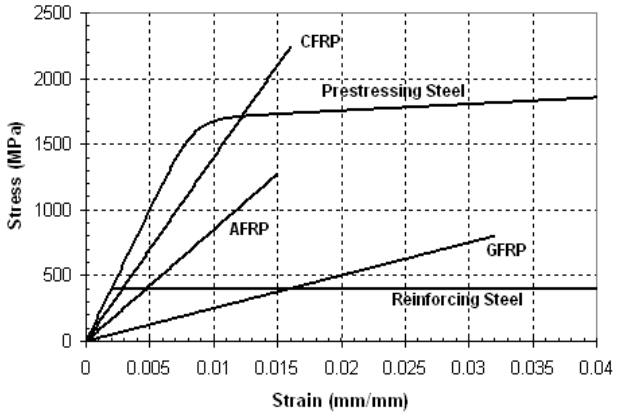

Figure 2-1 Stress and strain relationships of FRP and steel materials (ISIS Design Manual No.5 2008)

Although FRP composites are expensive and more susceptible to physical damage than steel, they have become an attractive substitute for steel in strengthening systems for concrete structures due to their many advantages: high strength-to-weigh ratio, corrosion resistance, and high fatigue resistance (Nanni 2003, ACI 440R 2007).

2.4 Flexural Strengthening with FRP

2.4.1 Strengthening methods

Two general methods for flexural strengthening with FRP are: the externally bonded (EB) system and the near-surface-mounted (NSM) system. The basic concept of these two systems is to improve flexural strength and stiffness by adding FRP material to the concrete tensile surface. For the EB system, FRP sheets or plates are bonded to the concrete surface using epoxy adhesives. To improve the bond strength between the concrete and the FRP, the concrete surface is usually treated by sandblasting. For the NSM system, FRP bars or plates are inserted into a groove that is made in the concrete surface with a concrete saw. The groove is then filled with epoxy adhesive to bond the FRP to the concrete. General strengthening procedures for these two systems are illustrated in Table 2-3.

Table 2-3 Strengthening procedures for EB and NSM systems

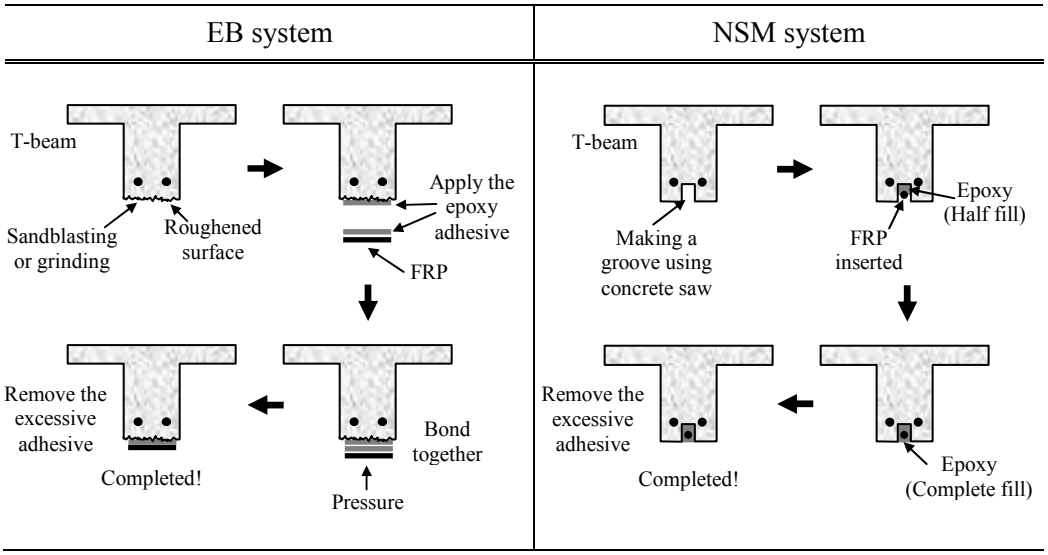

The EB system has been more generally applied due to its simple installation procedure, and guidelines and specifications have been also established well for this system (ACI 440.2R 2008, ISIS Design Manual No. 4 2008). On the other hand, the NSM system is a relatively new technique with fewer applications performed so far. The NSM system has shown an improvement of flexural capacity with a good bond property (Jung et al. 2005, El-Hacha et al. 2004a). A comparison study between the two systems showed that NSM system exhibited better load carrying capacity due to higher bond strength at the FRP-concrete interface (El-Hacha and Rizkalla 2004, Hassan and Rizkalla 2002). The NSM FRP composites are also protected from external mechanical damage since they are placed within a groove in the concrete cover and are completely covered by the epoxy adhesive.

2.4.2 Bond characteristics in FRP strengthened beams

The bond strength between the concrete and the FRP is extremely important to provide the composite behaviour. This bond property can be represented by the bond stress-slip relationship, which is derived from various bond tests: concrete pull-out test (single or double shear test), axial tension test, cantilever beam test, notched beam test, and hinged beam test (Nanni et al. 1995). Based on these bond tests, various bond stress-slip relationships have been proposed (Dai el al. 2005, Nakaba et al. 2001). Figure 2-2 shows the typical bond stress-slip relationship at the concrete-FRP interface.

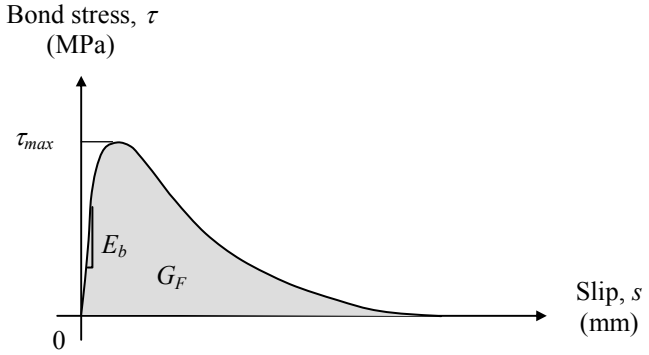

Figure 2-2 Typical bond stress-slip relationship of FRP strengthened beams

The maximum bond strength, τ_{max} is affected mainly by concrete strength, thickness and stiffness of the FRP, surface preparation, strength and stiffness of the adhesive, and the bonded length. Lorenzis et al. (2001) and Chen and Teng (2001) summarized the current bond strength models for predicting the bond strength at FRP-concrete interface considering the concrete strength, FRP stiffness, and the bonded length. The maximum bond strength is generally known to be between 4MPa and 8MPa depending on the main influencing factors (Dai el al. 2005). The fracture energy, G_F, is the area underneath the interfacial bond stress-slip diagram as shown in Figure 2-2. This fracture energy represents the energy required to induce debonding from the concrete interface. Because of this physical meaning, the fracture energy is often used in numerical analyses for the simulation of the debonding failure. The fracture energy mainly depends on the concrete tensile strength assuming that the debonding failure occurs at the concrete interface. The slip modulus, E_b, is the initial slope of the bond stress-slip curve. Lee et al. (1999) found that the slip modulus mainly depends on the properties of the adhesive, and that the slip modulus at the concrete-FRP interface is normally higher than that at the concrete-steel interface.

For the EB system, many simple shear tests were performed to investigate the bond strength at the FRP-concrete interface (Taljsten 1997, Chajes et al. 1996, Bizindavyi and Neale 1999). They found that the average bond strength is affected by the concrete strength (f'_c), stiffness of the FRP (E_fA_f), surface preparation, and adhesive type. Yuan et al. (2004) investigated the full range behaviour of FRP-concrete interface using a local bond slip relationship and solved differential equation at various stages. Malek et al. (1998) developed a method to calculate the shear and normal stress distribution along the beam length based on linear elastic material behaviour.

For the NSM system, Lorenzis et al. (2004) and Lorenzis and Nanni (2002) performed simple pullout tests for NSM bars with different variables. This research showed that the NSM groove size, type of FRP, type of epoxy, and concrete strength were the main factors affecting the maximum bond

strength of the NSM system. Hassan and Rizkalla (2004) tested beams strengthened with NSM reinforcement with different anchorage lengths. They reported that an effective anchorage length exists beyond which the bond strength no longer increases.

Figure 2-3 shows the typical shear and normal stress distribution along the beam length for the EB strengthened beams. Note that the shear and normal stress (peeling stress) are concentrated near the cutoff point of the FRP plate, which are main causes of premature debonding failures. The detailed failure modes of FRP strengthened beams are described in following section.

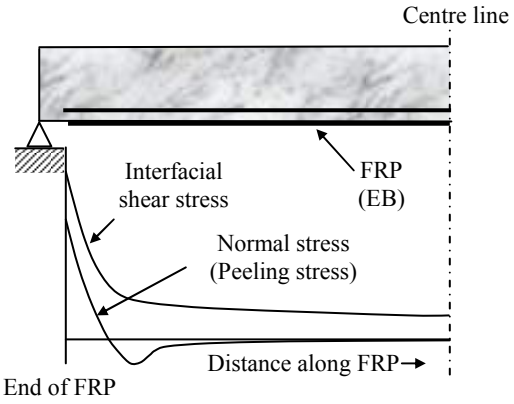

Figure 2-3 shear and normal stress distributions along the FRP length (ACI 440.2R 2008)

2.4.3 Failure modes of FRP strengthened beams

The EB system presents more failure modes in comparison to conventional reinforced concrete (RC) beams. Failure modes are classified into two types. The first type of failure includes the common failure modes such as concrete crushing and FRP rupture based on complete composite action. The second type of failure is a premature failure without reaching full composite action at failure. Figure 2-4 and Table 2-4 summarize the failure modes of FRP strengthened beams with the EB system. For the NSM system, premature debonding failure, such as splitting failure or pull-out failure, has been observed, but general failure modes have not been widely reported due to the lack of experimental data.

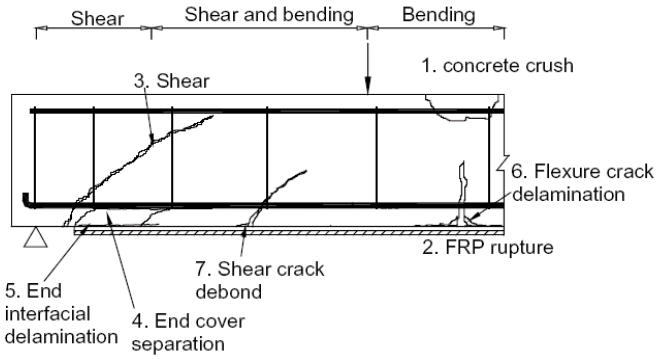

Figure 2-4 Failure modes of EB strengthened beams (Pham and Al-Mahaidi 2004)

Table 2-4 Description of failure modes for EB system

Failure modes		Description
Case I: Full composite action	Concrete crushing	• If premature failures are prevented, the ultimate flexural capacity of the beam is reached when either the FRP composite fails by tensile rupture or the concrete crushes in compression. This is similar to the classical flexural failure modes of RC beams except for the brittle failure of FRP rupture.
	FRP rupture	
Case II: Premature failure	End cover separation	• Failure of the concrete cover is initiated by the formation of a crack at or near the plate end due to high interfacial shear and normal stresses caused by the abrupt termination of the plate.
	End interfacial delamination	• This debonding failure is initiated by high interfacial shear and normal stresses near the end of the plate that exceed the strength of the weakest element (concrete or epoxy).
	Flexural crack induced debonding	• Flexural crack induced debonding happens when the concentrated bond stress at the crack location exceeds the shear strength in the weakest layer.
	Shear crack induced debonding	• Shear crack induced debonding occurs in the zone where both shear and bending moment are significant. It is caused by the combination of two mechanisms. The first one is similar to that of flexural crack induced debonding. The second is by the vertical movement of the inclined crack.

If FRP strengthened beams show complete composite action up to the ultimate state, the modes of failure are determined by the amount of FRP reinforcement. Based on strain compatibility and force equilibrium in a rectangular section, the *balanced FRP reinforcement*, $A_{f,b}$ can be calculated as shown in Figure 2-5. At this balanced FRP condition, the beam fails due to FRP rupture and concrete crushing at the same time. If the amount of FRP reinforcement is less than $A_{f,b}$, termed an *under-*

strengthened beam, the failure mode will be FRP rupture. On the other hand, if the FRP area is more than the balanced amount of FRP, termed an *over-strengthened beam*, the failure mode is concrete crushing (ISIS Design Manual No.4 2008).

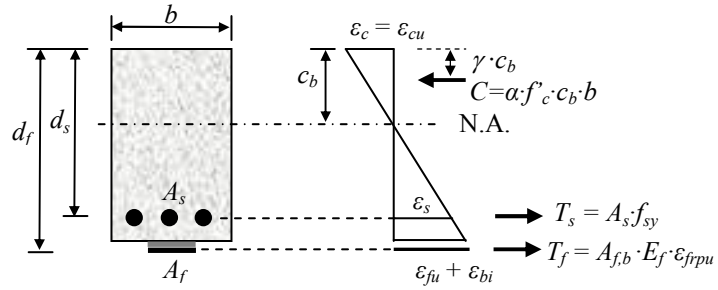

Figure 2-5 Strain compatibility at the balanced condition

FRP strengthened beams often fail prematurely without reaching the full capacity of the FRP or the concrete due to the limit of the bond strength between the FRP and the concrete. This type of failure occurs suddenly without warning. Many studies have been performed to explain each premature debonding failure mode; however, the exact mechanism for the premature bond failures has not yet been established due to numerous influencing factors affecting the bond strength at the FRP-concrete interface.

2.4.4 Strain limit and anchor system

The shear and normal stresses concentrated at the end of the bonded FRP composites are the main causes of premature end debonding failure in the EB system as described in previous section. To prevent or delay the end debonding failure, various anchor systems have been developed and the maximum FRP strain is limited to less than the rupture strain in many specifications and design guidelines. The normal and shear stress distributions of the NSM system are different from the EB system, so different provisions should be prepared to prevent debonding failure of the NSM system.

2.4.4.1 Strain limit

For the EB system, ACI 440.2R (2008) suggested a debonding strain, ε_{fd}, to limit the maximum FRP strain. This debonding strain, which is less than 90% of the ultimate strain, is proportional to the concrete strength and inversely proportional to the stiffness and thickness of the FRP. This means that an RC beam with low strength concrete strengthened with high stiffness and thick FRP has a greater possibility of experiencing a debonding failure. On the other hand, the Concrete Society (2004) takes a more conservative approach limiting the maximum FRP strain as a quantitative value regardless of the FRP type. The strain limits are summarized as follows.

1) ACI 440.2R (2008) – debonding strain, ε_{fd}

$$\varepsilon_{fd} = 0.41\sqrt{\frac{f'_c}{nE_f t_f}} \le 0.9\varepsilon_{frpu}$$

2) Concrete Society (2004)

$$\varepsilon_{f,max} = \begin{cases} 0.008 \text{ for uniform load} \\ 0.006 \text{ for concentrate load} \end{cases}$$

For the case of one ply of FRP plate (n = 1, E_f =165,000MPa, t_{frp} = 1.2 mm, and ε_{frpu} = 0.00169) applied to a beam that is subjected to a concentrated load, the effective strain of FRP will be 0.00668 and 0.006 based on ACI and Concrete Society guidelines, respectively (39.5% and 35.5% of the ultimate FRP strain, respectively). As such, the FRP strain is limited not to exceed these strain limits to prevent debonding failure for design purposes in the EB system.

For NSM system, although 70% of the ultimate strain is proposed as a debonding strain by ACI 440.2R (2008), further research is needed for this system.

2.4.4.2 Mechanical anchors for EB system

Various anchor systems such as bolts, mechanical anchors, or U-shaped sheets have been investigated as end anchors for the EB system. Hollaway and Mays (1999) investigated the effect of various anchor systems as shown in Figure 2-6. According to their research, the beams with end anchors

showed greater moment capacity and deformability than un-anchored beams by delaying premature debonding failure. Teng et al. (2002b) performed experiments using various U-shaped sheet anchors, and they found that the failure modes at the anchor were changed based on the amount of FRP U-shaped sheets. Eshwar et al. (2008) developed two different types of FRP based anchor system, namely, a near surface mounted (NSM) end anchor and a spike anchor. They found that each of these systems was highly effective in increasing the capacity of the strengthened member by delaying debonding failure.

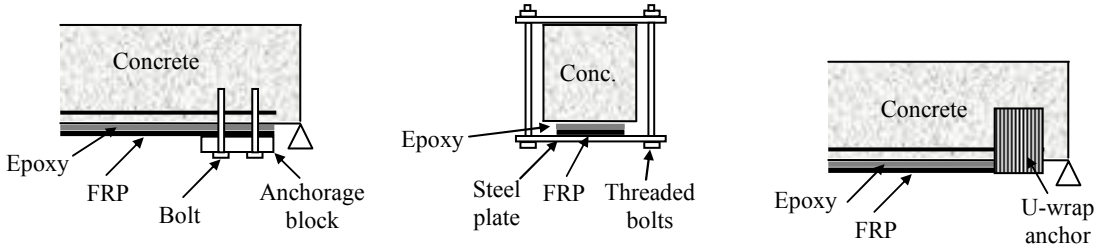

(a) Bolted anchor (b) Mechanical anchor (c) U-wrap anchor

Figure 2-6 Mechanical anchors for EB system (Hollaway and May 1999)

2.5 Prestressed FRP Strengthening System

2.5.1 Background

FRP composites are being investigated as an alternative material for prestressing due to their high tensile strength, low relaxation losses, and high corrosion resistance compared to conventional steel tendons. Numerous research and demonstration projects utilizing FRP prestressed tendons have been performed, and full scale FRP prestressed concrete bridges have been constructed around the world (ACI 440.4R 2004). In contrast, limited research is reported on the use of a prestressed FRP system for repair and strengthening purposes. The main advantage of this system is the recovery of the serviceability of structures, such as crack closure and deflection reduction. On the other hand, the disadvantages of prestressed FRP strengthening system are complicated installation procedure and low deformability compared to prestressed steel tendons.

Initial intensive research with regard to the strengthening with prestressed EB FRP plates was performed at EMPA in Switzerland from the 1990's. They developed an appropriate anchor system for prestressing the FRP plate that was successfully applied to real structures (Millar et al. 2004, Meier et al. 1992). Later, the EMPA researchers developed the gradient method that allows prestressing without anchors at the beam ends (Czaderski and Motavalli 2007). Prestressed FRP sheets were also investigated by Wight et al. (2001) and El-Hacha et al. (2003), and they concluded that prestressed CFRP sheets could remarkably improve the serviceability as well as the ultimate strength of the beam. One of the challenges of prestressed EB systems is the development of proper anchor system at the ends of the FRP because the shear stress (bond stress) and normal stress (peeling stress) become extremely high at the end of the FRP due to prestressing. As a result, various anchor systems have been developed and investigated (Stocklin and Meier 2001, Hollaway and Mays 1999). Their research showed that an improvement of the ultimate flexure response was achieved in prestressed strengthened beams with anchors compared to beams with no anchors.

On the other hand, prestressed NSM system utilizing carbon FRP (CFRP) bars or plates has been recently investigated. Nordin and Täljsten (2004, 2006) applied a prestressed NSM system to RC beams, and found that the ultimate load carrying capacity and the serviceability were greatly improved, and that the force transfer from the FRP to the structure was working well without an external anchor unlike EB prestressing system. Jung et al. (2007) tested prestressed NSM beams using both the CFRP bar and plate with the prestressing force of 20% of the ultimate CFRP strength, and also compared the test results with the non-prestressed beams. They concluded that the cracking load and the stiffness of the beam were greatly improved compared to the non-prestressed beams, and could prevent the premature debonding failure. Gaafar and El-Hacha (2007) tested prestressed NSM beams with various prestressing levels. They found that the serviceability and the ultimate load carrying capacity were improved as the level of the prestressing force was increased while

deformability was decreased when increasing the prestressing force. They concluded that the optimum prestressing limits was between 35% and 45% based on the test results. Badawi (2007) investigated the monotonic and fatigue performance of prestressed NSM strengthened beams. He found that the prestressed strengthened beams showed an improved performance of the static and fatigue resistance compared to unstrengthened beams.

2.5.2 Behaviour of prestressed FRP strengthened beams

The fundamental concept of prestressed FRP strengthened beams is to increase the resisting moment by providing an active force (prestressing force) to the concrete element. Figure 2-7 shows a typical prestressed FRP strengthened beam subjected to four-point load. The tensile stress at the concrete bottom face at mid-span under service loading becomes reduced or changed into compressive stress due to the effect of prestressing force as shown in Figure 2-7. In this way, the deflection is reduced and open cracks may be closed.

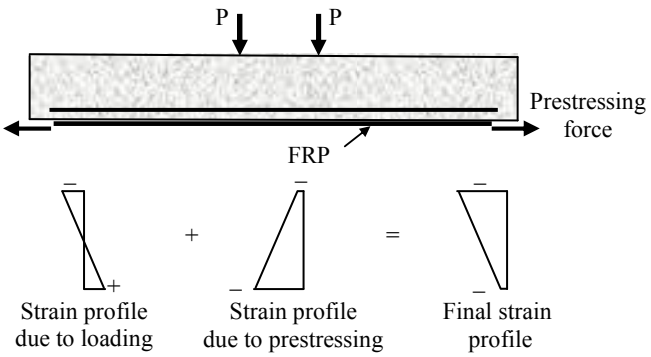

Figure 2-7 Mechanism of the prestressed FRP strengthening system

2.5.3 Application of prestressed FRP strengthening systems

In contrast to the steel, FRP materials have very low transverse load carrying capacity. Therefore, application of a prestressed FRP system requires development of an appropriate anchor system. General prestressed FRP strengthening systems developed so far are summarized in Table 2-5.

Table 2-5 Various prestressed FRP strengthening systems

System	Description	Examples
FRP sheet (EB)	• Strengthening using prestressed FRP sheets has been developed and investigated (Wight et al. 2001, El-Hacha et al. 2003, 2004b). Various anchor systems for prestressing FRP sheets, such as round bar anchor, elliptical anchor, and flat plate anchor, were developed. The figure shows an example of flat plate anchor for prestressing FRP sheets developed by El-Hacha et al. (2003).	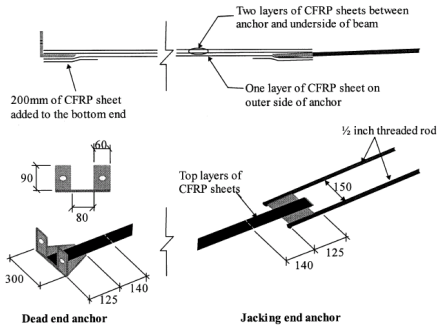
FRP plate (EB)	• Initial intensive research and development project with regard to the strengthening with prestressed FRP plates were performed at EMPA in the beginning of the 1990's. Various anchor systems for prestressed FRP plate have been developed and applied in the real structures (Garden and Mays 1999, Stocklin and Meier 2001, Millar et al. 2004). The figure shows one of the anchors for the prestressed EB plate system.	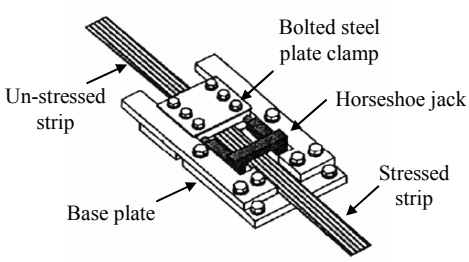
FRP bar (NSM)	• Strengthening with prestressed FRP bars can be applied effectively by the use of NSM bars. Shown is the prestressing set-up for prestressed NSM bars developed by Nordin and Taljsten (2004).	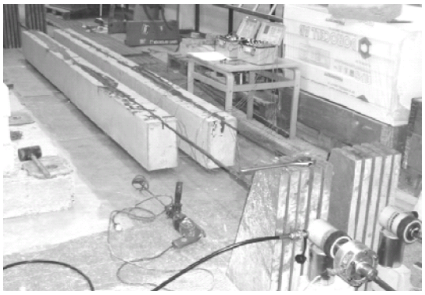
FRP bar (external tendon)	• Strengthening with prestressed FRP bars can be applied by the use of external tendons. Shown is the prestressing set-up for prestressed FRP bars developed at Waterloo (El Refai 2007).	

2.6 Ductility and Deformability

Concrete structures should be designed to provide sufficient warning and energy dissipation before failure in order to give sufficient time for repair or evacuation, and to prevent catastrophic failure. Adequate warning could be achieved by providing sufficient deformation capacity. Deformation of concrete structures can be classified as elastic deformation and plastic deformation. The term *ductility* has been used in steel reinforced concrete structures as a means to quantify plastic behaviour. However, since plastic behaviour is limited in FRP reinforced concrete structures, a new term *deformability* has been developed to quantify deformation capacity for FRP reinforced concrete structures. The term *deformability* was first used by Mufti et al. (1996) and they defined the deformability factor as the ratio of the deflection (curvature) at ultimate state to the deflection (curvature) at serviceability limit state (Mufti et al. 1996). Canadian Highway Bridge Design Code (CSA S6, 2006) and ISIS Design Manual No. 3 (2007) base this concept on the deformability of FRP reinforced beams.

2.6.1 Ductility

Ductility is conventionally defined as the ability of the structural members to sustain large plastic deformation, and thus dissipate energy before failure. Figure 2-8 shows the typical load-deflection diagram of RC beams and FRP reinforced beams. E_{tot} and E_{el} are the total energy (elastic energy plus dissipated plastic energy) and the elastic energy accumulated in the system, respectively. At failure this accumulated elastic energy in the system is dissipated. As shown in Figure 2-8, RC beams have large energy dissipation capacity before failure due to large plastic deformation. On the other hand, only a little energy is dissipated prior to failure in the FRP reinforced beams which may cause a sudden explosion at failure.

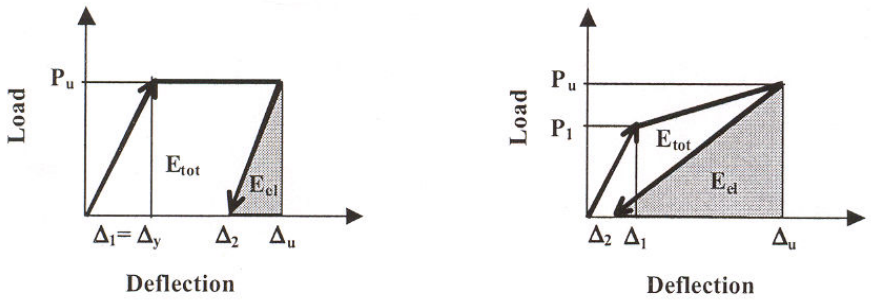

(a) Steel reinforced beam (b) FRP reinforced beam

Figure 2-8 Load-deflection behaviour of steel and FRP reinforced beams (ISIS Design Manual No.5 2008)

Ductility can be measured by two methods: deformation-based and Energy-based. Deformation based ductility is measured in terms of deflection or curvature, as demonstrated by Equations (2-1) and (2-2). Energy based ductility can be calculated by Equations (2-3) and (2-4). A large ductility index denotes ductile structural behaviour.

$$\text{Deflection ductility, } \mu_{\Delta 1} = \frac{\Delta_u}{\Delta_y} \tag{2-1}$$

$$\text{Curvature ductility, } \mu_{\phi 1} = \frac{\phi_u}{\phi_y} \tag{2-2}$$

$$\text{Energy ductility 1, } \mu_{E1} = \frac{E_u}{E_y} \tag{2-3}$$

$$\text{Energy ductility 2 (Naaman and Jeong 1995), } \mu_{E2} = \frac{1}{2}\left(\frac{E_{tot}}{E_{el}} + 1\right) \tag{2-4}$$

Where Δ_u, ϕ_u, and E_u are the deflection, the curvature, and the energy measured by the area under the load-deflection curve at the ultimate point; Δ_y, ϕ_y, and E_y, at the steel reinforcement yielding point.

2.6.2 Deformability

Deformability is defined as the amount of deformation that occurs prior to failure, and therefore no plastic work is necessary. As mentioned earlier, the concept of deformability is more applicable to

FRP reinforced beams and FRP strengthened RC beams than ductility because the FRP material does not yield. For FRP reinforced beams, the serviceability loading point (conditions at service load level) is introduced to determine deformability since there is no steel yielding point. For FRP strengthened RC beams, the steel yielding point can be used to define the deformability. Otherwise, the serviceability loading point can be applied when the steel yielding point is not clear. The basic equations to measure deformability are shown as follows:

$$\text{Deflection deformability (Tann et al., 2003), } \mu_{\Delta 2} = \frac{\Delta_u}{\Delta_s} \tag{2-5}$$

$$\text{Curvature deformability (ISIS Design Manual No. 5, 2008), } \mu_{\phi 2} = \frac{\phi_u}{\phi_s} \tag{2-6}$$

Where, Δ_s and ϕ_s are the deflection and the curvature at the service load; Δ_u and ϕ_u, at the ultimate load. A service load is defined as 67% of the ultimate load by Tann et al. (2003) in FRP strengthened beams, or as a load to produce tensile stress in the concrete of $0.25\sqrt{f'_c}$ in prestressed FRP beams (ISIS Design Manual No. 5, 2008).

2.6.3 Research for improvement of ductility and deformability

Only a few studies related to the enhancement of the deformability in FRP reinforced beams have been performed based on either a material or system perspective. For the material aspect, some researchers have tried to develop a new ductile FRP material called hybrid FRP. The hybrid FRP composites exhibit pseudo-plastic behaviour by combining two different FRP materials that have different elastic modulii and tensile strength. Harris and Somboonsong (1998) and Grace et al. (2002) investigated beams strengthened with hybrid FRP material for the improvement of ductility. They obtained improved ductility in hybrid FRP strengthened beams. However, the hybrid FRP composites are not commercially available and very expensive; therefore, more research is required in this field.

As for the structural aspect, both unbonded systems and partially bonded systems have been applied in flexure members to increase deformability. Burgoyne (1993) suggested an unbonded

system for FRP strengthened beams and schematically showed its potential to improve deformability. Lees and Burgoyne (1999, 2000) investigated experimentally and theoretically the behaviour of partially bonded prestressed AFRP concrete beams. They applied various bonding configurations: fully bonded, unbonded, and partially bonded. According to their research, an improvement of deflection deformability was attained while sustaining the load carrying capacity at the same level as the fully bonded system by partial unbonding of the AFRP tendon. Chahrour and Soudki (2005) also investigated a partially bonded FRP strengthening system. They used partially bonded CFRP plate with mechanical anchors to strengthen RC beams. According to their findings, strengthened beams with end-anchored partially bonded CFRP showed higher enhancement in load carrying capacity and deformability than the fully bonded beam with no end-anchorage.

2.7 Partially Bonded System

2.7.1 Background

Reinforced steel and prestressed tendons are typically completely bonded to the concrete along their length to provide composite action. Complete bond between the steel and the concrete is a critical factor to assure the ultimate load carrying capacity. On the other hand, the concept of a fully unbonded system in prestressed concrete (PC) beams, where the steel tendons are fully unbonded and the anchors are installed at the ends of the steel tendons to hold the steel tensile force under loading, has been developed due to following reasons.

1. Prevention of stress concentration of the tendon at the high moment region maintaining low stress level of the entire tendon;
2. Capability for retensioning and additional tensioning of the unbonded tendon; and
3. Easy inspection and maintenance of the unbonded tendon.

For steel reinforced RC or PC beams, it has not been necessary to consider a partially bonded concept to increase ductility, because ductility is always assured to some degree due to the highly

plastic behaviour of the steel reinforcement as described in previous section. On the other hand, the failure modes of beams strengthened with FRP are different from steel reinforced RC or PC beams as described in Section 2.4.3. FRP rupture could occur in under-strengthened beams, and premature bond failure could result at very low FRP strain levels. In these cases, the deformability of the beam is significantly decreased. In contrast, if the FRP is fully unbonded, large deformability may be assured, but the increase in flexural capacity provided by FRP strengthening will be limited.

To overcome these drawbacks in FRP strengthened beams, the concept of partially bonded system was developed. A *partially bonded* FRP strengthening system is similar to the fully bonded system except that a portion of the FRP length is intentionally unbonded. For a simply supported beam, the unbonded length is typically within the middle portion of the beam, while the end portions are bonded. Lees and Burgoyne (1999, 2000) suggested the concept that both deformability and improved moment capacity could be achieved by applying a partially bonded system as shown in Figure 2-9, and they verified the capacity by the experimental program and the theoretical approach as well.

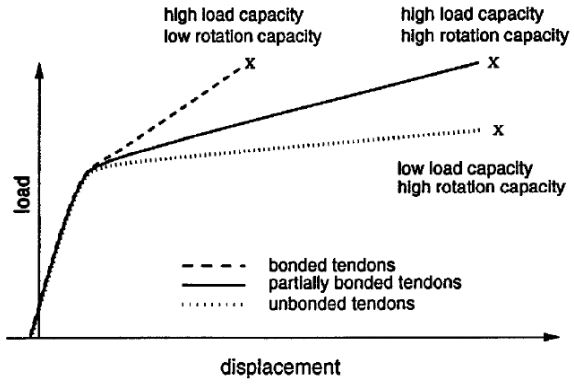

Figure 2-9 Concept of the partially bonded system (Lees and Burgoyne 1999)

2.7.2 Flexural behaviour of partially bonded beams

The tensile stress distribution for a fully bonded, a fully unbonded, and a partially bonded FRP strengthening systems are shown in Figure 2-10 for a simply supported beam subjected to four-point

loading. In the partially or fully unbonded system, the maximum tensile stress in the FRP is lower prior to the steel yielding compared to the fully bonded system due to intentional unbonding at mid-span as shown in Figure 2-10(a). The lower FRP stress means that the stresses in the steel reinforcement and the concrete are higher in comparison to the fully bonded case. However, at the post-yielding stage, the tensile force resultant of steel reinforcement is no longer increased due to yielding, and the total tension force resultant (steel plus FRP) is approximately constant without regard to the bonded condition under the same applied load. As a result, the stress in the FRP in the partially or unbonded beams becomes almost equal to that of the fully bonded system as shown in Figure 2-10(b). While the FRP stress is uniform within the unbonded length, the curvature increases significantly to satisfy the strain compatibility at the mid-span in the partially bonded or unbonded system. As a result, the rotation capacity and deflection are increased in the partially bonded or unbonded system as shown in strain profiles in Figure 2-10(b).

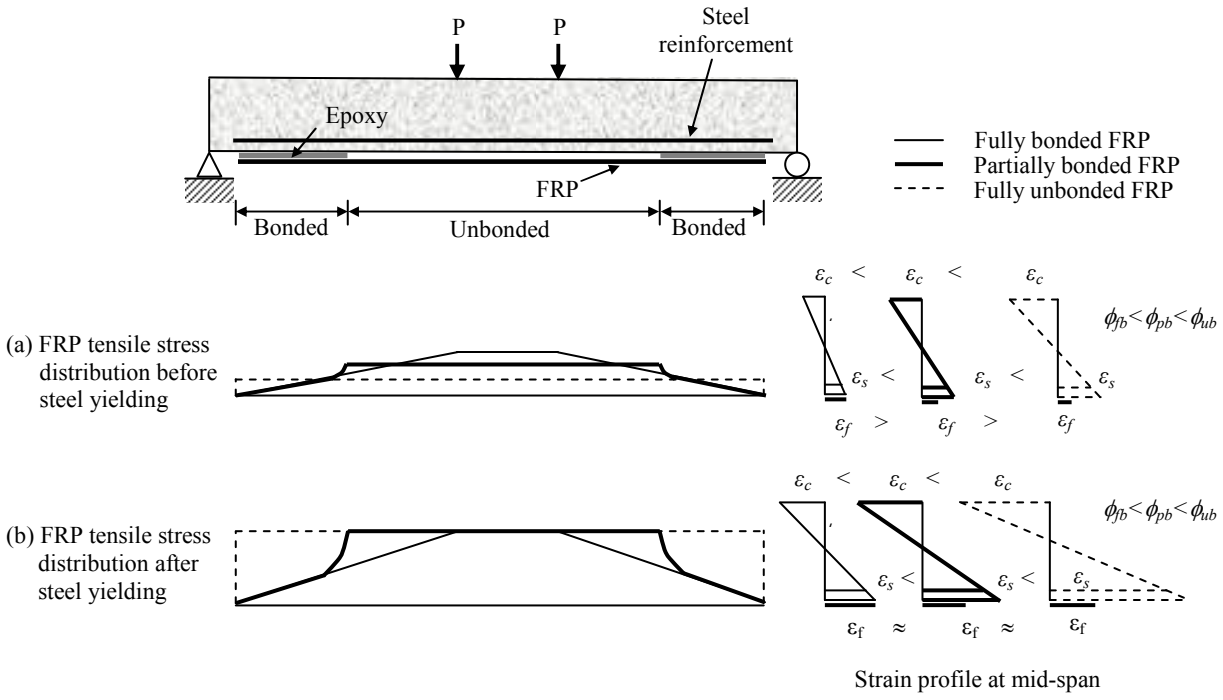

Figure 2-10 Flexural behaviour of fully bonded, partially bonded, and fully unbonded beams

FRP stresses in the fully bonded beams can be easily calculated at any section by using force equilibrium and strain compatibility. However, the FRP strains in the unbonded system can not be calculated directly from section analysis because sectional strain compatibility is not present due to the lack of bond. Instead, the strain in the unbonded FRP becomes the average strain of the concrete at the same level as the FRP (Collins and Mitchell 1987, Shin 2000). The concrete strain at the level of the FRP at any arbitrary unbonded section would be:

$$\varepsilon_c = \frac{f_c}{E_c} = \frac{1}{E_c} \cdot \frac{Me_f}{I} \tag{2-7}$$

Therefore, total deformation of the concrete in the unbonded region is

$$\Delta l = \int_{unbonded} \varepsilon_c \cdot dx = \int_{unbonded} \frac{1}{E_c} \cdot \frac{Me_f}{I} dx \tag{2-8}$$

Average strain of the concrete becomes

$$\frac{\Delta l}{L_{ub}} = \int_{unbonded} \frac{1}{L_{ub} E_c} \cdot \frac{Me_f}{I} dx \tag{2-9}$$

As a result, the average stress of the FRP due to the external load becomes

$$f_f = E_f \cdot \frac{\Delta l}{L_{ub}} = \int_{unbonded} \frac{E_f}{L_{ub} E_c} \cdot \frac{Me_f}{I} dx = \frac{E_f}{L_{ub} E_c} \int_{unbonded} \frac{Me_f}{I} dx \tag{2-10}$$

Within the elastic range of behaviour prior to cracking, f_f can be easily calculated because the moment of inertia, I, is constant in the unbonded region. However, after cracking and steel yielding, moment of inertia is no longer constant and this procedure can not be applied.

For PC beams with fully unbonded tendons, the ultimate stress in the tendon was suggested by Namman (1991a, b) by applying bond reduction factor. This reduction factor is mainly affected by span to depth ratio and loading pattern, and was statistically derived based on numerous test data. He also showed that this factor can be applied to the prestressed beams with fully unbonded FRP tendons (Naaman et al. 2002).

For beams with partially bonded FRP tendons, Lees and Burgoyne (1999, 2000) suggested an analytical model based on rigid body behaviour of the beam, and compared the model to experimental results. This model is based on a discrete crack approach in which the rotation of the beam is assumed to occur only at crack locations. Based on the geometry of the deflected beam, the stress in the tendon and the bond stress were calculated, and following additional crack formation, loss of bond, or tendon rupture, were predicted. This procedure was repeated until complete bond failure or tendon rupture happens.

For partially bonded FRP strengthened beams, an experimental research program was performed by Chahrour and Soudki (2005) for beams with different unbonded lengths. However, to the Author's knowledge, an analytical model to predict general behaviour of partially bonded FRP strengthened beams has not been developed.

2.8 Finite Element Analysis

2.8.1 Background

With the advent of computers in the 1940s, the finite element (FE) modeling technique has been rapidly developed. Soon thereafter FE modeling has been applied for the analysis of the reinforced concrete (RC) structures. Ngo and Scordelis (1967) first applied FE modeling to the RC structures as shown in Figure 2-11. They used predetermined cracks to simulate the cracks in the concrete. However, the development of the cracks with applied load was not considered. They also applied the link element between the steel reinforcement and the concrete to investigate the behaviour of the bond slip at the concrete-steel reinforcement interface.

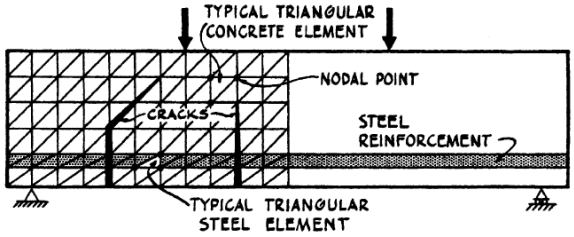

Figure 2-11 Finite element modelling of the reinforced concrete beam (Ngo and Scordelis 1967)

Nilson (1968) applied the same discrete cracks to the modeling of RC structures, but he also considered the development of the cracks at their tips as the applied load increases by utilizing the average value of the principal tensile stress in two adjacent elements for the detection of the crack initiation and development. However, this modeling still had a problem that the stresses at the crack tip could be changed depending on the mesh size, or the stress singularity at the crack tip could be not considered.

The use of discrete type of cracks for the modeling of RC structures is defined as a *discrete crack approach*. This approach is suitable when the location of cracks and their propagation can be easily estimated. On the other hand, a completely different approach for the modeling of the crack was introduced by Rashid (1968). He used the *smeared crack approach* for the simulation of the RC structures. The basic concept of the smeared crack approach is to utilize the changed constitutive relationships after the crack initiation as shown in Figure 2-12 while maintaining the element mesh unchanged.

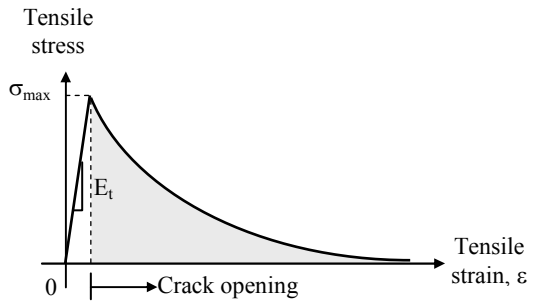

Figure 2-12 Softening curve of concrete tension

The main advantage of the smeared crack model is that re-meshing of the elements or the use of the interfacial element at the crack location is not needed. Therefore, the smeared crack model became more popular and has been widely used due to this computationally convenient procedure. The classical smeared crack model has a similar problem to discrete crack model called *strain localization*, where the strains near cracks are highly dependent on the mesh size (non-objective). The increases of the strain and the stress are concentrated at the crack location (crack bands) once the crack forms and this concentration should be independent of the mesh size (Bazant 1976). To avoid this mesh sensitivity, various types of *localization limiters* have been introduced and implemented to the modeling. The simplest localization limiter is the modification of the constitutive model, where the descending curve is dependent on the mesh size. On the other hand, this localization problem might be negligible and not affect the overall behaviour if the failure is not controlled by the cracks in the RC structures (Dodds et al. (1984)).

Most commercial FE software adopts the *fixed orthogonal crack model* for the formation and development of the cracks due to its simple formulation, where the crack occurs perpendicular to the direction of the principal tensile stress and this direction is not changed once the crack forms. A problem that may occur in this model is known as *shear stress locking*, where the shear strength does not decrease at the crack plane when the direction of the principal stress is changed, and the shear stress is acting on the crack plane. One of the solutions to avoid the shear stress locking problem is to use a *multi-directional* or *rotating crack model*, where the direction of the initially formed crack can be changed when the angle between the principal tensile stress and the direction of the original crack is greater than a certain value (Rots and Blaauwendraad 1989).

An iterative incremental procedure is required for the solution of the nonlinear load-deflection behaviour of the RC beams. The general Newton-Raphson iteration method has been widely used for nonlinear problems, where iterations are required with an increase of the load or deflection until the

internal equilibrium condition is satisfied and convergence is obtained. Every step requires the formation of the new stiffness matrix of the entire model to achieve the equilibrium (HKS 1997). To reduce the large computational cost caused by the calculation of the stiffness matrix at every incremental step and to avoid a possible non-convergence problem, an explicit integration method was developed mainly for the purpose of the simulation of the dynamic analysis with high nonlinearity. The explicit integration method determines a solution from the dynamic equilibrium equation, $P - I = m\ddot{u}$, without iterating by explicitly advancing the kinematic state from the previous increment. Solving a problem explicitly does not require the formation of tangent stiffness matrices, in contrast to the Newton-Raphson iteration method (HKS 1997). Therefore, this method can reduce the computational cost and time for many nonlinear problems.

For the simulation of the nonlinear concrete compression behaviour and the steel reinforcement hardening effect, appropriate types of *hardening rules* and *flow rules* are required. The hardening rule defines the motion of the subsequent yield surface during plastic loading. The flow rule is a link to connect the loading function to the stress-strain relation, and is generally defined by $d\varepsilon_{ij}^{\ p} = d\lambda \frac{\partial g}{\partial \sigma_{ij}}$. If a plastic potential function, *g*, has the same shape as a loading surface, *f*, then the flow rule is called an *associate flow rule*, and can be written by $d\varepsilon_{ij}^{\ p} = d\lambda \frac{\partial f}{\partial \sigma_{ij}}$. On the other hand, if there is no relationship between *g* and *f*, then the flow rule follows a *non-associate flow rule* (Chen 1982).

2.8.2 Application to FRP strengthened concrete beams

Nonlinear finite element analysis using general purpose FE software has been used to simulate the behaviour of the FRP strengthened beams (Arduini et al. 1997, Hu et al. 2003, Chansawat et al. 2006). These studies predicted the general behaviour of the FRP strengthened beams well in terms of load-deflection relationship; however, these models did not consider the debonding phenomenon which is

prevalent in the externally bonded (EB) FRP strengthened beams. As described in the previous section, the mechanism of debonding is complicated due to many influencing factors, such as surface preparation quality, evenness of the surface, and workmanship. Therefore, the accurate mechanism of the debonding failure has not been established although extensive experimental investigations have been carried out on the subject.

To simulate debonding phenomenon in the FE analysis, Wong and Vecchio (2003) and Pham and Al-Mahaidi (2005) applied an interfacial (link) element connecting the concrete and FRP, where the tangential property follows general bond stress-slip relationship shown in Figure 2-2, which can be obtained from shear tests. Kishi et al. (2005) applied discrete crack model at the concrete crack locations to simulate the effect of the cracks on the debonding failure. Coronado and Lopez (2005) utilized the material modeling based on the damage mechanics in order to simulate the debonding phenomenon. These research studies showed reasonable agreement with the experimental result for their specimens.

2.9 Summary

In this chapter, an extensive review on flexural strengthening methods with FRP material was performed and the basic concept of the partially bonded system was introduced. Figure 2-13 summarizes the development in the use of FRP material for flexural members and the key literature for each system. In this study, the flexural behaviour of partially bonded FRP strengthened beams is intensively investigated as in the shaded area of Figure 2-13.

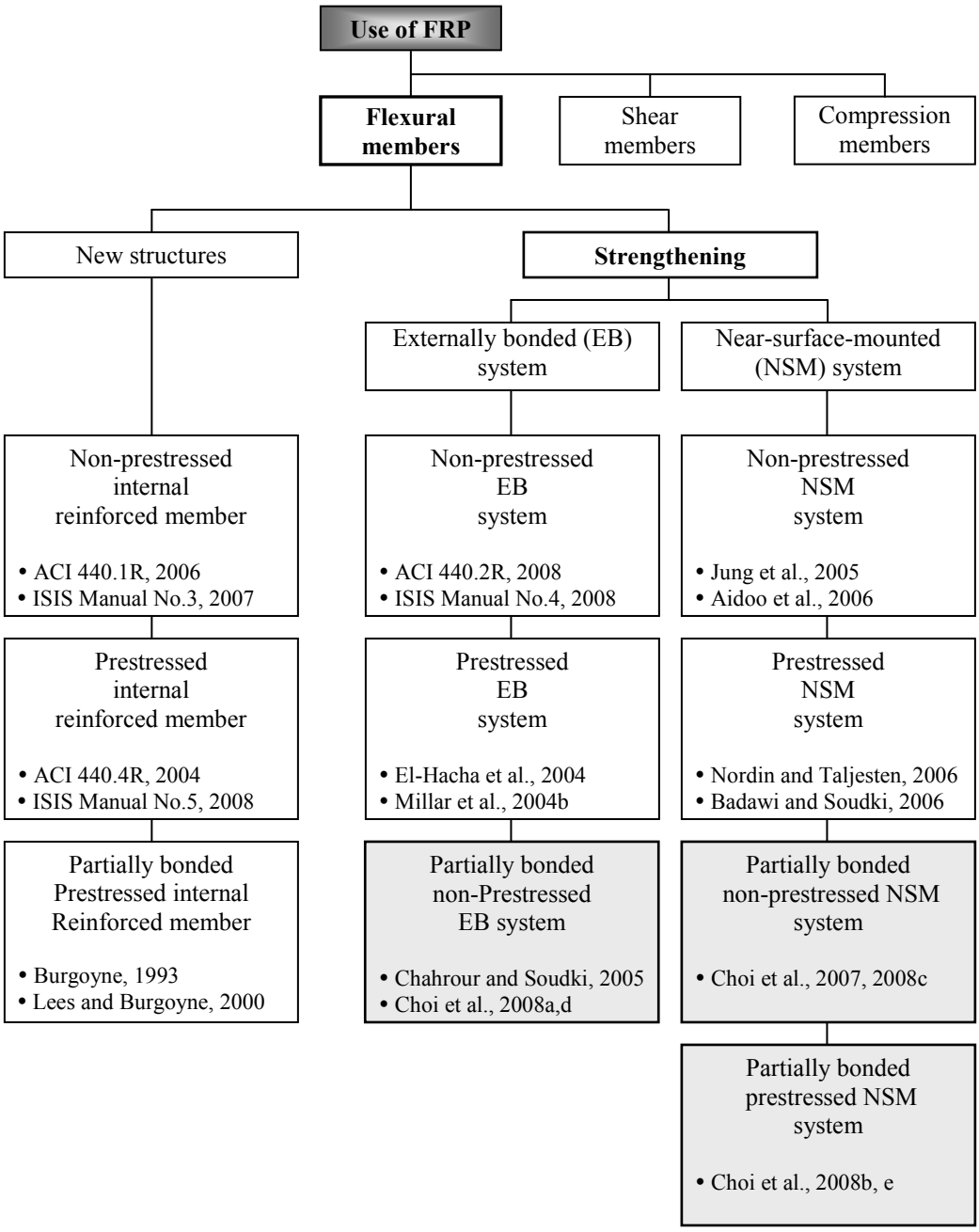

Figure 2-13 Use of FRP material as flexural reinforcement

Chapter 3
Analysis of Partially Bonded FRP Strengthened Beams

3.1 General

An appropriate method for the analysis of a partially bonded FRP strengthening system has not been developed to date as discussed in Section 2.7. In this chapter, a new, simple analytical model was developed based on the curvature approach. This model was used to investigate the effect of partial unbonding with various unbonded lengths and the potential of the improvement of deformability in the partially bonded system (Section 3.2). A linear elastic finite element analysis was also performed in order to investigate the shear and normal stress distributions at the FRP-concrete interface (Section 3.3). Based on this analytical investigation, a detailed experimental program was designed and carried out in Chapter 4.

3.2 Development of the Analytical Model

3.2.1 General

The analysis of unbonded or partially bonded system is fundamentally different from the fully bonded system. For the case of a fully bonded system, the moment-curvature response is calculated using section analysis. In a partially bonded system, a conventional section analysis can no longer be applied due to strain incompatibility at the FRP-concrete interface within the unbonded length. The strain in the partially bonded FRP remains as an average value of the concrete strains at the same location as FRP in the beam section, as illustrated in Figure 2-10 in Section 2.7.2. The response of the partially bonded system, therefore, becomes member dependent as well as section dependent, so the deformed shape of the unbonded region must be considered to calculate the FRP strain at any applied load.

Analytical methods to predict the deflection of RC beams include the discrete crack approach and the curvature approach (Park and Paulay, 1975). The discrete crack approach calculates the rotation and deflection of the beam by assuming that the rotation occurs only at the crack locations. However, this approach is based on complete composite action to find the rotation angle using elongation of steel reinforcement at each element between cracks. Therefore, it is difficult to apply this approach to the analysis of a partially bonded system.

On the other hand, the curvature approach uses the curvature distribution along the beam length to calculate deflection of the beams by direct integration; therefore, it is not needed to calculate the crack locations and spacing. This approach is used to analyze partially bonded FRP strengthened beams in this study. The analysis involves determining the curvature diagram of the partially bonded FRP strengthened beam based on the applied loading (moment diagram) while addressing the overall strain compatibility of the partially bonded system.

3.2.2 Fundamentals of analysis

Presuming that a premature debonding failure does not occur and that the internal steel reinforcement reaches yield level, the failure of a partially bonded FRP strengthened beam may occur in one of three modes: concrete crushing, FRP rupture, or balanced failure (simultaneous concrete crushing and FRP rupture). These failure modes are the same as a fully bonded FRP strengthened beam. However, the failure mode of a partially bonded beam depends not only on the failure mode of the beam in the fully bonded condition, but also on the unbonded length, L_{ub}.

If the failure mode of the beam in the fully bonded condition is FRP rupture (an *under-strengthened* beam, see Section 2.4.3), then the failure mode can change from FRP rupture to concrete crushing as the unbonded length increases. This change in failure mode occurs because the rate of the FRP stress increase decreases with increasing unbonded length, while the concrete and steel stresses increase faster as described in Section 2.7.2. The unbonded length at which the failure

mode changes from FRP rupture to concrete crushing in an under-strengthened beam corresponds to the balanced failure condition, and is referred to as the *balanced unbonded length*, L_{ubb}. If the unbonded length is less than L_{ubb}, then the failure mode will be FRP rupture. If the unbonded length exceeds L_{ubb}, then the failure mode will be concrete crushing.

If the failure mode is concrete crushing in the fully bonded condition (an *over-strengthened* beam, see Section 2.4.3), partial unbonding will not change the failure mode; the partially bonded beam will fail due to concrete crushing regardless of the unbonded length. As such, the balanced unbonded length, L_{ubb}, does not exist for an over-strengthened beam. Therefore, the effect of unbonded length, L_{ub}, on the expected failure mode is a key concept in the development of the analytical model for partially bonded beams.

For illustration purposes, the analytical model is presented using the case of a simply-supported partially bonded beam subjected to four-point loading at the ultimate limit state, as shown in Figure 3-1. The analysis is simplified by considering several critical sections of interest, and assuming that the variation of curvature occurs linearly between these sections (Figure 3-1(b)). Critical sections of interest are the loading point section (section u-u), steel yielding section (section y-y), cracking moment section (section c-c), and the transition section (section t-t). The distances between mid-span of the beam and these critical sections are defined as L_p, L_{uby}, L_{ubcr}, and L_{ub}, as shown in Figure 3-1. The transition section denotes the section where the FRP bond condition is changed from the bonded to unbonded state. The discontinuity of the curvature and strain distributions at the transition section is caused by the sudden change of bond condition.

The concrete strain distribution at the level of FRP is similar in shape to the curvature distribution (Figure 3-1(c)). The FRP strain is constant throughout the unbonded region (Figure 3-1(d)) and is equal to the average concrete strains at the FRP level in the unbonded region (Figure 3-1(c)).

Therefore, the area A_1 is equal to A_2. This relationship defines the *overall strain compatibility* for partially bonded FRP strengthened beams.

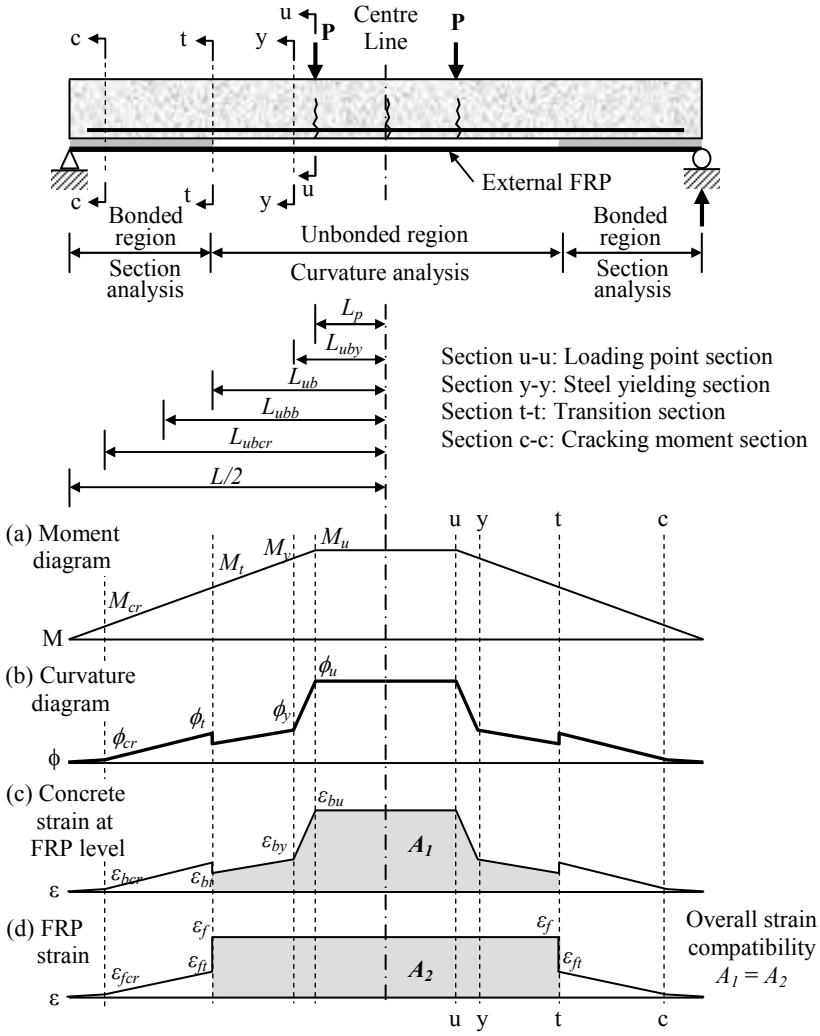

Figure 3-1 Moment, curvature, and strain distributions for a partially bonded FRP strengthened simply supported beam

Based on overall strain compatibility and force equilibrium equations at each critical section, the FRP strain, concrete strain, and curvatures are calculated. Within the bonded regions of the beam, a conventional section analysis may be used to determine section curvature. Once the analysis is concluded, the curvature diagram can then be used to compute the beam deflection.

3.2.3 Assumptions

The following assumptions were used in the calculation procedure.

1. Perfect bond exists between the concrete and the FRP in the bonded region with no slip.
2. There is no friction between the concrete and the FRP within the unbonded length.
3. No premature bond failure occurs before concrete crushing or FRP rupture.
4. Strain distribution over the section depth remains linear up to ultimate (plane section remains plane) except at the level of the FRP in the unbonded region.
5. Curvature and strain distributions along the beam at any loading condition change linearly between the critical sections.
6. Conventional section analysis is valid in the bonded region.
7. The effect of strain discontinuity at transition point is small.
8. A parabolic concrete stress-strain relationship is used in compression, and the ultimate compressive strain is 0.0035 (Collins and Mitchell, 1987).

$$\frac{f_c}{f_c'} = 2 \cdot \frac{\varepsilon_c}{\varepsilon_c'} - \left(\frac{\varepsilon_c}{\varepsilon_c'} \right)^2, \ \varepsilon_c' = 2 \cdot \frac{f_c'}{E_{ct}}, \ E_{ct} = 5{,}500\sqrt{f_c'}$$

9. The stress-strain relationship of concrete in tension is linear elastic, and tensile stress after cracking is neglected. The flexural tensile strength is given by $f_r = 0.6\sqrt{f_c'}$ (CSA A23.2 2004).
10. The stress-strain curve for the steel reinforcement is linear elastic-perfectly plastic.

$$f_s = \begin{cases} \varepsilon_s E_s & \varepsilon_s \le \varepsilon_{sy} \\ f_{sy} & \varepsilon_{sy} \le \varepsilon_s \le \varepsilon_{su} \end{cases}$$

11. The FRP stress-strain relationship is idealized as linear elastic to failure, $f_f = \varepsilon_f E_f \le f_{frpu}$.

3.2.4 Calculation procedure

The general analysis procedure for the calculation of the ultimate response of a partially bonded FRP strengthened beam with any unbonded length is illustrated by the flowchart in Figure 3-2. The

analysis procedure involves various subroutines (A through J) which are dependent on the relationship between L_{ub}, L_{ubb}, and L_{uby}. Detailed flowcharts for each subroutine can be found in Appendix A.

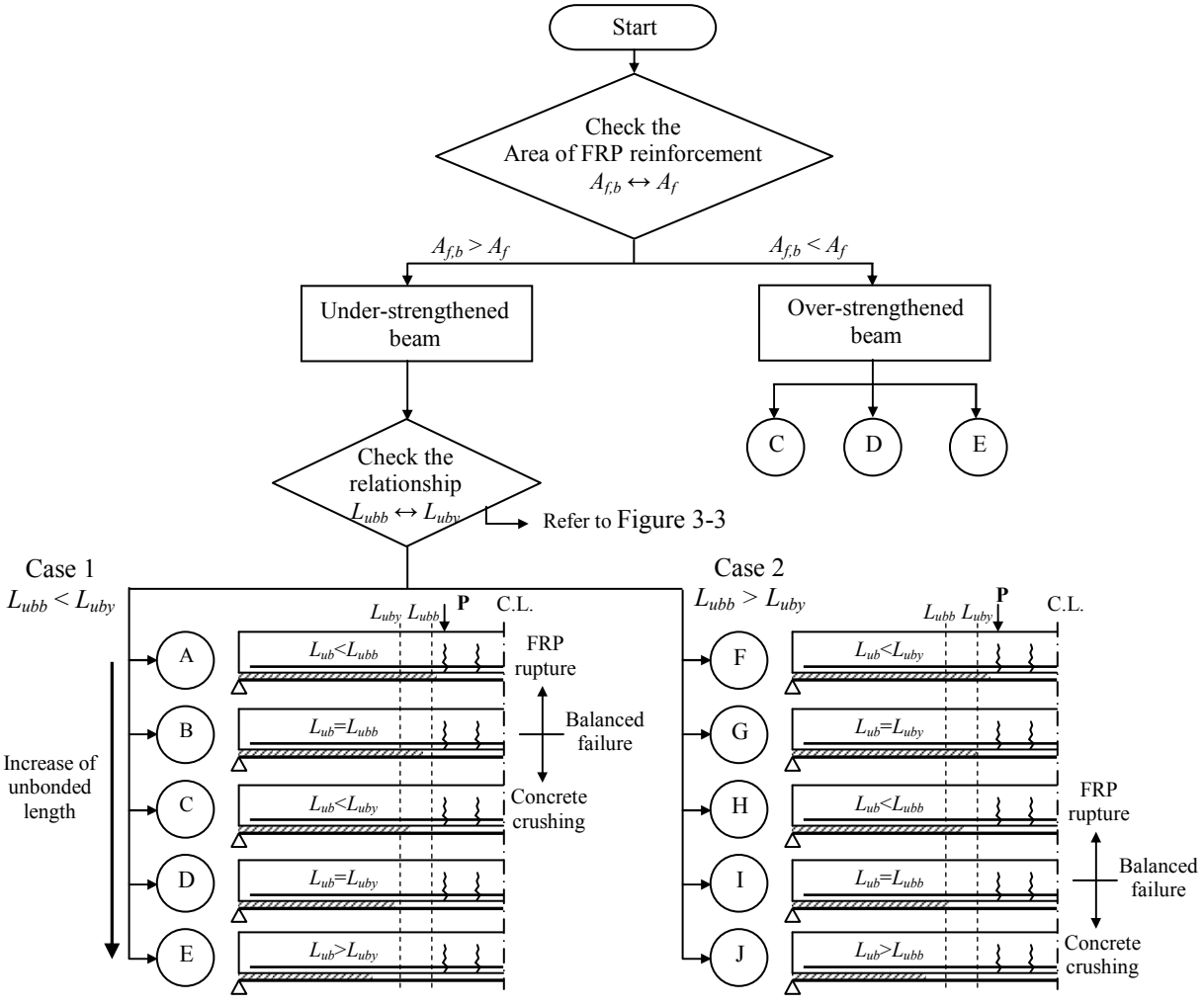

Figure 3-2 Flowchart for analysis of partially bonded FRP strengthened beams with various unbonded lengths

The analysis begins by computing the balanced area of FRP ($A_{f,b}$) since the failure mode of partially bonded beams depends on the failure mode of the beam in the fully bonded condition. The balanced area of FRP ($A_{f,b}$) can be calculated based on force equilibrium and section compatibility in the fully

bonded beam (See Figure 2-5 in Section 2.4.3). If the beam is under-strengthened ($A_f < A_{f,b}$), the calculation procedure will follow one of the subroutines A though J depending on the unbonded length as shown in Figure 3-2. If $L_{ubb} < L_{uby}$, subroutines A and B are used for the FRP rupture failure and balanced failure modes, respectively. Subroutine C, D, or E is used for the concrete crushing failure mode, depending on the unbonded length. If $L_{ubb} > L_{uby}$, F, G, or H is used for the FRP rupture failure mode, depending on the unbonded length. Subroutines I and J are used for the balanced failure and concrete crushing failure modes, respectively. If the beam is over-strengthened ($A_f > A_{f,b}$), the calculation procedure would be the same as the subroutines for the under-strengthened beam where concrete crushing occurs; subroutine C, D, or E would be used, depending on the unbonded length.

As discussed earlier, the failure mode of an under-strengthened beam can change according to the relationship between the unbonded length, L_{ub} and balanced unbonded length, L_{ubb}. Moreover, the critical sections and overall compatibility equations depend on the relationship between the unbonded length and the location where steel yielding occurs (L_{uby}). If the unbonded length is less than L_{uby}, there are two critical sections: the ultimate section and the transition section (since the steel yielding section exists outside the transition section), and the overall strain compatibility is given by Eq. (3-1).

$$\varepsilon_f = \frac{\frac{1}{2}\cdot\left(\varepsilon_{bt}+\varepsilon_{bu}\right)\cdot\left(L_{ub}-L_p\right)+\varepsilon_{bu}\cdot L_p}{L_{ub}} \tag{3-1}$$

On the other hand, if the unbonded length is greater than L_{uby}, three critical sections must be considered: the ultimate section, the steel yielding section, and the transition section, and the overall strain compatibility is given by Eq. (3-2).

$$\varepsilon_f = \frac{\frac{1}{2}\cdot\left(\varepsilon_{bt}+\varepsilon_{by}\right)\cdot\left(L_{ub}-L_{uby}\right)+\frac{1}{2}\cdot\left(\varepsilon_{by}+\varepsilon_{bu}\right)\cdot\left(L_{uby}-L_p\right)+\varepsilon_{bu}\cdot L_p}{L_{ub}} \tag{3-2}$$

As discussed previously, overall strain compatibility dictates that the FRP strain within the unbonded length is equal to the overall concrete strain at the level of FRP reinforcement in the unbonded region. Thus, Eq. (3-1) and (3-2) are derived from the strain distributions shown in Figure 3-1(c) and Figure 3-1(d) by setting the area A_1 equal to the area A_2 and solving for ε_f.

As such, the relationship between L_{ub}, L_{ubb}, and L_{uby} should be known for the case of the under-strengthened beam. The relationship between L_{ubb} and L_{uby} is first checked using the flowchart in Figure 3-3. This procedure determines whether L_{ubb} is greater or less than L_{uby} by assuming that L_{ubb} equals L_{uby}, but does not compute these lengths directly. Depending on the section details and the loading conditions, the balanced unbonded length, L_{ubb}, can be less than L_{uby} (Case 1), or greater than L_{uby} (Case 2). Once this relationship is determined, L_{ubb} can be computed using the subroutines for Case B or I, as appropriate, by solving for the unbonded length required to produce a balanced failure (i.e., set $L_{ub} = L_{ubb}$). The length to the yield point, L_{uby}, can be also computed using the subroutines for Case D or G, as appropriate, by solving for the unbonded length needed to produce steel yielding at the transition section (i.e., set $L_{ub} = L_{uby}$). Based on the relationships between L_{ub}, L_{ubb}, and L_{uby}, the calculation for the beam with any unbonded length can be completed.

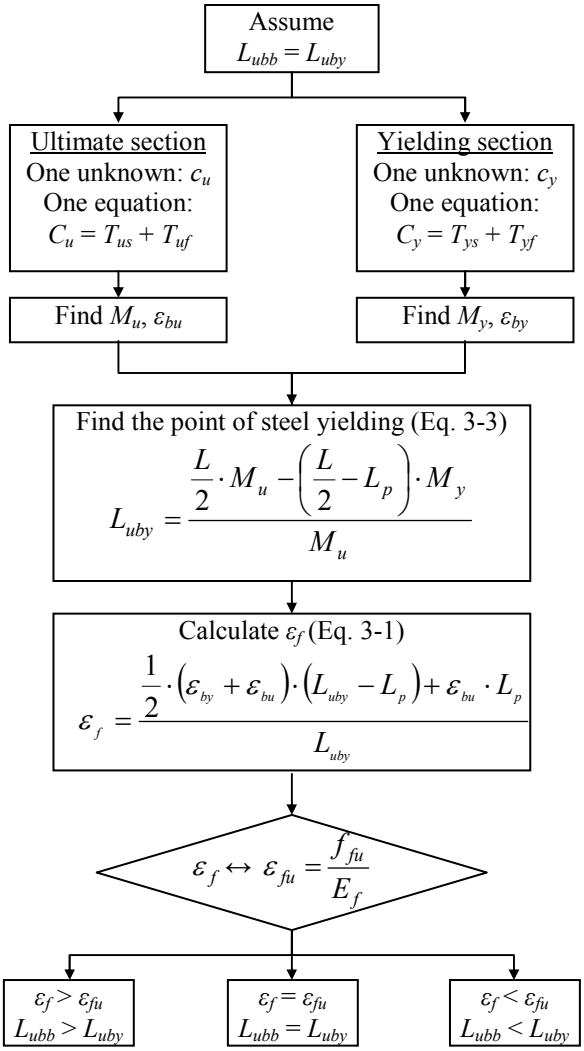

Figure 3-3 Flowchart for determining the relationship between L_{ubb} and L_{uby}

The analysis procedure for the beam shown in Figure 3-1 is Case H since $L_{uby}<L_{ub}<L_{ubb}$. The detailed analysis procedure for Case H is shown in Figure 3-4. For this case, the failure mode is FRP rupture because L_{ub} is less than L_{ubb}. The critical sections are the ultimate, the steel yielding, and the transition section, and the overall strain compatibility equation is Eq. (3-2).

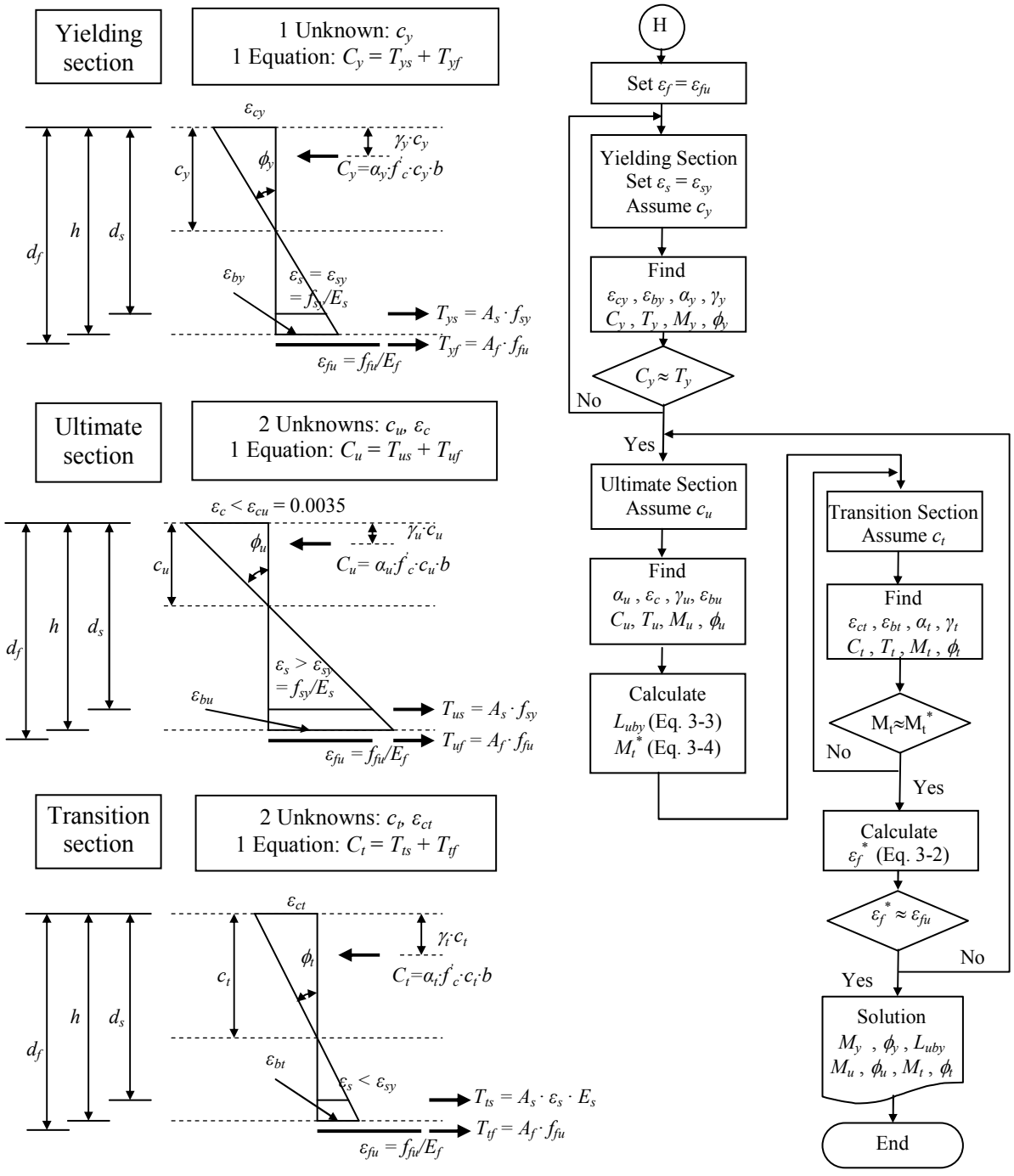

Figure 3-4 Force equilibrium at the critical sections and the flowchart of Case H

Figure 3-4 shows the force equilibrium equations at each critical section and the solution subroutine for Case H. The steel yielding section analysis can be completed independently (one equation and one unknown). However, section analyses at the ultimate section and transition section can not be solved explicitly, since the number of unknowns exceeds the number of equations (two equations and four unknowns). In addition to its role in overall strain compatibility, the strain profile at each section defines the concrete and internal steel reinforcement stresses and strains, allowing the internal moment at the section to be computed. The moments at each critical section are related by the moment diagram (Figure 3-1(a)), as given by Eq. (3-3) and (3-4).

$$M_y = \frac{M_u \cdot \left(L/2 - L_{uby}\right)}{L/2 - L_p} \tag{3-3}$$

$$M_t = \frac{M_u \cdot \left(L/2 - L_{ub}\right)}{L/2 - L_p} \tag{3-4}$$

The distance to the steel yielding point, L_{uby}, is unknown, so these expressions provide two additional equations and one additional unknown. The solution is completed using the overall strain compatibility relationship, Eq. (3-2), as the sixth equation.

In summary, the analysis is performed using the force equilibrium equations for each critical section, the overall strain compatibility equation, and the relationship between bending moments at the critical sections to solve the unknowns. Although a direct solution process could be developed, the solution is simplified by taking an iterative approach following the flowchart shown in Figure 3-4.

A similar approach is used to analyze the complete response of a beam at the cracking, yielding and ultimate stages for any unbonded length. For the response at the steel yielding and cracking stages, the number of critical sections is reduced and the overall strain compatibility equation is simplified.

3.2.5 Numerical example

Using the analytical model developed, an investigation was performed for the beams that have the same configuration as the beams used in the experimental program with various unbonded lengths. The summary of the sectional and geometric properties are as follows. Further details of the beam can be found in Chapter 4.

- Concrete: b_f = 400 mm, b_w = 150 mm, t_f = 50 mm, h = 300 mm, (T-section), f'_c = 52.5MPa
- Steel: A_s = 400 mm^2, E_s = 200,000MPa, f_{sy} = 400MPa, d_s = 254 mm
- FRP: A_f = 36.0 mm^2, E_f = 165GPa, f_{frpu} = 2800MPa, ε_{frpu} = 0.0169, d_f = 302.0 mm
- L = 3300 mm, L_p = 150 mm, 4-point bending.

Step 1. Determine whether beam is under-strengthened or over-strengthened ($A_{f,b} \leftrightarrow A_f$)

$$A_{f,b} = \frac{\alpha_1 \beta_1 f'_c \left\{ t_f (b_f - b_w) + c_b b_w \right\} - A_s f_{sy}}{E_f \varepsilon_{fu}}$$ (Equation from Figure 2-5, modified for T-section)

$$\alpha_1 = 0.85 - 0.0015 f'_c = 0.771$$

$$\beta_1 = 0.97 - 0.0025 f'_c = 0.839$$

$$c_b = \frac{\varepsilon_{cu}}{\varepsilon_{fu} + \varepsilon_{bi} + \varepsilon_{cu}} \cdot d_f = 51.56mm$$ (Equation from Figure 2-5, assume b_i = 0)

$A_{f,b}$ = 187.94 mm^2 > A_f = 36.0 mm^2

→ Under-strengthened beam

Step 2. Check the relationship between L_{ubb} and L_{uby} (refer to flowchart in Figure 3-3)

Assume $L_{ubb} = L_{uby}$

- Ultimate section (One equation and one unknown → solved independently)

M_u = 78.92 kN-m, ε_{bu} = 0.0510

- Yielding section (One equation and one unknown → solved independently)

M_y = 75.33 kN-m, ε_{by} = 0.0031

$$L_{uby} = \frac{\frac{L}{2} \cdot M_u - \left(\frac{L}{2} - L_p\right) \cdot M_y}{M_u} = 218mm$$

$$\varepsilon_f = \frac{\frac{1}{2} \cdot \left(\varepsilon_{by} + \varepsilon_{bu}\right) \cdot \left(L_{uby} - L_p\right) + \varepsilon_{bu} \cdot L_p}{L_{uby}} = 0.044 \quad > \quad \varepsilon_{fu} = 0.017$$

$\rightarrow$ $L_{ubb} > L_{uby}$ $\rightarrow$ Case 2

Step 3. Calculate L_{ubb} (subroutine Case I) (refer to flowchart I in Appendix A)

Set $L_{ub} = L_{ubb} > L_{uby}$

Critical sections

- Ultimate section (One equation and one unknown $\rightarrow$ solved independently)
- Yielding section (One equation and one unknown $\rightarrow$ solved independently)

  L_{uby} = 216 mm
- Transition section (One equation and two unknowns

  $\rightarrow$ solved using overall strain compatibility equation)

  $M_t^* = M_t$ = 54.5kN-m

Equation of overall strain compatibility (Eq. 3-2)

$$\varepsilon_f^* = \frac{\frac{1}{2} \cdot \left(\varepsilon_{bt} + \varepsilon_{by}\right) \cdot \left(L_{ub} - L_{uby}\right) + \frac{1}{2} \cdot \left(\varepsilon_{by} + \varepsilon_{bu}\right) \cdot \left(L_{uby} - L_p\right) + \varepsilon_{bu} \cdot L_p}{L_{ub}}$$

Iterate L_{ub} until ε_f^* equals ε_{fu}

$\therefore$ M_u = 78.92 kN-m, $\phi_u = 180.9 \times 10^{-6}$ rad/mm, L_{ubb} = 614 mm

Calculate associated applied load and mid-span deflection

$\therefore$ P_u = 105.23 kN, Δ_u = 61.77 mm

Step 4. Calculate L_{uby} (subroutine Case G) (refer to flowchart G in Appendix A)

Set $L_{ub} = L_{uby} < L_{ubb}$

Critical sections

• Ultimate section (One equation and two unknowns → solved using overall strain compatibility equation)

• Transition section (One equation and one unknown → solved independently)

Equation of overall strain compatibility (Eq. 3-1)

$$\varepsilon_f = \frac{\frac{1}{2}\cdot\left(\varepsilon_{bt}+\varepsilon_{bu}\right)\cdot\left(L_{ub}-L_p\right)+\varepsilon_{bu}\cdot L_p}{L_{ub}}$$

Iterate L_{ub} until ε_f equals ε_f^* (where, ε_f^* = FRP strain at the ultimate section)

$\therefore M_u = 78.40$ kN-m, $\phi_u = 71.93\times10^{-6}$ rad/mm, $L_{uby} = 219$ mm

$\therefore P_u = 104.53$ kN, $\Delta_u = 43.55$ mm

Step 5. Calculate response when $L_{ub} = 450$ mm

$L_{uby} < L_{ub} < L_{ubb}$

Subroutine Case H (illustrated in Section 3.2.4 with Figure 3-4)

$\therefore M_u = 78.86$ kN-m, $\phi_u = 134.40\times10^{-6}$ rad/mm

$\therefore P_u = 105.15$ kN, $\Delta_u = 51.30$ mm

Step 6. Calculate response when $L_{ub} = 850$ mm

$L_{uby} < L_{ubb} < L_{ub}$

Subroutine Case J (refer to flowchart J in Appendix A)

$\therefore M_u = 72.97$ kN-m, $\phi_u = 192.4\times10^{-6}$ rad/mm

$\therefore P_u = 97.29$ kN, $\Delta_u = 64.51$ mm

The analysis for other unbonded lengths can be calculated in a similar manner. Figure 3-5 shows the analysis results of this example in terms of moment-curvature response at the mid-span section.

Results are shown for the unstrengthened beam, fully bonded FRP strengthened beam (solid lines), and partially bonded FRP strengthened beam with increasing unbonded lengths (dashed lines). At the balanced point ($L_{ub} = L_{ubb}$ = 614 mm), where the beam fails due to FRP rupture and concrete crushing at the same time, the moment capacity was increased by 59% compared to the unstrengthened beam. This is the same improvement as the fully bonded beam, and the ultimate curvature in the partially bonded beam was increased by 192% compared to the fully bonded beam. After passing the balanced point ($L_{ub} > L_{ubb}$), the failure mode changes to concrete crushing. At this stage, the ultimate curvature continues to increase, but the ultimate moment is reduced. Therefore, the balanced unbonded length is the key value to improve deformability without loss of the load carrying capacity.

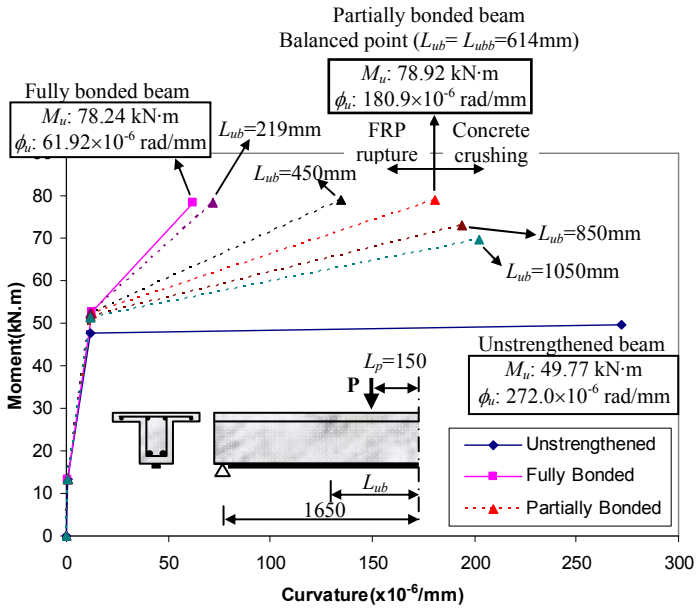

Figure 3-5 Moment-curvature diagrams of unstrengthened, fully bonded, and partially bonded beams (under-strengthened beam, $A_{f,b} > A_f$)

Load-deflection diagrams with increasing the unbonded length shows the same pattern as the moment-curvature diagrams. The deflection was increased without loss of the load carrying capacity up to the balanced unbonded length and the applied load was decreased after passing the balanced

point. The predicted load-deflection diagrams were compared with the experimental results in Section 5.3.1.

3.2.6 Application to the beam subjected to the uniform load

The analytical model was developed based on the assumption of a linear variation of a curvature along the beam length between the critical points of the beams subjected to the 4-point bending. However, if the beam is subjected to a uniform load, the curvature distribution is not linear. In order to maintain the assumption of a linear variation of curvature between analysis points (critical section), many more sections must be considered along the beam length. This will significantly increase the computational effort required to analyze the beam. As an alternative approach, an equivalent 4-point load is suggested for the analysis of partially bonded beams subjected to a uniform load.

The curvature distribution of the partially bonded beam subjected to a uniform load (ω) can be assumed as shown in Figure 3-6(a) by the solid line. Since the FRP of the partially bonded beams is fully unbonded within the unbonded length, the curvature distribution within the unbonded length is similar to that of the unstrengthened beam; therefore, the equivalent 4-point load is derived using the analysis of the unstrengthened beam. The dotted line in Figure 3-6(a) represents the curvature diagram subjected to the 4-point load of the partially bonded beam. To obtain the equivalent 4-point load, the loading distance (L_p) and the equivalent load (P) should be known. Those unknowns can be calculated using two conditions that the deflection and the moment at mid-span due to the two loading conditions (uniform and 4-point load) are the same. Figure 3-6(b) shows the curvature diagrams of the unstrengthened beam subjected to a uniform load (ω) and 4-point loading with different loading distances (L_p) at the ultimate stage. The same beam configurations used in the previous section were used for this analysis.

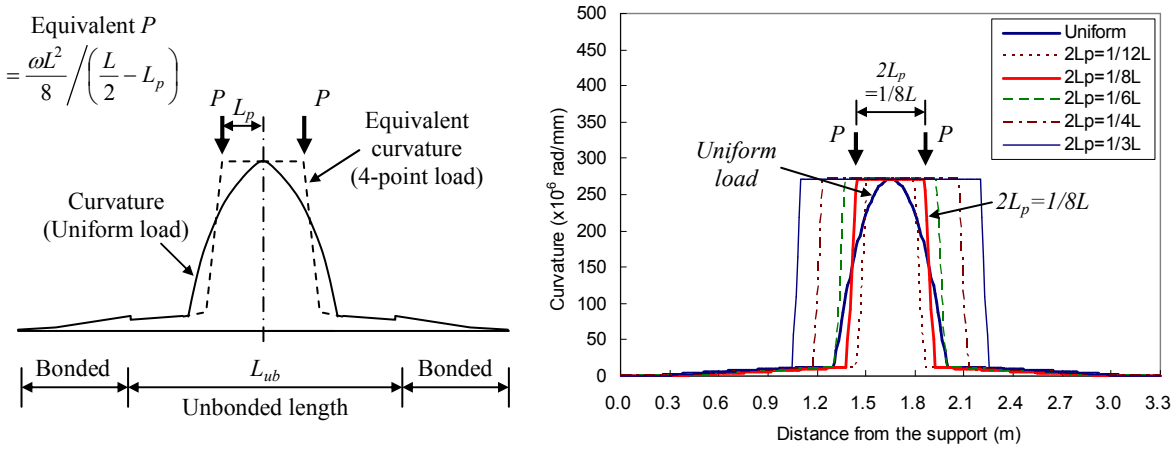

(a) Equivalent curvature diagram of the partially bonded beam

(b) Comparison of curvature diagrams of the unstrengthened beam

Figure 3-6 Equivalent 4-point load subjected to the uniform load

Table 3-1 shows the deflections at mid-span at ultimate and the deflection ratios between the uniform load and the 4-point loading. The deflection due to the uniform load was very similar to the deflection due to 4-point loading of $2L_p$=1/8L as shown in Table 3-1 and Figure 3-6(b). Therefore, the partially bonded beam subjected to the uniform load with this configuration can be assumed to be a beam subjected to an equivalent 4-point loading of $2L_p$=1/8L. The equivalent load is $\frac{\omega L^2}{8}\Big/\left(\frac{L}{2}-L_p\right)$ to make the equal moment at mid-span. For the different beam configuration, the same procedure can be used to obtain the equivalent 4-point loading for the analysis of the partially bonded beams.

Table 3-1 Comparison of deflection between uniform loading and 4-point loading at ultimate

Load condition	Deflection (mm)	Ratio*
Uniform	104.39	-
$2L_p$=1/12L	80.34	0.77
$2L_p$=1/8L	106.02	1.02
$2L_p$=1/6L	130.62	1.25
$2L_p$=1/4L	176.13	1.69
$2L_p$=1/3L	216.87	2.08

* Deflection ratio between uniform and 4-point loads

The analytical model is derived from force equilibrium, overall strain compatibility, and moment relationships between the critical sections where the strains and curvatures are significantly changed. Therefore, this model can be applied to other loading conditions and support conditions once the critical sections and the related equations are properly determined. That is, Eq. (3-1), (3-2), (3-3), and (3-4) must be adapted to the new load and support conditions. The analytical model can also be applied to the concrete beams with initial cracks and strains by considering the initial strains (ε_{bi}) for the formation of overall strain compatibility equation and force equilibrium equations.

3.3 Elastic Finite Element Analysis

In this section, two-dimensional linear elastic finite element (FE) analysis was performed. An analytical model developed in previous section has some assumptions to simplify the calculation procedure, so it is limited for the model to observe the stress distributions at FRP-concrete interface along the FRP length. High shear (bond) stress and normal (peeling) stress at the end of FRP in the fully bonded system are known to be main causes for premature bond failure of FRP strengthened beams, as described in Section 2.4.2. Therefore, the objective of elastic FE analysis is to investigate the general distribution of these stresses in partially bonded beams. A more rigorous three-dimensional nonlinear FE analysis considering the effect of concrete cracks and crushing, strain hardening of the steel reinforcement, and the interactions at the interface are carried out to investigate the debonding failure in Section 5.4.

The SAP2000 commercial FE analysis package was used to analyze the behaviour of EB FRP strengthened T-beams. The same geometry and material properties of the beam were used as in Section 3.2.5. A four-node quadrilateral shell element was used to model the epoxy adhesive, FRP plate, and the concrete, and only half of the beam was considered due to symmetry. In this stage, the FRP-epoxy interface and epoxy-concrete interface were considered to be perfectly bonded. Figure 3-7 show the two-dimensional modeling mesh for the EB FRP strengthened beam. Very fine mesh was

used for concrete, epoxy, and FRP reinforcement at the interface as shown in Figure 3-7 in order to investigate the behaviour of the interfacial stresses.

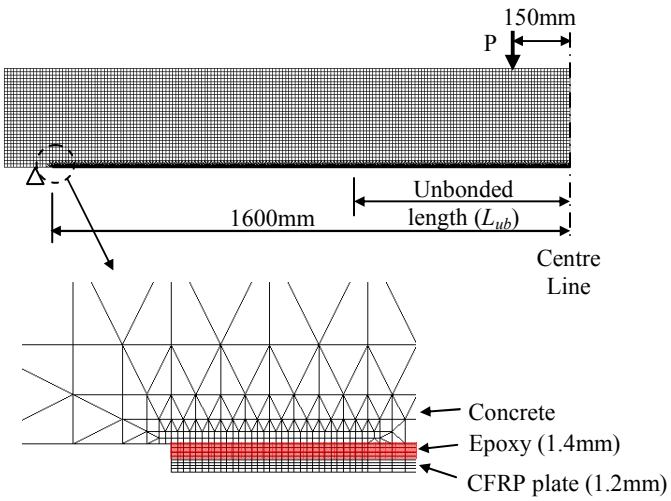

Figure 3-7 Finite element mesh of EB FRP strengthened beams

Figure 3-8 shows the normal stress (peeling stress) distributions at the FRP-concrete interface along the beam length at the elastic stage (P = 10kN). The normal stresses were concentrated at the end of the FRP due to the sudden termination of FRP without regard to the bond condition. On the other hand, this normal stress was also high at the bonded point in the partially bonded beam as shown in Figure 3-8. This normal compressive stress at the tip of the bonded point was changed into the normal tensile stress right after the bonded point, and this tensile stress decreased rapidly to almost zero as shown in Figure 3-8. This is because the epoxy elements were removed to make the unbonded condition within the unbonded length, so the normal stresses were increased at the bonded point due to the sudden gap at that point. Therefore, a sudden gap at the bonded point should be avoided in order to reduce or remove this concentrated normal stress at the bonded point. For this reason, the epoxy adhesive was applied even to the unbonded region to remove the gap and a thin plastic sheet was used to make the unbonded length in the experimental program in the following chapter.

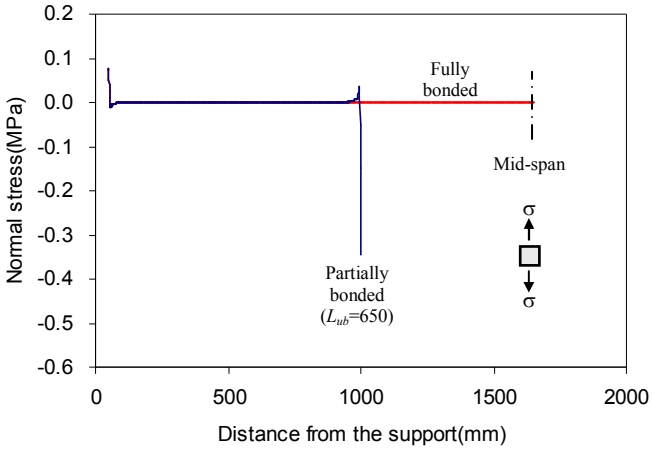

Figure 3-8 Normal stress distributions at the FRP-concrete interface along the beam length (P = 10kN)

The shear (bond) stress distributions along the FRP length were similar to the normal stress distributions at the interface as shown in Figure 3-9(a). Shear stress was concentrated at the end of the FRP without regard to the bond condition and this stress was also high at the bonded point in the partially bonded beam. Due to the sudden change of the bond condition at the transition section, the sudden change of the FRP tensile stress occurred at the bonded point as shown in Figure 3-9(b) and as a result the shear stress was increased at that point. For this reason, CFRP wrapping was applied at the high stress zone to increase the bond strength in the experimental program in the following chapter.

Although the analysis performed in this section is valid only at the elastic stage and should consider the effect of the nonlinear properties of the materials, the general behaviour of the interfacial stresses and the differences in stress distributions between fully bonded and partially bonded beams were represented well by the FE analysis.

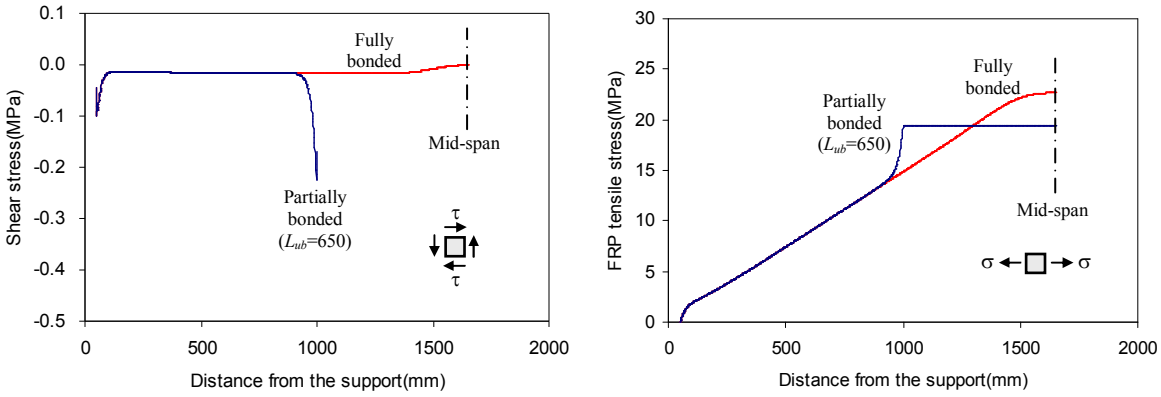

(a) Shear stress distribution (b) Tensile stress distribution of FRP

Figure 3-9 Shear stress distribution at interface and FRP tensile stress distribution along the beam length (P = 10kN)

3.4 Summary

In this chapter, an analytical model was introduced for the analysis of the partially bonded system. The development of the model and the numerical example were presented. Linear elastic finite element analysis was also performed to investigate the stress distributions at the concrete-FRP interface. The specific conclusions are as follows:

1. An analytical model was developed based on the curvature approach for the analysis of the partially bonded beams. The analytical model determines the curvature diagram of the partially bonded FRP strengthened beam at critical sections based on the applied loading (moment diagram) while addressing the overall strain compatibility of the partially bonded system and force equilibrium equations at critical sections.
2. This model represents the general behaviour of the partially bonded beams with various unbonded lengths well. A balanced condition and a balanced unbonded length exist in under-strengthened partially bonded beams, where the deformability of the beam was maximized without the loss of the flexural strength. The developed model showed that the partially

bonded FRP strengthening system has a high potential to improve the beam deformability in comparison to the fully bonded system.

3. An equivalent 4-point loading pattern was proposed for the analysis of partially bonded beams subjected to uniform loading based on the equivalent deflection and moment of the beam.
4. A linear elastic finite element (FE) analysis was performed to investigate the interfacial stress distributions. The analysis showed that the interfacial stresses were concentrated at the end of the FRP plate without regard to the bond condition. In the partially bonded beam, the interfacial shear and normal stresses were also concentrated at the bonded point due to the sudden change of the bond condition. These high stresses at the end of the plate and at the bonded point must be considered in the design of the partially bonded system.

Chapter 4
Experimental Program

4.1 General

An experimental program was developed to verify the analytical model developed in Chapter 3 and to investigate the actual flexural behaviour of partially bonded FRP strengthened beams. Section 4.2 shows the whole test matrix of the experimental program. The specimen fabrication and strengthening with both the externally bonded (EB) CFRP and the near-surface-mounted (NSM) CFRP are described in Section 4.3 and 4.4. In section 4.5, material properties used in the experiments are reported. The description of test setup and instrumentations are in Section 4.6. Test results and discussion for each strengthening system are described in consecutive chapters (Chapter 5~Chapter 7).

4.2 Test Matrix

A total of seventeen, simply supported, 3.5m long, T-shaped RC beams were constructed and tested. One of them is a control beam without strengthening and the other 16 beams consist of four test groups that have different strengthening systems. Each group has different unbonded lengths including the fully bonded beam in order to investigate the effect of partial unbonding on the behaviour of the beams. Three strengthening systems were applied: non-prestressed EB system (Group I), non-prestressed NSM system (Group II), and prestressed NSM system (Groups III and IV). The detailed test matrix is shown in Table 4-1.

The configuration for non-prestressed CFRP strengthened beams (Group I and II) was selected to induce CFRP rupture in the fully bonded condition (under-strengthened beam, $A_f < A_{fb}$) in order to maximize the effect of partial unbonding. The area of CFRP reinforcement was selected to provide an increase of approximately 60% in ultimate load carrying capacity compared to the unstrengthened beam.

Table 4-1 Test matrix

Beam No.	Test group	Beam name*	Strengthening system	Unbonded length (L_{ub}×2) (mm)
1	-	Control	-	-
2	Group I	NPFB	Non-prestressed EB CFRP plate	Fully Bonded
3		NPPB2		650×2
4		NPPB3		850×2
5		NPPB4		1050×2
6	Group II	NBFB	Non-prestressed NSM CFRP bar	Fully Bonded
7		NBPB2		650×2
8		NBPB2.5		750×2
9		NBPB3		850×2
10		NBPB4		1050×2
11	Group III	PBFB	Prestressed NSM CFRP bar (40%)	Fully Bonded
12		PBPB2		650×2
13		PBPB3		850×2
14		PBPB4		1050×2
15		PBPB5		1250×2
16	Group IV	PBFB-60	Prestressed NSM CFRP bar (60%)	Fully Bonded
17		PBPB4-60		1050×2

* Specimen naming convention:

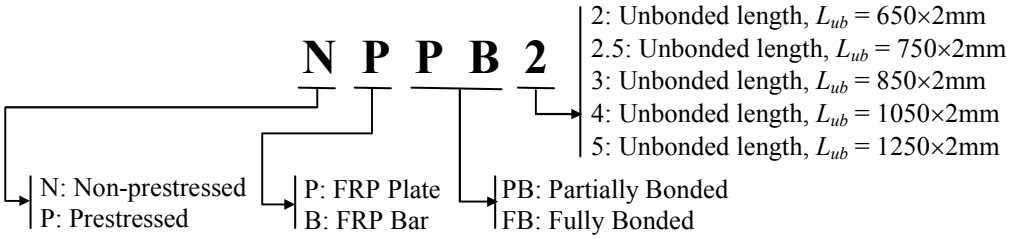

Based on the beam configuration selected, the balanced unbonded length for non-prestressed CFRP was estimated to be approximately 650 mm as calculated in Section 3.2.5. Therefore, a lower bound for the unbonded length of 650 mm was selected to maximize partial unbonding effect, while the other longer unbonded lengths were selected to investigate the effect of the unbonded length on the

behaviour of the beams. For the prestressed CFRP strengthened beams (Group III, IV), the same amount of CFRP reinforcement and unbonded lengths as the non-prestressed CFRP were applied for comparison purposes. The prestressing levels for Group III and Group IV beams are selected to be 40% and 60% of the CFRP tensile strength based on the specified values, respectively, considering that prestressing work is normally performed with the prestressing levels of 40% to 60% in the existing prestressed FRP concrete beams.

4.3 Fabrication of RC T-beams

The basic shape and dimensions of the RC T-beams are shown in Figure 4-1. The basic beam geometry is height of 300 mm, flange thickness of 50 mm, web width of 150 mm, and flange width of 400 mm. The T-shape cross section was selected because this shape typically represents integrated beam-slab construction.

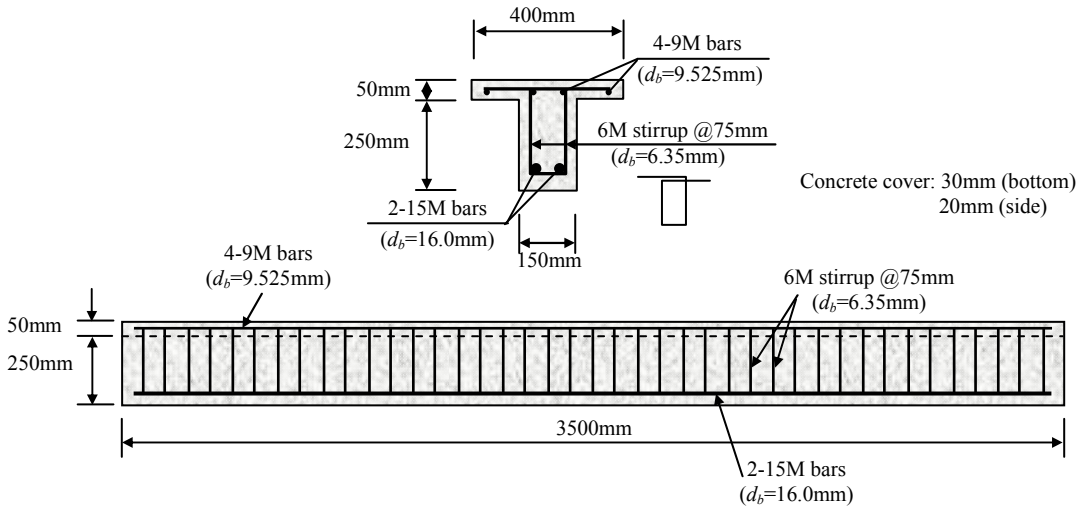

Figure 4-1 Beam geometry and reinforcement details

The bottom tension reinforcement consisted of two 15M deformed steel bars. The area of bottom reinforcement was selected as a similar reinforcement ratio to the field construction ($\rho = A_s / b_w \cdot d_s$ = 0.0105, ρ_{min} = 0.00362, ρ_{max} = 0.0788). Shear reinforcement consisted of double-legged T-shaped

steel stirrups with a nominal diameter of 6.35 mm. The stirrups were uniformly spaced at 75 mm, centre to centre, to avoid shear failure. The tension test of reinforcing steel bars was performed and their engineering properties were reported in Section 4.5.

Figure 4-2 shows the construction procedure for the RC T-beams following typical construction practice. The strain gages mounted on the reinforcing steel bars were coated with wax to provide protection from damage during concrete casting (Figure 4-2(a)). All of the cages were placed inside wooden formwork (Figure 4-2(b) and (c)). Plastic spacers were placed underneath the steel reinforcement at several points to provide the desired clear cover (30 mm) at the bottom of the beams. Ready-mixed concrete was used with a specified compressive strength of 35 MPa (Figure 4-2(d)). The concrete slump was 95 mm at the time of casting. After casting the concrete, the beams were moist cured for 7 days, followed by 21 days of curing in air (Figure 4-2(e) and (f)). A total of 30 cylinders were made for the concrete compressive strength test according to CSA A23.2 (2004).

(a) Strain gage installed (b) Steel cage constructed (c) Wooden forms and cages

(d) Concrete casting (e) 7 days moisture curing (f) Stripping

Figure 4-2 Construction process of RC T-beams

4.4 Strengthening of RC T-beams with CFRP

4.4.1 General

After 28 days of curing, four beams were strengthened with externally bonded CFRP plates (Group I), five beams were strengthened with near-surface-mounted CFRP bars (Group II), and the other seven beams were strengthened with prestressed NSM system (Group III and IV).

One 1.2mm×30mm CFRP plate (Sika® CarboDur® - Sika Canada Inc.) was used for Group I beams, while one 7.9 mm diameter CFRP bar (Leadline® – Mitsubishi Chemical Functional Products, Inc.) was used for Group II, III, and IV beams. The CFRP bars used in the experimental program were selected to have a similar axial stiffness (E_fA_f) to the CFRP plate for comparison purposes between two groups. Material properties of the CFRP plates and bars provided by manufacturers are summarized in Table 4-2. The material test for both the CFRP plate and the CFRP bar was carried out to obtain actual properties (see Section 4.5).

Table 4-2 CFRP material properties (provided by manufacturers)

Type of CFRP	Dimensions (mm)	Nominal Area (mm^2)	Elastic modulus (GPa)	Ultimate tensile strength (MPa)	Ultimate tensile strain	Axial stiffness (E_fA_f) (kN)
Plate	1.2×30	36.0	165	2,800	0.0169	5940
Bar	7.9 (diameter)	46.1	147	2,400	0.0163	6777

Commercially available epoxy adhesive (Sikadur® 30– Sika Canada Inc.) was used for bonding the CFRP plates and bars to the concrete. The maximum tensile strength of the Sikadur® 30 adhesive is 24.8MPa, Modulus of elasticity is 4.5GPa, and compressive strength 59.3MPa at 7days at 23°C based on the data provided by manufacturer.

4.4.2 Non-prestressed EB system (Group I)

Figure 4-3 shows the strengthening scheme of the beams with EB CFRP plate and the detailed configuration of the strengthened section. The beam was strengthened with one CFRP plate (30×1.2×3200 mm) by bonding it to the concrete tensile surface using the epoxy adhesive. The epoxy adhesive was applied to the entire concrete surface even in the partially bonded beams to remove the gap between the CFRP plate and the concrete. This is based on the results of the FE analysis in Section 3.3. For the partially bonded beams, a thin plastic sheet was used to make the unbonded region in the mid-span as shown in Figure 4-3. CFRP U-wraps were used at the end of the plate and at the bonded point, as shown in Figure 4-3, where the bond stress is concentrated (see Section 3.3), to prevent or delay the premature debonding failure.

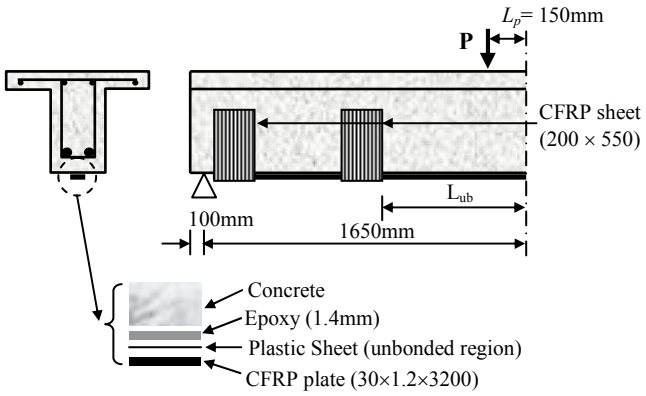

Figure 4-3 Detailed configuration of the EB CFRP strengthening system

The detailed strengthening procedure for a concrete beam with CFRP plate is shown in Figure 4-4. First, the bottom surface of the concrete beams was prepared by sandblasting to provide a rough surface to improve bond capacity (Figure 4-4(a)). The surface was cleaned by washing and air-brushing to remove dust or debris and fine particles (Figure 4-4(b)). A uniform 1.5 mm thin layer of the epoxy adhesive was applied by putty knife to both the bottom surface of the concrete and the CFRP plate (Figure 4-4(c), (d)). The measured thickness of the adhesive was 1.4 mm after curing.

The CFRP plate was placed in position on the concrete surface and pressed onto the epoxy using a hard rubber roller until the epoxy was forced out on both sides. To ensure a good bond with concrete, a uniform pressure should be applied along the entire length of the plates (Figure 4-4(e)). Strengthening of RC beams with EB CFRP plate was completed by cleaning the excessive epoxy (Figure 4-4(f)).

(a) Sandblasting (b) Cleaning the surface (c) Applying the epoxy

(d) Applying the epoxy (e) Pressing with rube roller (f) Removing the excessive epoxy

Figure 4-4 Procedure for EB CFRP plate installation

After 7 days curing of the adhesive, U-shaped CFRP sheets with 200 mm width were placed around the web of the concrete beams at both ends of fully bonded and partially bonded beams. For the partially bonded specimens, additional transverse CFRP sheets were installed at the bonded point in order to reduce the concentrated bonded stress in this area. Figure 4-5 shows the detailed procedure for installing the CFRP sheets. First, the epoxy adhesive (Sikadur® 330 for sheets – Sika Canada Inc.) was applied to the concrete surface and the CFRP sheet was placed in position and pressed with a

roller as shown in Figure 4-5(a) and (b). Additional epoxy was applied and pressed with a rubber plate and the excessive adhesive was removed and cleaned (Figure 4-5(c) and (d)).

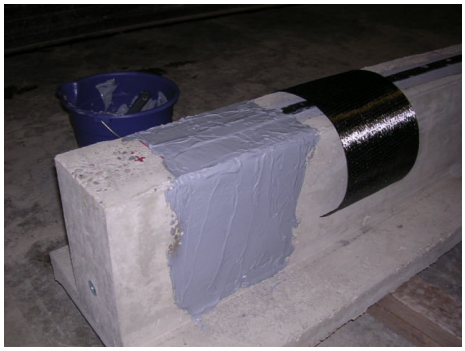

(a) Applying the epoxy (1.0 mm thick)

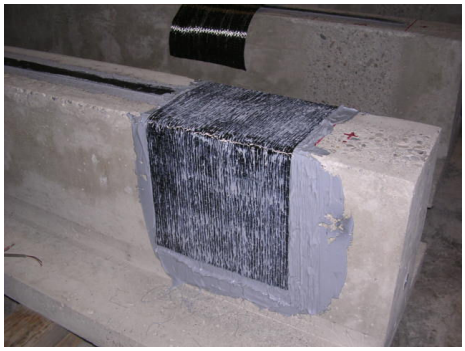

(b) Applying the CFRP sheet and press with roller

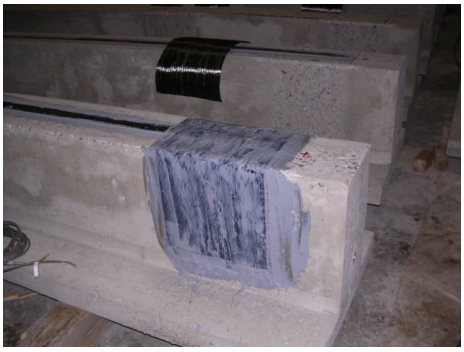

(c) Applying additional epoxy (0.5 mm thick)

(d) Cleaning the excessive epoxy with putty knife

Figure 4-5 Procedure for CFRP sheet installation

4.4.3 Non-prestressed NSM system (Group II)

Figure 4-6 shows the general procedure for NSM CFRP strengthening and detailed dimensions of the NSM grooves. The beam was strengthened with one CFRP bar (7.9 mm diameter) inserted into a NSM groove made in the concrete tensile surface and bonded using the epoxy adhesive. For the partially bonded beams, a thin plastic tube (9.525 mm diameter) was used to make the unbonded region in the mid-span as shown in Figure 4-6. The epoxy adhesive was applied to the entire concrete surface even in the partially bonded beams to maintain the location of the bar under loading.

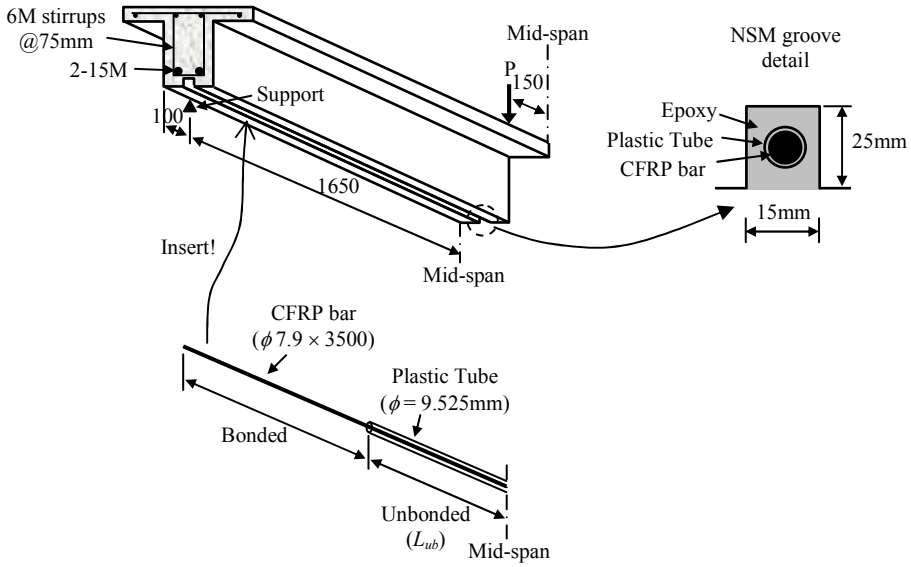

Figure 4-6 Detailed configuration of the NSM CFRP strengthening system

Installation of the NSM CFRP reinforcing bars begins by making the specified grooves in the concrete cover on the tension surface of the beams. A special concrete saw with a diamond blade was used to cut the grooves. Figure 4-7 shows the groove making procedure.

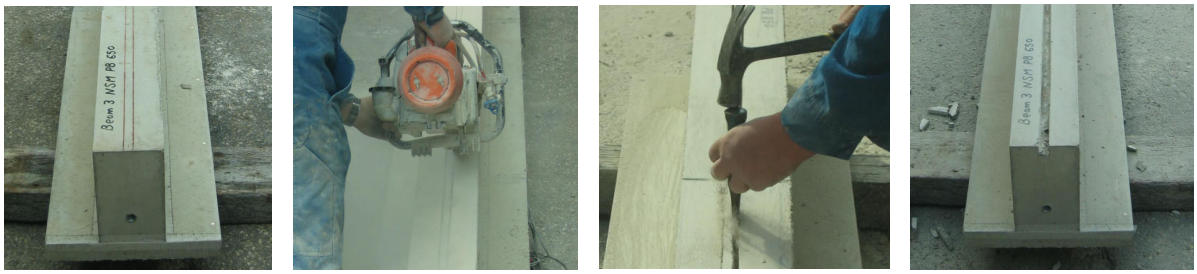

(a) Drawing cut lines (b) Cutting the groove (c) Chipping the concrete (d) Finished NSM groove

Figure 4-7 Process of making NSM groove

The groove size was selected to be approximately 15 mm wide and 25 mm deep for 7.9 mm CFRP bars, as shown in Figure 4-6. Based on current research by Lorenzis and Nanni (2002) and Hassan and Rizkalla (2004), larger groove sizes produce larger bond strength than smaller groove sizes. On

the other hand, the depth of the groove is limited by the bottom steel reinforcement, and the width should not be excessive to limit construction cost.

Figure 4-8 shows the detailed procedure for installation of the CFRP bars. First, the grooves were cleaned and compressed air was used to remove debris and fine particles to ensure proper bond between the epoxy adhesive and the concrete (Figure 4-8(a)). The epoxy adhesive was then applied into the groove before inserting the CFRP bars. Each groove was half-filled with the epoxy adhesive. The CFRP reinforcing bar was inserted in the groove and lightly pressed to displace the epoxy (Figure 4-8(b)). The groove was then filled with more paste and the surface was leveled (Figure 4-8(c), (d)). The excessive adhesive was removed with a putty knife. The epoxy adhesive was cured for 7 days.

(a) Cleaning the groove (b) Installing the CFRP (c) Filling the epoxy (d) Leveling and cleaning

Figure 4-8 Procedure for NSM CFRP bar installation

4.4.4 Prestressed NSM system (Group III and IV)

A self-anchored prestressing system considering field applications was applied to strengthen the concrete T-beams as shown in Figure 4-9. The live end consists of a steel frame, two clamp anchors, one hydraulic jack, and one screw adjustor (Figure 4-9(b)), while the dead end consists of a steel reaction plate and a clamp anchor (Figure 4-9(c)). A steel clamp anchor was developed at the University of Waterloo (Al-Mayah 2004) and modified to fit the Leadline CFRP bar. Load cells were installed at both ends to measure the prestressing force during prestressing and releasing.

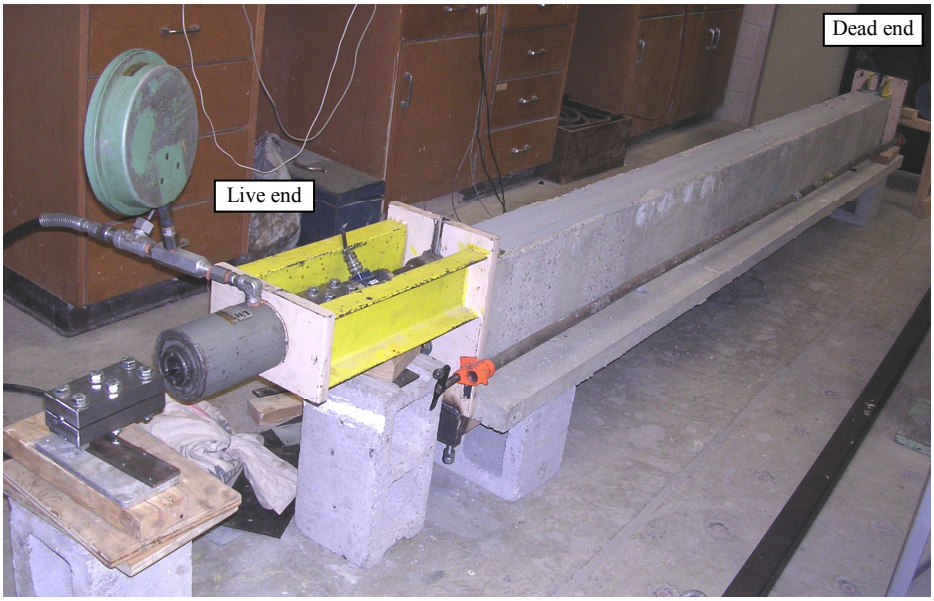

(a) Prestressing setup

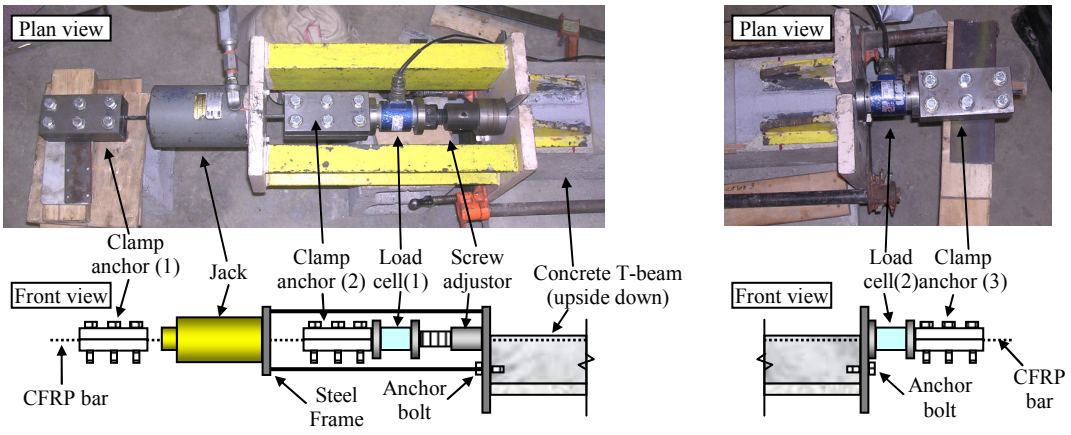

(b) Live end (c) Dead end

Figure 4-9 Self-anchored prestressing setup

The beam was positioned upside down to facilitate the prestressing procedure (see Figure 4-9(a)). A steel frame prestressing assembly was attached to the concrete T-beam using an anchor bolt as shown in Figure 4-9(b) and (c), and a CFRP bar was inserted to be prestressed. A prestressing force was applied using a hydraulic jack with a capacity of 30-Ton and a 75 mm stroke. As the hydraulic jack pushed clamp anchor (1), the CFRP bar was tensioned and the compressive prestressing force

was applied to the beam. Once the desired force was reached, the prestressing force acting on the clamp anchor (1) was transferred to clamp anchor (2) by releasing the jacking force after locking the prestressing force using a screw adjustor. Epoxy adhesive was filled halfway in the groove before inserting the CFRP bar. After inserting the bar and applying the prestressing force, the epoxy adhesive was completely filled in the groove. The epoxy adhesive was cured for 7 days. The prestressing procedure to make the NSM prestressed beam is shown in Figure 4-10.

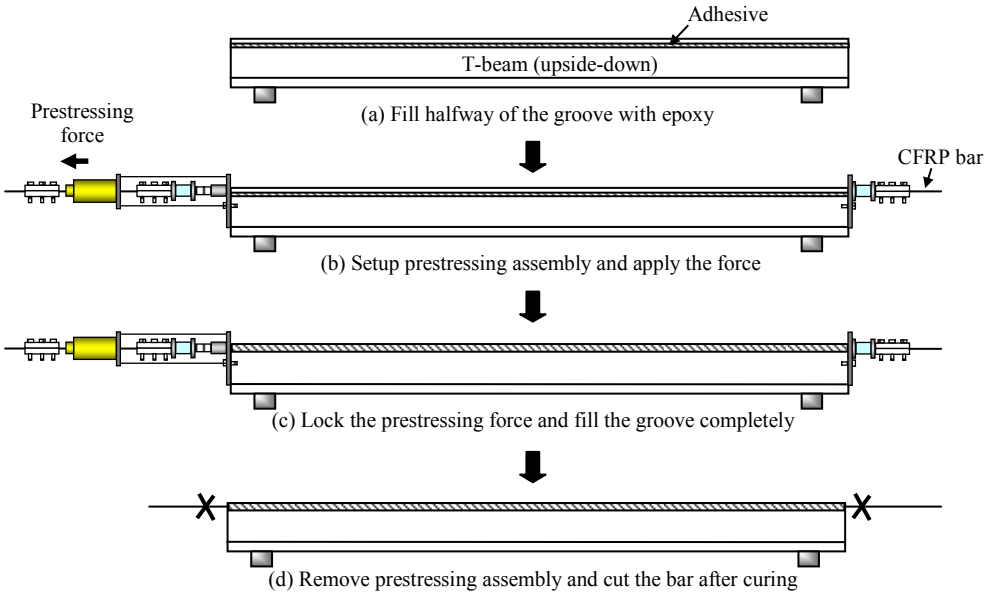

Figure 4-10 Prestressing procedure for prestressed NSM system

The prestressing forces at both ends were measured during the 7 days after applying the epoxy adhesive to investigate the loss of the prestressing force. A typical prestressing force versus time diagram was plotted in Figure 4-11(a), which shows that the prestressing loss was very small during curing process and the prestressing loss was less than 1% of the initial prestressing force after transfer regardless of the prestressing level. The prestressing loss diagrams for other prestressed beams are shown in Appendix B. Figure 4-11(b) shows the CFRP strain distribution at mid-span during curing. There was almost no change in the CFRP strain after releasing the prestressing force.

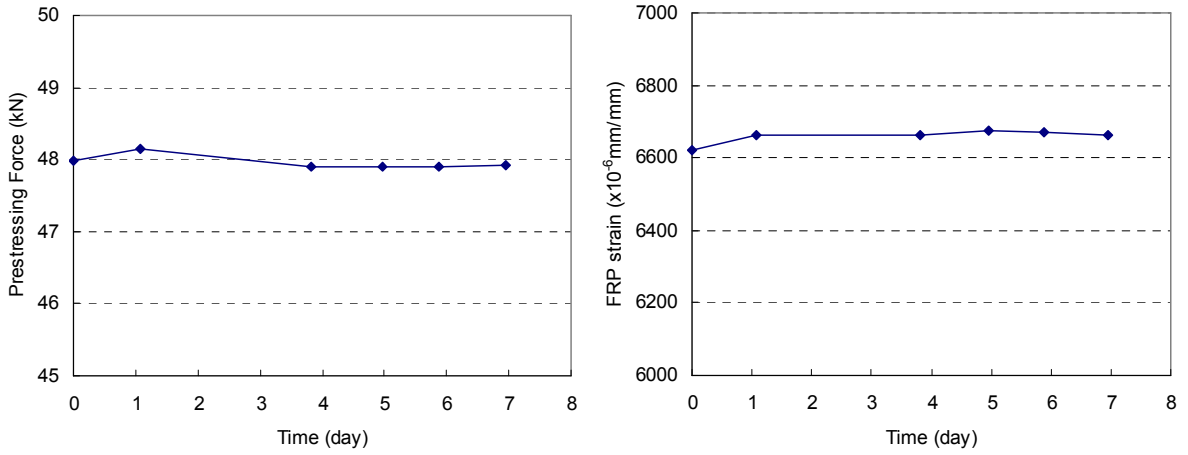

(a) Prestressing loss during curing (b) CFRP strain distribution at mid-span with time

Figure 4-11 Prestressing force and CFRP strain diagrams with time (beam PBFB)

The prestressing force was completely released after 7 days by loosening the bolts of the clamp anchors. To prevent the sudden release of the prestressing force which may cause bond cracking at the end of the beam, a gradual release was carried out by loosening and re-fastening the bolts repeatedly. Figure 4-12 shows the gradual release of the prestressing force with time. A gradual release improves the bond strength and decreases the transfer length in the prestressed strengthened beam (Badawi 2007).

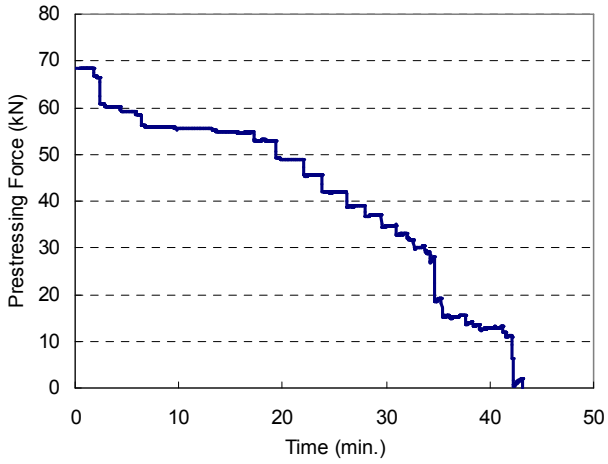

Figure 4-12 Gradual release of the prestressing force (beam PBPB4-60)

4.5 Material Properties

The materials used in the experiments are concrete, steel reinforcement, CFRP plate, and CFRP bar. In this section, their engineering properties are reported.

4.5.1 Concrete

Concrete compression testing was carried out based on CSA A23.2 (2004) at 7 days, 14 days, 28 days of curing, and at the time of testing. Three cylinders were tested each time and the average strength was calculated. Figure 4-13 shows the average concrete cylinder strength with time.

The average compressive strength was 52.6MPa at 28days and 52.5 ~ 52.7MPa at the time of testing. A concrete compressive strength of 52.5MPa was used for the analysis of the beam. The flexural tensile strength of concrete was estimated using the equation of $f_r = 0.6\sqrt{f_c'}$ from CSA A23-3 standard (2004). The calculated value of concrete tensile strength was 4.35MPa.

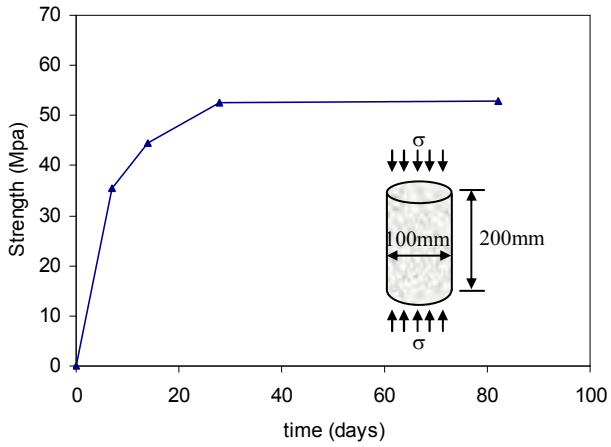

Figure 4-13 Concrete compressive strength with time

4.5.2 Steel reinforcement

Four 15M deformed steel bars were tested based on ASTM A370 (2007). An extensometer with 50 mm gage length was installed to measure the strains. The test setup and the ruptured steel bar are shown in Figure 4-14. The extensometer was removed before failure to prevent possible damage from the sudden rupture. The ultimate strain at rupture was calculated by measuring the final elongation

between two points marked on the bar. The average yield strength and ultimate strength was 473MPa and 618MPa, respectively. The average ultimate strain at rupture was 0.173 (17.3%).

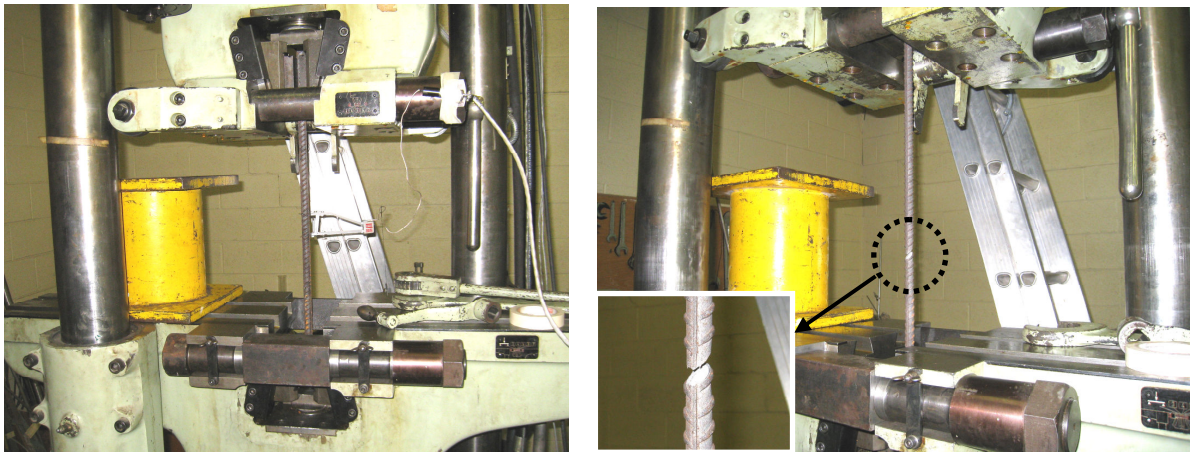

(a) Test setup of steel bar (b) Rupture of steel bar

Figure 4-14 Test setup and failure mode of M15 steel bar

The stress-strain curve of one of the tested bars is shown in Figure 4-15. Steel yielding and strain hardening were clearly observed. For the nonlinear FE analysis (Section 5.4) and the advanced analytical model (Section 6.3), a tri-linear elastic-plastic constitutive model was assumed to represent the strain hardening effect with the yielding strength of 460MPa and the modulus of elasticity at the hardening part is assumed to be 2GPa, as shown in Figure 4-15.

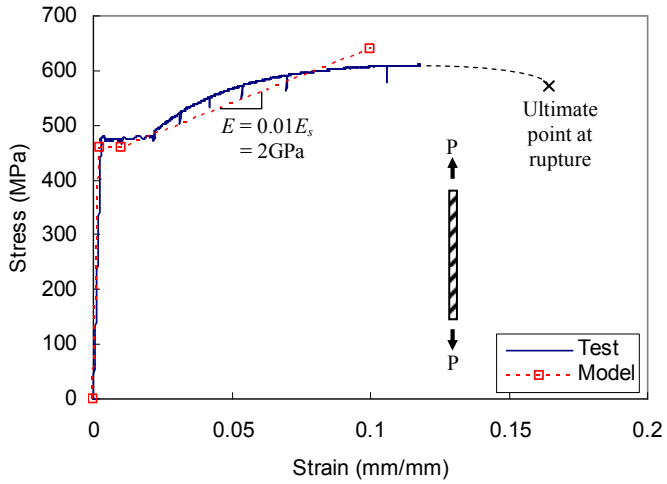

Figure 4-15 Stress-strain curve of steel reinforcement

4.5.3 CFRP plate

A tension test of the CFRP plate was carried out based on CSA S806 (2007). Five specimens were prepared with a length of 280 mm, width of 15 mm, and thickness of 1.2 mm. Steel tabs (thickness of 1.2mm) were sandblasted and bonded to both ends of the specimen with epoxy adhesive. An extensometer with 50 mm gage length was installed to measure the CFRP strains. The test setup and failure mode of CFRP plate are shown in Figure 4-16. The failure was very explosive, as shown in Figure 4-16(b). The average ultimate tensile strength and elastic modulus of CFRP plate was 3415MPa and 170GPa, respectively. These values are 22% and 3% higher than the strength and elastic modulus provided by manufacturer (2800MPa and 165GPa), respectively.

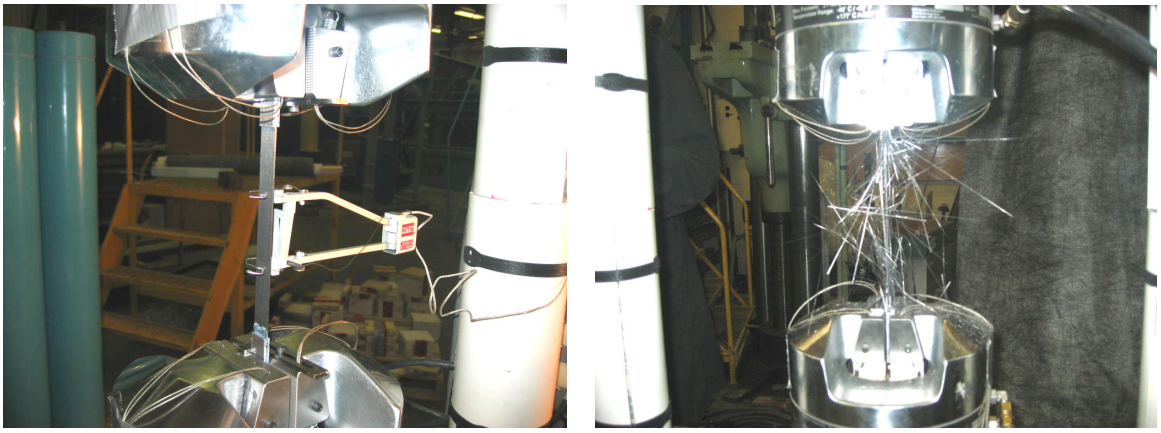

(a) CFRP plate test setup (b) Failure mode of CFRP plate

Figure 4-16 CFRP plate test setup and failure mode

4.5.4 CFRP bar

A tension test of five CFRP bars was carried out using wedge anchors at both ends of the bar, as shown in Figure 4-17(a). The use of wedge anchors is not a standard way based on CSA S806 (2007), but can easily be applied to the tension test to measure the material properties. A strain gage (5mm gage length) was installed on the bar to measure the strains. The average ultimate tensile strength and elastic modulus of the CFRP bar were 2134MPa and 160GPa, respectively. However, the ultimate

strength of the CFRP bar appears to be small and invalid considering that the guaranteed strength provided by manufacturer is 2400MPa. This is because equipment setup (use of wedge anchors) did not follow standard, so complete explosive failure did not happen and the failure was initiated from the wedge anchors as shown in Figure 4-17(b).

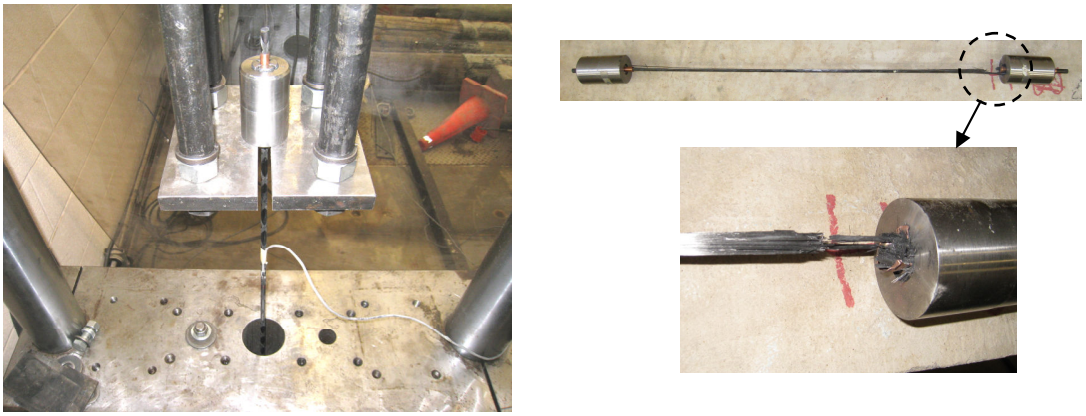

(a) CFRP bar test setup (b) Failure mode of CFRP bar

Figure 4-17 Test setup and failure mode of CFRP bar

Applied loads and CFRP strains were also measured during prestressing work for prestressed NSM beams as described in Section 4.4.4. From these data, the elastic modulus of CFRP bar was calculated to be 155~158GPa, which is similar to the value obtained from the tension test. Since the ultimate strength from the tension test was not valid due to an improper failure mode, the ultimate strength was estimated from the beam test results. The ultimate CFRP strains obtained from the tested beams that failed by CFRP rupture were 0.0183~0.0188. From this value, the ultimate tensile strength is calculated to be 2836~2970MPa, which is approximately 21% higher than the values provided by manufacturer (2400MPa). This is similar to the behaviour of the CFRP plate that showed 22% higher strength than the specified value. For the analysis of the beams, an ultimate strength of 2800MPa and an elastic modulus of 155GPa were used.

4.6 Test Setup and Instrumentation

The testing frame and the test setup are shown in Figure 4-18. All of the beams were tested to failure in a four point bending using a Servo-controlled hydraulic actuator of 155 kN (35 kips) capacity. The rate of loading was 1.0 mm/min in a stroke-control mode.

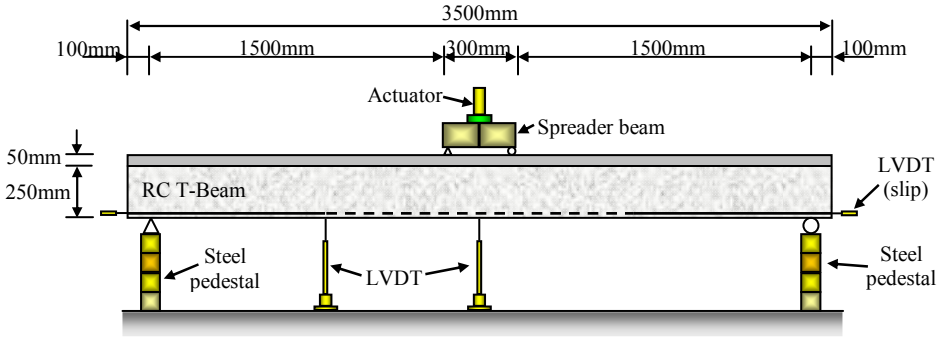

Figure 4-18 Test setup

Two linear variable differential transducers (LVDTs) were used to measure the deflection at mid-span and at the bonded point and two LVDTs were installed at the ends of the CFRP plate and the CFRP bar in order to measure the end slip of the CFRP (relative displacement between the CFRP and

the concrete) during testing as shown in Figure 4-18. The detailed configuration of the LVDTs for slip measurement are shown in Figure 4-19

(a) Group I beams (b) Group II, III, IV beams

Figure 4-19 Slip measurement device at the end of the CFRP

Figure 4-20 shows the location of the strains in concrete, steel reinforcement, and CFRP reinforcement during testing. 5 mm strain gages (120Ω, gage factor: 2.11) were used for the measurement of strains in steel and CFRP reinforcement while 60 mm strain gages (120Ω, gage factor: 2.09) were used for concrete. For the partially bonded beams, strain gages were installed at the mid-span of the beam and on either side of the transition point (transition between unbonded and bonded zone) as shown in Figure 4-20. Two strain gages were used at each location for measuring the strains in steel and concrete. For the fully bonded beams, strain gages were installed at the same location as the partially bonded beam with unbonded length of 650 mm for comparison purposes.

The data were automatically collected using a National Instrument SCXI data acquisition system. The location of cracks and their propagation was clearly marked on concrete surface at load increments of 10 kN.

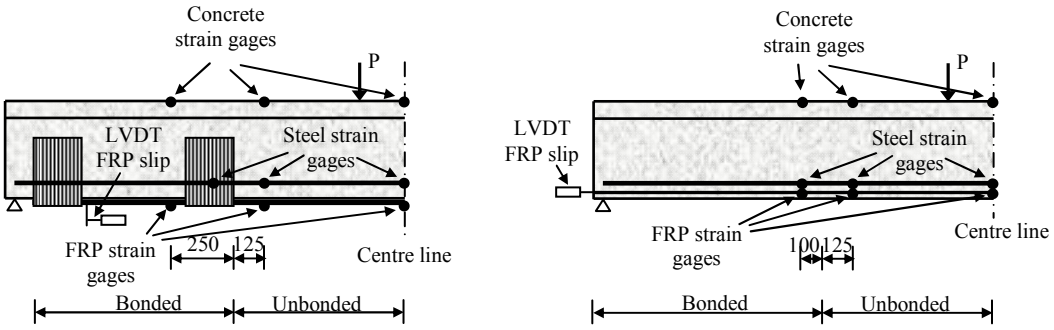

(a) Group I beams (b) Group II, III, IV beams

Figure 4-20 Location of the strain gages

Chapter 5
Non-prestressed EB Strengthened Beams

5.1 General

The test results and discussion for the non-prestressed EB partially bonded CFRP strengthened beams (Group I) are presented in this chapter. Failure modes and load-deflection behaviour of the beams are discussed in Section 5.2. Comparison studies between analytical predictions and experimental results are performed in Section 5.3. A nonlinear finite element (FE) analysis is presented to investigate the premature debonding failure of the beams in Section 5.4.

5.2 Test Results and Discussions

The test results for the non-prestressed EB CFRP strengthened beams in terms of applied load and deflection at cracking, at steel yielding, and at ultimate state are summarized in Table 5-1, along with a description of the failure mode.

Table 5-1 Summary of non-prestressed EB strengthened beam (Group I) test results

Test Group	Beam Name	P_{cr} (kN)	Δ_{cr} (mm)	P_y (kN)	Δ_y (mm)	P_u (kN)	Δ_u (mm)	Deform-ability, μ (Δ_u / Δ_y)	Failure mode*
-	Control	13.37	0.69	68.13	14.03	79.39	108.70	7.75	CC
Group I	NPFB	14.10	0.79	74.01	16.26	83.90	28.30	1.74	FD
	NPPB2	15.24	0.77	71.59	15.01	97.58	58.01	3.86	FD+FR
	NPPB3	14.26	0.69	67.33	13.78	86.80	42.34	3.07	FD+FR
	NPPB4	13.99	1.00	68.61	16.62	82.12	38.89	2.33	FD+FR

* CC: Concrete Crushing, FD: FRP Debonding, FR: FRP Rupture

5.2.1 Failure modes and load-deflection behaviour

Figure 5-1 shows the failure modes of the fully bonded beam (NPFB) and the partially bonded beams (NPPB2, NPPB3, and NPPB4). All four strengthened beams failed by FRP debonding, and the failure

of the three partially bonded beams was accompanied by FRP rupture near the bonded point as shown in Figure 5-1.

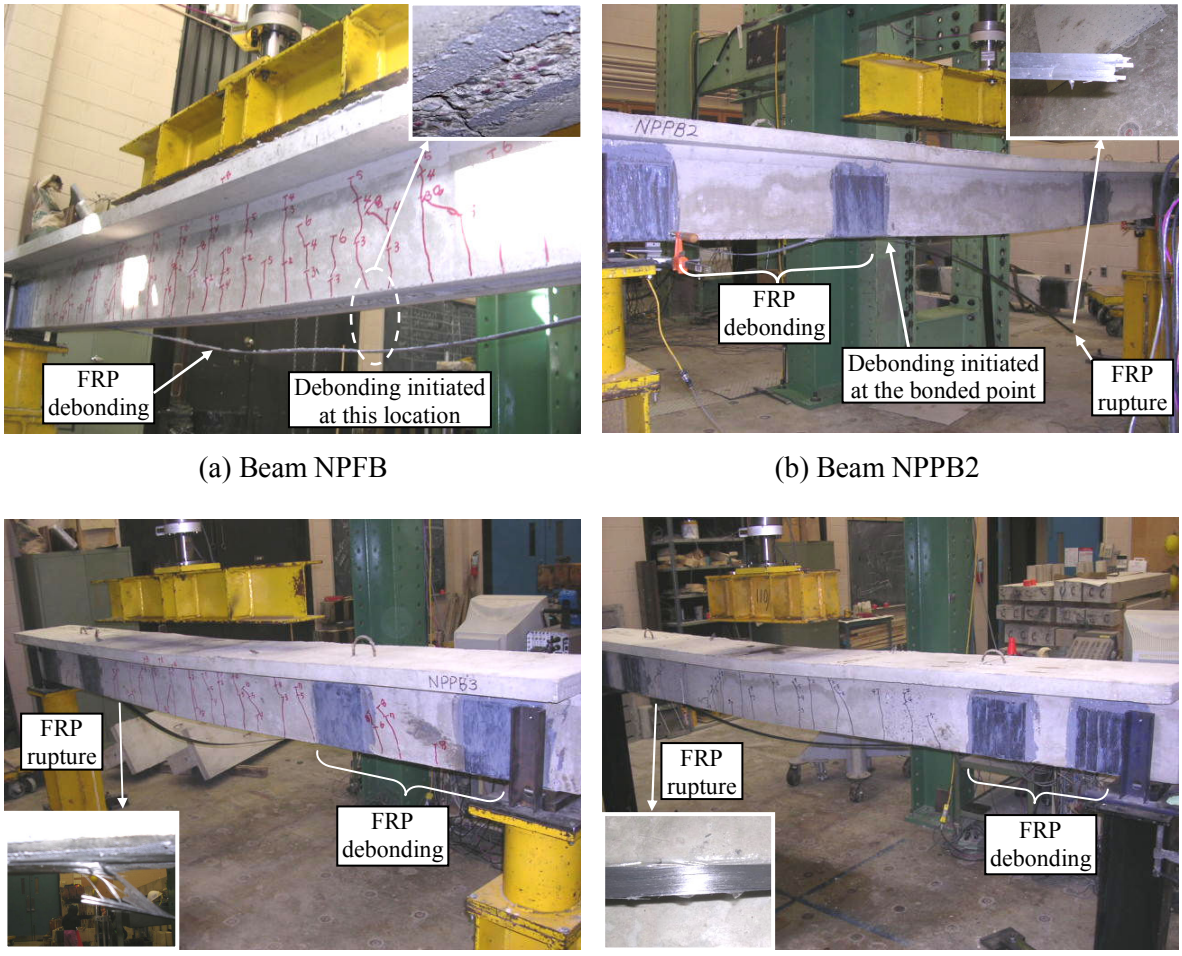

(a) Beam NPFB (b) Beam NPPB2

(c) Beam NPPB3 (d) Beam NPPB4

Figure 5-1 Failure modes of EB strengthened beams (Group I)

For the fully bonded beam (NPFB), debonding was initiated from one of the flexural cracks near the loading point. This crack propagated to the beam end along the interfacial layer, followed by sudden complete debonding as shown in Figure 5-1(a) accompanied by a big sound. This debonding failure is a typical flexural crack induced debonding failure where the interfacial shear stress is concentrated at the tip of the flexural cracks inducing debonding failure, as described in Section 2.4.3. Failure occurred along the epoxy-concrete interface which is the weakest part of the system. The

concrete surface of the epoxy-concrete interface after debonding failure is shown in the enlarged figure of Figure 5-1(a). In contrast, for the partially bonded beams, this typical flexural crack-induced debonding was avoided and debonding failure at the bonded point was delayed with more deflection and greater applied load. This is because the FRP is intentionally unbonded at mid-span and the U-wraps at the bonded point increase the bond strength. The debonding failure occurred simultaneously with FRP rupture at the opposite bonded point as shown in Figure 5-1(b), (c) and (d). This rupture was caused by the impact energy released from sudden debonding. Complete FRP rupture happened in beam NPPB2 (Figure 5-1(b)) and this rupture intensity was decreased as the unbonded length increased as shown in Figure 5-1(c) and (d). This is because the released elastic energy from CFRP debonding failure was decreased as the unbonded length increased (CFRP elastic strain at the time of debonding was less as the unbonded length is increased).

Figure 5-2 shows the load deflection diagrams for the Group I beams. The behaviour up to cracking is almost identical without regard to the bond condition. The applied load level corresponding to steel yielding was slightly higher in the fully bonded beam compared to the partially bonded beams, but the stiffness of the beam (slope of load-deflection diagram) up to steel yielding was almost identical between the strengthened beams. The flexural stiffness of the beam is determined by the geometry of the beam and the axial stiffness (EA) of the steel and the FRP reinforcement. The stiffness, and thus the behaviour, of the beam up to steel yielding was mainly governed by the axial stiffness of the steel reinforcement. This is because the area of the FRP reinforcement is only one-tenth that of the steel reinforcement in the beams. As well, the elastic modulus of the FRP plate is approximately 85% of the steel elastic modulus. Since the strains in the FRP and the steel are similar in magnitude prior to steel yielding (≤ 0.002) regardless of the FRP bonded length, the flexural behaviour of the beam is dominated by the higher axial stiffness of the steel and the load-deflection behaviour of the strengthened beams is almost identical without regard to the FRP bond condition.

On the other hand, the rate of increase in the FRP strain is decreased as the unbonded length is increased because the FRP strain is distributed within the unbonded length. As a result, the applied load at steel reinforcement yielding was slightly higher in the fully bonded beam compared to the partially bonded beams.

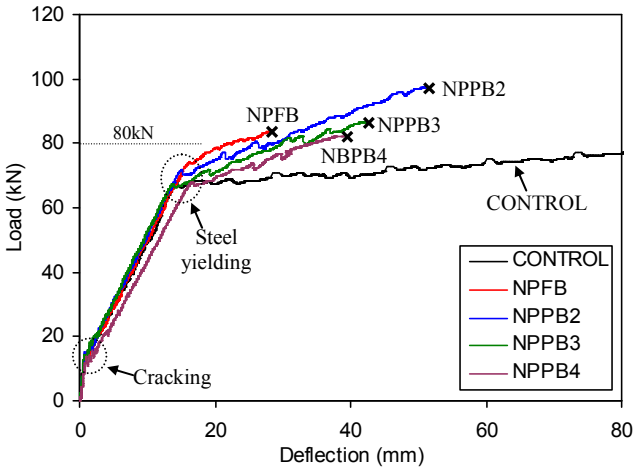

Figure 5-2 Load-deflection diagram of the beams (Group I)

The points marked "x" in Figure 5-2 denote the ultimate points at which the premature debonding failure occurred. The ultimate deflection and the ultimate load were improved in the partially bonded beams compared to the fully bonded beams (except the ultimate load of beam NPPB4) due to the avoidance of the flexural crack induced debonding that occurred in the fully bonded beam as described earlier. The ultimate load and deflection of NPPB2 were improved by 16% and 105%, respectively, compared to the fully bonded beam. Beam NPPB3 also showed improvement of the ultimate load and deflection of 3% and 50%, respectively compared to beam NPFB. On the other hand, beam NPPB4 showed an ultimate deflection improvement of 37%, but the ultimate load carrying capacity was decreased by 2% compared to the fully bonded beam (NPFB). This is because the bonded length (anchorage length) of beam NPPB4 was only 550mm at each end, apparently inducing a debonding failure at a lower applied load. It is also notable that the ultimate capacity

among partially bonded beams was decreased as the unbonded length was increased. This is because decreased bonded or anchorage length induced earlier debonding failure at the bonded point. If the deformability index, μ, is defined by the ratio of the ultimate deflection (Δ_u) to the deflection at steel yielding (Δ_y), then the indices are 1.74, 3.86, 3.07, and 2.33 in the NPFB, NPPB2, NPPB3, and NPPB4 beams, respectively.

The stiffness of the beams (the slope of load-deflection diagram) at the post yielding stage (from steel reinforcement yielding to failure) was slightly decreased as the unbonded length is increased. The stiffness reduction was not clearly visible in the load-deflection diagrams due to early debonding failure of all beams, but this reduction was remarkable in the NSM strengthened beams (see load-deflection diagrams in Figure 6-2 and Figure 7-2). Once the steel reinforcement yields the load-deflection response is mainly governed by the axial stiffness of the FRP reinforcement since the axial stiffness of the steel reinforcement is negligible due to yielding. In addition, the unbonded length of the FRP affects the stiffness of the beam after steel yielding; the beam stiffness is decreased as the unbonded length is increased. For a given load level or moment, the total tension force resultant (steel plus FRP) is approximately constant regardless of unbonded length. After steel yielding, the force in the steel remains essentially constant, indicating that increases in applied load correspond to increases in the force (strain) in the FRP. The FRP strain is constant within the unbonded length and represents the average concrete strain at the level of the FRP within the unbonded length. Thus, as the unbonded length increases, the maximum strains in the concrete must increase to sustain the same uniform strain in the FRP for a given load level. This produces increased curvature of the section as the unbonded length increases, and corresponds to a decrease in the flexural stiffness of the beam.

Since the occurrence of a debonding failure is undesirable, most design guidelines place a limit on the maximum FRP strain at the strength limit state to avoid debonding failure as described in Section 2.4.4. For example, ACI 440.2R (2008) applies the debonding strain, ε_{fd}, that limits the maximum

FRP strain depending on the concrete strength and the FRP stiffness (see Equation in Section 2.4.4). Based on the properties of the FRP plate used, the debonding strain, ε_{fd}, is calculated to be 0.00668 (39.5% of ε_{frpu}). If the capacity of the strengthened beam is defined by this strain limit, the corresponding maximum applied load for the test beams was determined to be approximately 80kN regardless of the unbonded length because the total tensile force resultant (steel plus FRP) must be almost identical as discussed earlier. Corresponding deflections at this strain limit ($\Delta_{u,ACI}$) can be found from Figure 5-2 to be 21.7mm, 25.5mm, 29.9mm, and 34.7mm in the NPFB, NPPB2, NPPB3, and NPPB4 beams, respectively. The deformability indices corresponding to these limited deflections are calculated to be 1.33, 1.70, 2.17, and 2.08 in the same order. This shows an improvement of the deformability for partially bonded FRP strengthened beams without reduction of the ultimate load carrying capacity based on the limited FRP strain.

5.2.2 Strain distribution

The strain gages were installed at three locations along the beam length to investigate the strain distributions of the FRP, steel reinforcement, and concrete top flange. Detailed locations of strain gages can be found in Section 4.6. In this section, strain distributions and comparisons between fully bonded and partially bonded beams are discussed.

5.2.2.1 FRP strain distribution

The variation of FRP strains with applied load in the Group I beams is shown in Figure 5-3. The FRP strains of beam NPFB increased for strain gages that were closer to the mid-span (gage 1 > gage 2 > gage 3) for a given applied load as shown in Figure 5-3(a). This is because the FRP was fully bonded along the beam length and strains were proportional to the moment at that section. After steel yielding at mid-span, the increase rate of strain at gage 1 was faster, as shown in Figure 5-3(a), since the force in the steel reinforcement increased very slow due to yielding. On the other hand, the FRP strains at

gage 1 and gage 2 of the partially bonded beams are almost identical, as shown in Figure 5-3(b), (c) and (d), because these gages were installed within the unbonded length.

The strains measured at gage 3 location, within the bonded region, were decreased as the unbonded length of the partially bonded beams increased because the gage location became closer to the support (see Figure 5-3(b), (c) and (d)). When comparing the strains at gage 3 location between the fully bonded beam (NPFB) and the partially bonded beam with the unbonded length of 650 mm (NPPB2), the values were almost the same at load levels beyond cracking because the gages were installed at the same location within the bonded region (see Figure 5-3(a) and (b)).

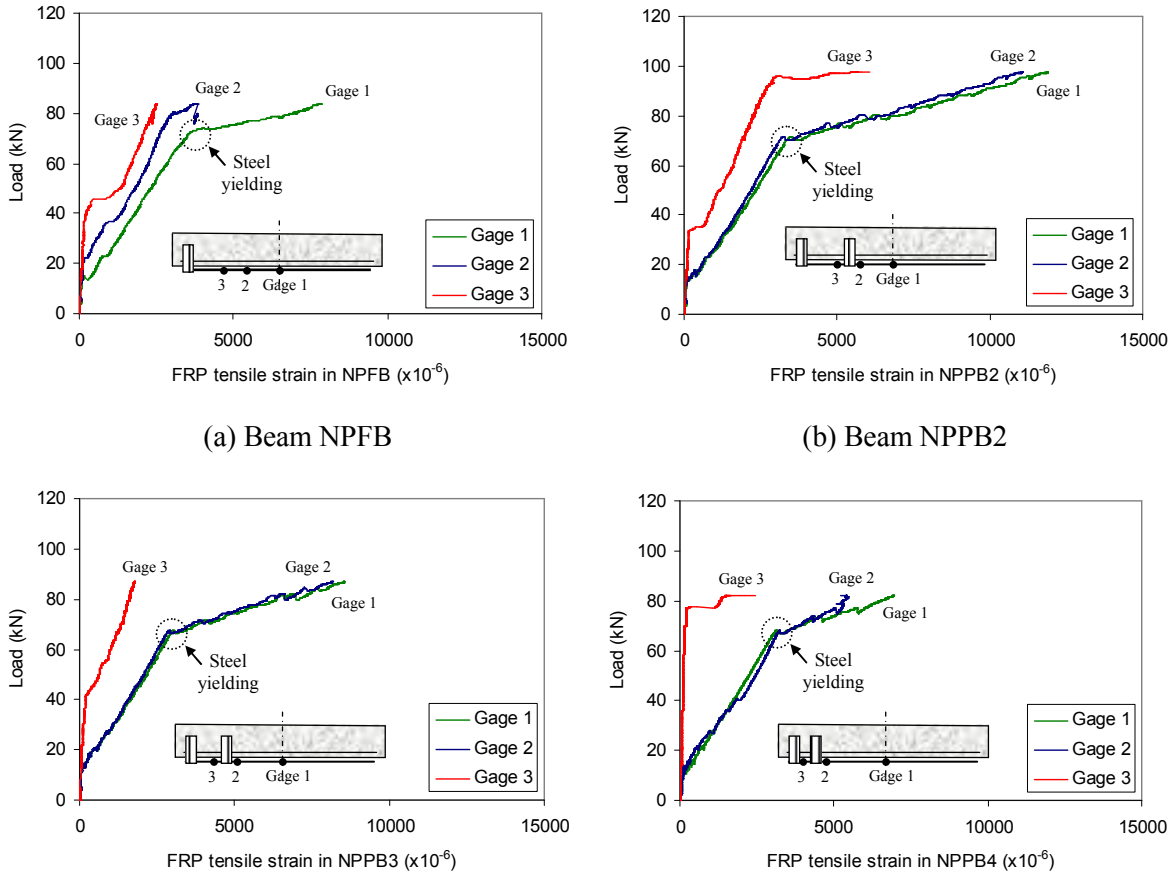

(a) Beam NPFB

(b) Beam NPPB2

(c) Beam NPPB3

(d) Beam NPPB4

Figure 5-3 Variation of FRP tensile strains with applied load (Group I beams)

A comparison of the FRP strains at mid-span for all Group I beams is shown in Figure 5-4. The FRP strain behaviour was almost identical without regard to bond condition, which verifies that the FRP strain must be similar under the same applied load at the post-yielding stage regardless of the unbonded length as discussed earlier. The resultant tensile force in the steel reinforcement remains essentially constant after steel yielding, indicating that increases in applied load correspond to increases in the force in the FRP. Therefore, the strains in FRP reinforcement are almost identical without regard to bond condition for a given applied load.

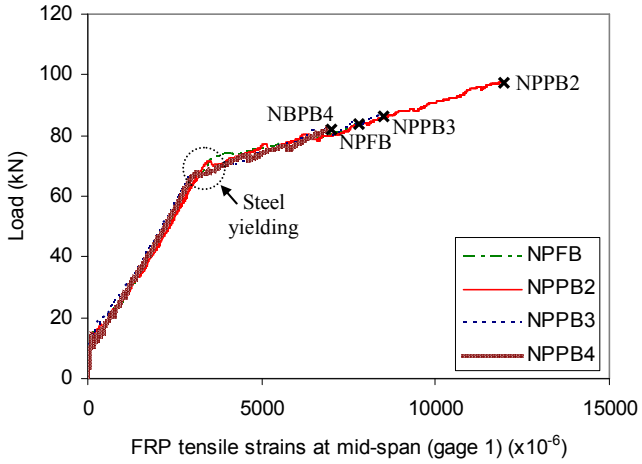

Figure 5-4 Comparison of FRP tensile strains at mid-span (Group I beams)

5.2.2.2 Concrete strain distribution

Variation of the concrete compressive strain at the top fibre with applied load is shown in Figure 5-5. For the fully bonded beam, the proximity to the mid-span affects the strain values (gage 1 > gage 2 > gage 3), which is the same result as the FRP strain distribution in the previous section because the FRP reinforcement is fully bonded. On the other hand, in the partially bonded beams the strains in gage 2 were much less compared to the strains in gage 1, and closer to the strains in gage 3 (see Figure 5-5(b), (c) and (d)). This is because FRP strains at the bonded point (gage 2) are high due to unbonding, so steel and concrete strains are reduced at this location. The strains in gage 3, installed in

the bonded region, were decreased as the unbonded length is increased because the location of the strain gages was farther from the mid-span (see Figure 5-5(b), (c) and (d)).

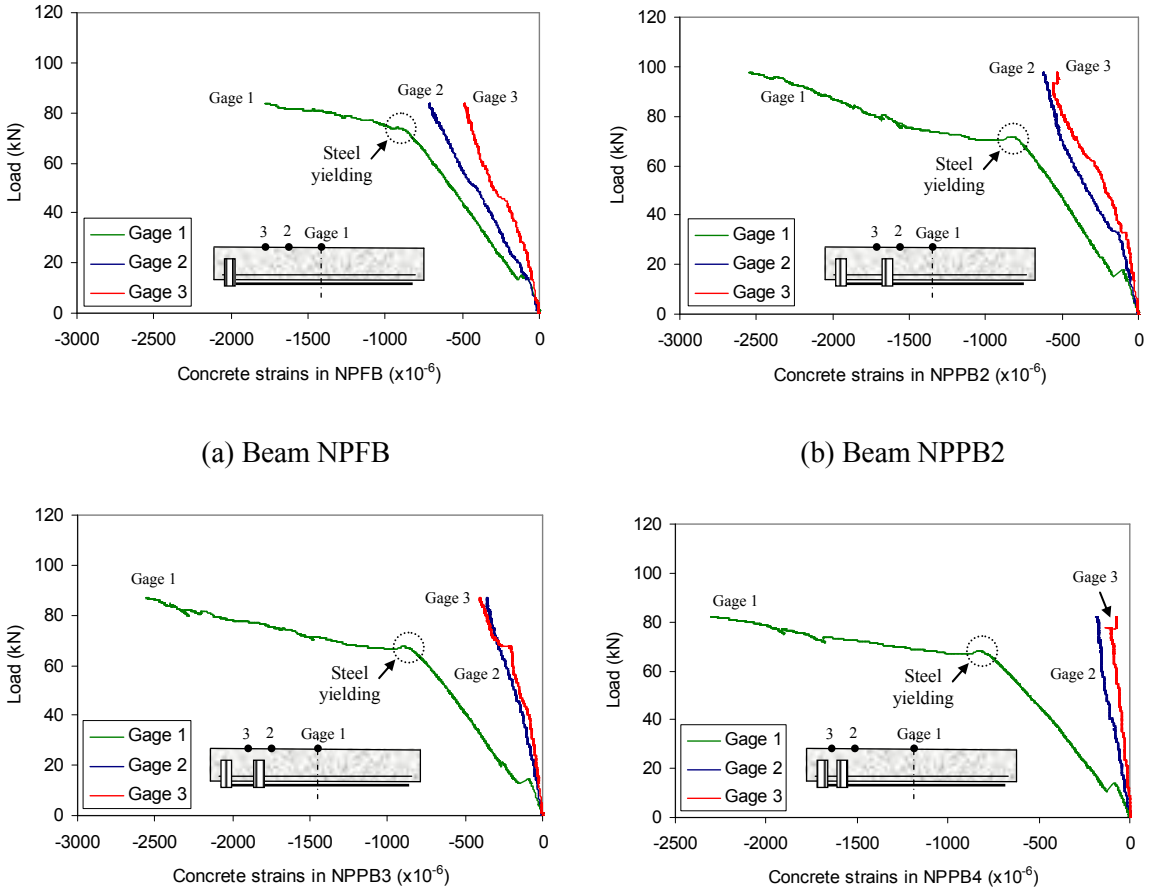

(a) Beam NPFB

(b) Beam NPPB2

(c) Beam NPPB3

(d) Beam NPPB4

Figure 5-5 Variation of concrete compression strains at top fibre with applied load (Group I beams)

Figure 5-6 shows a comparison of the concrete strains at mid-span. In contrast to the distributions of the FRP strains at mid-span in Figure 5-4, the concrete strains were greater for a given applied load after steel reinforcement yielding as the unbonded length is increased. This verifies that the concrete strains increase more rapidly as the unbonded length increases because the rate of increase in the FRP strain is reduced as the unbonded length is increased. This high concrete strain produces greater

curvature at mid-span, resulting in the stiffness reduction of the beam. Therefore, the deflection at the post-yielding stage is increased at the same applied load as the unbonded length increases.

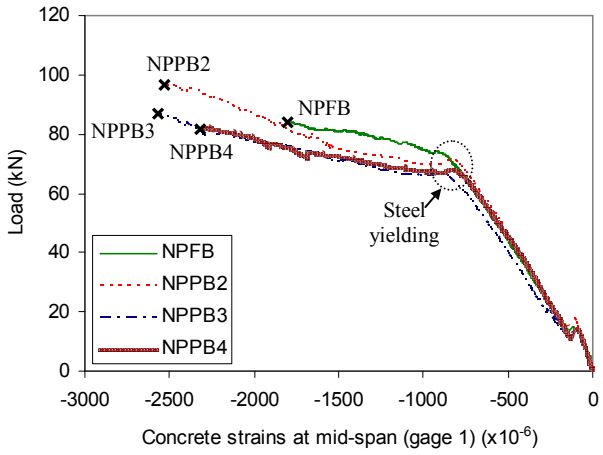

Figure 5-6 Comparison of concrete compressive strains at top fibre at mid-span (Group I beams)

5.2.2.3 Steel reinforcement strain distribution

The variation of the steel reinforcement with applied load is shown in Figure 5-7. At cracking, the strains in steel reinforcement at mid-span were suddenly increased as shown in Figure 5-7. This is because the tension stress in concrete is released at the time of cracking, and therefore the steel reinforcement takes more tension force. The measured steel reinforcement strains (gage 1) at yielding were between 2500×10^{-6} and 3000×10^{-6} based on the Figure 5-7, which is slightly higher than the average yield strain of 2365×10^{-6} for tested steel bars (see Section 4.5). This is possibly because the grinding of steel bars for the installation of strain gages affects the yield strain.

The general pattern of strain variation was similar to that of the concrete strains. One typical observation is that the strains measured in gage 2 showed a slope change at the occurrence of steel reinforcement yielding at mid-span. The rate of strain increase with applied load of gage 2 was decreased at steel yielding (the slopes were steeper) in the partially bonded beams as shown in Figure

5-7(b), (c), and (d). This is because the FRP stress within the unbonded length increases fast at post-yielding stage due to yielding, and therefore the rate of strain increase in the steel reinforcement at gage 2 is decreased at the post-yielding stage. In the fully bonded beam, no slope change was observed for gage 2 at the yielding point as shown in Figure 5-7(a).

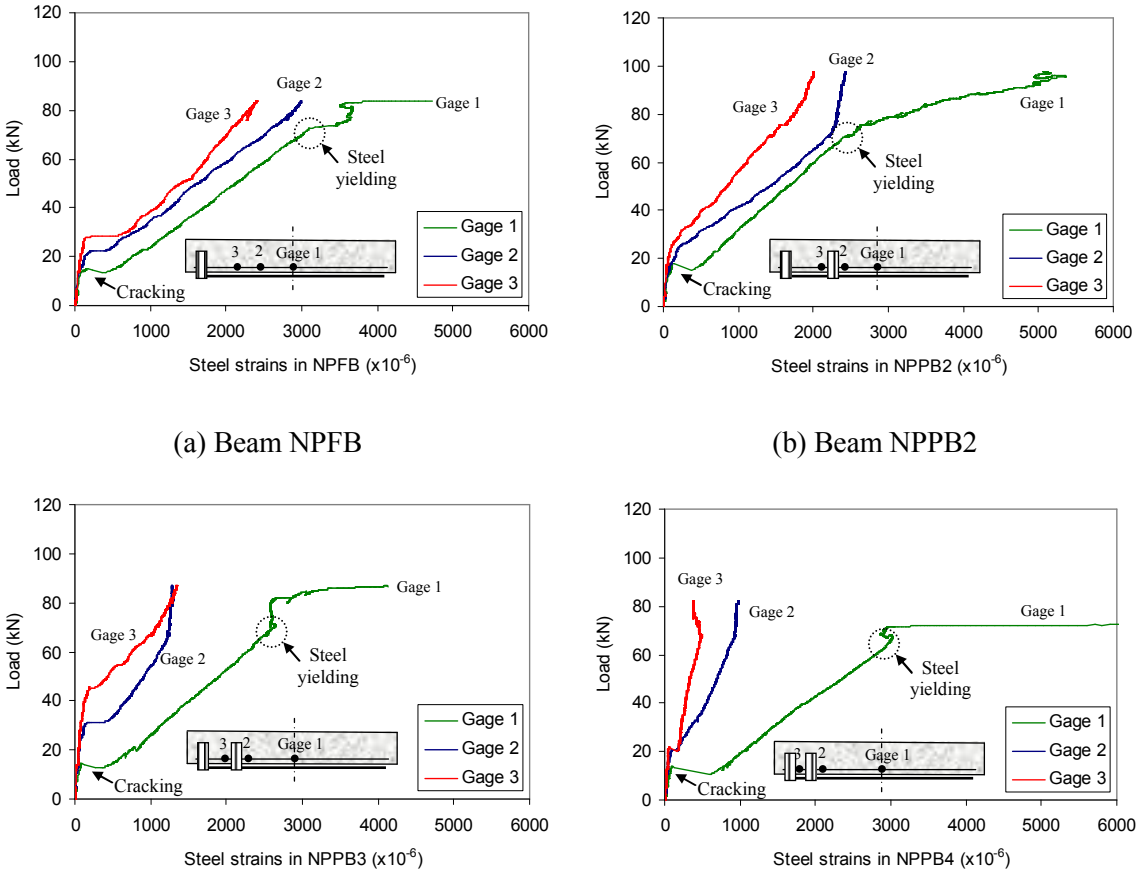

(a) Beam NPFB

(b) Beam NPPB2

(c) Beam NPPB3

(d) Beam NPPB4

Figure 5-7 Variation of steel reinforcement strains with applied load (Group I beams)

Figure 5-8 shows the comparison of the steel reinforcement strains (gage 1) at mid-span. Typical behaviour was not observed in this figure, and the steel strain patterns were similar to the FRP strain distributions. This is because the behaviour of the beam before steel yielding was mainly governed by the steel reinforcement without regard to the bond condition as discussed earlier (see Section 5.2.1).

The rate of steel strain increase after steel yielding must be greater as the unbonded length is increased for the same reason as the concrete strain distribution at mid-span in Figure 5-6. However, this behaviour was not observed in Figure 5-8 because the strains in the steel reinforcement can be affected by concrete tension stiffening effect. That is, the strains in the steel reinforcement at the crack location are higher than those where the steel bar is enclosed by the concrete because the concrete takes some tension force. Therefore, the comparison of steel strains after steel yielding does not give a significant conclusion.

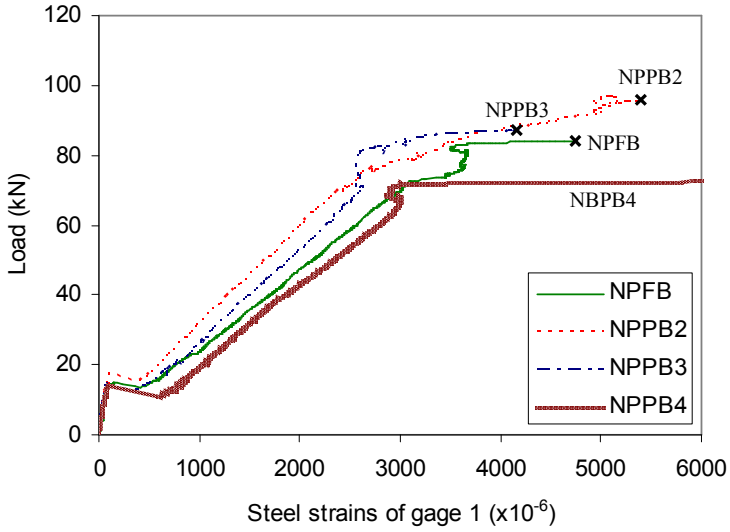

Figure 5-8 Comparison of steel reinforcement strains at mid-span (Group I beams)

5.2.3 Crack distribution

Cracks were marked at applied load increment of every 10kN. Figure 5-9 shows the beams where the cracks are marked up to failure and the sketches of the crack development at the applied load of 60kN. Because the crack control is a concern under service load conditions, the comparison of crack patterns was performed at a service load of 60kN, which is almost the half of the ultimate load of the strengthened beams when no premature debonding failure occurs, and less than the ultimate load of the unstrengthened beam.

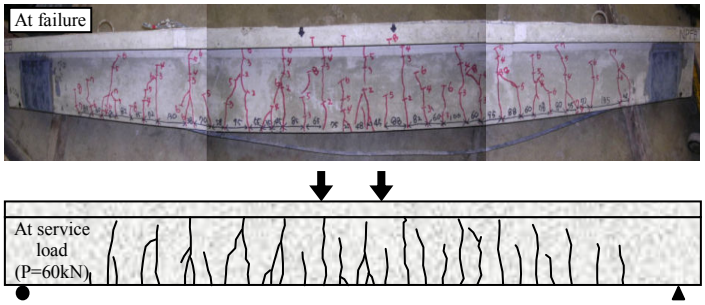

(a) Beam NPFB

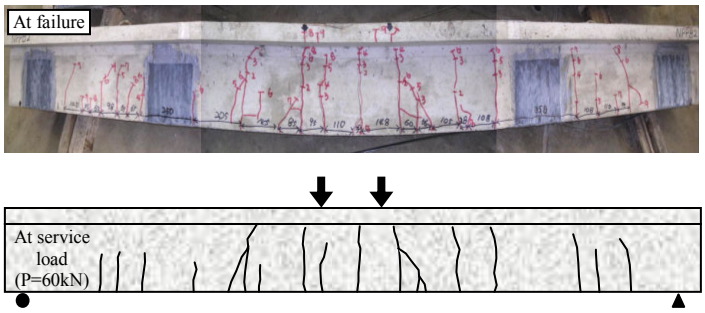

(b) Beam NPPB2

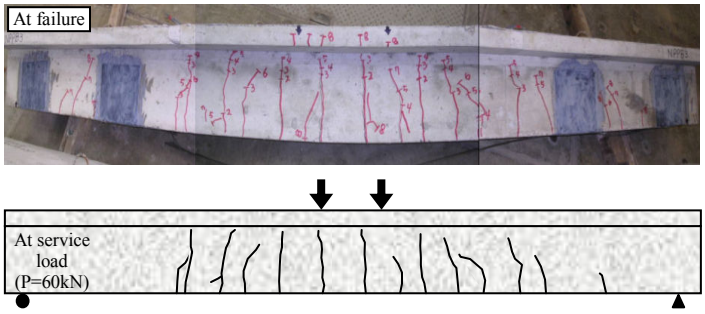

(c) Beam NPPB3

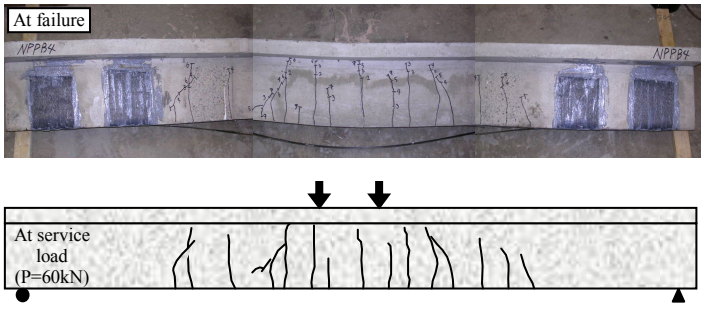

(d) Beam NPPB4

Figure 5-9 Crack patterns at failure and at service load (P = 60kN) of Group I beams

At the applied load of 60kN (service load condition), the cracks were almost developed to the bottom of the flange in all beams. When comparing the crack distributions between the fully bonded and partially bonded beams, the spacing between the cracks was much smaller and the number of the cracks was greater in the fully bonded beams. In addition, the length over which the cracks occurred was slightly wider in the fully bonded beams as shown in Figure 5-9. This is because the FRP stress in the fully bonded beam can be directly transferred to the concrete due to the bond between the FRP and the concrete, so more cracks can occur, and thus the spacing was less compared to the partially bonded beams. The crack width was not measured, but the crack width in the partially bonded beam appears to be slightly wider than that of the fully bonded beam. Based on the discrete crack approach, where the rotation of the beam is assumed to occur only at the crack locations (see Section 2.7.2), there must be wider cracks in the partially bonded beams compared to the fully bonded beam because the beam deflections at the applied load of 60kN were almost same without regard to the bond condition, but the number of cracks was greater in the fully bonded beam. The difference in the crack patterns between the partially bonded beams was not prominent as shown in Figure 5-9. This is because the cracks at service load occurred mainly within the unbonded length of the beam. Therefore, the difference in the unbonded length between the partially bonded beams did not make the big difference on the crack patterns.

5.2.4 Slip of CFRP plate

Two LVDT's were used to measure the CFRP slip at the end of the CFRP plate during testing. However, no slip was observed up to the debonding failure. Only a sudden increase of slip was measured at that time of failure due to sudden debonding of all strengthened beams. The debonding failure was initiated near the mid-span in the fully bonded beam and at the transition point in the partially bonded beams. Therefore, the slip might occur at mid-span or bonded point before failure but the slip at the end of the CFRP plate was not affected by this early debonding failure.

5.3 Comparison between Analytical Prediction and Experimental Results

In this section, a comparison is performed between the experimental results and the predictions based on the analytical model developed in Chapter 3 to verify the appropriateness of the analytical model. The load-deflection behaviour is compared in Section 5.3.1 and comparisons of the strain variations and strain distributions along the FRP length are discussed in Section 5.3.2.

5.3.1 Comparison of load-deflection diagrams

Figure 5-10 shows the load-deflection comparison between predicted and measured values at mid-span. Dotted lines with solid squares denote analytical predictions, while solid lines are the measured values. The analytical model predicted the general behaviour of the beams well, including the stiffness changes at the cracking and steel yielding points. The stiffness degradation with the increase of the unbonded length described in Section 5.2.1 was also represented well by the model. However, the measured ultimate responses (load and deflection) were much less compared to the predicted values. This is because all of the beams failed by premature debonding of the FRP, while the analytical model assumes perfect bond with no slip up to ultimate state. To investigate the ultimate response considering the debonding failure, nonlinear finite element (FE) analysis was conducted and the results of the analysis were compared to the measured values in Section 5.4.

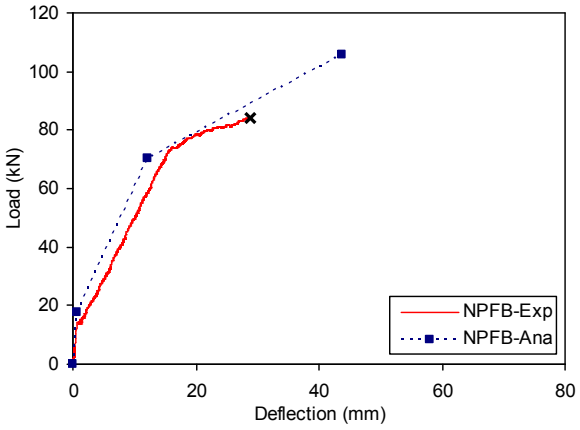

(a) Beam NPFB

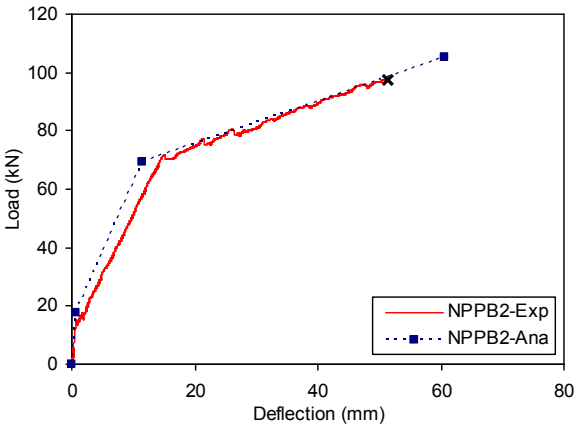

(b) Beam NPPB2

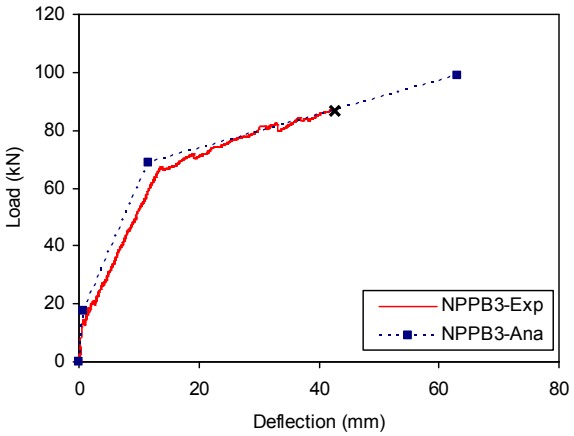

(c) Beam NPPB3

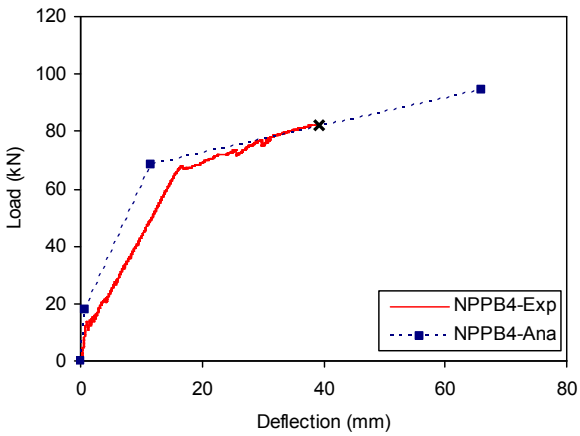

(d) Beam NPPB4

Figure 5-10 Comparison of experimental and predicted load-deflection diagrams

5.3.2 Comparison of strain distributions

A comparison between measured and predicted strain distributions is performed in this section. Predicted strains in the FRP, the concrete, and the steel reinforcement with the applied load are compared with the measured strains in Section 5.3.2.1. Strain profiles along the FRP length are investigated and compared in Section 5.3.2.2.

5.3.2.1 Strain variation with applied load

Measured and predicted strains in the FRP at mid-span are plotted in Figure 5-11. The variation of measured strains at mid-span after steel yielding was almost identical without regard to the bond condition as described earlier. The analytical predictions represented this behaviour well as shown in Figure 5-11. The predictions at the ultimate state were greater compared to the measured strains due to early debonding failure of the beams.

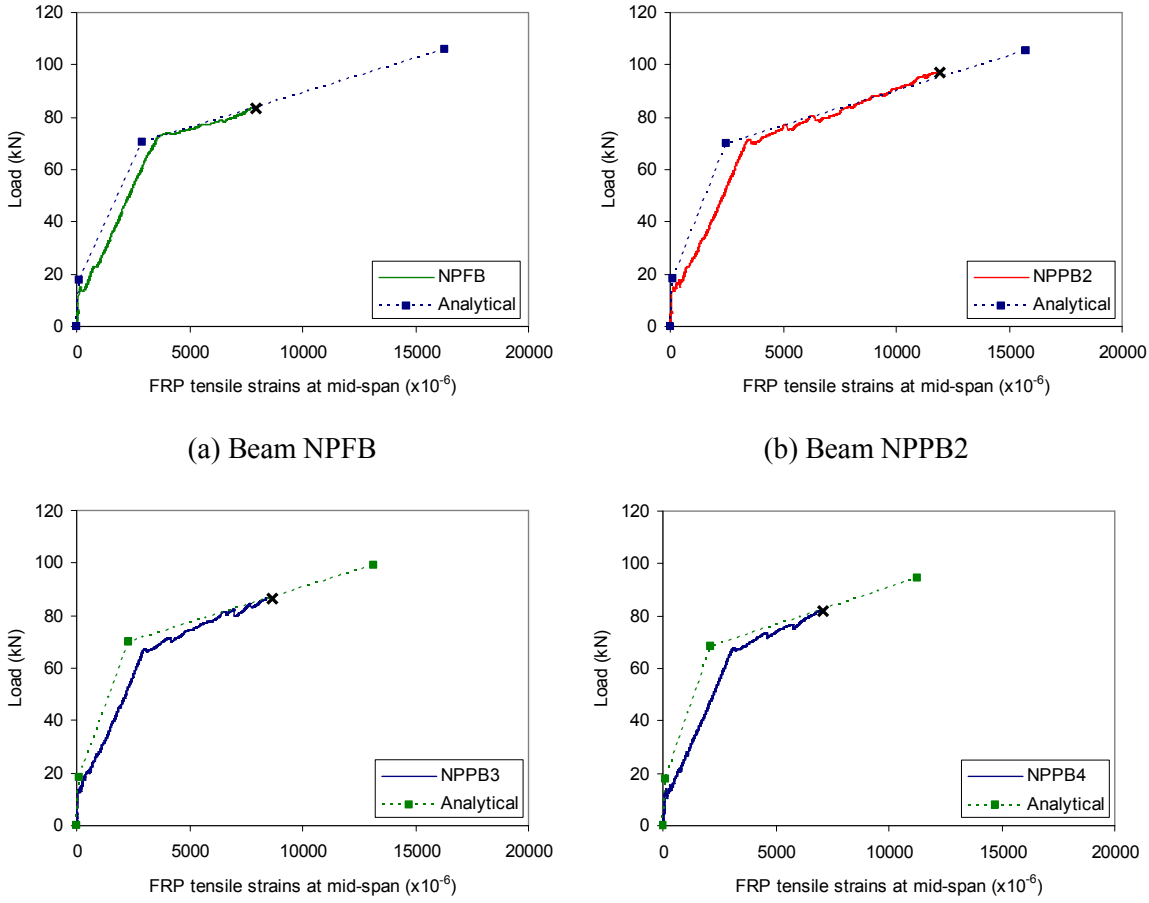

(a) Beam NPFB

(b) Beam NPPB2

(c) Beam NPPB3

(d) Beam NPPB4

Figure 5-11 Comparison of measured and predicted FRP strains at mid-span

Concrete strain distributions with applied load are compared in Figure 5-12. For the fully bonded beam (NPFB), the measured stiffness of load-strain diagram at post-yielding stage was lower than the

predicted stiffness as shown in Figure 5-12(a). This may be caused by partial FRP debonding near mid-span before complete debonding failure in the fully bonded beam. For the partially bonded beams, the general behaviour including the stiffness change at cracking and steel yielding and the stiffness decrease after steel yielding as the unbonded length increased, was represented well by the analytical model as shown in Figure 5-12(b), (c), and (d).

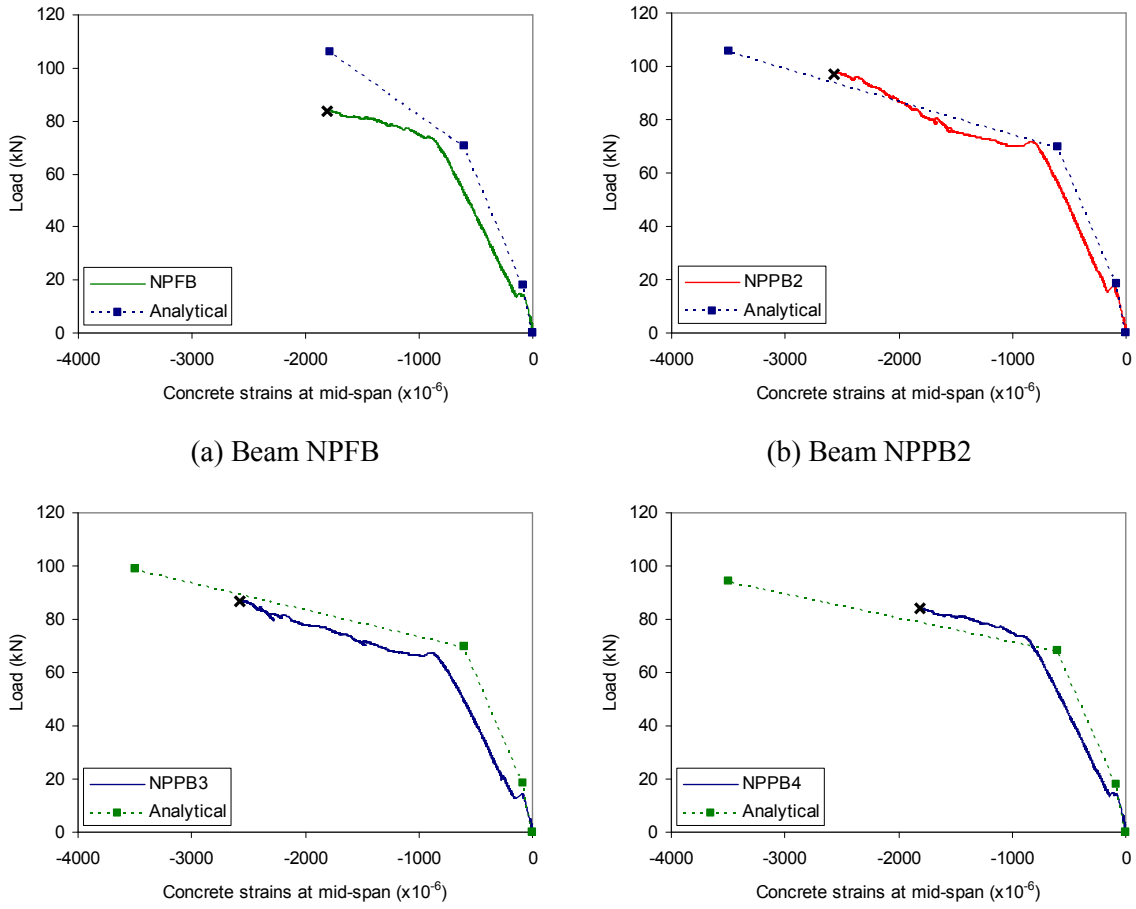

(a) Beam NPFB

(b) Beam NPPB2

(c) Beam NPPB3

(d) Beam NPPB4

Figure 5-12 Comparison of measured and predicted concrete strains at mid-span

Predicted and measured strains in the steel reinforcement are compared in Figure 5-13. The steel strains were predicted well up to steel yielding. However, the predicted strains after yielding were much higher compared to the measured values as shown in Figure 5-13. This is because the strain

gages may not be located at a crack location, and the steel strains between cracks will be less than those at crack locations due to the tension stiffening effect as discussed earlier. On the other hand, the analytical model uses a cracked section analysis and does not consider the tension stiffening effect. As a result, the measured strains showed lower values than the predicted strains after steel yielding.

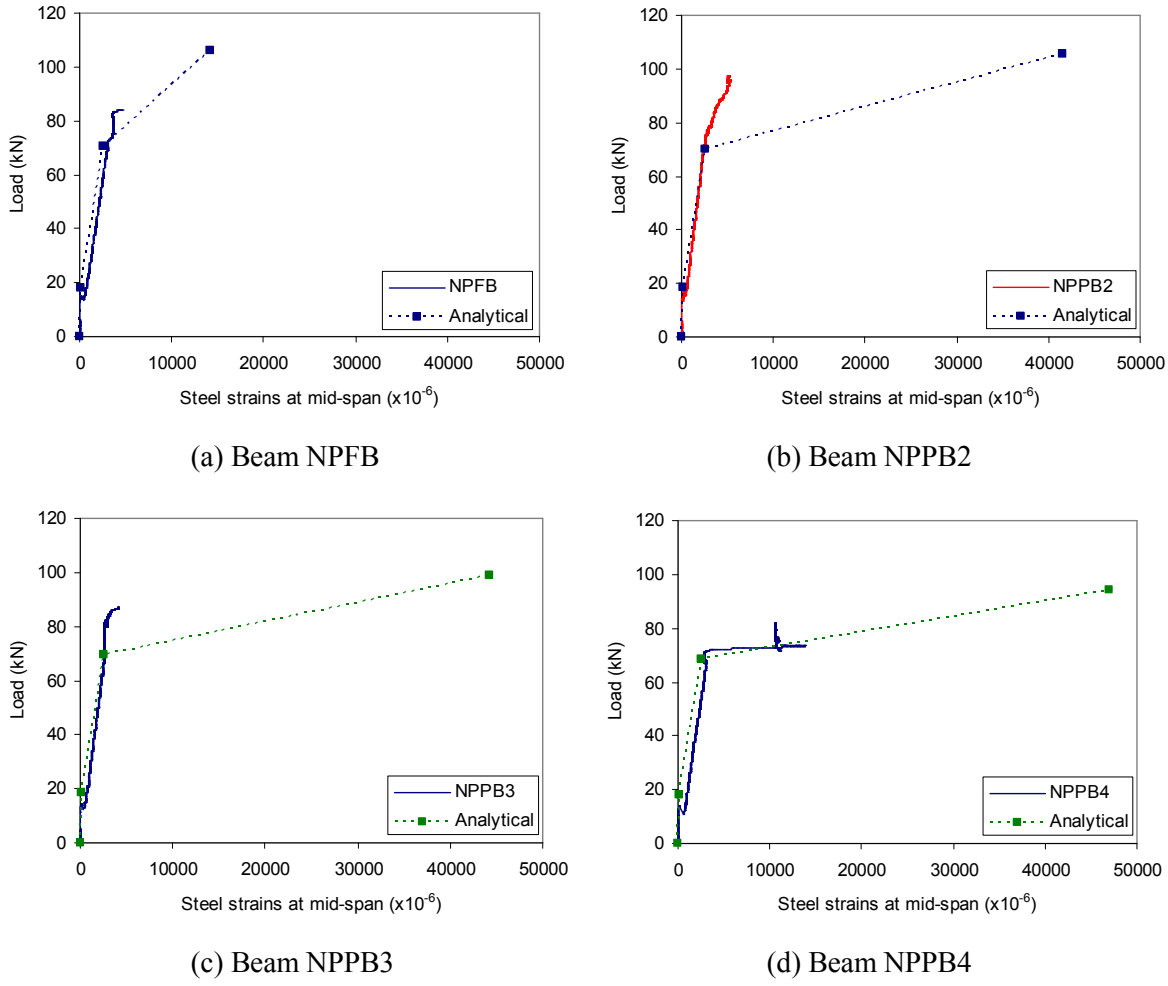

(a) Beam NPFB (b) Beam NPPB2

(c) Beam NPPB3 (d) Beam NPPB4

Figure 5-13 Comparison of measured and predicted steel strains at mid-span

Strain variations in the FRP, the concrete and the steel reinforcement with the applied load at bonded point (gage 2) are compared in Figure 5-14, Figure 5-15 and Figure 5-16. The strain variation at this location is relatively less important compared to the strains at mid-span because the effect of the strains at this location on the overall beam behaviour is relatively small compared to the strains at

mid-span. However, the behaviour at the bonded point in partially bonded beams is distinct compared to fully bonded beams, and therefore an appropriate strain prediction at this location is also needed.

A comparison of the FRP strain variation at gage 2 location is shown in Figure 5-14. In contrast to the strain distribution at mid-span, the FRP strains of partially bonded beams at bonded point are greater than those of the fully bonded beam due to partial unbonding. The analytical model predicted this behaviour well as shown in Figure 5-14.

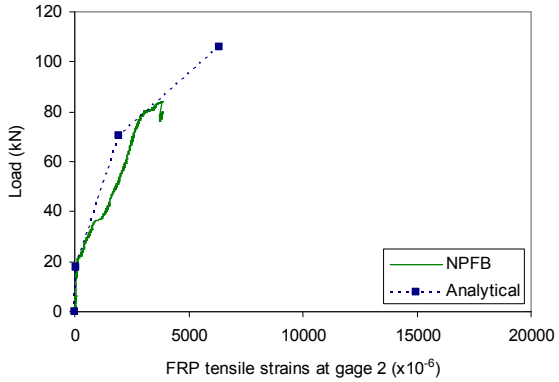

(a) Beam NPFB

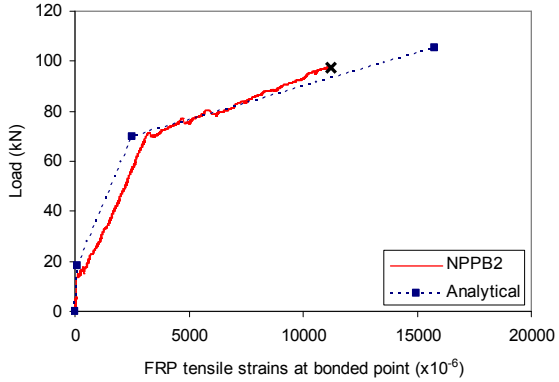

(b) Beam NPPB2

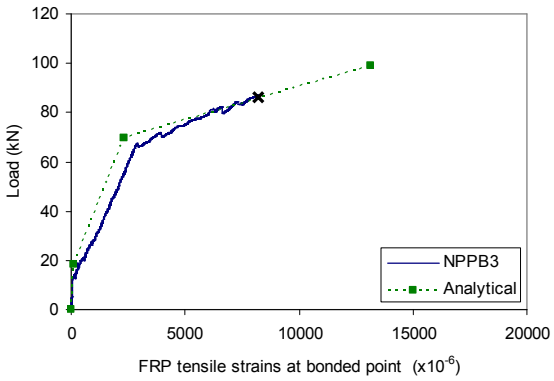

(c) Beam NPPB3

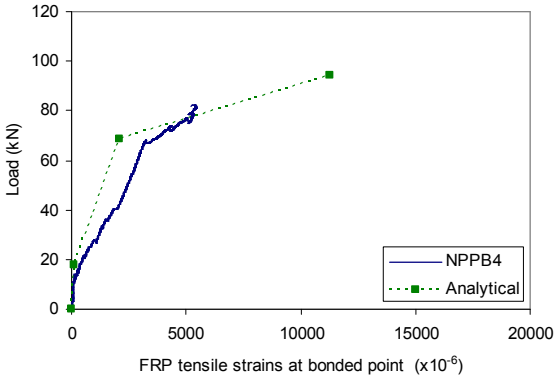

(d) Beam NPPB4

Figure 5-14 Comparison of measured and predicted FRP strains at bonded point (gage 2)

Comparisons of the strains in the concrete at gage 2 locations are shown in Figure 5-15. The analytical model predicted that the stiffness of load-concrete strain diagram in the fully bonded beam

was slightly decreased after the steel yielding point (see Figure 5-15(a)) while the stiffness in the partially bonded beams was increased after steel yielding (see Figure 5-15(b), (c), and (d)). The measured stiffness change was not as prominent as the predicted values, but can be clearly observed in Beam NPPB2 as shown in Figure 5-15(b). This stiffness change is caused by the high FRP strains at the bonded point as discussed earlier, delaying concrete strain increases at the bonded point in the partially bonded beams and resulting in an apparent increase of stiffness.

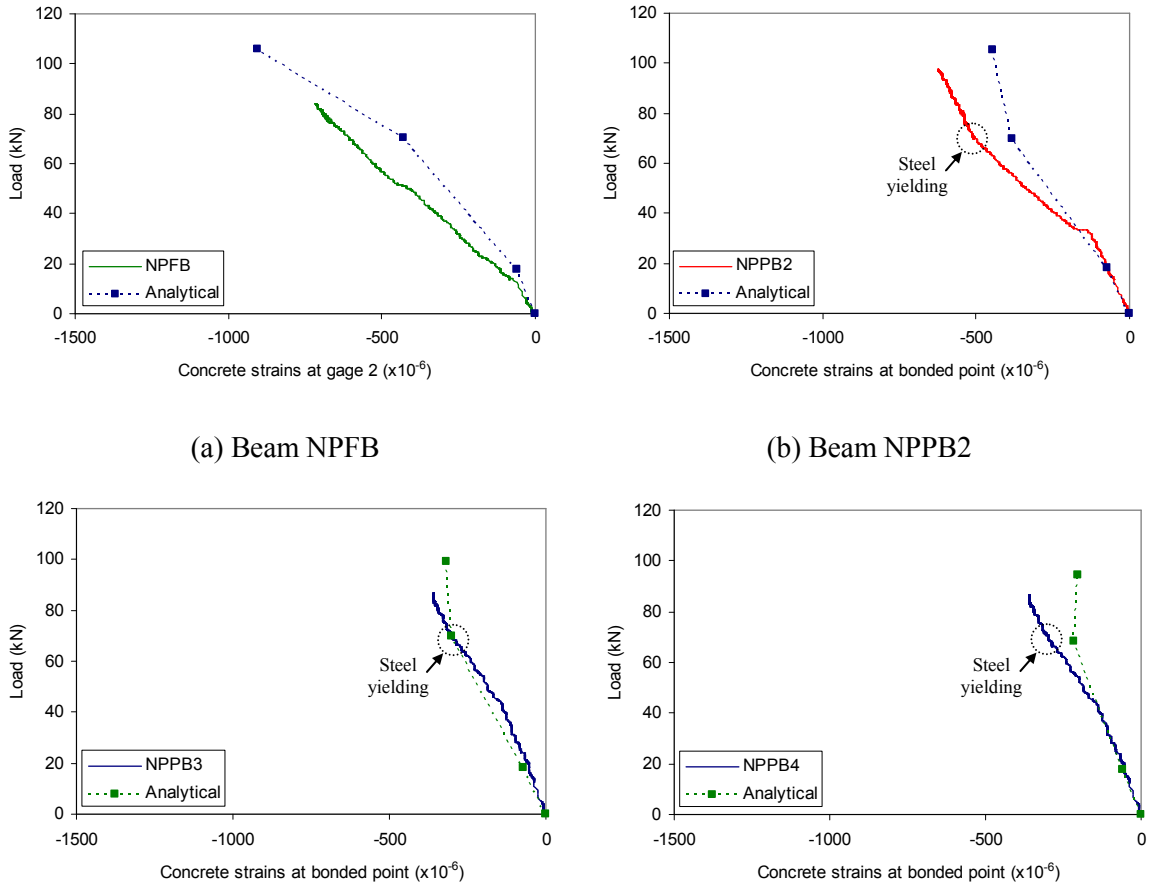

(a) Beam NPFB

(b) Beam NPPB2

(c) Beam NPPB3

(d) Beam NPPB4

Figure 5-15 Comparison of measured and predicted concrete strains at bonded point (gage 2)

Figure 5-16 shows the steel strain variations with applied load at the gage 2 location. The pattern of strain variation was similar to the concrete strains, although the stiffness change at steel yielding was

more prominent as shown in Figure 5-16. This is because the high FRP tensile strains at the bonded point had a greater effect on the steel strains due to the close distance between the FRP and steel reinforcement.

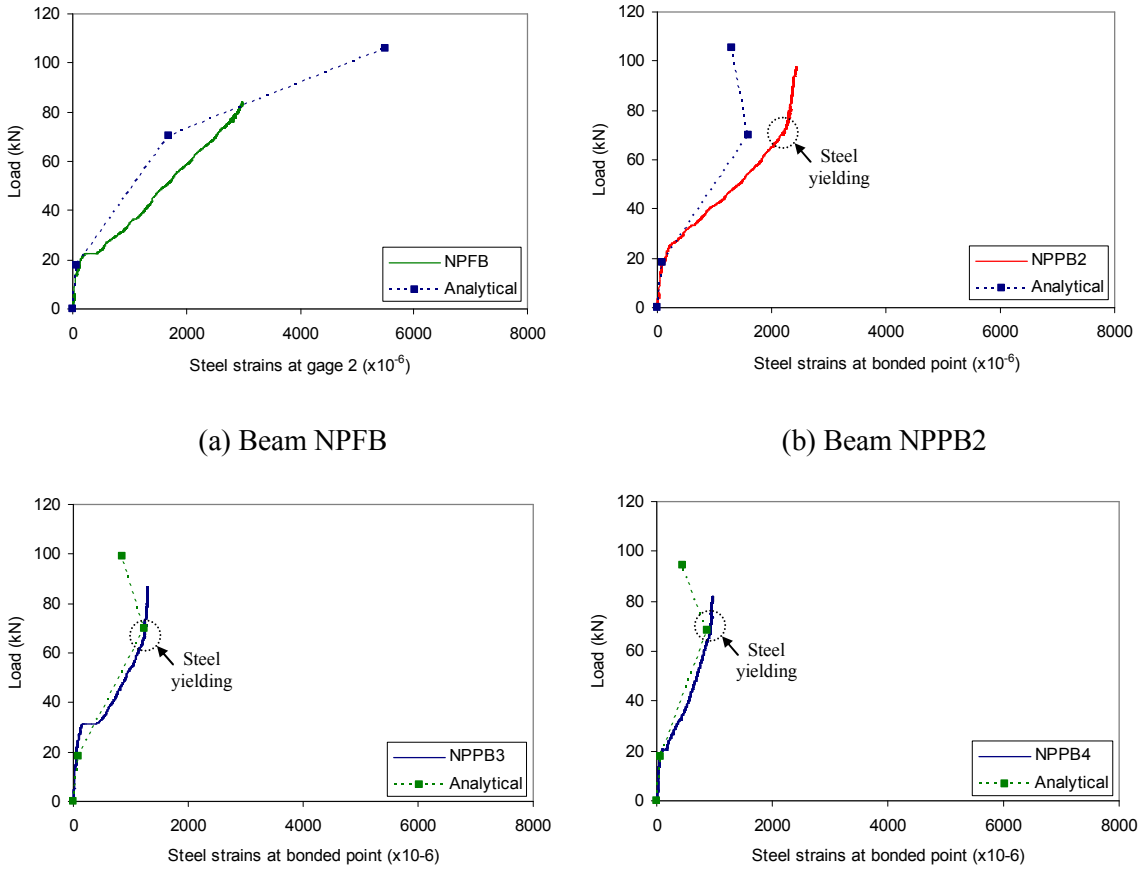

(a) Beam NPFB

(b) Beam NPPB2

(c) Beam NPPB3

(d) Beam NPPB4

Figure 5-16 Comparison of measured and predicted steel strains at bonded point (gage 2)

5.3.2.2 Strain distribution along the beam length

The strain gages of the fully bonded beam (NPFB) were installed at the same locations of those in beam NPPB2 to investigate the distinction of the strain distributions between the fully bonded and the partially bonded beams. The comparison of the strain profile along the beam length is performed before steel yielding (P = 60kN, service load) and after steel yielding (P = 80kN).

Figure 5-17 shows the FRP strain distribution for the fully bonded beam (NPFB) and the partially bonded beam (NPPB2) at the applied load of 60kN and 80kN. At the service load stage (P = 60kN), the strain distributions were similar for the two systems (see Figure 5-17(a) and (b)), while the difference was prominent at the post yielding stage (P = 80kN) at the bonded point as shown in Figure 5-17(c) and (d). The analytical predictions showed a good agreement with the measured values.

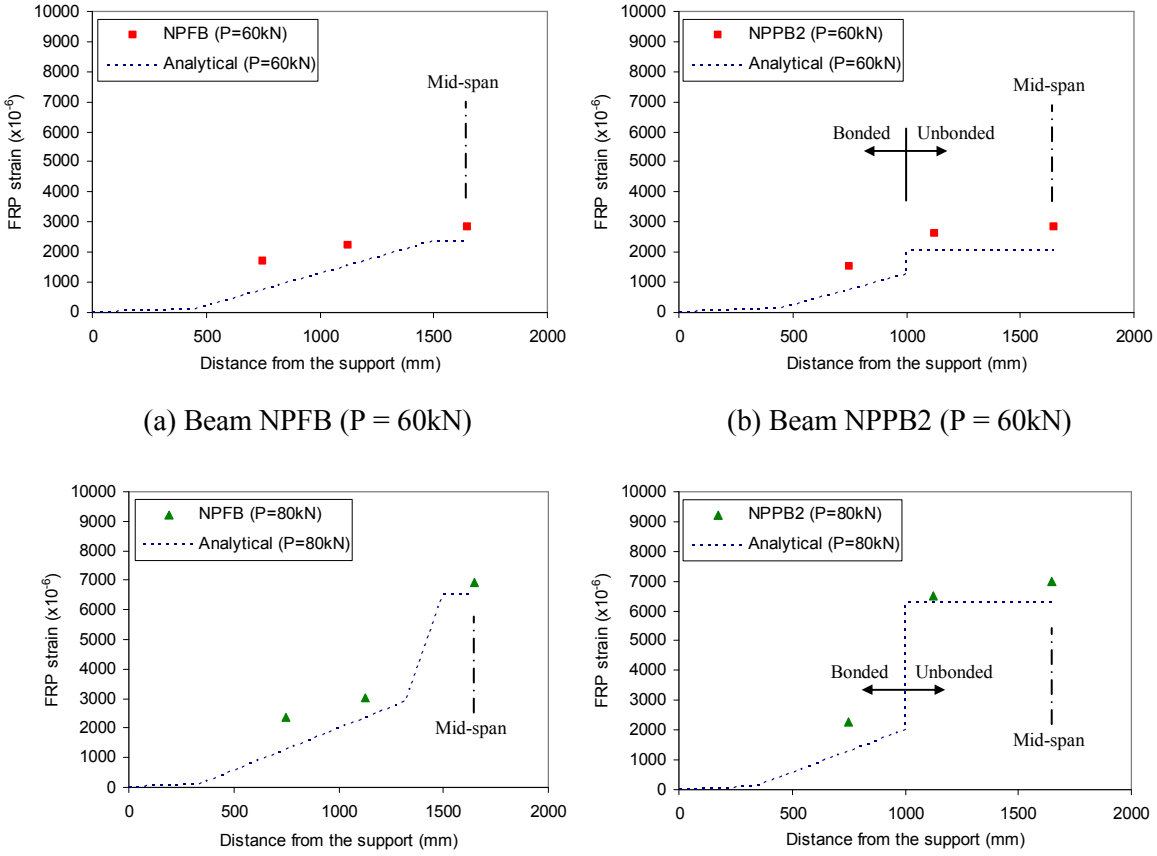

(a) Beam NPFB (P = 60kN)

(b) Beam NPPB2 (P = 60kN)

(c) Beam NPFB (P = 80kN)

(d) Beam NPPB2 (P = 80kN)

Figure 5-17 Comparison of measured and predicted FRP strain profiles (P = 60kN and 80kN)

Figure 5-18 shows comparisons of measured and predicted concrete strain profiles along the beam length at the applied load of 60kN and 80kN. At the service load stage (P = 60kN), the strain distributions were almost the same for the partially bonded and fully bonded beams (Figure 5-18(a) and (b)). In contrast to the FRP strain distribution, the magnitude of the concrete strains was

significantly different at mid-span between the fully bonded and partially bonded beams as shown in Figure 5-18(c) and (d). The predicted strains were slightly lower (approximately 200~300×10^{-6}) than the measured values; however, the general pattern of the strain distributions predicted by the model represented the measured strain distribution accurately.

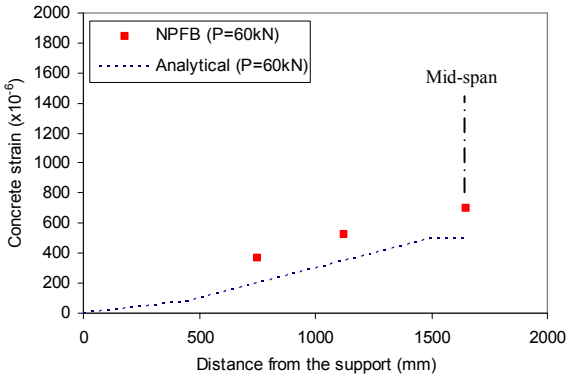

(a) Beam NPFB (P = 60kN)

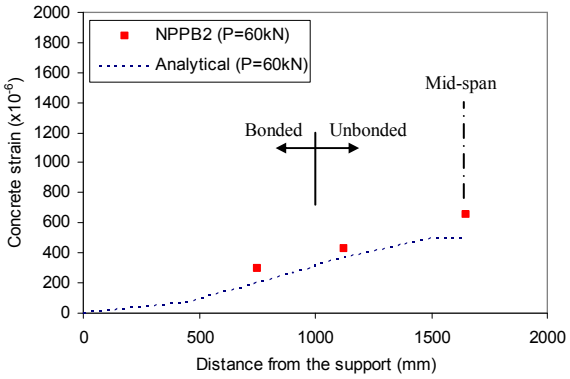

(b) Beam NPPB2 (P = 60kN)

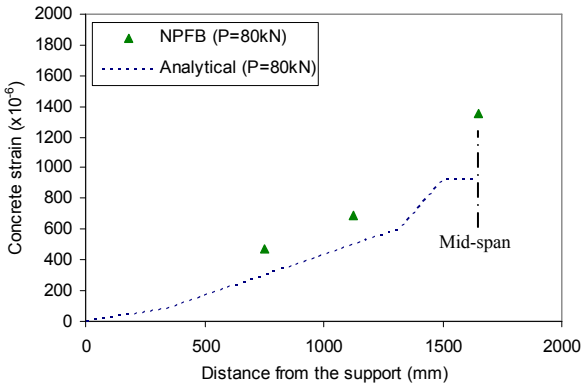

(c) Beam NPFB (P = 80kN)

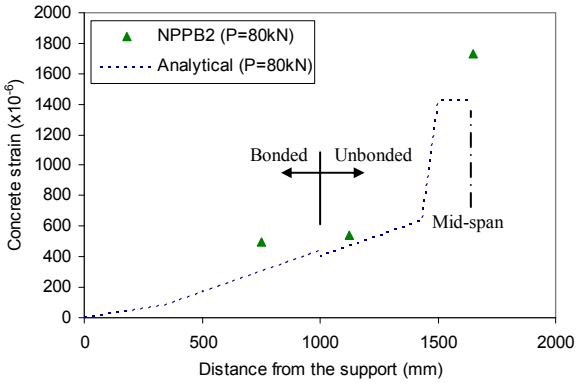

(d) Beam NPPB2 (P = 80kN)

Figure 5-18 Comparison of measured and predicted concrete strain profiles (P = 60kN and 80kN)

Comparisons of steel strain distributions are shown in Figure 5-19. The general pattern of the strains was the same as the concrete strain profiles. The strains in the steel reinforcement were predicted well up to steel reinforcement yielding at service load stage (P = 60kN), but the measured

strains at mid-span after steel yielding were much less compared to the predicted values because of the tension stiffening effect as discussed earlier.

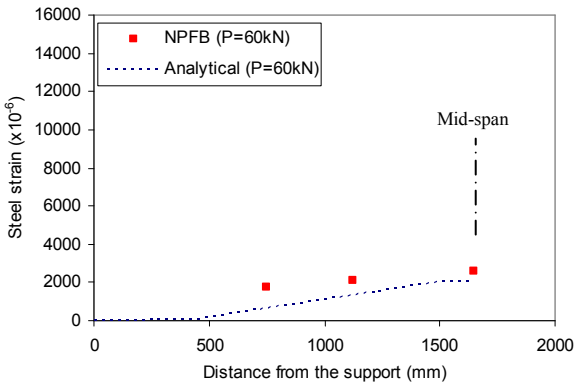

(a) Beam NPFB (P = 60kN)

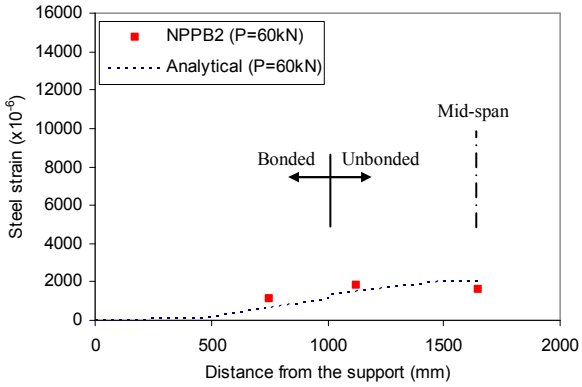

(b) Beam NPPB2 (P = 60kN)

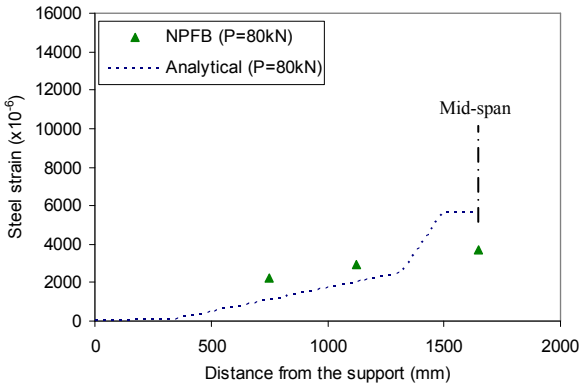

(c) Beam NPFB (P = 80kN)

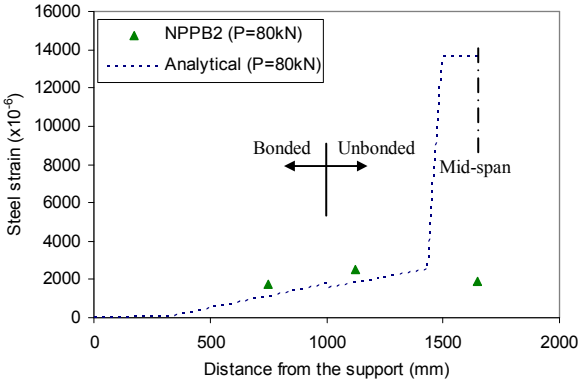

(d) Beam NPPB2 (P = 80kN)

Figure 5-19 Comparison of measured and predicted steel reinforcement strain profiles (P = 60kN and 80kN)

The strain distributions of NPPB3 and NPPB4 beams along the beam length are not included because the general pattern of the strain profiles was the same as that of beam NPPB2.

5.3.3 Summary

The analytical model predicted the overall behaviour of the beams well in terms of the load-deflection diagrams. However, the predicted ultimate response at failure was over-estimated due to the

premature debonding failure that happened in the tested beams. The prediction of the strain variation in the FRP, in the concrete, and in the steel reinforcement at the mid-span and at the bonded point also showed good agreement with the experimental results. The strain distributions along the beam length were represented well by the model.

5.4 Nonlinear Finite Element Analysis

5.4.1 General

The analytical model predicted the general behaviour of the beams including the strain variations very well. However, the model did not consider the premature debonding failure, and therefore the ultimate response of all beams was over-estimated. Therefore, the ultimate response governed by debonding failure needs to be investigated in more detail for both the fully bonded and partially bonded beams.

Although the linear elastic FE analysis was able to investigate the general pattern of interfacial stress distributions as presented in Section 3.3, this is only valid prior to the concrete cracking, and the ultimate behaviour including the debonding phenomenon can not be simulated. Therefore, a rigorous analysis of the EB strengthened beams up to failure is required that considers the concrete cracking in tension, the tension stiffening effect, the nonlinear concrete compression behaviour, and the strain hardening effect of the steel reinforcement. In addition, an appropriate bond stress-slip relationship at the FRP-concrete interface, as described in Section 2.4.2, should be considered in order to simulate the premature debonding failure.

In this section, a three-dimensional nonlinear FE analysis was performed for the analysis of the FRP strengthened beams with the consideration of bond stress-slip relationship and contact properties in the partially bonded beams. The general purpose commercial FE software ABAQUS was used based on the smeared, fixed orthogonal crack model for concrete crack modeling (see Section 2.8).

An explicit integration method was applied to solve nonlinear problems, which determines solutions based on the dynamic equilibrium by explicitly advancing the kinematic state from the previous increment. Details of the explicit integration method are described in Section 2.8.

5.4.2 Material constitutive model

For the concrete nonlinear compression behaviour, a plastic-damage model developed by Lubliner et al. (1989) and modified by Lee and Fenves (1998) was used for the simulation of the stiffness degradation in concrete material. This model makes use of a non-associated flow rule based on the Drucker-Prager hyperbolic potential function. For this model, a uniaxial nonlinear stress-strain relationship proposed by Collins and Mitchell (1987) was used as a basic stress-strain curve, and linear behaviour was assumed up to $0.7f'_c$ as shown in Figure 5-20. The strength was reduced to 10% of f'_c at the ultimate concrete strain of 0.0035 to simulate the concrete crushing at failure. The Poisson's ratio and the angle of dilatancy of the concrete were assumed to be 0.18 and 30°, respectively, which were based on the recommendations by Coronado and Lopez (2005). They performed sensitivity analysis of FRP strengthened beams by changing main parameters of the beams, and proposed general values needed for FE simulation.

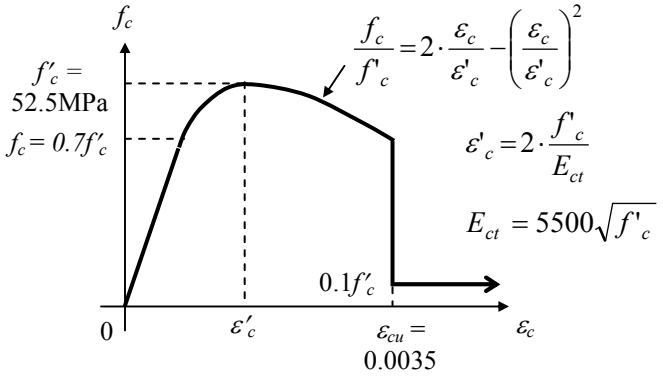

Figure 5-20 Stress-strain behaviour of concrete under uniaxial compression

For the concrete in tension, a brittle crack model based on a simple Rankine criterion was applied, where the cracks occur when the maximum principal tensile stress exceeds the tensile strength of the material. The tension stiffening effect due to the concrete between the cracks is also important and should be evaluated appropriately. This effect can be considered utilizing the softening curve of the uniaxial tensile stress-strain relationship after crack initiation. Hilleborg et al. (1976) suggested a linear softening curve for concrete tension behaviour, as shown in Figure 5-21(a), and proposed a crack opening width, ω_c, of 0.01~0.02mm based on experiments. The CEB-FIP model code (1990) and Gopalaratnam and Shah (1985) proposed a bilinear curve and an exponential curve, respectively, as shown in Figure 5-21(b) and (c). FE analyses were performed in the current study using these three types of tension stiffening model, but there was almost no difference in term of overall load-deflection behaviour between different tension stiffening models. Therefore, the bi-linear tension stiffening model proposed by CEB-FIP (1990) was adopted in the further simulation.

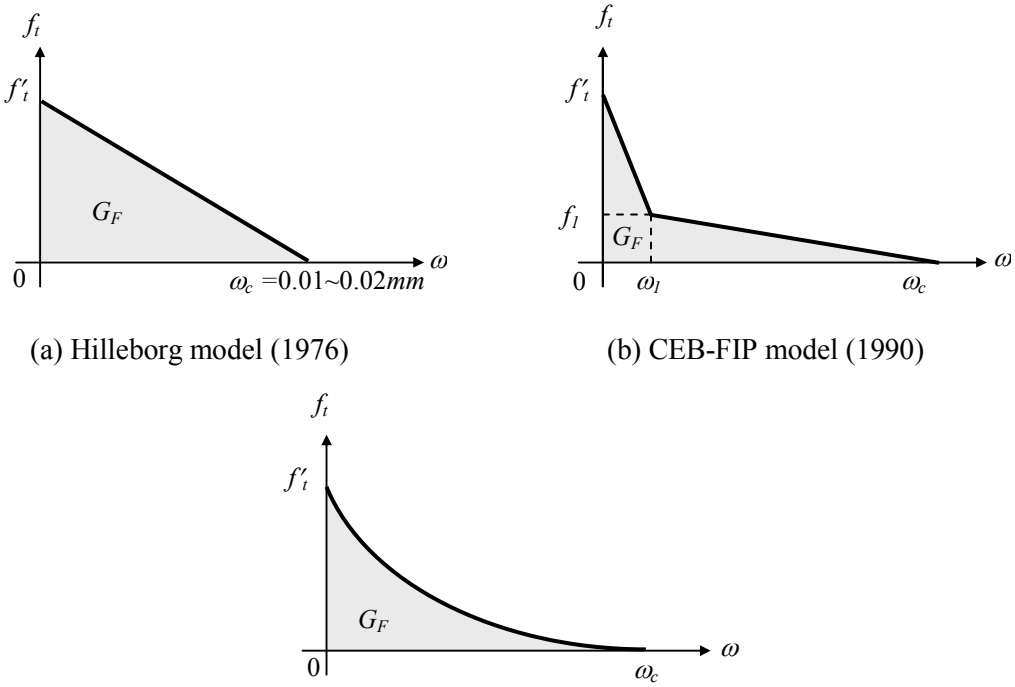

(a) Hilleborg model (1976)

(b) CEB-FIP model (1990)

(c) Gopalaratnam and Shah model (1985)

Figure 5-21 Concrete tension stiffening models

The constitutive behaviour of the steel reinforcement was defined using a tri-linear elastic-plastic constitutive model (Malvar 1998, MacGregor and Bartlett 2000) to represent the strain hardening effect based on the steel bar test results (see Section 4.5), while the CFRP plate was assumed to be a linear elastic material up to rupture as shown in Figure 5-22.

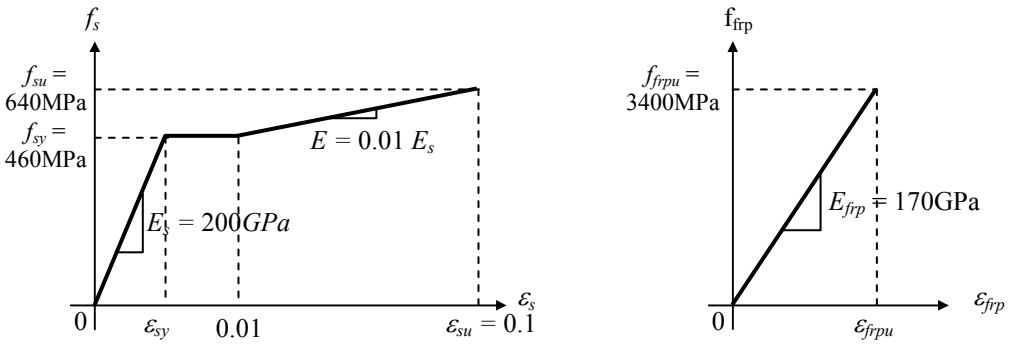

(a) Steel reinforcement (b) CFRP plate

Figure 5-22 Stress-strain relationship for steel and CFRP plate

5.4.3 Interfacial element model

The interfacial debonding failure is initiated by high interfacial stresses that exceed the strength of the weakest element (epoxy adhesive or concrete) as described in Section 2.4.3. The failure usually occurs along the concrete interfacial layer because the tensile strength of epoxy adhesive is usually higher than that of concrete. The epoxy adhesive layer can be simulated using an interfacial or link element that is able to represent the bond (shear) stress-slip relationship between the concrete and the FRP. This interfacial element was first adopted by Ngo and Scordelis (1967) to simulate the bond stress-slip behaviour between steel reinforcement and concrete as shown in Figure 5-23(a). The same concept of the interfacial element was used in this study to simulate the property at the FRP-concrete interface.

Various bond stress-slip relationships have been proposed, and this relationship is affected by many factors as described in Section 2.4.2. Therefore, it is very difficult to select a typical relationship that is appropriate for a particular FRP-concrete interface. Moreover, this relationship is usually derived

from a simple shear test, which has a limited applicability to beam specimens because the curvature and the cracks of the beam are not considered. In this study, a simple linear-elastic bond stress-slip relationship was applied as shown in Figure 5-23(b) because the load-deflection behaviour of CFRP strengthened beams was almost linear up to premature debonding failure and the complete debonding failure happened suddenly at the end of the response. For the maximum bond stress, τ_{max}, an appropriate value was selected by simulating the beams with various maximum bond strengths until it matched the experimental load-deflection response. The shear stiffness (E_b) normally varies between 50MPa/mm and 150MPa/mm, and has little influence on the load-deflection behaviour (Kishi et al. 2005, Pham and Al-Mahaidi 2005). A value of 100MPa/mm was assumed for the current analysis.

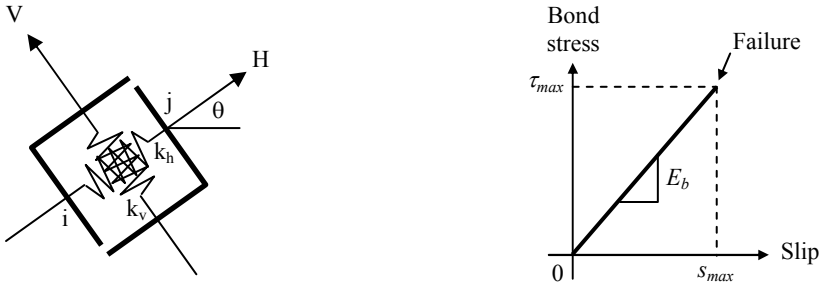

(a) Link element (Ngo and Scordelis 1967) (b) Bond stress-slip relationship

Figure 5-23 Interfacial element and bond stress-slip relationship

5.4.4 Contact model

Contact properties at the concrete-FRP interface within the unbonded length in partially bonded beams should be considered to ensure that shear force is not transferred between the FRP and the concrete in the unbonded region, while the pressure (normal) force from the concrete is transmitted to the FRP reinforcement. A *hard* contact property provided by ABAQUS (HKS 1997) was applied for the simulation of the normal direction to prevent the penetration between concrete and FRP material but transmitting the pressure force. On the other hand, no friction was ensured between the two faces

for the tangential behaviour at FRP-concrete interface so that the CFRP could move freely as shown in Figure 5-24.

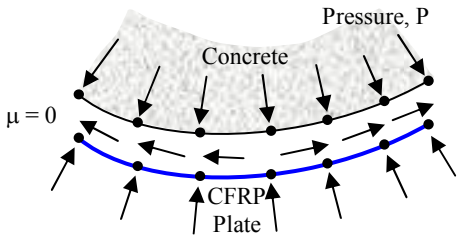

Figure 5-24 Contact model at the FRP-concrete interface within unbonded length

5.4.5 Geometric model

One-quarter of the T-shaped reinforced concrete beam was modeled due to symmetry as shown in Figure 5-25(a). An eight-node brick element was used to model the concrete and a four-node shell element was used for the CFRP plate. A two-node truss element was used for modeling the steel reinforcement. This element was embedded to the concrete as shown in Figure 5-25(b) assuming that there is a perfect bond between the concrete and steel reinforcement. An interfacial element was applied between the FRP and concrete in the FRP bonded length to allow simulation of the debonding failure, while the contact modeling was assigned within the unbonded region for the partially bonded beams as shown in Figure 5-25(a). The element types used in the modeling are summarized in Table 5-2.

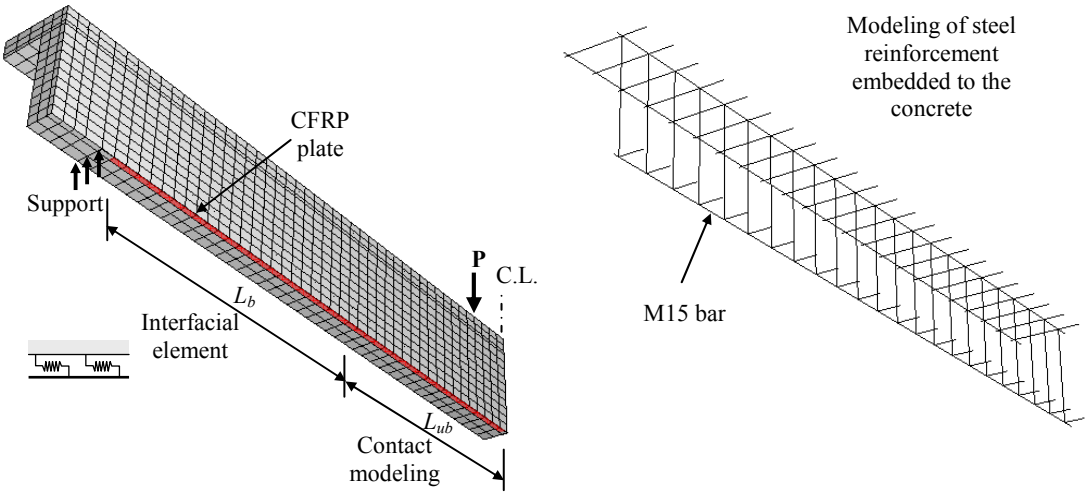

(a) Modeling of the beam (b) Embedded steel reinforcement

Figure 5-25 Finite element mesh and the steel reinforcement element

Table 5-2 Element types used in FE analysis

Material	Description	Code	Remarks
Concrete	Eight-node brick	C3D8R	Reduced integration
Steel	Two-node truss	T3D2	Embedded element
Epoxy	Connector	CONN3D2	Interfacial element
CFRP	Four-node shell	S4R	Reduced integration

To verify the FE analysis and mesh sensitivity, three different mesh sizes were selected for the simulation of the unstrengthened beam as shown in Figure 5-26(a), (b), and (c). The results were compared with the measured load-deflection curve, and FE models with the different mesh sizes were found to represent the behaviour of T-beams well as shown in Figure 5-26(d). Although the beam stiffness was slightly stiffer and the ultimate load was slightly higher as the mesh size was finer, the difference was negligible as shown in Figure 5-26(d). Therefore, mesh 2 (fine mesh) in Figure 5-26(b) was selected for the rest of the simulations.

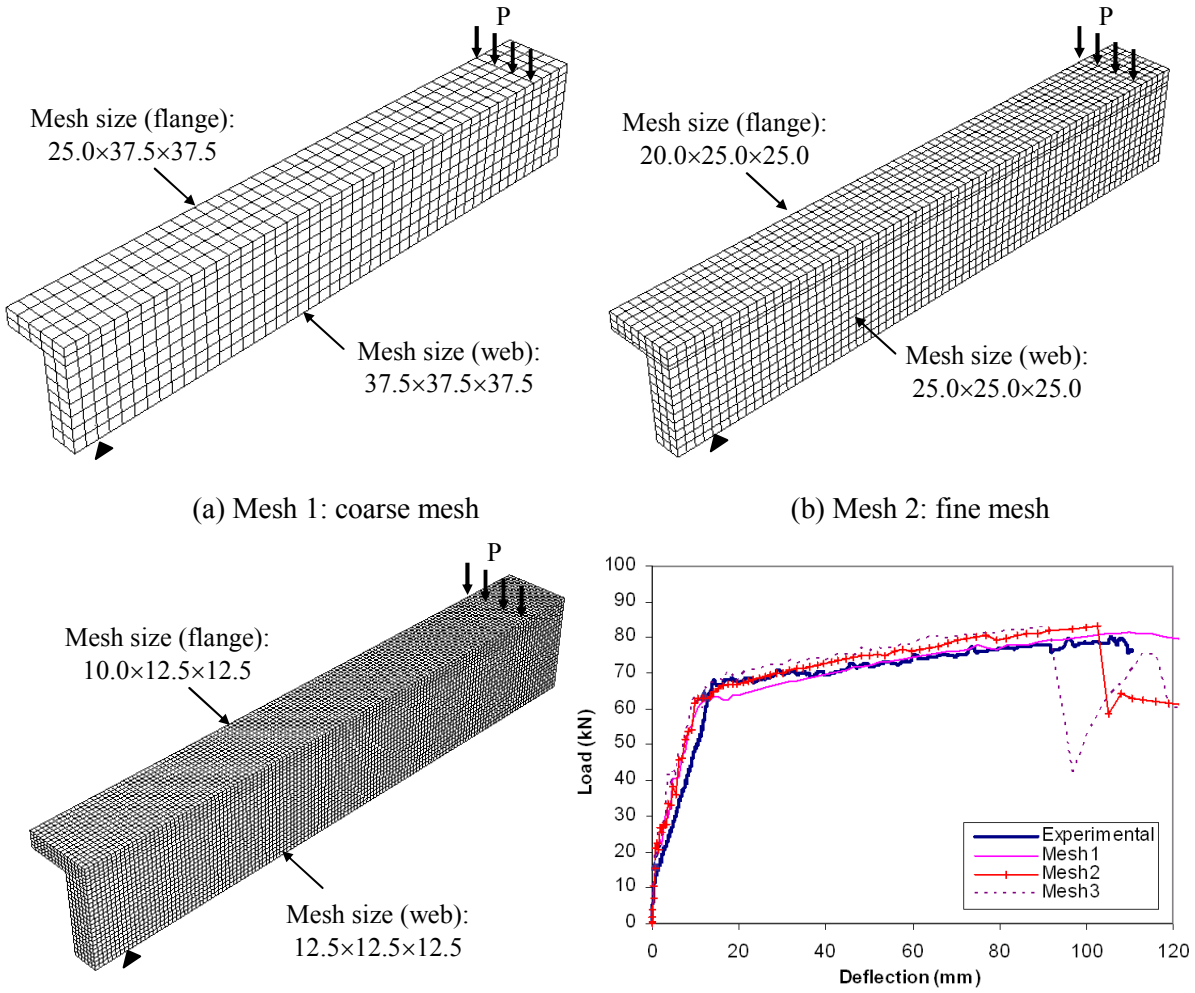

(a) Mesh 1: coarse mesh

(b) Mesh 2: fine mesh

(c) Mesh 3: very fine mesh

(d) Load-deflection comparison

Figure 5-26 Various modeling meshes and load-deflection comparison with mesh size

5.4.6 Results of FE analysis and comparisons

5.4.6.1 Load deflection comparisons

Comparisons of the load-deflection diagrams for the fully bonded and partially bonded beams are shown in Figure 5-27. For the fully bonded beam (NPFB), an experimental result and five FE analyses with different maximum bond strength, τ_{max}, values were compared (Figure 5-27 (a)). 'FEA-PB' denotes a perfect bond without limitation of the bond strength, while the maximum bond strength

of 4MPa, 6MPa, 8MPa, and 9MPa were applied to 'FEA-4MPa', 'FEA-6MPa', 'FEA-8MPa' and 'FEA-9MPa' models, respectively, to simulate the debonding failure.

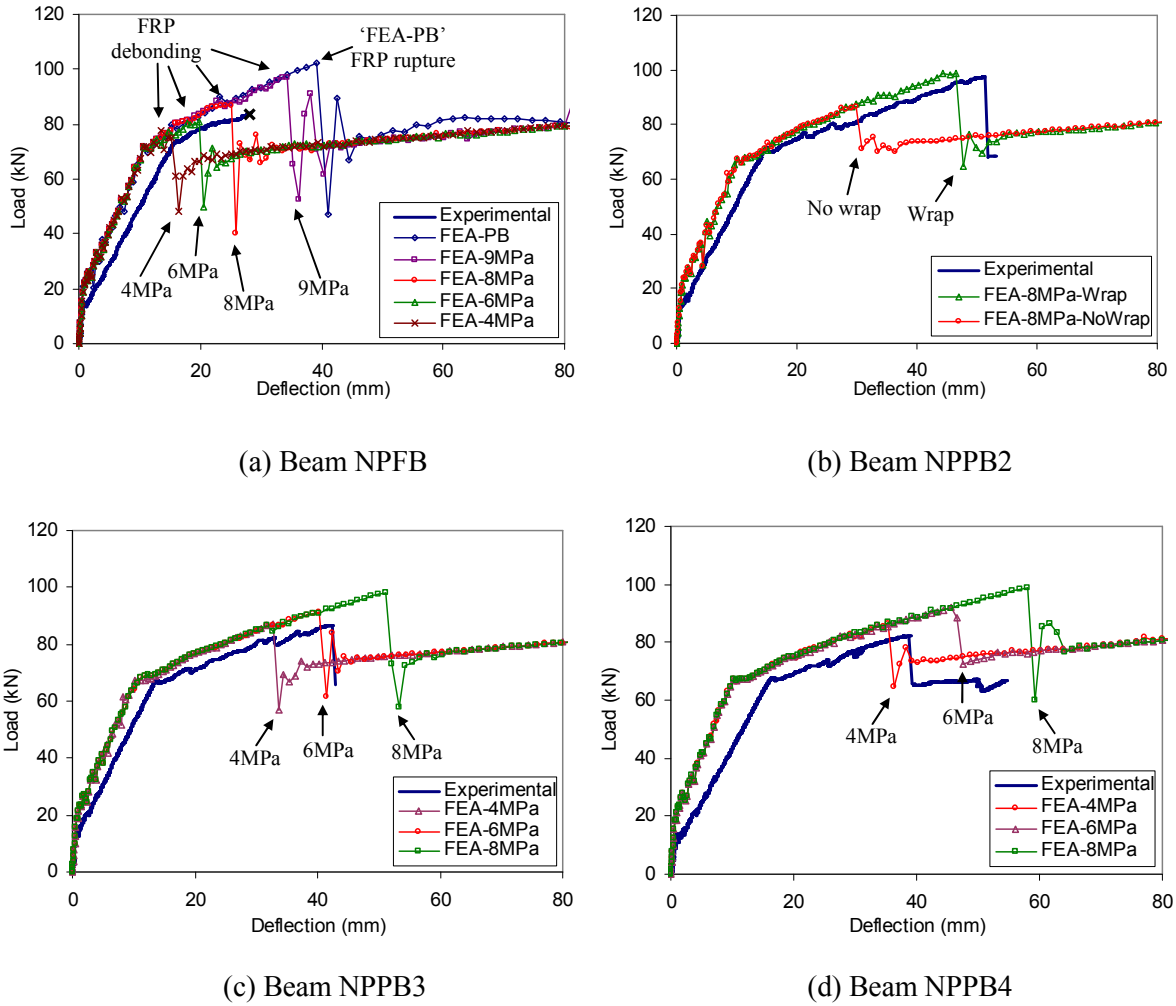

(a) Beam NPFB

(b) Beam NPPB2

(c) Beam NPPB3

(d) Beam NPPB4

Figure 5-27 Comparison of load-deflection curves between FE analysis and test results

The beam stiffness of the FE analysis was slightly higher than that of the tested beam, which is possibly caused by the material variations, such as the difference of the stiffness and the strength of the steel reinforcement and the CFRP plate. For beam NPFB, if the debonding failure does not happen and full composite action is exhibited, the beam will fail by FRP rupture as predicted by 'FEA-PB'. On the other hand, the analysis case with an assumed maximum shear strength of 8MPa

showed a close behaviour to the tested beam (NPFB) as shown in Figure 5-27(a). Therefore, the maximum bond strength for the tested beams can be considered to be 8MPa. This bond strength is at the upper bound of the existing proposed maximum bond strengths, generally taken to be between 4MPa and 8MPa (Dai et al. 2005, Chajes et al. 1996). However, considering the high concrete compressive strength (52.5MPa) and the good surface preparation (sandblasting) applied to the specimens, the high bond strength of the beams may be possible.

Figure 5-27(b) shows the comparison of the load-deflection diagram of beam NPPB2. If no U-wrap is considered at the bonded point with the maximum bond strength of 8MPa, then the ultimate response is well below the experimental results as shown in Figure 5-27(b). To simulate the effect of U-wraps at the bonded point, interfacial elements were added within the U-wrap (resulting in the bond strength was doubled) to simulate the increased bonded area due to the U-wraps. The FE simulation considering this wrapping effect (FEA-8MPa-Wrap) represented the ultimate behaviour of the beam well as shown in Figure 5-27(b). This shows that U-wraps at the bonded point can greatly improve the bond strength.

A comparison of the load-deflection diagrams of the beam NPPB3 and the beam NPPB4 between FE analysis and the experimental results are shown in Figure 5-27(c) and (d). For these cases, the ultimate response of the beam was over-estimated with the maximum bond strength of 8MPa. For beam NPPB3, FE simulation with the maximum bond strength of 6MPa showed similar behaviour to the experimental results, while FE analysis with maximum bond strength of 4MPa in beam NPPB4 showed a close response to the experimental results as shown in Figure 5-27(c) and (d). This implies that the maximum bond strength is affected by the bonded length and decreased as the unbonded length increased, inducing the debonding failure earlier as the unbonded length increased as observed in the tested beams.

5.4.6.2 Analysis of the bond stress distribution

Bond stress distributions along the CFRP plate in the fully bonded and the partially bonded beam are shown in Figure 5-28. Due to the relatively coarse mesh modeling compared to the linear elastic FE analysis shown in Figure 3-7, the bond stress distributions were not shown as a smooth pattern. However, it could investigate the general trend of the bond stress distributions in both the fully bonded and the partially bonded beams.

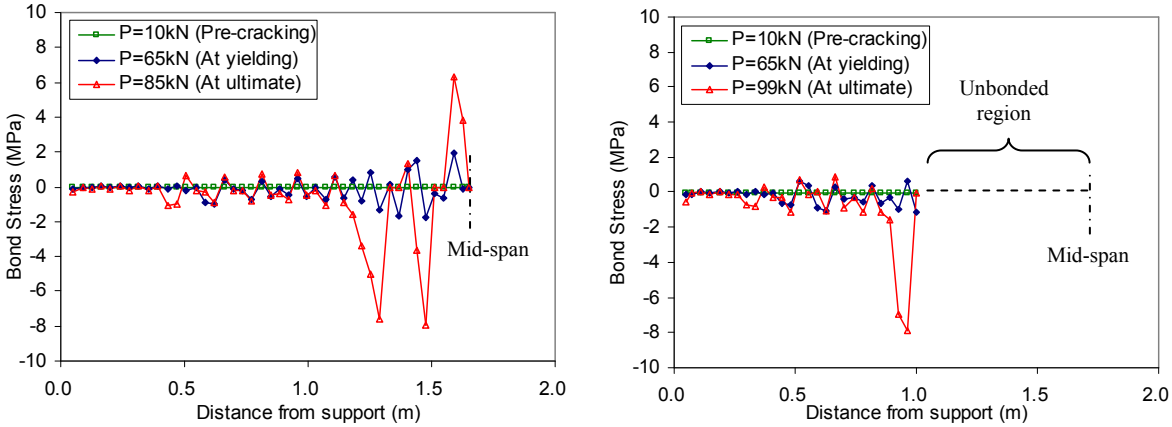

(a) Beam NPFB (b) Beam NPPB2

Figure 5-28 Bond stress distributions along the CFRP plate with various loading stages

Each figure contains the bond stress distributions at the elastic stage (pre-cracking, P=10kN), at the time of the steel reinforcement yielding (P=65kN), and at the ultimate stage of each beam. As expected, the bond stresses were increased as the applied load increased. For the fully bonded beam (NPFB), high bond stresses occurred near the loading point and FRP debonding was initiated at this location (Figure 5-28(a)), which is the same debonding failure phenomenon observed in the fully bonded beam during testing (the flexural crack induced debonding failure; see Figure 5-1(a)).

On the other hand, the bond stress was concentrated at the bonded point in the partially bonded beam (Figure 5-28(b)) due to the sudden change in the bond condition at this location. This concentrated bond stress induced the debonding failure of the bonded point, which shows the same result as the debonding failure observed in the partially bonded beams tested (see Figure 5-1(b)).

5.4.6.3 Comparison of FRP strain distributions

Three FRP strain gages were installed at the same locations in beams NPFB and NPPB2 for comparison purposes. The location of strain gages can be found in Section 4.6. The comparisons of the measured and predicted FRP strain distributions are shown in Figure 5-29 and Figure 5-30 at the service load stage (P = 60kN) and at the post yielding stage (P = 80kN), respectively.

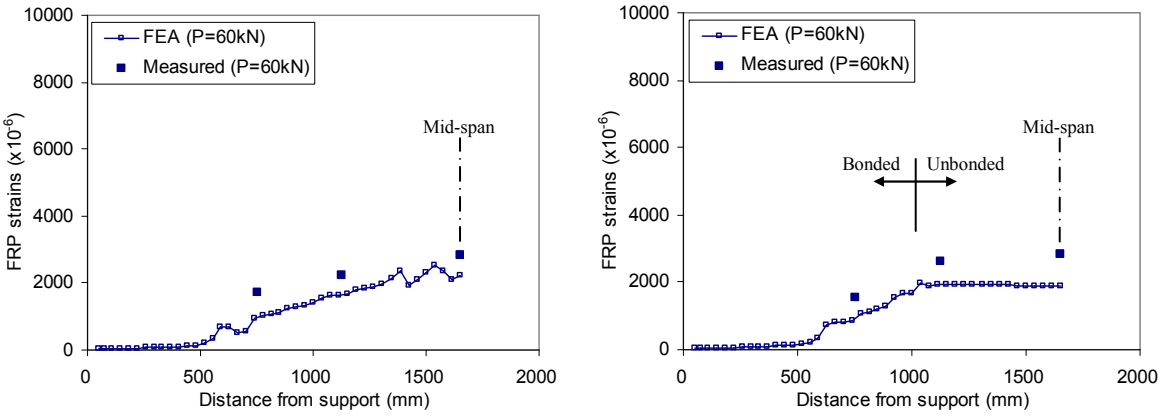

(a) Beam NPFB (b) Beam NPPB2

Figure 5-29 Comparison of FRP strain distribution along CFRP plate at service load condition (P = 60kN)

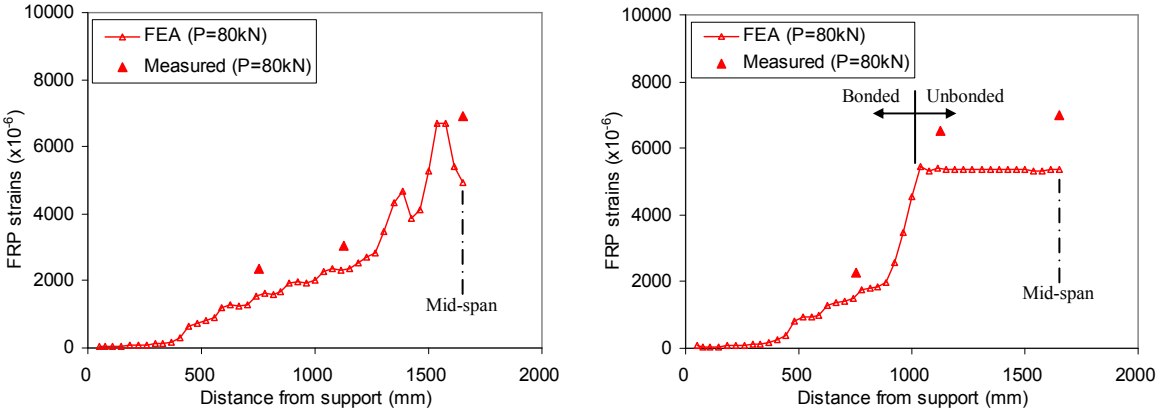

(a) Beam NPFB (b) Beam NPPB2

Figure 5-30 Comparison of FRP strain distribution along CFRP plate at post-yielding stage (P = 80kN)

The strains in the FRP plate from experiments were generally higher than those predicted by FE modeling. The difference between the strain distribution for the fully bonded and the partially bonded beams was prominent at the bonded point after steel yielding as shown in Figure 5-30. The FRP strains in the partially bonded beams were suddenly increased at the bonded point and remained constant within the unbonded region, while the strains of the fully bonded beam near the bonded point increased gradually compared to the partially bonded beams. For the measured FRP strains within the unbonded region, the mid-span strain was slightly higher than that near bonded point. This is because there might be a slight friction between the FRP and the concrete. Overall, the FRP strains predicted by FE analysis showed a reasonable agreement with the experimental results.

5.5 Summary

The test results of externally bonded (EB) CFRP plate strengthened RC T-beams were presented and discussed in this chapter. The test results were compared with the predictions by the proposed analytical model. Three-dimensional nonlinear finite element analysis was also performed to investigate the debonding failure and the interfacial stress distributions. The specific conclusions from this investigation are as follows:

1. Typical flexural crack induced debonding failure was observed in the fully bonded beam (NPFB). The debonding was initiated from one of the flexure cracks near the loading point and the debonding was propagated along the concrete interface followed by the complete debonding.
2. For the partially bonded beams, the debonding failure was initiated at the bonded point with greater load capacity in comparison to the fully bonded beam. This was because the flexural crack induced debonding was avoided due to intentional unbonding and the U-wraps at the bonded point increased the bond strength in the partially bonded beams.

3. The measured FRP strains at the mid-span were almost identical between the strengthened beams without regard to the bond condition, while the concrete strains at mid-span were greater in the partially bonded beam compared to the fully bonded beam inducing more curvature and deflection.
4. The predicted load-deflection behaviour and the strain distribution matched the experimental results well except that the ultimate response at failure was over-estimated due to early debonding failure that occurred in the tested beams.
5. Three-dimensional nonlinear finite element (FE) analysis utilizing interfacial elements and contact modeling showed that the maximum bond stress in the fully bonded beam was approximately 8MPa; the effect of U-wraps at transition point was significant to improve the flexural capacity; and the maximum bond strength in the partially bonded beams was decreased with the increase of the unbonded length. FE analysis also showed that the bond stress in the fully bonded beam was high near loading point at the crack location, inducing a debonding failure at that location. High bond stress occurred at the transition point where the debonding was initiated in the partially bonded beams.

Chapter 6
Non-prestressed NSM Strengthened Beams

6.1 General

Test results and discussions on the behaviour of non-prestressed NSM CFRP strengthened beams (Group II) are presented in this chapter. Failure modes and load-deflection diagrams are discussed in Section 6.2, and comparisons between analytical predictions and experimental results are described in Section 6.3. An advanced model is proposed to address the complete behaviour of the beams including the effect of the FRP slip and the gradual concrete failure in Section 6.3. Test results of NSM beams are also compared with the EB strengthened beams to investigate the effectiveness of each strengthening system in Section 6.4.

6.2 Test Results and Discussions

Test results of non-prestressed NSM FRP strengthened beams in terms of applied load and deflection at cracking, at steel yielding, and at ultimate state are summarized in Table 6-1, along with a description of the failure mode.

Table 6-1 Summary of non-prestressed NSM strengthened beam test results (Group II)

Test Group	Beam Name	P_{cr} (kN)	Δ_{cr} (mm)	P_y (kN)	Δ_y (mm)	P_u (kN)	Δ_u (mm)	Deform-ability, μ (Δ_u / Δ_y)	Failure mode*
-	Control	13.37	0.69	68.13	14.03	79.39	108.70	7.75	CC
Group II	NBFB	17.39	0.97	74.36	16.21	124.09	86.35	5.33	FR
	NBPB2	15.98	0.74	72.55	14.15	111.45	93.12	6.58	CC
	NBPB2.5	13.48	0.89	69.39	12.65	111.69	90.12	7.12	CC
	NBPB3	14.23	0.68	70.60	14.36	109.39	99.74	6.95	CC
	NBPB4	14.44	1.21	69.95	17.01	104.58	114.29	6.72	CC

* CC: Concrete Crushing, FR: FRP Rupture

6.2.1 Failure modes and load-deflection behaviour

Failure modes of the fully bonded beam (NBFB) and the partially bonded beam (NBPB4) in Group II beams are shown in Figure 6-1. The other partially bonded beams with different unbonded lengths (NBPB2, NBPB2.5, and NBPB3) showed the same failure mode as beam NBPB4. Photographs of the failure mode for all tested beams can be found in Appendix C. Unlike the typical premature debonding failure observed in the conventional EB strengthened beams (see Section 5.2.1), almost the full capacity of the FRP bar was exhibited without a sudden premature failure in this system.

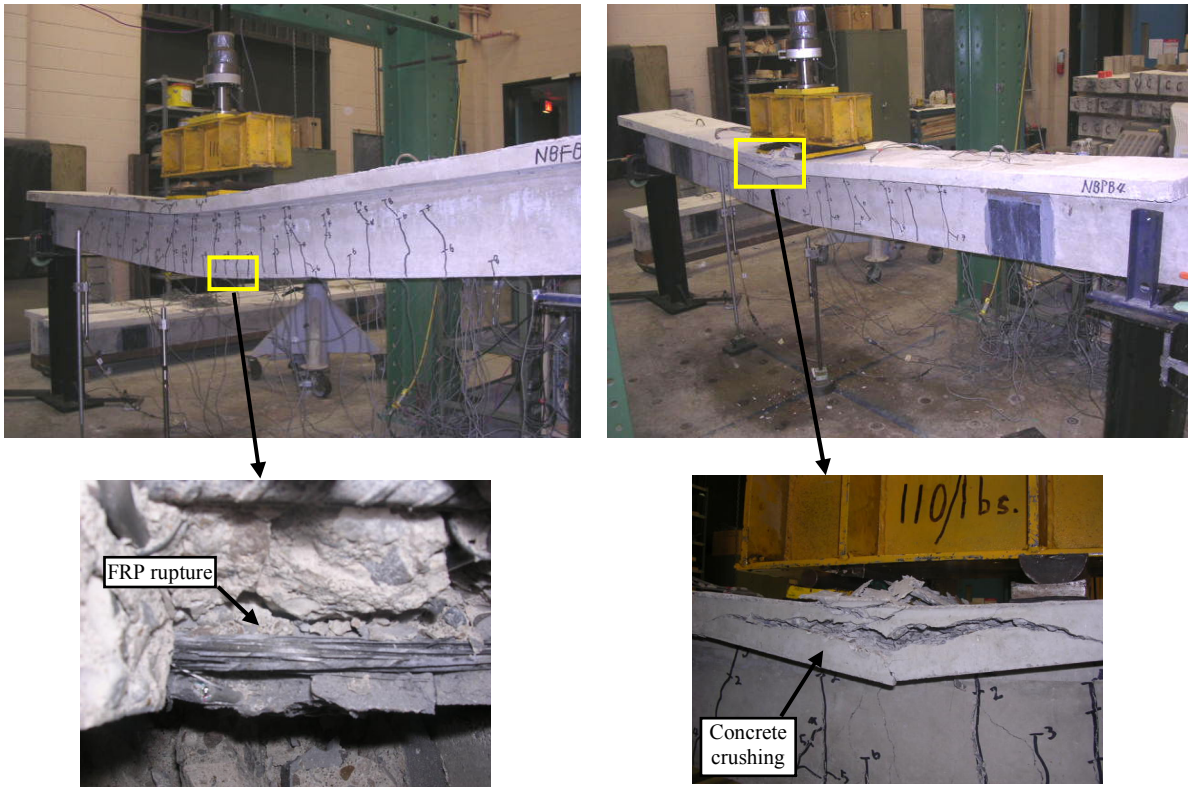

(a) Beam NBFB (b) Beam NBPB4

Figure 6-1 Failure modes of NSM strengthened beams

For the fully bonded beam (NBFB), the FRP bar ruptured inside the epoxy adhesive after sustaining a large applied load with a large deflection. The location of the FRP bar rupture was near the mid-span between the loading points as shown in Figure 6-1(a). At the time of FRP rupture, a

limited number of concrete compression cracks were observed at the top flange of the section. The failure mode of four partially bonded beams (NBPB2, NBPB2.5, NBPB3, and NBPB4) was concrete crushing at the mid-span as shown in Figure 6-1(b). This concrete crushing occurred gradually with a gradual loss of the section at top fibre in the beam's cross-section. The applied load did not drop suddenly at the initiation of the concrete crushing at the top fibre, but instead the beam sustained almost the same level of load capacity with increasing the beam deflection. Finally, the complete crushing of the concrete flange happened with a significant load drop when one of the compression steel reinforcements in the flange buckled after significant section loss of the concrete at the mid-span. For beams NBPB2 and NBPB3, although the top fibre of the concrete flange was severely damaged (Figure C-2 in Appendix C) the applied load did not drop, and the test was stopped since the maximum stroke of the actuator was reached. Thus, the ultimate deflection response of these beams may not have been achieved. Subsequently, beam NBPB2.5 with an unbonded length of 2×750mm was tested to failure because the ultimate deflection response of beams NBPB2 (L_{ub}=2×650mm) and NBPB3 (L_{ub}=2×850mm) could not be obtained. For beams NBPB2.5 and NBPB4, a sudden drop of the load was observed after severe section loss of the concrete with high deflection.

The load-deflection diagrams of the beams are shown in Figure 6-2. The load-deflection curve of the fully bonded beam (NBFB) increased linearly up to the steel yielding point and became nonlinear close to the ultimate state. No FRP slip was measured at both ends of the beam, but some slip marks were found at the epoxy-FRP interface near the mid-span during the post-failure investigation of segments taken from the tested beams at several locations as shown in Figure 6-3. Based on these slip marks and the nonlinear load-deflection behaviour (Figure 6-2), it is assumed that partial FRP debonding occurred in the mid-span region, resulting in the large nonlinear deflection in the response of the fully bonded beam near the ultimate stage.

For the partially bonded beams, the load-deflection curves did not suddenly drop at onset of the concrete crushing, but became almost flat while sustaining almost the same applied load as shown in Figure 6-2 (individual load-deflection curves can also be seen in Figure 6-6). This is due to a gradual concrete failure and redistribution of compression stresses after the onset of the concrete crushing. The stresses were redistributed from the crushed concrete to the compression steel reinforcement and the undamaged concrete section, so that the beam could sustain almost same applied load with increased the deflection. This gradual failure in the concrete is described in more detail in Section 6.3.3.

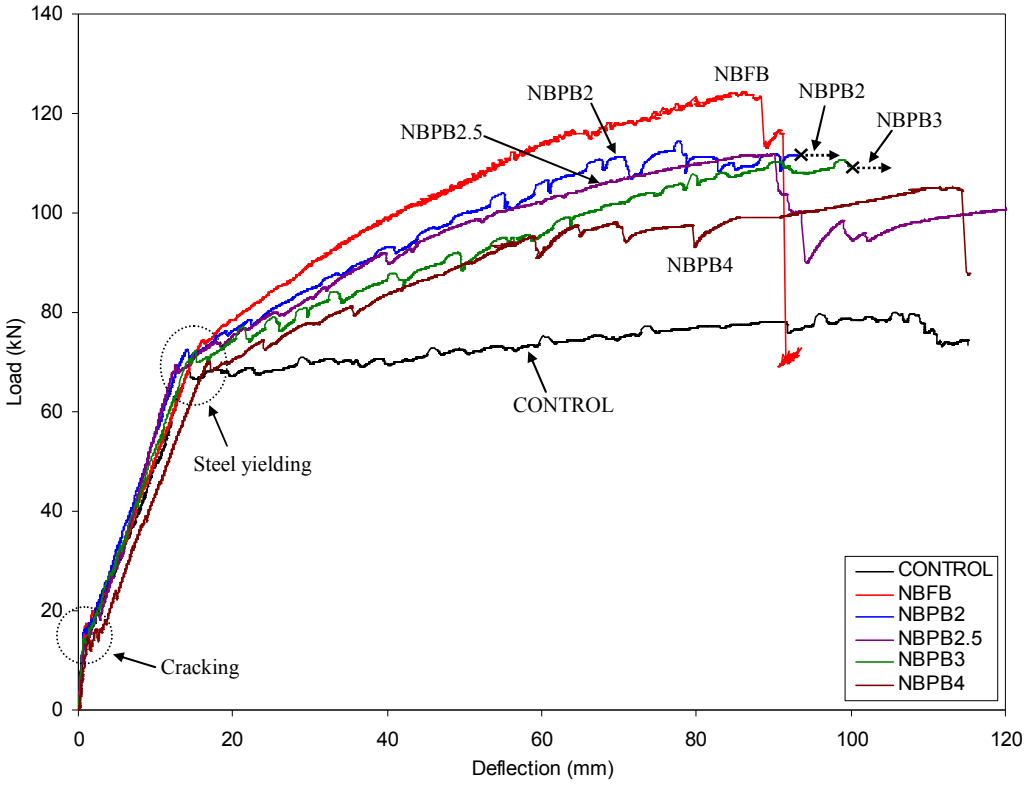

Figure 6-2 Load-deflection diagrams of Group II beams

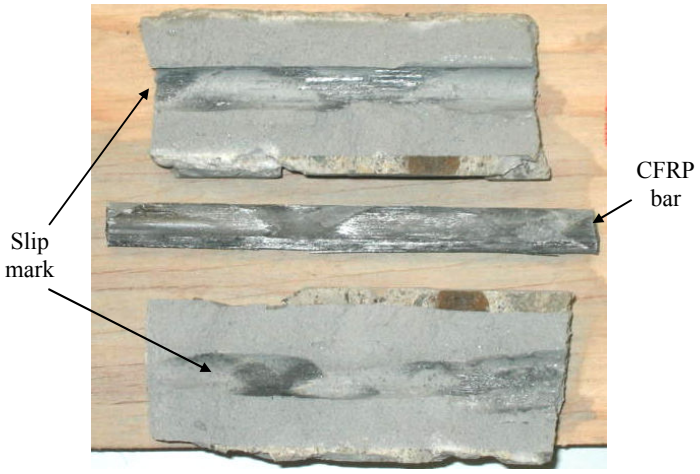

Figure 6-3 Slip marks at the epoxy-FRP interface of beam NBFB at mid-span

The ultimate response of beams NBPB2 and NBPB3 is expected to go further as indicated in the dotted arrows in Figure 6-2 because the tests stopped at the maximum stroke. The load-deflection response of beam NBPB2.5 was between those of beams NBPB2 and NBPB3 as expected. However, the ultimate deflection was slightly less than that of beam NBPB2. This is because the complete concrete crushing failure happened when one of the compression steel reinforcing bars in the flange buckled, and therefore is dependent on the actual location of the top steel bars and the geometry of the beam flange which may vary for each beam. For beam NBPB4, the ultimate deflection was greater than any other beams, but the ultimate load carrying capacity was reduced.

The load-deflection behaviour up to steel reinforcement yielding was almost identical without regard to the bond condition. At the post yielding stage, the stiffness of the beams was decreased as the unbonded length increased as shown in Figure 6-2. As a result, the deflection of the partially bonded beams was improved at the same applied load compared to the fully bonded beam. However, the ultimate deflection at failure in the partially bonded beams showed only a slight increase compared to the fully bonded beam (4.4% ~ 32.4%) due to the complex behaviour including slip of FRP reinforcement and the gradual concrete failure. The ultimate load in the partially bonded beams

was slightly decreased compared to the fully bonded beam (10.0% ~ 15.7%) as the unbonded length increased. This is because the ultimate response was controlled by FRP in the fully bonded beam while the failure was controlled by the concrete in the partially bonded beams due to the increase of the concrete strains with the increase of the unbonded length.

6.2.2 Strain distributions

Strain gages were installed at mid-span and near the bonded point to measure the strains in the concrete, the steel reinforcement, and the FRP reinforcement. The general pattern of the strain distributions was similar to the strains in the beams strengthened with EB CFRP plate (see Section 5.2.2), so detailed investigations and discussions are not presented in this section. The complete measured strains for all beams are found in Appendix D.

Comparisons of load versus strain curves at mid-span for the test beams are shown in Figure 6-4. The load-FRP strain diagrams were almost identical without regard to the bond condition (Figure 6-4 (a)). This is because there is almost no stress increase in the steel reinforcement at the post-yielding stage due to steel yielding, and as a result the stresses in the FRP reinforcement must be almost identical at the same applied load without regard to the bond condition in order to satisfy the moment equilibrium at the mid-span. Note that since many FRP strain gages failed near ultimate stage, the measured ultimate strains were less than expected values at failure.

On the other hand, the concrete strains at a given load were increased in the post-yielding stage as the unbonded length increased (Figure 6-4(b)). The FRP strain is constant within the unbonded length and represented the average concrete strain at the level of the FRP within the unbonded length. Thus, the concrete strains must increase to sustain the same uniform strain in the FRP for a given load level as the unbonded length increases. The same behaviour was observed in EB strengthened beams, and a detailed description of this behaviour can be found in Section 5.2.2.

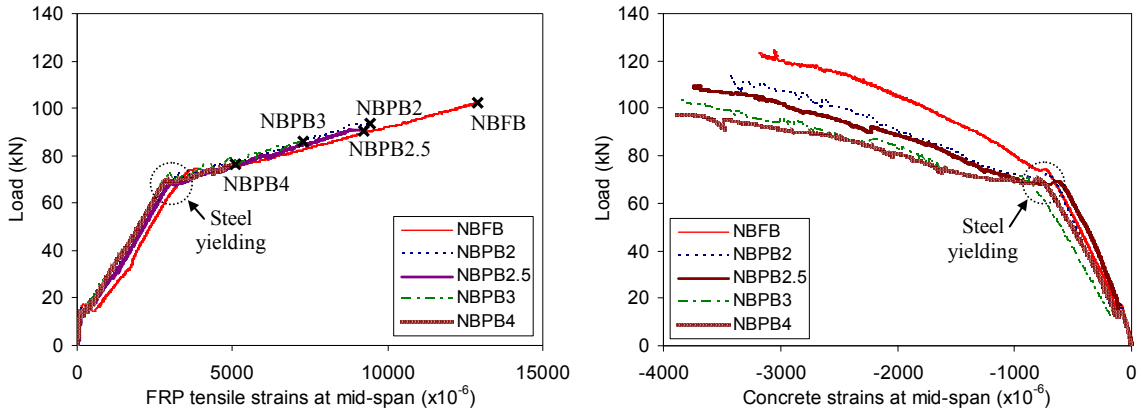

(a) FRP strains with load (b) Concrete strains with load

Figure 6-4 Comparison of load-strain curves at mid-span

6.2.3 Crack distributions

The sketches of the crack distribution at the applied load of 60kN in Group II beams are shown in Figure 6-5. The crack distributions at failure, as well as at service load (P=60kN), are shown in Appendix E. In general, the crack patterns for the NSM beams were similar to those in the EB strengthened beams. The spacing of the cracks in the fully bonded beam (NBFB) was generally smaller compared to the partially bonded beams due to the complete bond between the concrete and the FRP bar in the fully bonded beam, as described in Section 5.2.3. However, this crack spacing difference between fully bonded and partially bonded beams was not much prominent compared to the EB system beams. The comparison of the crack patterns between the two systems (EB and NSM systems) is performed in Section 6.4.2.

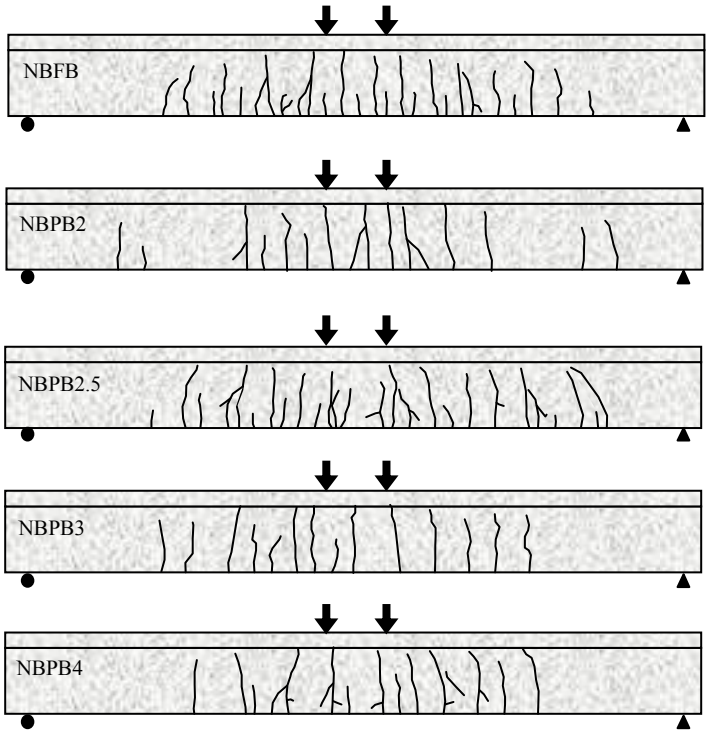

Figure 6-5 Crack distributions at service load (P = 60kN) (Group II beams)

6.3 Advanced Analytical Model

An advanced analytical model is proposed in this section. The basic model developed in Chapter 3 does not consider the effect of FRP reinforcement slip and the gradual concrete failure that occurred in the NSM strengthened beams (Section 6.3.1). An idealized reduced flange section is applied in Section 6.3.3 to simulate the progressive concrete crushing failure. An FRP slip model is proposed in Section 6.3.4.

6.3.1 Comparison between basic model and experimental results

Experimental load-deflection curves were compared to the predictions based on the analytical model with no FRP slip and without consideration of the stress redistribution (concrete gradual failure) in Figure 6-6. The general behaviour of the beam could be represented well up to near failure. However,

the post-crushing stage with the nonlinear behaviour could not be predicted as shown in Figure 6-6. Therefore, a more advanced model is required to demonstrate the complete behaviour of the beam including the effect of the FRP slip and the progressive concrete crushing failure.

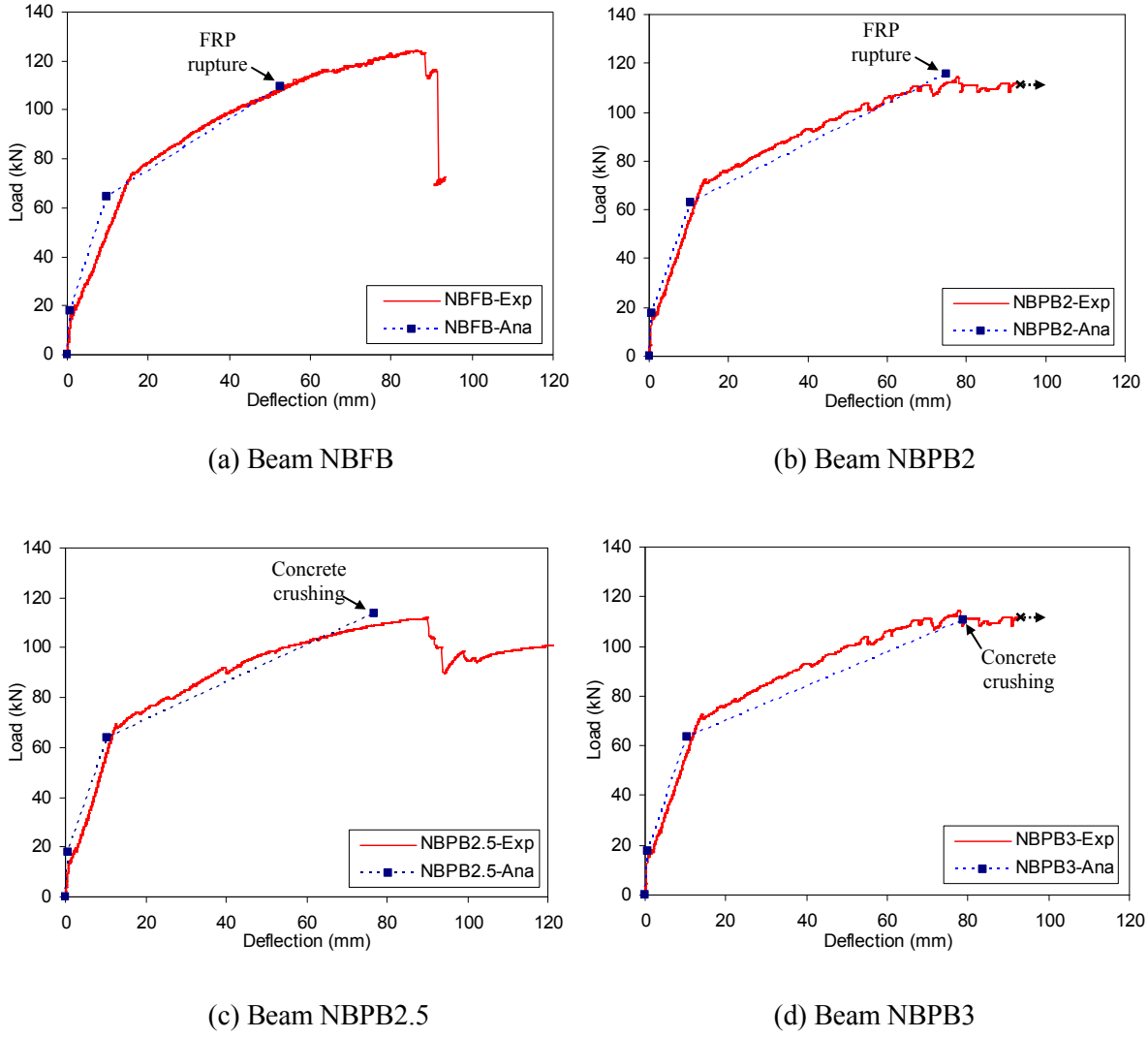

(a) Beam NBFB

(b) Beam NBPB2

(c) Beam NBPB2.5

(d) Beam NBPB3

Figure 6-6 Load-deflection comparison between measured values and predictions without considering the effect of the FRP slip and the concrete gradual failure

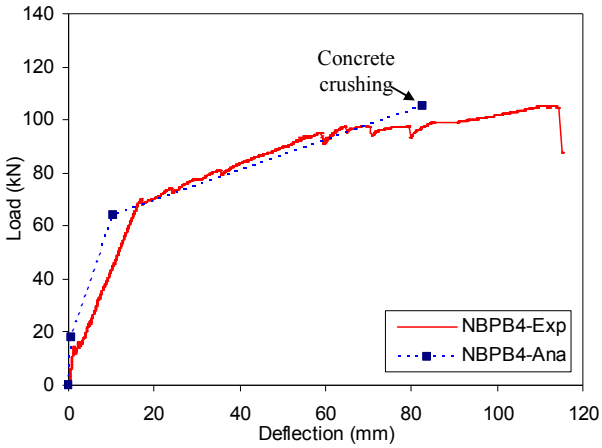

(e) Beam NBPB4

Figure 6-6 Load-deflection comparison between measured values and predictions without considering the effect of the FRP slip and the concrete gradual failure (continued)

6.3.2 Material constitutive model

For the concrete compression behaviour, the same parabolic concrete stress-strain curve as the basic model proposed by Collins and Mitchell (1987) is used. However, the ultimate strain at onset of the concrete crushing was increased to 0.0045 based on the real concrete compressive strain at onset of crushing. On the other hand, the tension strength of the concrete was neglected at the post-cracking stage and the effect of the tension stiffening was not considered. The constitutive model of the steel reinforcement was defined using a tri-linear elastic-plastic model, the same as the model used in FE analysis, to represent the strain hardening effect of the steel reinforcement. The CFRP bar was assumed to be a linear elastic material up to failure. The material constitutive models for the advanced analytical model are shown in Figure 6-7.

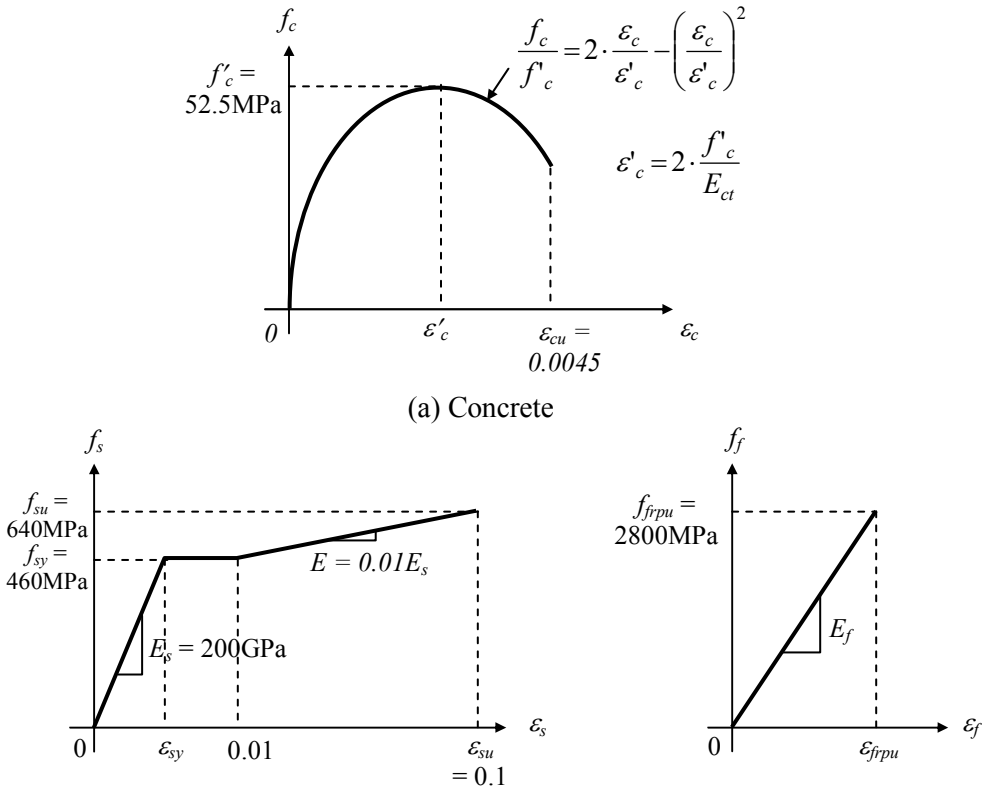

Figure 6-7 Stress-strain relationship for concrete, steel reinforcement, and CFRP bar

6.3.3 Model for concrete gradual failure

As discussed in the Section 6.2, the partially bonded beams exhibited large deflections beyond the onset of concrete crushing while the load capacity was maintained, as shown in Figure 6-6. To predict this behaviour, gradual stress redistribution after initial concrete crushing must be considered in the analytical model.

Figure 6-8 shows a typical gradual failure observed in a T-beam from the initiation of the concrete crushing to the complete crushing at failure. During this period, the deflection was significantly increased without a reduction in the load capacity of the beam. At complete crushing, accompanied by buckling of the compression reinforcement (last figure in Figure 6-8), the applied load drops suddenly.

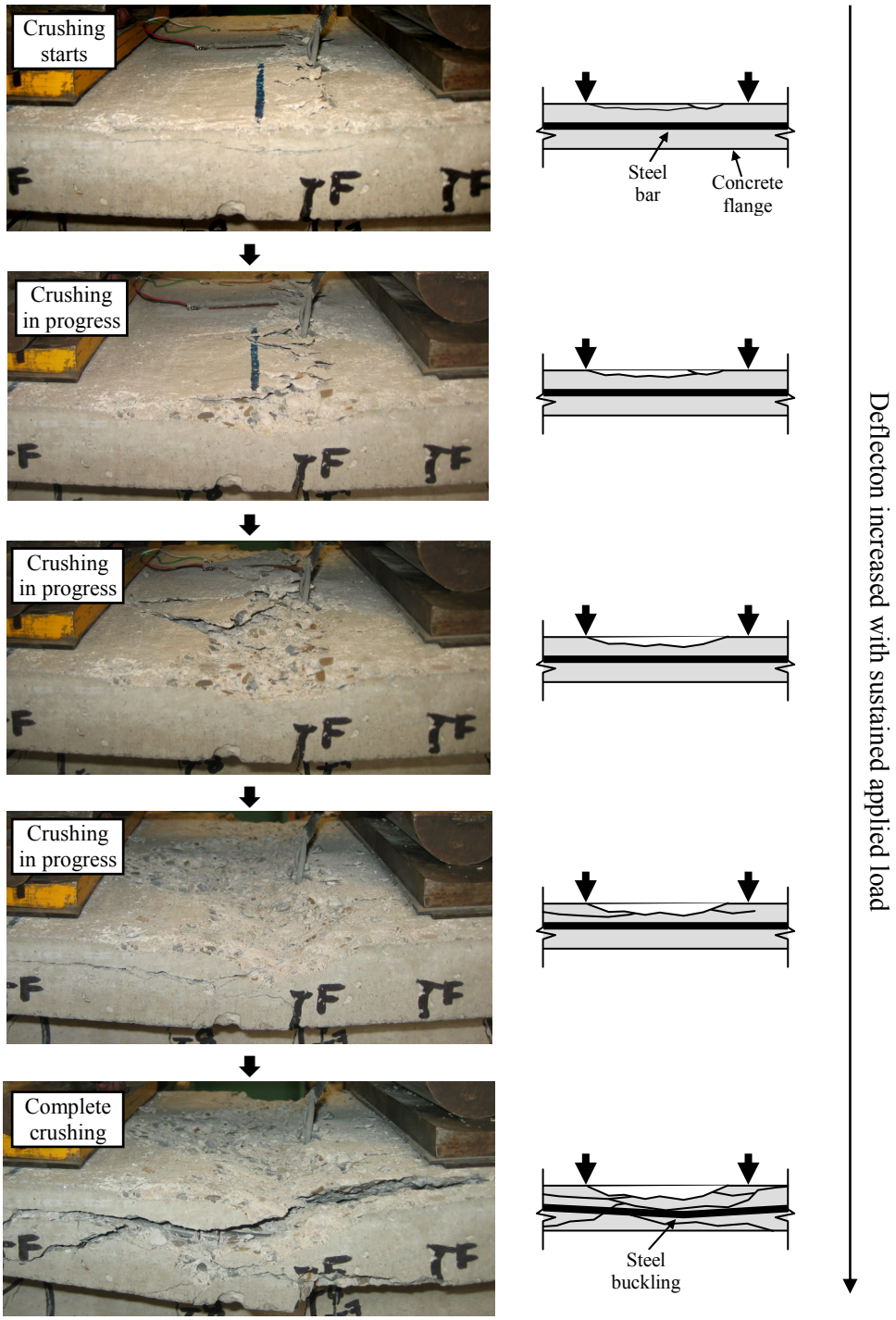

Figure 6-8 Gradual failure of the RC T-beam at mid-span

The basic mechanism of this progressive failure is due to stress redistribution in the T-beam flange. Once the concrete strain goes beyond the ultimate strain, the stress in the concrete is decreased to near zero. The reduction in compressive stress at the extreme fibre must be redistributed elsewhere in order for the beam to continue to sustain the applied load. For the T-beams, the large flange width results in a shallow compression zone (small neutral axis depth). Thus, the loss of compression area due to crushing can be accommodated by redistribution of compression stresses to the compression steel reinforcement and other parts of the undamaged concrete flange. As the flange thickness decreased (crushing in progress), the strains at the top and bottom fibre keep increasing. As a result, the curvature increases between the loading points and deflection increases as shown in Figure 6-9.

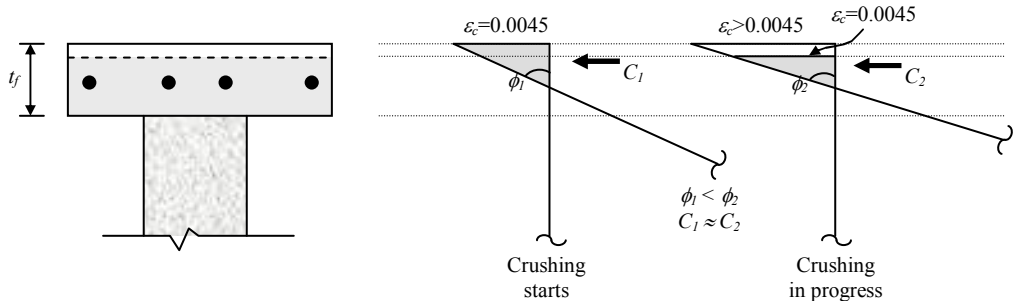

Figure 6-9 Strain profiles of concrete gradual failure

Figure 6-10 shows the idealized section model of a T-beam at the post-crushing stage. Beyond a concrete strain of 0.0045, crushing continues and destroys parts of the concrete flange as shown in Figure 6-10(a). To simulate the progressive crushing in the flange, the flange thickness was reduced in increments of 5mm uniformly between the loading points (See Figure 6-10(b)) and the analysis was repeated. 5mm increments of the reduced flange thickness were chosen to be enough to represent the behaviour of the beam. The maximum reduced thickness of the flange was assumed to be 35mm at which the compression steel reinforcement buckled and complete concrete crushing occurred.

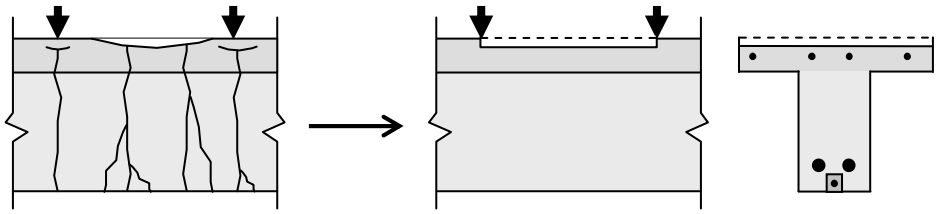

(a) Progressive failure (b) Idealized model

Figure 6-10 Idealized Model for gradual failure at post-crushing stage

The predicted load-deflection diagrams considering concrete gradual failure with no FRP slip are plotted in Figure 6-11. There was no modification in the predicted behaviour for Beams NBFB and NBPB2 because the predicted failure was FRP rupture for these beams; therefore, the consideration of concrete gradual failure does not affect the predictions of these beams. For the beams with longer unbonded lengths, the ultimate deflection behaviour was increased by the gradual crushing failure and decreased thickness of concrete flange as shown in Figure 6-11(c), (d), and (e). However, the predicted ultimate failure in beams NBPB2.5 and NBPB3 was FRP rupture at the reduced flange thicknesses of 45.54mm and 39.95mm, respectively, while the observed failure was concrete crushing. For beam NBPB4, the beam fails at the flange thickness of 35mm, but the predicted ultimate load was overestimated compared to the measured ultimate load. In addition, the nonlinear behaviour that occurred in all tested beams could not be represented well by the model that only considered the concrete gradual failure as shown in Figure 6-11. Therefore, the effect of possible slip of the FRP reinforcement must also be considered in addition to the concrete gradual failure to address complete behaviour of the beams.

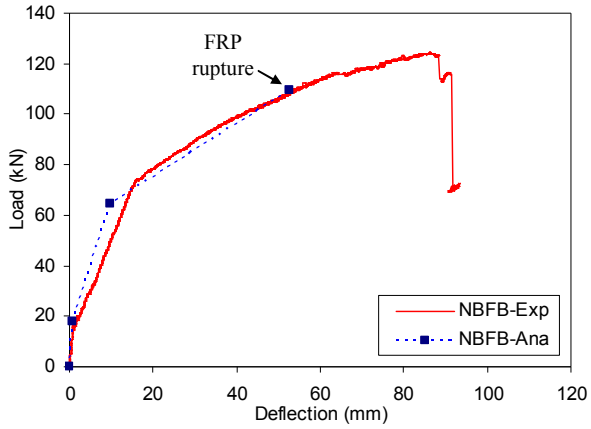

(a) Beam NBFB

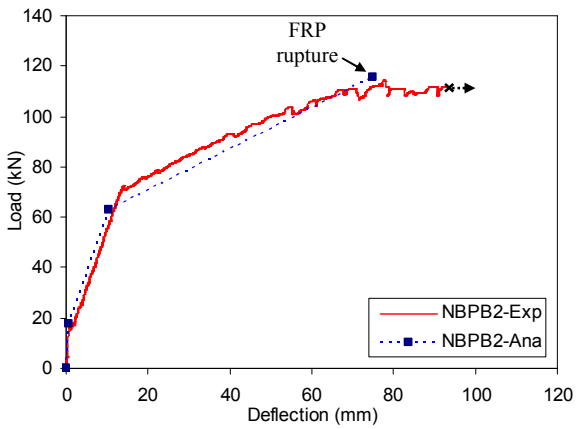

(b) Beam NBPB2

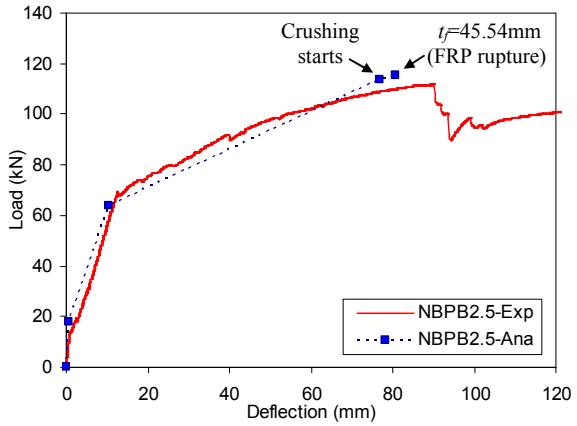

(c) Beam NBPB2.5

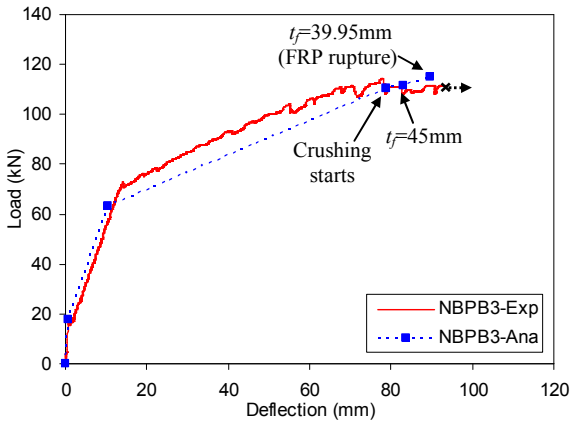

(b) Beam NBPB3

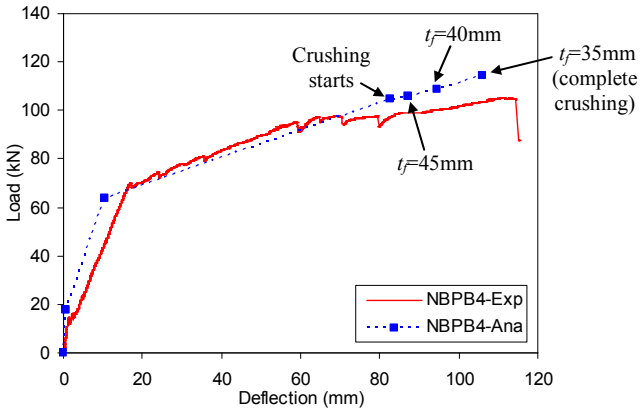

(e) Beam NBPB4

Figure 6-11 Load-deflection comparison between measured values and predictions considering the effect of concrete gradual failure with no FRP slip

6.3.4 FRP slip model

Although extensive concrete crushing was not observed in the fully bonded beam (NBFB) before FRP rupture, the deflection was much greater than the prediction based on conventional section analysis as shown in Figure 6-11. As discussed in Section 6.2, this behaviour is assumed to be caused by FRP slip at high stress levels. The FRP slip was evident based on the slip mark found at the FRP-epoxy interface (Figure 6-3) and the non-linearity in the load-deflection and load-concrete strain diagrams (Figure 6-1 and Figure 6-4). However, it is not possible to determine the exact slip initiation point and propagation region. Some researchers (Lorenzis 2004, Lorenzis and Nanni 2002) have suggested bond stress-slip relationships for NSM strengthened beams. However, it is difficult to apply those proposed relationships to the tested beams since the material and geometry properties are different. For this reason, the slip initiation and its propagation were chosen based on the observation of the test results.

It is assumed that slip initiated at 95% of the ultimate FRP strength in the fully bonded beam (NBFB) because the initiation of the nonlinear behaviour was prominent at approximately 95% of the ultimate load. For beam NBPB2 (unbonded length of 2×650mm), the initiation of slip was also assumed at 95% of the ultimate FRP strength for the same reason as the beam NBFB. The initiation of FRP slip is directly related to the bond (shear) stress at the FRP to concrete interface as described in Section 2.4.2, and the bond stress, τ, is proportional to the difference in the normal FRP stress, $d\sigma$, over a unit length, as illustrated in Figure 6-12. In the partially bonded beams, the normal stress changes significantly at the transition point, as shown in Figure 6-13, and the slip initiation is assumed to be caused by this difference in the FRP stress and resulting large bond stress at the transition point. Based on the assumption that slip initiated at a FRP stress of 95% of the ultimate FRP strength for beam NBPB2, the applied load corresponding to that value was determined. The FRP stress at the transition point (bonded part) at this load level was calculated to be 21% of the FRP

ultimate strength using a section analysis. Considering the bonded and unbonded FRP stress levels at the transition point, the normal stress difference is calculated to be 74% of the FRP strength in beam NBPB2 (see Figure 6-13).

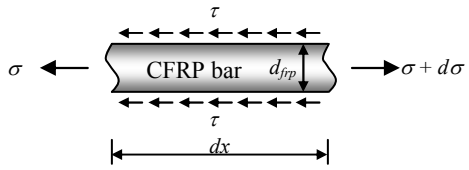

$$\frac{\pi d_{frp}^{\,2}}{4}\sigma + \pi d_{frp}\tau\, dx = \frac{\pi d_{frp}^{\,2}}{4}(\sigma + d\sigma)$$

$$\therefore \tau = \frac{d_{frp}}{4}\frac{d\sigma}{dx}$$

Figure 6-12 Relationship between bond (shear) and normal stresses

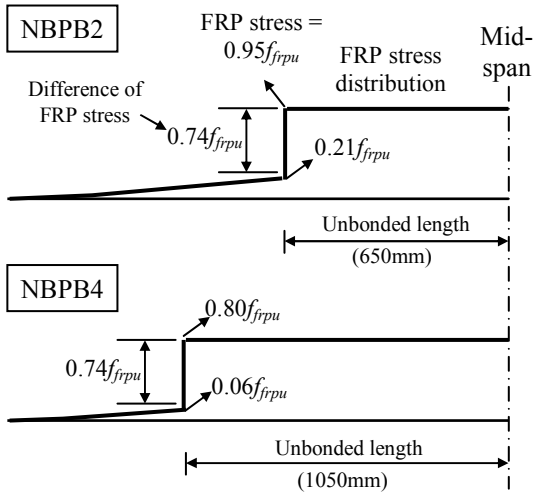

Figure 6-13 Determination of the FRP stresses at slip initiation

Based on the assumption that the slip initiates at the bond stress corresponding to the same normal stress difference (74% of the ultimate FRP strength) for all of the partially bonded beams, the slip initiation FRP stress for beams NBPB2.5, NBPB3 and NBPB4 beams was determined. In this manner, the FRP stresses at the bonded point and unbonded point for beam NBPB4 are calculated to be 6% and 80% of the FRP strength, respectively, as shown in Figure 6-13. Similarly, the FRP stress at slip

initiation for beams NBPB2.5 and NBPB3 were also calculated to be 90% and 85% of the FRP strength, respectively.

Once the FRP stress level reaches the slip initiation stress, an unbonded region was assumed to develop in the fully bonded beams to simulate the propagation of slip. In the partially bonded beams, the unbonded length was increased to simulate slip, as shown in Figure 6-14. As slip propagates, the FRP stress is maintained at the same level while the concrete strains are increased as shown in Figure 6-14. Therefore, the beam deflection is increased while sustaining the applied load.

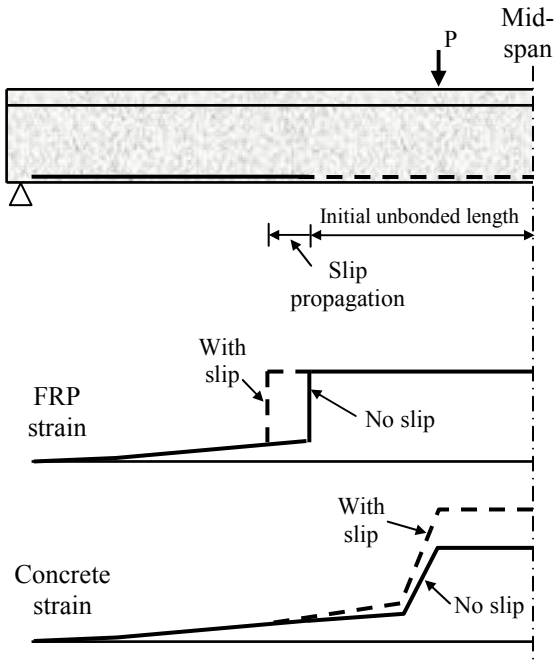

Figure 6-14 Modeling of FRP slip propagation

For the fully bonded beam, the unbonded region was created at mid-span when the FRP stress reaches 95% of the FRP strength, and this unbonded region was increased to simulate the slip propagation. The analysis was repeated at unbonded length increments of 100mm and the final stage of the analysis was done by setting the FRP stress as the ultimate strength since the failure mode was by FRP rupture. 100mm increments of the unbonded length were selected to be enough to represent

the behaviour of the beam. For the partially bonded beams, soon after the initiation of slip and the increase of the unbonded region, the concrete strain reached its ultimate strain (0.0045) and started to crush. From this point, both slip and concrete crushing progressed. The analysis was performed by decreasing the flange thickness in increments of 5mm while finding the required unbonded length due to slip to maintain the same FRP stress. The analysis was repeated until the thickness of the concrete flange was 35mm which corresponds to complete concrete crushing of the flange.

6.3.5 Comparison with test results and discussions

A comparison of the load-deflection diagrams between the predictions considering the concrete gradual failure and FRP slip and experimental results is shown in Figure 6-15. For the fully bonded beam (NBFB) the ultimate deflection was predicted well, while the ultimate load carrying capacity of the beams was slightly less than the experimental results. This is possibly caused by the deviation of the material properties and the model assumptions.

For beams NBPB2, NBPB2.5, and NBPB3, concrete crushing started right after onset of FRP slip as shown in Figure 6-15(b), (c) and (d). The ultimate load carrying capacity of the NBPB2, NBPB2.5, and NBPB3 beams was well predicted, but the ultimate deflection predicted by the model was slightly higher than that of the experimental results. For beams NBPB2 and NBPB3, the tests were stopped due to the limitation of the stroke, so the actual ultimate deflection might be higher as indicated by dotted arrows in Figure 6-15(b) and (d). For beam NBPB2.5, the ultimate crushing happened at the flange thickness of around 40mm as shown in Figure 6-15, where one side of the concrete flanges completely crushed with the bucking of one of the compression steel bars.

For beam NBPB4, the concrete crushing happened first followed by the FRP slip initiation since the concrete strain became much higher for this beam due to the longer unbonded length. A sudden load drop was observed at the flange thickness of approximately 35mm. As such, the predicted response represented the measured ultimate behaviour well.

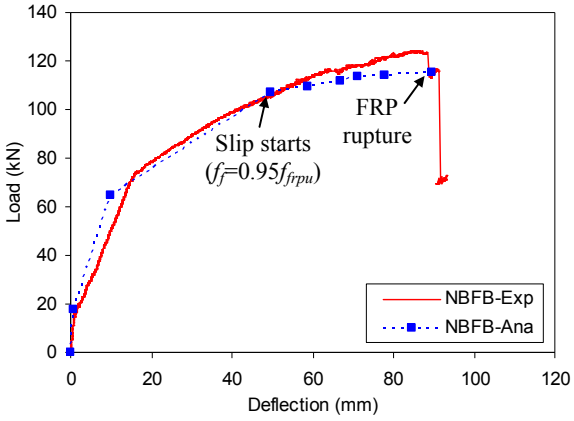

(a) Beam NBFB

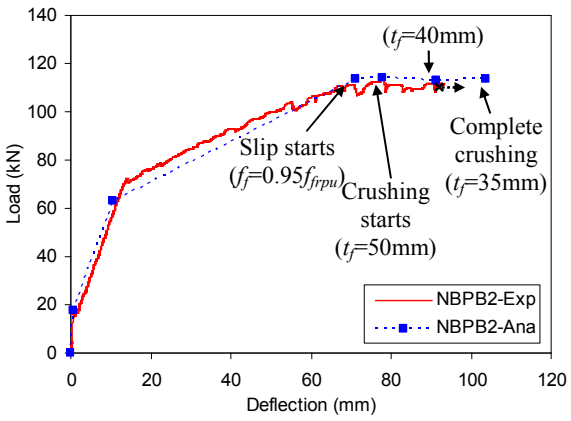

(b) Beam NBPB2

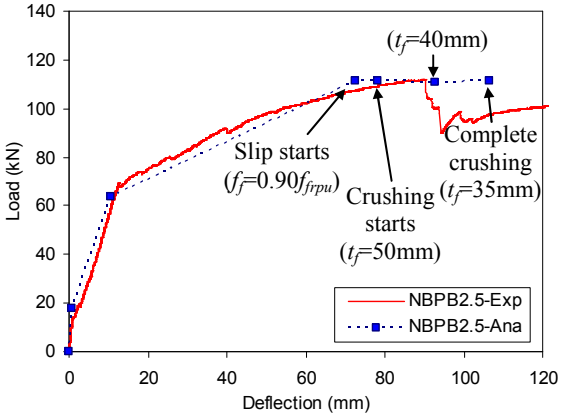

(c) Beam NBPB2.5

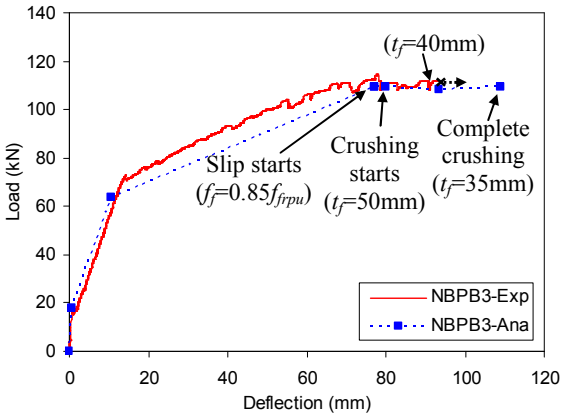

(d) Beam NBPB3

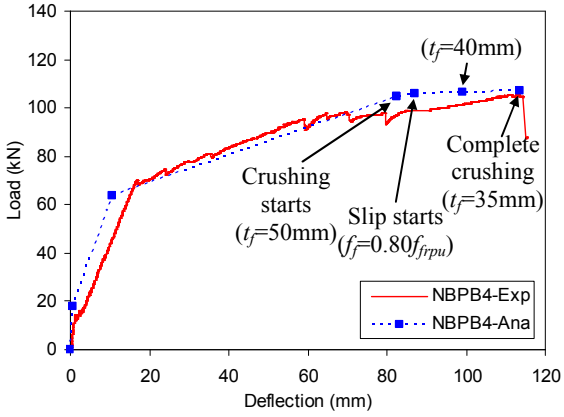

(e) Beam NBPB4

Figure 6-15 Load-deflection comparison between measured values and predictions considering the effect of FRP slip and the stress redistribution

6.4 Comparison with Non-prestressed EB Strengthened Beams

A comparison study between non-prestressed EB and NSM strengthened beams (Group I and Group II beams) was performed in this section to evaluate the overall performance of two strengthening systems. The load-deflection behaviour is compared in Section 6.4.1, and the crack distributions and the deflections at the service load condition were compared in Section 6.4.2.

6.4.1 Load-deflection behaviour

Figure 6-16 shows the load-deflection comparisons between EB FRP strengthened beams (Group I) and NSM FRP strengthened beams (Group II). Prior to failure, the load-deflection behaviour of the two systems with the same unbonded length was almost identical as shown in Figure 6-16. This is because the FRP areas were selected to provide a similar axial stiffness (E_fA_f) for the two systems (see Table 4-2). All of the beams strengthened with the NSM bar (Group II) reached its full capacity (the beams failed by FRP rupture or concrete crushing), while the beams strengthened with EB plate (Group I) failed prematurely by complete debonding before reaching the ultimate FRP strength.

The ultimate loads were greater by 47.9%, 14.2%, 22.6%, and 27.4%, in the NSM beams NBFB, NBPB2, NBPB3 and NBPB4, respectively, compared to the EB beams with the same unbonded lengths. The ultimate deflections in the NSM beams were also higher by 205.1%, 60.5%, 135.6%, and 193.9% compared to the EB beams. This shows that the NSM system was much more effective than the EB system to improve the flexural capacity for all bond conditions due to the apparent high bond strength in the NSM system.

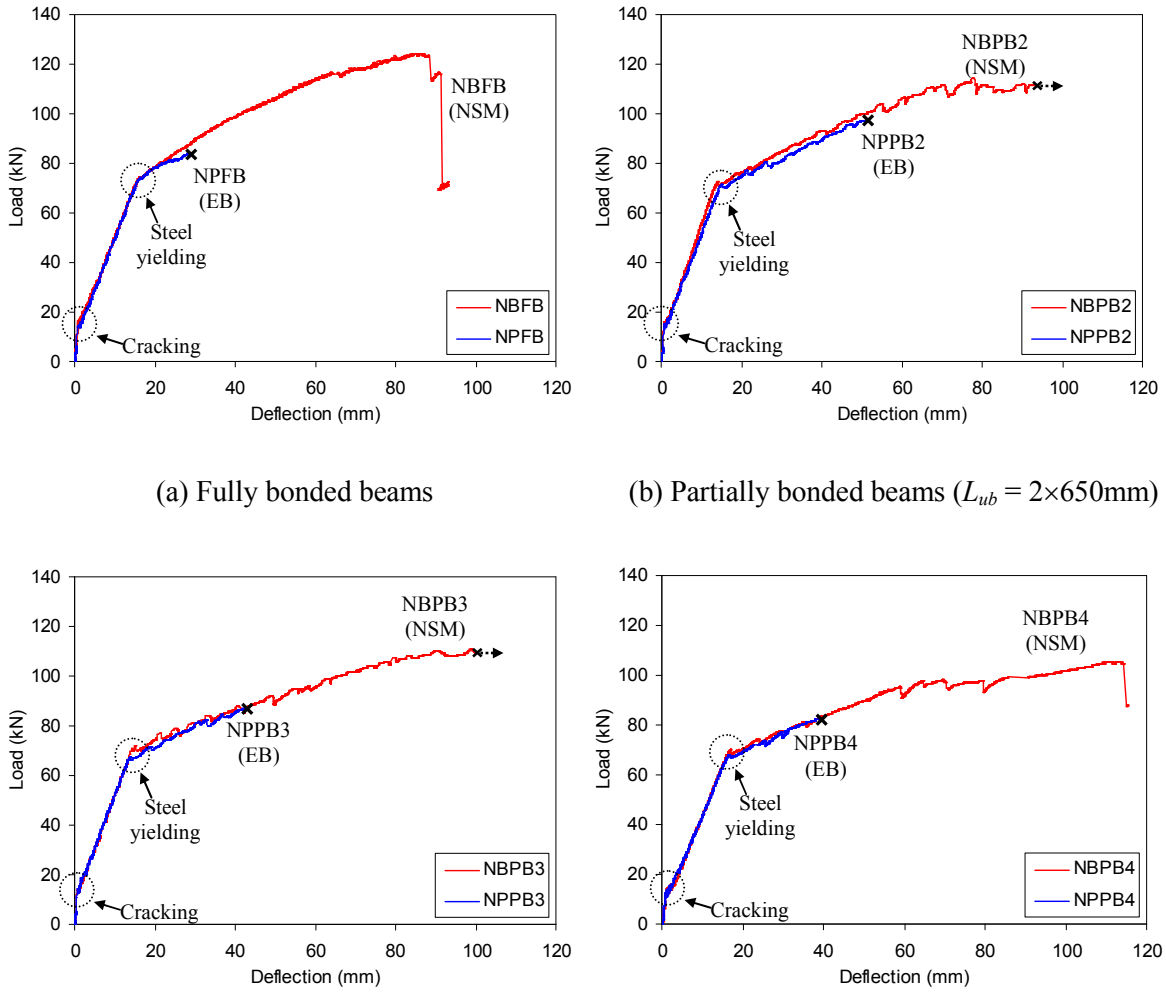

(a) Fully bonded beams

(b) Partially bonded beams (L_{ub} = 2×650mm)

(c) Partially bonded beams (L_{ub} = 2×850mm)

(d) Partially bonded beams (L_{ub} = 2×1050mm)

Figure 6-16 Comparison of load-deflection behaviour between EB and NSM beams

6.4.2 Crack distributions

The crack distributions at the service load condition (P = 60kN) were compared between the fully bonded beams and the partially bonded beams with the unbonded length of 2×1050mm in Figure 6-17. Although the cracks were slightly more widely distributed in the EB beams compared to the NSM beams, the overall crack patterns and spacing were almost identical between two systems regardless of the bond condition. This suggests that the type of strengthening system does not significantly affect

the crack behaviour. The deflections at service load levels were also almost identical as shown in Figure 6-16. Overall, the serviceability is not strongly influenced by the type of strengthening system (EB or NSM) if the same axial stiffness (A_fE_f) of FRP is used.

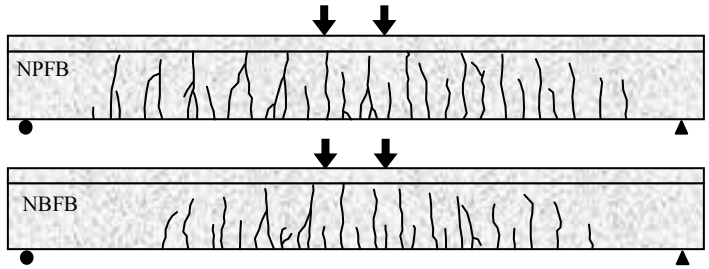

(a) Fully bonded beams

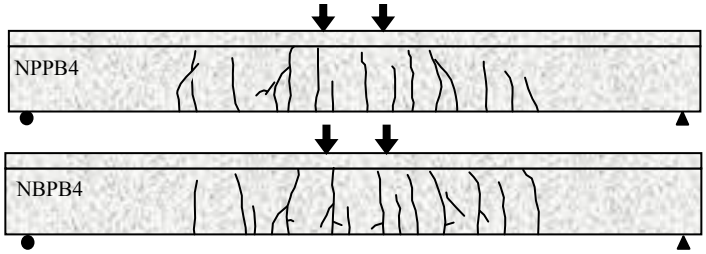

(b) Partially bonded beams (L_{ub} = 2×1050mm)

Figure 6-17 Comparison of crack distributions at serviced load (P = 60kN) between EB and NSM beams

6.5 Summary

The test results of near surface mounted (NSM) FRP bar strengthened RC T-beams were presented and discussed in this chapter. An advanced analytical model was proposed to address the complete behaviour of the beams including the effect of FRP slip and concrete gradual crushing failure. Test results were also compared with externally bonded (EB) FRP plate strengthened beams to evaluate the effectiveness of the strengthening system. The specific conclusions from this investigation are as follows:

1. For the fully bonded beam (NBFB), the full capacity of the FRP bar was reached and the failure mode was FRP rupture while sustaining a large applied load and large deflection. On the other hand, the failure mode of the partially bonded beams was gradual concrete crushing in the T-beam flange.
2. The experimental results showed that the stiffness of the beams at the post-yielding stage was decreased as the unbonded length increased. As a result, the deflection of the partially bonded beams was increased at any given applied load above yielding. However, the ultimate deflection in the partially bonded beams at failure showed only a slight increase compared to the fully bonded beam due to the complex behaviour of the beams including FRP slip and concrete gradual failure. The ultimate load carrying capacity was slightly decreased as the unbonded length increased because the failure mode was changed from FRP rupture to concrete crushing.
3. The basic analytical model could not predict the ultimate behaviour involving the FRP slip and the stress redistribution at the post-crushing stage. An advanced model was proposed to demonstrate this behaviour. For the simulation of the progressive failure, an idealized progressively reduced flange depth was assumed, and a FRP slip model was proposed for the simulation of the FRP slip. The advanced analytical model represented the nonlinear behaviour in both the fully bonded and the partially bonded beams well.
4. The NSM system is much more effective compared to the EB system for the improvement of the ultimate flexural capacity due to the apparent higher bond strength at the concrete and FRP interface. However, the serviceability of the two systems in terms of cracking and deflections (prior to yielding) was similar since the axial stiffness of the systems was similar.

Chapter 7
Prestressed NSM Strengthened Beams

7.1 General

In this chapter, test results of the prestressed NSM partially bonded CFRP strengthened beams (Group III and Group IV) are discussed. Section 7.2 describes failure modes and load-deflection behaviour of tested beams. A comparison study is performed between predictions and experimental results in Section 7.3. Test results of prestressed beams are compared to those of the non-prestressed NSM strengthened beams in Section 7.4.

7.2 Test Results and Discussions

Test results for the prestressed NSM FRP strengthened beams (Group III and Group IV) in terms of applied load and deflection at cracking, at steel yielding, and at ultimate state are summarized in Table 7-1, along with a description of the failure mode.

Table 7-1 Summary of prestressed strengthened beam test results (Group III and IV)

Test Group	Beam Name	P_{cr} (kN)	Δ_{cr} (mm)	P_y (kN)	Δ_y (mm)	P_u (kN)	Δ_u (mm)	Deform-ability, μ (Δ_u / Δ_y)	Failure mode*
-	Control	13.37	0.69	68.13	14.03	79.39	108.70	7.75	CC
Group III	PBFB	27.70	2.18	94.44	18.50	123.78	48.06	2.60	FR
	PBPB2	32.44	2.19	91.24	17.05	119.99	49.66	2.91	FR
	PBPB3	33.55	1.88	90.49	17.52	119.73	56.35	3.22	FR
	PBPB4	32.63	1.96	87.17	17.32	115.77	63.51	3.67	FR
	NBPB5	32.08	1.79	86.85	15.39	109.66	55.22	3.59	FD
Group IV	PBFB-60	39.84	2.06	105.85	16.86	124.55	30.76	1.82	FR
	PBPB4-60	37.87	2.44	93.53	16.26	116.26	52.65	3.24	FR

* CC: Concrete Crushing, FR: FRP Rupture, FD: FRP Debonding

7.2.1 Failure modes and load-deflection behaviour

The failure modes of the fully bonded beam (PBFB) and the partially bonded beam with the unbonded length of 2×1250mm (PBPB5) are shown in Figure 7-1. The failure mode for all other tested beams in Group III and Group IV was the same as the fully bonded beam (PBFB), and can be found in Appendix C. For the beams strengthened with 40% prestressing force, the failure mode of the fully bonded beam (PBFB) and three partially bonded beams (PBPB2, PBPB3 and PBPB4) was FRP rupture near the mid-span as shown in Figure 7-1(a). When the ultimate FRP strain was reached, the CFRP bar ruptured inside the epoxy adhesive with a loud explosive sound. The broken bar in beam PBFB can be seen in Figure 7-1(a). No concrete crushing was observed at the top flange of beams PBFB, PBPB2, and PBPB3, while a limited number of concrete compressive cracks were observed in beam PBPB4 at that time of FRP rupture (see Figure C-3(d) in Appendix C).

On the other hand, one partially bonded beam with the longest unbonded length (PBPB5, L_{ub} = 2×1250mm) failed by FRP debonding as shown in Figure 7-1(b). At the applied load of 109kN and the deflection of 55mm, one side of the CFRP bar suddenly slipped inside the epoxy adhesive and complete debonding occurred with a loud sound. The total slip from the end was 93mm as shown in Figure 7-1(b). This debonding failure was pull-out type debonding since no damage or cracks was observed on the surface of the epoxy adhesive. FRP crushing was observed within the unbonded region due to the impact energy released from the sudden debonding at the other bonded point (see Figure C-3(e) in Appendix C). This is the same phenomenon observed in the partially bonded EB strengthened beams.

Based on the test results for the 40% prestressed strengthened beams, the development length of the beams strengthened with 40% prestressing force to induce the FRP rupture can be considered to be between 500mm and 700mm because beam PBPB5 with 500mm anchorage length failed by FRP debonding while beam PBPB4 with 700mm anchorage length failed by FRP rupture. For this reason,

only two beams, a fully bonded beam (PBFB-60) and a partially bonded beam with 700mm anchorage length (PBPB4-60), were tested to investigate the behaviour of the strengthened beams with a higher level of the prestressing force (60%). The failure mode of these two 60% prestressed strengthened beams (Group IV) was the same FRP rupture at mid span as observed for the 40% prestressed beams. This was expected because the available FRP strains after prestressing were decreased due to the higher prestressing force. The failure mode for these beams can be found in Figure C-4 of Appendix C.

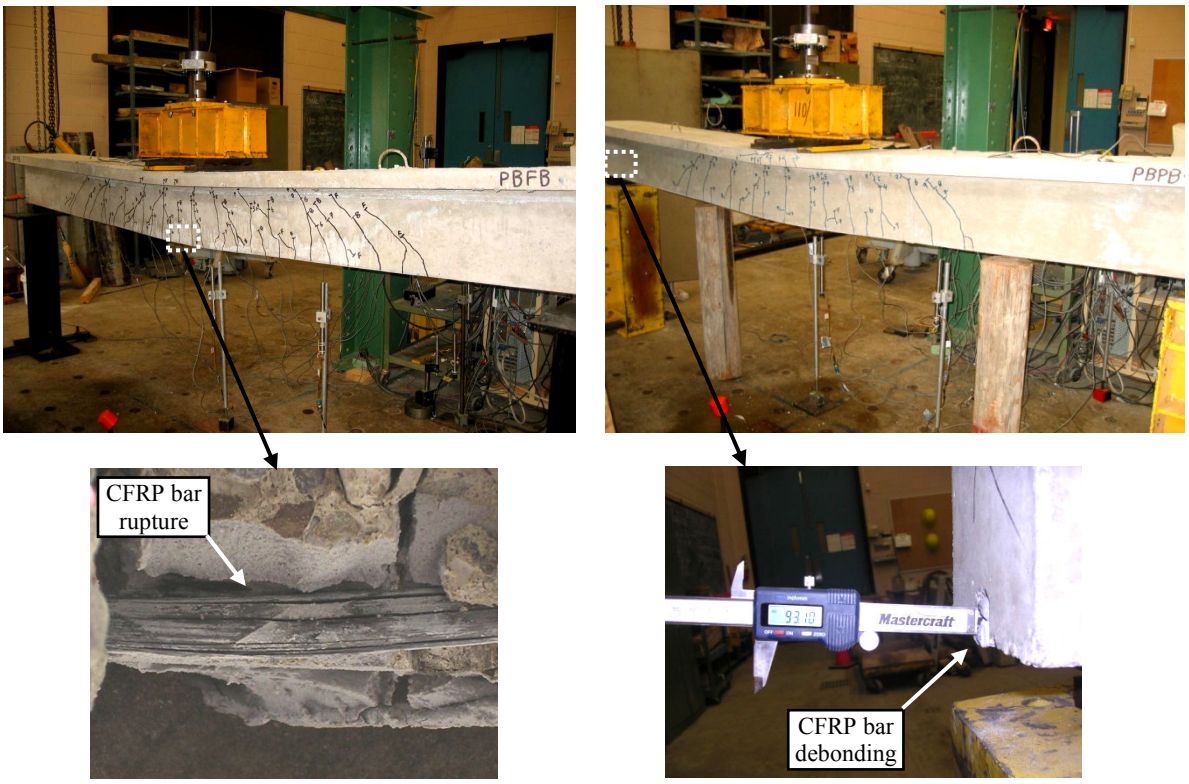

(a) FRP rupture failure (PBFB) (b) FRP debonding failure (PBPB5)

Figure 7-1 Failure modes of prestressed FRP strengthened beams (Group III)

Load-deflection diagrams for Group III beams (40% prestressing) are shown in Figure 7-2. All of the strengthened beams showed a significant improvement compared to the unstrengthened beam (control beam) in terms of the cracking load (P_{cr}), beam deflection at the service load (P = 60kN), and

the ultimate load (P_u) as shown in Figure 7-2, while the ultimate deflection (Δ_u) was decreased compared to the unstrengthened beam. The load-deflection diagrams of all the strengthened beams were almost identical up to the steel yielding point regardless of the bond condition, while the stiffness (slope) of the curve was decreased in the post-yielding state as the unbonded length was increased as shown in Figure 7-2. As a result, the ultimate deflection increased as the unbonded length increased compared to the fully bonded beam.

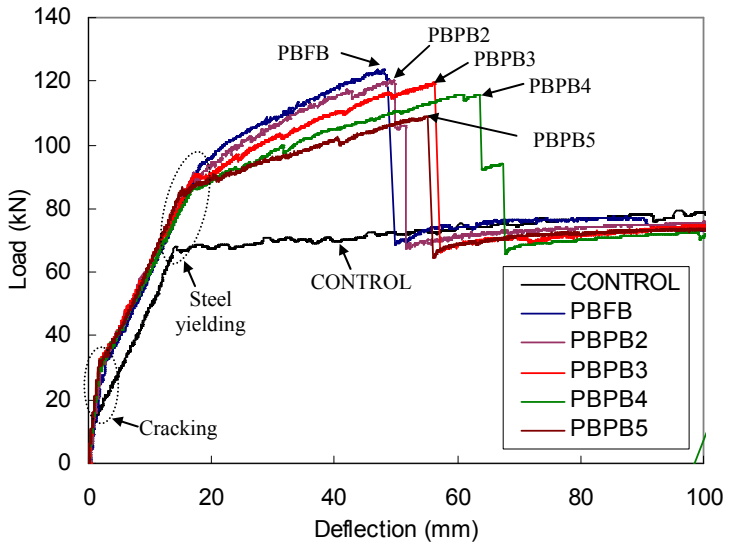

Figure 7-2 Comparison of the load-deflection diagrams of prestressed beams (Group III)

If the deformability index, μ, is defined by the ratio of the ultimate deflection (Δ_u) to the deflection at steel yielding (Δ_y), the deformability of the fully bonded beam (PBFB) and the partially bonded beam (PBPB4) is 2.60 and 3.67, respectively, which shows an improvement of the deformability (41.15%) due to partial unbonding. On the other hand, the ultimate load (P_u) and the load at steel reinforcement yielding (P_y) were slightly decreased as the unbonded length increased. In the fully bonded beam, the CFRP reinforcement carries more tension force up to steel yielding since it is completely bonded to the beam, and therefore there is a slight decrease in the yield load as the unbonded length is increased. On the other hand, at the post-yielding stage, the CFRP reinforcement

carries almost the same tension force without regard to the bond condition as described in previous chapters. The reason for the slight decrease of the ultimate load in the partially bonded beams, even though all beams failed by CFRP rupture, is possibly due to the greater rotation angle change at mid-span as the unbonded length is increased. Figure 7-3 shows the rotation angle and the deflected shape of the beams based on the analytical model at the ultimate state. The angle change between the loading points is greater as the unbonded length is increased, as shown in Figure 7-3. Due to this greater angle change, the stress in the outer fibres of the CFRP bar is increased, inducing the FRP rupture failure earlier as the unbonded length is increased. In addition to this angle change, other secondary effects caused by the use of the plastic tube could reduce the strength further. The decrease of the ultimate load was only 6.47% between beam PBFB (fully bonded) and beam PBPB4 (partially bonded), which is not significant considering the increase of the deformability (41.15%) between the two beams.

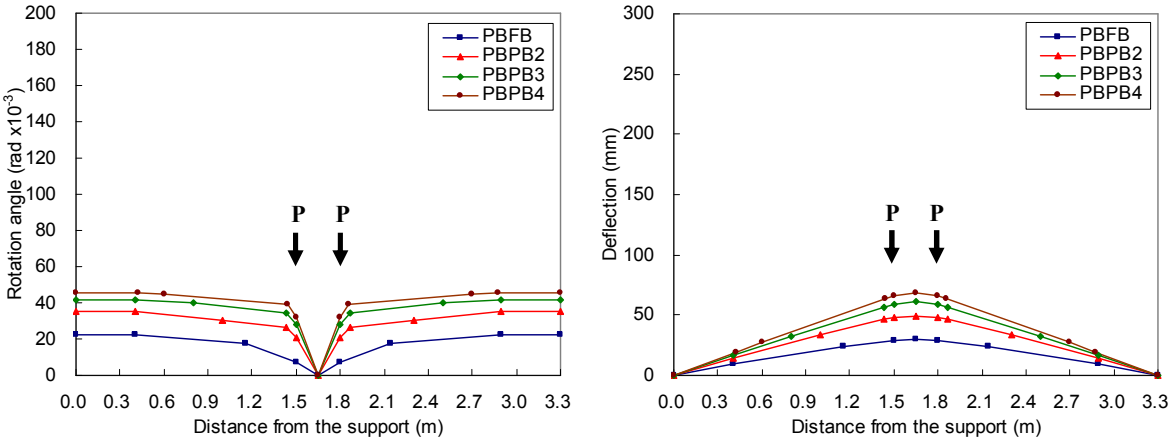

(a) Rotation angle (b) Beam deflection

Figure 7-3 Rotation angle and deflected shape of the beams (Group III)

Beam PBPB5 experienced premature debonding failure and as such the ultimate load was lower than beam PBPB4. However, the stiffness of beam PBPB5 at the post-yielding stage was decreased as

expected, so the ultimate deflection was still greater (14.9% increase) compared to the fully bonded beam (PBFB).

The load-deflection diagrams for the fully bonded and partially bonded beams strengthened with 60% prestressed FRP are shown in Figure 7-4. The general behaviour of the beams was similar to the beams strengthened with 40% prestressing force. The cracking load, deflection at service load, and the ultimate load were greatly improved compared to the unstrengthened beam. Moreover, the cracking load and deflection at service load were improved compared to the beams strengthened with 40% prestressing force (both the fully bonded beam and the partially bonded beam). The ultimate load was almost identical for the two different prestressing levels since the failure was governed by CFRP rupture in both cases. However, the ultimate deflection of beams with a higher prestressing level was reduced since the maximum effective CFRP strain was decreased due to prestressing to the higher level. The deformability index of beam PBFB-60 was 1.82, which is smaller than that of beam PBFB ($\mu = 2.60$). The deformability index for the partially bonded beam (PBPB4-60) was 3.24, showing a 78% improvement over the fully bonded beam (PBFB-60). This showed that partial unbonding was more effective to improve the deformability at higher prestressing level. On the other hand, the ultimate load was slightly decreased from 124kN (beam PBFB-60) to 116kN (beam PBPB4-60) (6.66% of decrease), similar to the 40% prestressed beams.

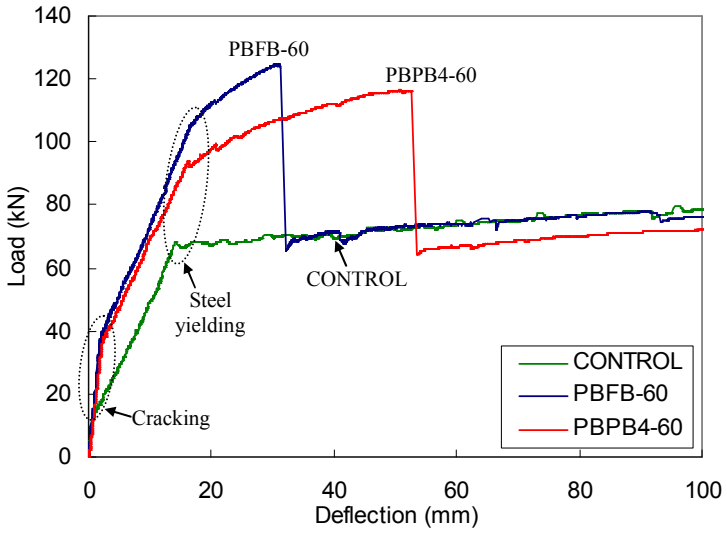

Figure 7-4 Comparison of the load-deflection diagrams of prestressed beams (Group IV)

7.2.2 Strain distribution

Load versus FRP strain and load versus concrete strain at mid-span are plotted in Figure 7-5. The initial strains in the CFRP reinforcement due to prestressing were 6600×10^{-6} and 9600×10^{-6} for the 40% and 60% prestressed beams, respectively. The strains in Figure 7-5 (a) and (c) represent the CFRP strain during testing and do not include the initial strains due to prestressing. The initial concrete strains due to prestressing were less than 30×10^{-6}, and as such, can be neglected.

The load versus FRP strain diagrams were almost identical without regard to the bond condition at the same prestressing level (Figure 7-5 (a) and (c)), while the concrete strains at the post-yielding stage increased with longer unbonded length (Figure 7-5 (b) and (d)). The load-concrete strain diagrams in Figure 7-5 (b) and (d) showed almost the same pattern as the load-deflection diagrams in Figure 7-2. This is the same behaviour observed in the strain distributions of non-prestressed EB and NSM beams (see Section 5.2.2 and Section 6.2.2). All of the other measured strains for all prestressed beams can be found in Appendix D.

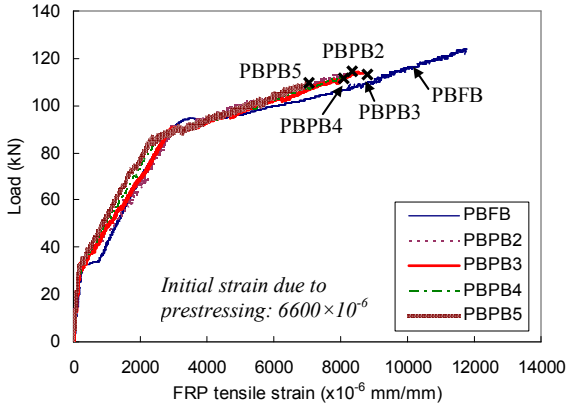

(a) Load-FRP strain diagrams (40%)

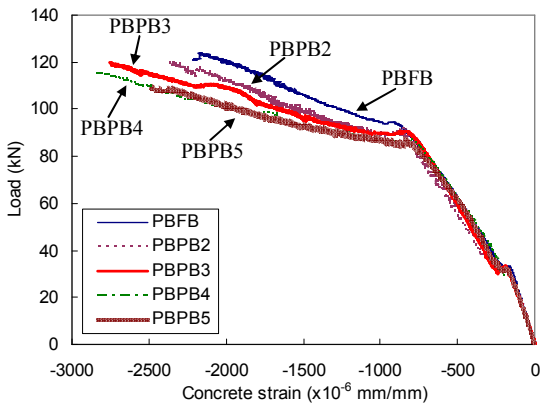

(b) Load-concrete strain diagrams (40%)

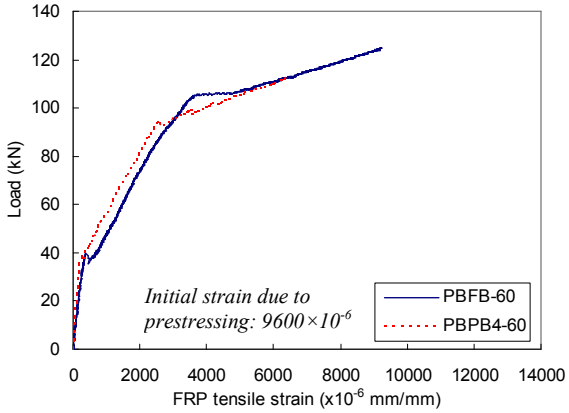

(c) Load-FRP strain diagrams (60%)

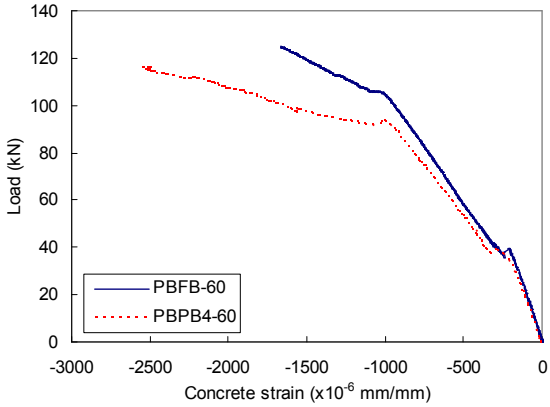

(d) Load-concrete strain diagrams (60%)

Figure 7-5 FRP and concrete strain distributions at mid-span with the applied load

7.2.3 Crack distribution

The crack distributions for the fully bonded beams (PBFB and PBFB-60) and partially bonded beams (PBPB4 and PBPB4-60) at an applied load of 60kN are shown in Figure 7-6. The crack patterns for the other prestressed beams can be found in Appendix E. The spacing between the cracks was smaller and the number of cracks was greater in the fully bonded beams in comparison to the partially bonded beams regardless of the prestressing level. In addition, the beam length over which the cracks occurred was also wider, and the crack depth was slightly less in the fully bonded beams as shown in

Figure 7-6(a) and (b). These crack patterns were almost the same as those observed in the non-prestressed EB or NSM strengthened beams, but the distinction between the fully bonded and partially bonded beams were more prominent in the prestressed beams. This is because the number of cracks and the beam length where cracks occurred were decreased due to the prestressing effect, so the distinction could be more easily observed. A comparison of crack patterns for non-prestressed and prestressed beams is reported in Section 7.4.2.

When comparing the crack distributions between beams with 40% and 60% prestressing forces in Figure 7-6, the 60% prestressing force further reduced the number and length of cracks in comparison to the 40% prestressing force. Therefore, it is evident that the higher FRP prestressing force is more effective to reduce cracking, and therefore improves the serviceability of the beam.

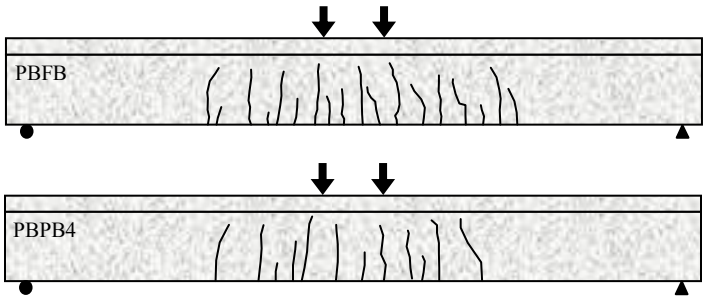

(a) Beams PBFB and PBPB4 (40% prestressing force)

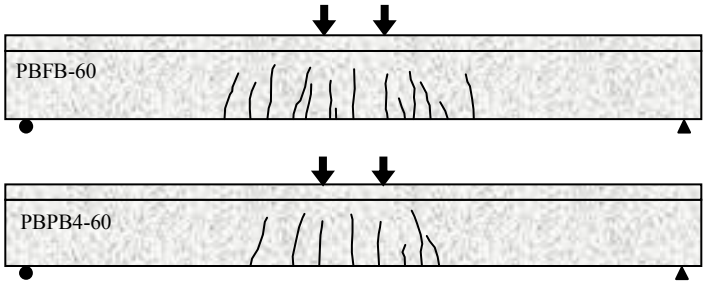

(b) Beams PBFB-60 and PBPB4-60 (60% prestressing force)

Figure 7-6 Comparison of crack patterns at service load (P = 60kN)

7.3 Comparison between Analytical Prediction and Experimental Results

A comparison of the measured and the predicted load-deflection diagrams of the fully bonded beams is shown in Figure 7-7(a). The same analytical model developed in Chapter 3 was used for the analysis. Since the FRP reinforcement is prestressed, the initial effective stress (f_{pe}) and strain (ε_{pe}) were considered when deriving force equilibrium equations at critical sections and the overall strain compatibility equation.

The general behaviour of the beam, including the stiffness change at critical points, was reasonably predicted by the basic analytical model. The stiffness of the predicted load-deflection diagrams was greater than the measured values, and the measured ultimate load was higher than the predicted values. These differences are mainly caused by variations in material properties and the modeling assumptions. FRP slip was also found in the FRP to epoxy interface in the fully bonded beams, which could affect the behaviour as observed in the non-prestressed NSM beams. However, the slip of FRP reinforcement in the prestressed beams would be smaller in comparison to the non-prestressed beam because the bond stress at mid-span is decreased due to the initial prestressing.

The comparison between the predicted and measured load-deflection diagrams of the partially bonded beams is shown in Figure 7-7(b), (c) and (d). The general behaviour, such as the stiffness change with increasing unbonded length, was well predicted by the analytical model and reasonably matched with the experimental results. However, the stiffness of the beams and the predictions of critical points, such as the ultimate point or the steel yielding point, are slightly different between the predicted and the measured responses. This is mainly caused by the analytical assumptions, the material variation, and possible CFRP internal slip.

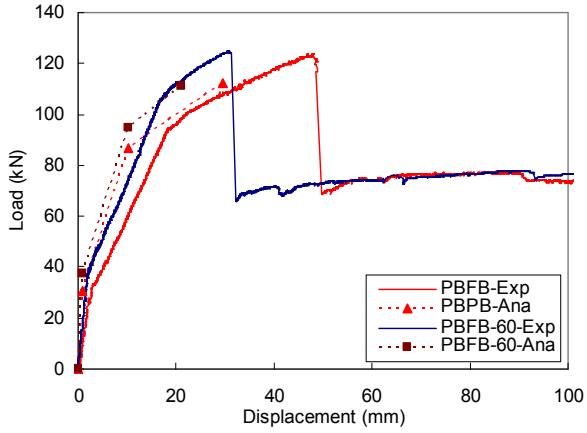

(a) Beams PBFB and PBFB-60

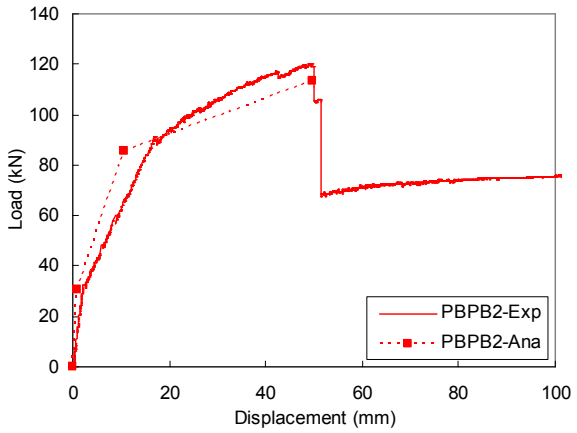

(b) Beam PBPB2

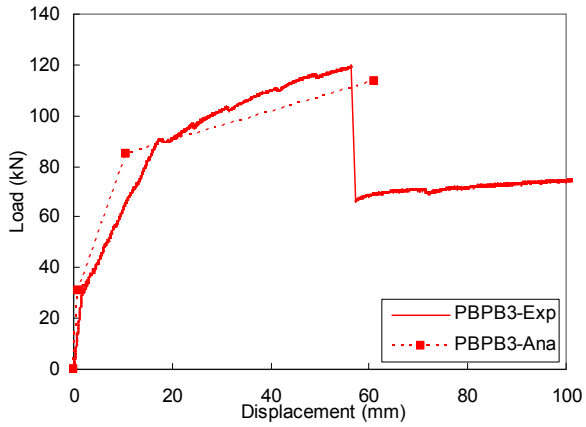

(c) Beam PBPB3

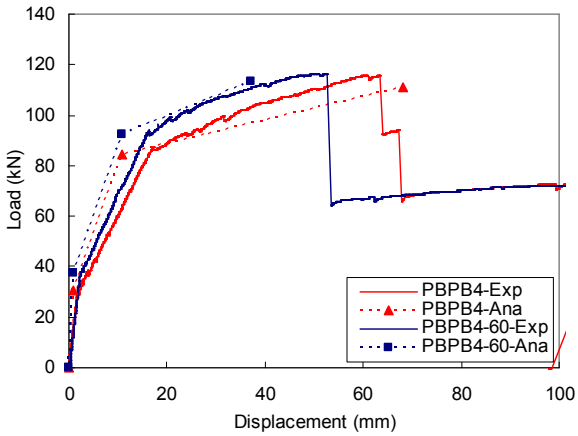

(d) Beams PBPB4 and PBPB4-60

Figure 7-7 Comparison of load-deflection diagrams between measured and predicted values

7.4 Comparison with Non-prestressed NSM Strengthened Beams

A comparison study between non-prestressed and prestressed NSM strengthened beams (Group II and Group III, IV beam) is performed in this section to evaluate the overall performance between the two strengthening systems. The failure mode and the load-deflection behaviour are compared and discussed in Section 7.4.1 and the serviceability comparison including crack distributions and the deflections is presented in Section 7.4.2.

7.4.1 Failure mode and load-deflection comparison

The load-deflection comparisons with increasing prestressing levels (0%, 40%, and 60%) in the fully bonded and partially bonded NSM strengthened beams are shown in Figure 7-8. FR and CC in Figure 7-8 denote FRP rupture failure and concrete crushing failure, respectively. The failure mode in the fully bonded beam was the same for the non-prestressed and prestressed beams (Figure 7-8(a)), while the failure mode was changed from concrete crushing to FRP rupture in the partially bonded beams by applying the prestressing force (Figure 7-8(b), (c), and (d)).

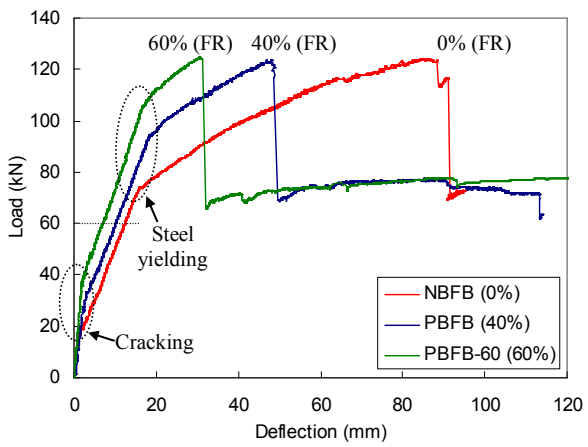

(a) Fully bonded beams

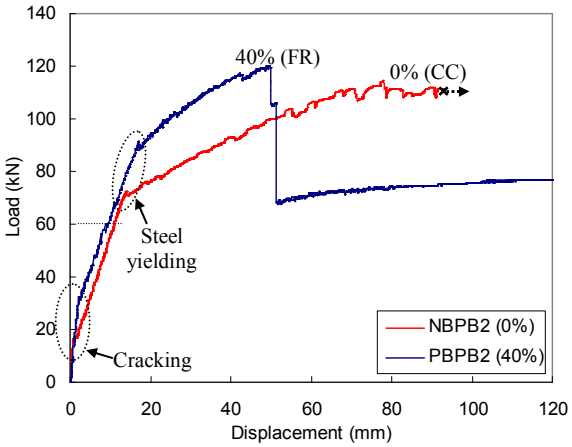

(b) Partially bonded beams (L_{ub} = 2×650mm)

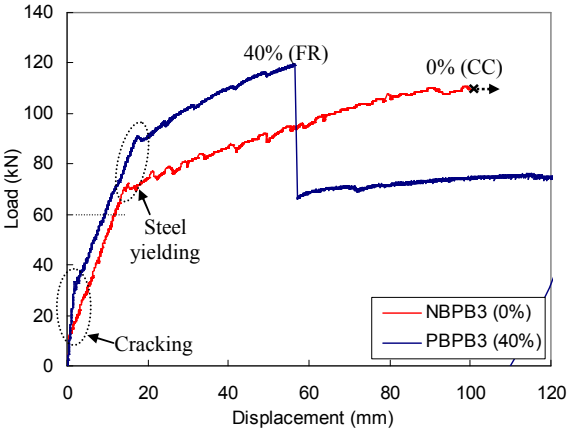

(c) Partially bonded beams (L_{ub} = 2×850mm)

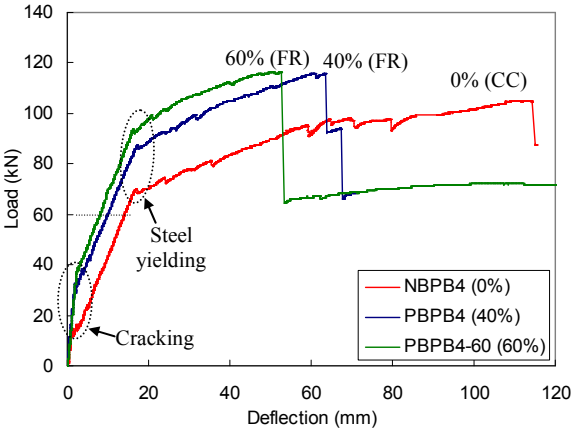

(d) Partially bonded beams (L_{ub} = 2×1050mm)

Figure 7-8 Comparison of the load-deflection behaviour between non-prestressed NSM beams (Group II) and prestressed NSM beams (Group III and IV)

For the fully bonded condition (Figure 7-8(a)), the ultimate load was almost identical for the non-prestressed and prestressed beams because the failure modes of all beams were FRP rupture. However, the cracking load and the steel yielding load were increased by 59.3% and 27.0% in beam PBFB and 129.1% and 42.3% in beam PBFB-60, respectively, compared to the non-prestressed beam NBFB. The ultimate strength was also improved in the partially bonded 40% prestressed strengthened beams compared to the non-prestressed beams due to the failure mode change from concrete crushing to FRP rupture. Strength increases of 7.7%, 9.5%, and 10.7% were observed in the prestressed partially bonded beams with unbonded lengths of 2×650mm, 2×850mm, and 2×1050mm, respectively, as shown in Figure 7-8(b), (c), and (d). However, the ultimate deflection of the prestressed beams was decreased compared to the non-prestressed beam as the prestressing level was increased without regard to the bond condition.

7.4.2 Serviceability comparison

The deflections at service load of 60kN were 11.56mm, 10.95mm, 11.70mm, and 14.07mm in non-prestressed beams, NBFB, NBPB2, NBPB3, and NBPB4, respectively. Deflections were decreased to 10.05mm, 9.83mm, 9.28mm, and 9.96mm in the 40% prestressed beams, PBFB, PBPB2, PBPB3, and PBPB4, respectively, and further decreased to 6.86mm and 7.99mm in 60% prestressed beams, PBFB-60 and PBPB4-60, respectively. As such the beam deflection can be reduced by applying the prestressing system at the service load condition, as illustrated in Figure 7-8 at the applied load of 60kN.

A comparison of the crack patterns at service load (P=60kN) is shown in Figure 7-9. The number of cracks and the beam length where cracks occurred were decreased due to the prestressing effect. The depth of cracks in the prestressed beams was also less in comparison to the non-prestressed beams (neutral axis depth is increased in the prestressed beam).

Overall, it is evident that the prestressed CFRP strengthening system is very effective to improve the serviceability of the beam, including crack control and deflection under service load.

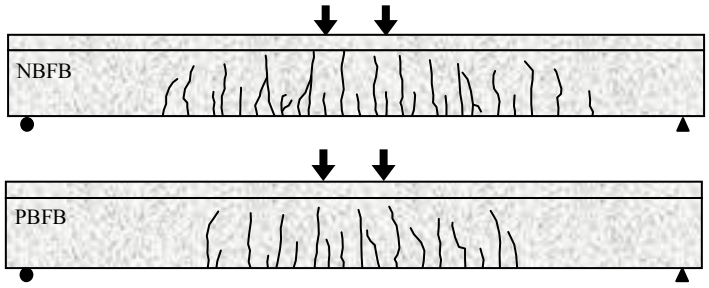

(a) Fully bonded beams

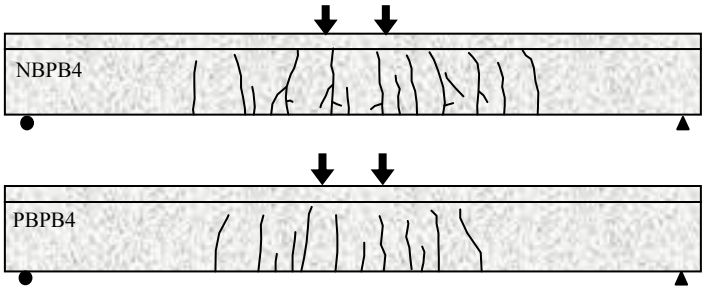

(b) Partially bonded beams (L_{ub} = 2×1050mm)

Figure 7-9 Comparison of crack distributions between non-prestressed NSM beams (Group II) and prestressed NSM beams (Group III) (P = 60kN)

7.5 Summary

The test results of prestressed NSM strengthened RC T-beams with different prestressing levels were presented and discussed in this chapter. The flexural response of partially bonded beams was compared to that of fully bonded beams, and the test results were also compared with the predictions. The behaviour of the prestressed beams was compared to the non-prestressed beams to evaluate the effectiveness of the strengthening system. The specific conclusions from this investigation are as follows:

1. The failure mode of the FRP prestressed beams was by FRP rupture except for one beam (PBPB5), which has the shortest bonded length and failed by FRP pull-out. Premature FRP pull-out debonding failure could be prevented if a proper anchorage length is provided. The anchorage length to ensure FRP rupture was found to be approximately 700mm for the 40% prestressed beams used in this study.
2. Prestressed strengthened beams were very effective to improve the cracking load, to decrease the deflection at service load, and to increase ultimate load compared to the unstrengthened beams. This improvement was greater as the prestressing force was increased. However, the deformability was decreased as the prestressing level increased.
3. Partially bonded prestressed beams showed an improvement of deformability compared to the fully bonded beams without a significant loss of ultimate load carrying capacity and without significantly affecting serviceability. The improvement provided by partial unbonding was more effective at higher levels of prestressing force.
4. The analytical model developed in Chapter 3 could predict the general behaviour of the prestressed strengthened beams well and showed good agreement with the experimental results.
5. The prestressed NSM system is more effective to improve the ultimate load carrying capacity and the serviceability in comparison to the non-prestressed NSM system. However, the deformability of the prestressed beams was decreased compared to the non-prestressed beams.

Chapter 8
Design Recommendations

8.1 General

In this chapter, general conclusions are drawn from all of the experimental results for the fully bonded and partially bonded beams in various strengthening systems (Section 8.2), and an evaluation of the analytical model is performed by comparing with the test results (Section 8.3). A parametric study is carried out on various beam configurations to investigate the effect of main variables on the behaviour of partially bonded beams, and design charts and procedures are proposed for the effective use of the partially bonded system (Section 8.4).

8.2 Analysis of Test Results

Test results in terms of load-deflection diagrams for all test groups (Group I ~ Group IV) are shown in Figure 8-1. One typical behaviour is that the load-deflection behaviour of the strengthened beams up to steel reinforcement yielding is almost identical regardless of the bonded length. However, the stiffness (slope) of the beams was decreased after steel yielding as the unbonded length at mid-span was increased. This stiffness reduction was prominent in the NSM strengthened beams as shown in Figure 8-1(b), (c), and (d). As discussed in previous chapters, the flexural stiffness of the beam is determined by the geometry of the beam and the axial stiffness (EA) of the steel and the FRP reinforcement. The stiffness of the beam up to steel yielding was mainly governed by the axial stiffness of the steel reinforcement. This is because the area of the FRP reinforcement is only one-tenth that of the steel reinforcement in the beams tested. As well, the elastic modulus of the FRP is approximately 80% of the steel elastic modulus. Since the strains in the FRP and the steel are similar in magnitude prior to steel yielding (≤ 0.002) regardless of the FRP bonded length, the flexural

behaviour of the beam is dominated by the higher axial stiffness of the steel and the load-deflection behaviour of the strengthened beams is almost identical without regard to the FRP bond condition.

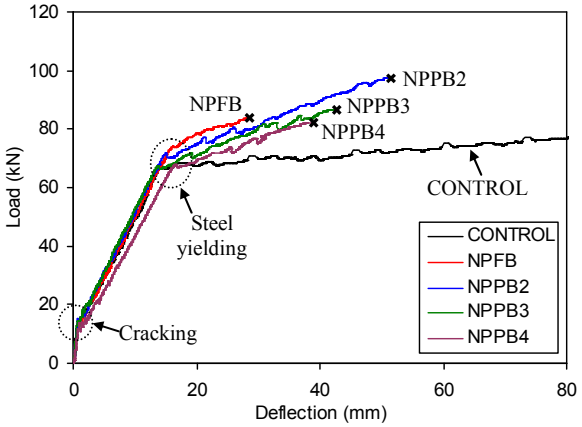

(a) Group I beams (EB plate)

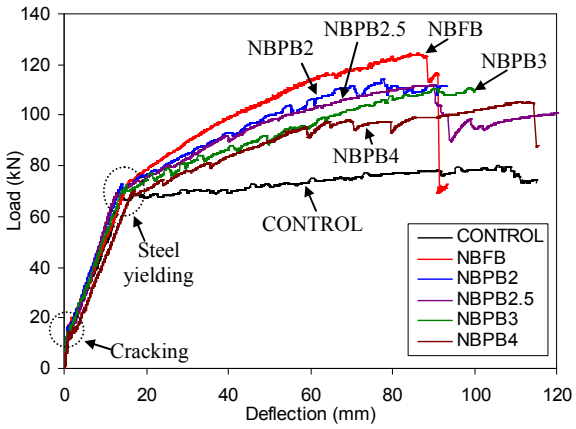

(b) Group II beams (NSM bar)

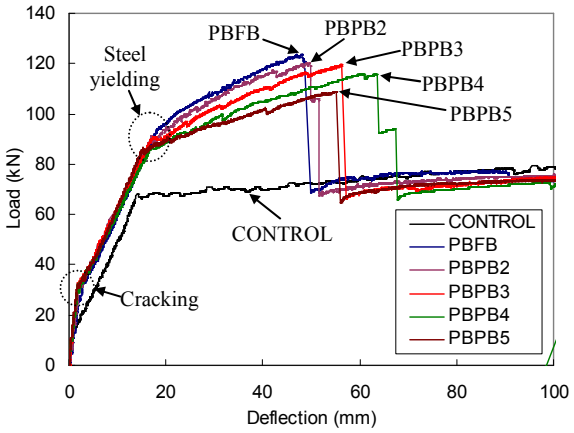

(c) Group III beams (40% prestressed NSM bar)

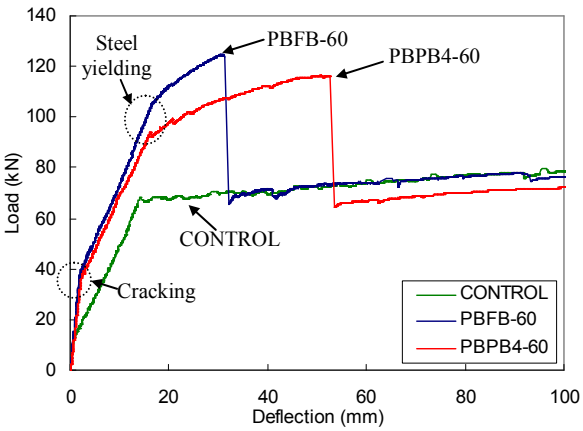

(d) Group IV beams (60% prestressed NSM bar)

Figure 8-1 Load-deflection diagrams of FRP strengthened beams

On the other hand, once the steel reinforcement yields the load-deflection response is mainly governed by the axial stiffness of the FRP reinforcement since the axial stiffness of the steel reinforcement is negligible due to yielding. In addition, the unbonded length of the FRP affects the stiffness of the beam after steel yielding; the beam stiffness is decreased as the unbonded length is

increased. For a given load level or moment, the total tension force resultant is approximately constant regardless of unbonded length. After steel yielding, the force in the steel remains essentially constant, indicating that increases in applied load correspond to increases in the force (strain) in the FRP. The FRP strain is constant within the unbonded length and represents the average concrete strain at the level of the FRP within the unbonded length. Thus, as the unbonded length increases, the maximum strains in the concrete must increase to sustain the same uniform strain in the FRP for a given load level. This produces increased curvature of the section as the unbonded length increases, and corresponds to a decrease in the flexural stiffness of the beam.

Another typical behaviour observed in the diagrams is that the load-deflection diagrams are approximately linear up to near the ultimate state with stiffness changes at the cracking load and at the steel yielding point. This is because the beam was under-reinforced (based on the steel reinforcement) and was not heavily strengthened with FRP. Nonlinear behaviour developed near the ultimate state in the non-prestressed NSM strengthened beams (Figure 8-1(b)). This is mainly due to the slip of the FRP and the gradual failure of the concrete. For design purposes, a linear response can be assumed for under-reinforced beams for simplicity.

For the EB FRP plate strengthened beams (Figure 8-1(a)), the failure mode of all beams was premature debonding failure. The debonding failure is known to be prevalent in the EB strengthened beams, and various premature debonding failures have been reported (see Section 2.4.3). For design purposes, the maximum strain of the FRP is often limited to avoid the debonding failure as described in Section 2.4.4.1. If the maximum strain of the FRP is limited in this manner and the failure of the beam section is tension controlled (i.e., the FRP strain reaches its limiting value before the concrete reaches its ultimate strain), the nominal resistance of the strengthened beam is not significantly affected by the unbonded length. This is because the total tension resultant force is essentially constant since the steel reinforcement is yielding and the strain in the FRP is equal to the specified

limiting value (i.e., constant). Since the maximum concrete strain may be less than the ultimate concrete strain depending on the unbonded length, the location of the concrete compression resultant may vary with unbonded length. However, changes in the location of the concrete compression resultant will be very minor in comparison to the magnitude of the lever arm of the internal moment couple, and thus the nominal flexural resistance of the strengthened section is not significantly affected by the unbonded length. On the other hand, the deflection of the beam corresponding to the limiting FRP strain is affected by the unbonded length. As discussed previously, as the unbonded length increases the maximum strains in the concrete must increase to produce the same uniform FRP strain in the unbonded length. As a result, the section curvature and the beam deflection both increase as the unbonded length increases. In summary, if the strain in the FRP is limited to a specified level to prevent debonding failure, the nominal resistance corresponding to that limit is essentially independent of the unbonded length. However, the deflection corresponding to the nominal resistance will increase as the unbonded length is increased, effectively increasing the deformability of the beam.

Overall, the test results of the partially bonded beams showed an improvement of the ultimate deformation while minimizing the reduction of the ultimate strength in comparison to the fully bonded beams. As well, there was little or no effect of partial unbonding on the serviceability of the beams.

8.3 Verification of Analytical Model as Design Model

The verification of the model has been performed by comparing the load-deflection diagrams with the experimental results. Figure 8-2 shows a comparison of the fully bonded beam and the partially bonded beam with the unbonded length of 1050×2mm of each test group. As shown in the figure, the general behaviour of the beams was predicted well, including the stiffness change at the cracking load and at the steel yielding point, and the stiffness reduction in the post-yielding stage in the partially bonded beams.

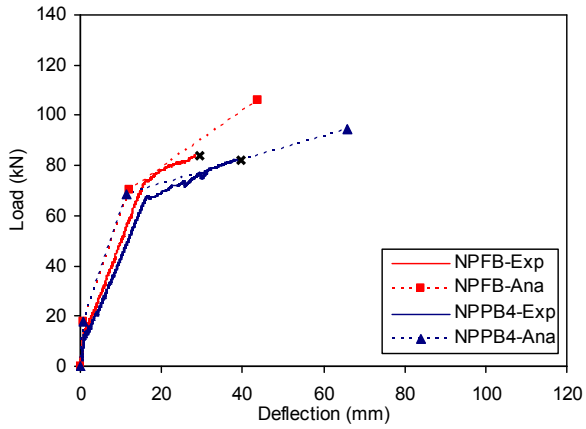

(a) Group I beams (EB plate)

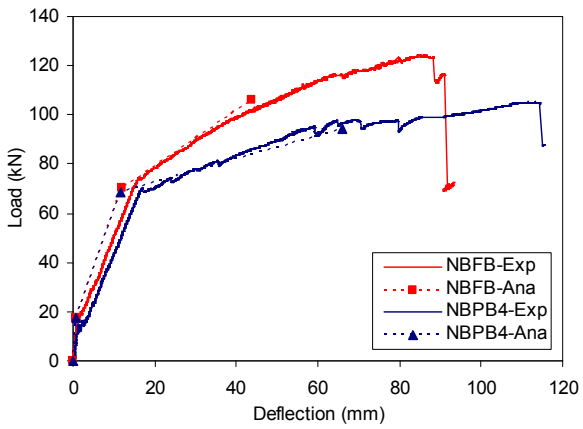

(b) Group II beams (NSM bar)

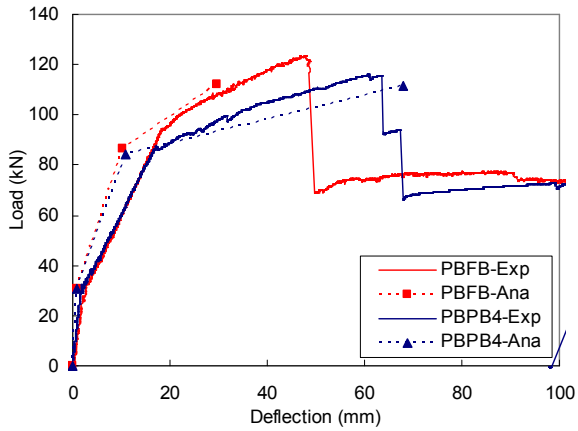

(c) Group III beams (40% prestressed NSM bar)

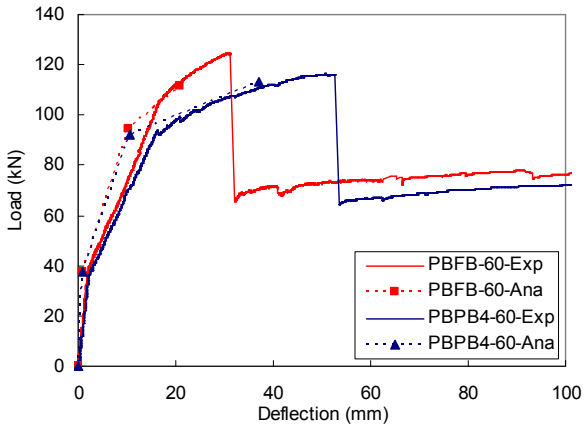

(d) Group IV beams (60% prestressed NSM bar)

Figure 8-2 Comparison between predicted and measured load-deflection diagrams

On the other hand, there was some discrepancy between the ultimate responses of the predicted and the measured values. This is due to the early debonding failure in the EB strengthened beams (Figure 8-2(a)), and the FRP slip and the concrete gradual failure in the NSM strengthened beams (Figure 8-2(b)) as discussed in Chapter 5 and Chapter 6. For design purposes, the debonding failure in the EB system and the FRP slip in the NSM system are unfavorable and are very difficult to predict. If the limited FRP strain concept described in Section 2.4.4.1 is applied for design purposes, these

unpredictable responses can be avoided and the analytical model described herein can be used to predict the behaviour corresponding to the nominal resistance of the beam.

8.4 Parametric Study and Design Recommendations

8.4.1 Effect of partial unbonding on the beams

The basic concept of the improvement of the ultimate deformability in the partially bonded beams is to utilize the beam where failure is controlled by FRP rupture in the fully bonded condition (an under-strengthened beam). By increasing the unbonded length, the rate of the FRP strain increase is decreased while the concrete strain is increased, resulting in an increase in the curvature and the deflection at ultimate. At certain unbonded length, the FRP strain and the concrete strain reach their ultimate strains at the same time, which is referred to as the balanced condition as defined in Section 3.2.2. The unbonded length at this condition is defined as the balanced unbonded length, L_{ubb}. Up to the balanced point, the deflection is increased without reduction of the ultimate strength since the failure is governed by the FRP rupture. Once the unbonded length is greater than the balanced unbonded length, the ultimate strength decreases since the concrete governs the failure mode before the FRP strain reaches its ultimate strain. If the beam fails by concrete crushing in the fully bonded condition (an over-strengthened beam), no balanced point exists and the failure mode is always concrete crushing regardless of the unbonded length. Therefore, the behaviour of the over-strengthened beam is similar to that of an under-strengthened beam with the unbonded length greater than the balanced unbonded length. The details for the behaviour of the partially bonded beams are described in Section 3.2.

Figure 8-3 shows the balanced condition for a fully bonded beam (Figure 8-3(a), the same as Figure 2-5) and a partially bonded beam (Figure 8-3(b)), where the beam fails by concrete crushing and FRP rupture at the same time. From the force equilibrium and the strain compatibility, the

balanced FRP reinforcement area of the fully bonded beam, $A_{f,b}$, can be calculated as shown in Figure 8-3(a). If the FRP reinforcement is prestressed, the FRP has an initial effective strain (ε_{pe}) due to prestressing force and ε_{fu} equals ε_{frpu} minus ε_{pe}. Otherwise, the ε_{fu} equals ε_{frpu} in non-prestressed FRP strengthened beams. If the area of the FRP used, A_f, is less than $A_{f,b}$, then the beam is under-strengthened, while if A_f, is greater than $A_{f,b}$, the beam is an over-strengthened beam.

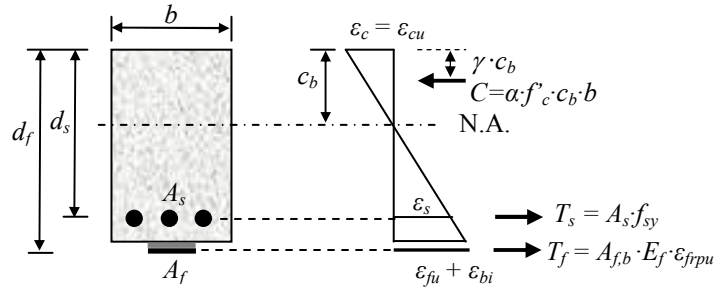

(a) Fully bonded beam

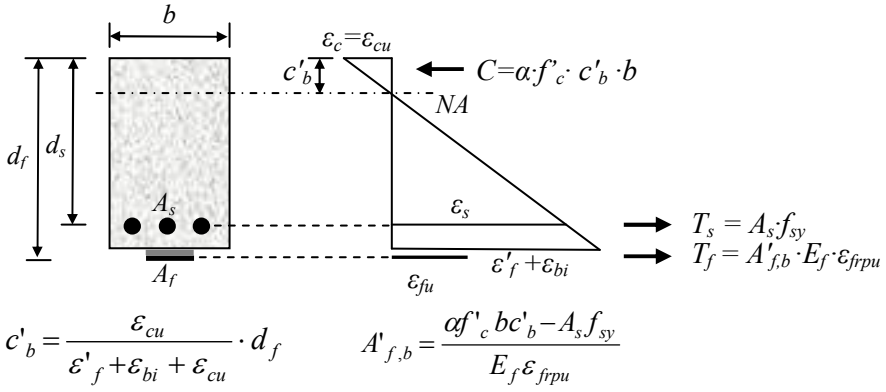

(b) Partially bonded beam

Figure 8-3 Strain compatibility at the balanced condition

Figure 8-4(a) shows the load-deflection behaviour of a T-beam strengthened with CFRP with various unbonded lengths including the fully bonded beam. The same beam configuration presented in Section 3.2.5 with L_p = 0.05L was used for the analysis. The balanced area of this beam configuration based on the Figure 8-3(a), $A_{f,b}$, is 252mm^2 which is greater than the FRP area used, A_f;

therefore, the beam is under-strengthened beam. As shown in the Figure 8-4(a) the behaviour of the beam up to steel yielding is almost identical without regard to the bond condition, while the stiffness of the beam is decreased at the post-yielding stage as the unbonded length is increased up to the balanced unbonded length. This results in an increase in the ultimate deflection while sustaining the ultimate load. If the unbonded length is greater than the balanced unbonded length, the ultimate deflection continues to increase with further increases in unbonded length, but the ultimate strength is decreased as shown in Figure 8-4(a). Therefore, the balanced length is important to improve the deformability without the loss of strength.

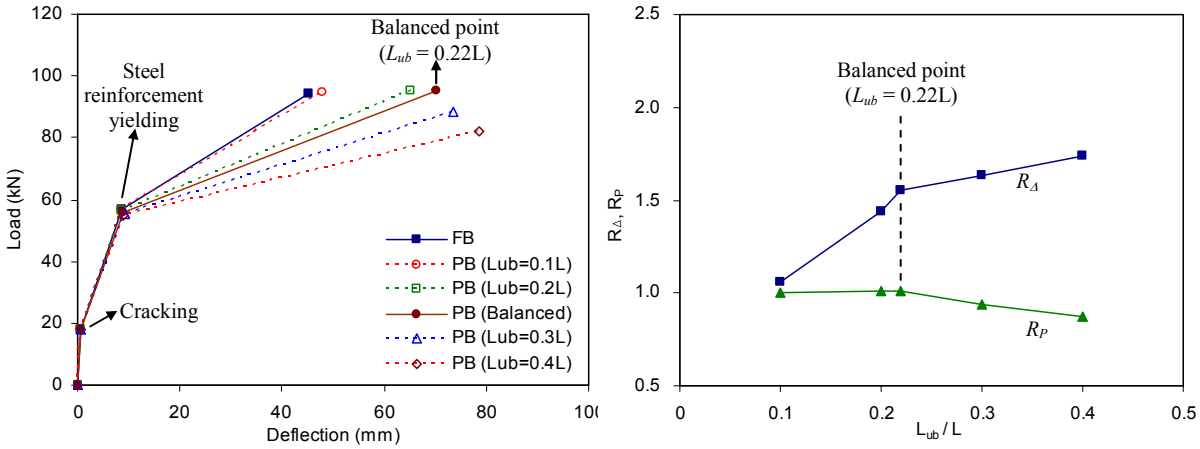

(a) Load-deflection curves with the increase of the unbonded length

(b) Effect of partial unbonding on the ultimate strength and deflection

Figure 8-4 Load-deflection response with different unbonded lengths and the effect of the partial unbonding on the strength and the deflection

Figure 8-4(b) shows the deflection ratio ($R_\Delta = \Delta_p / \Delta_f$) and the strength ratio ($R_P = P_p / P_f$) between the fully bonded and the partially bonded beams, where Δ_p and Δ_f are the ultimate deflections of the partially bonded and fully bonded beams, respectively, while P_p and P_f are the ultimate load of the partially bonded and fully bonded beams, respectively. Up to the balanced point, the deflection in the partially bonded beam was increased by approximately 1.5 times compared to the fully bonded beam

without a reduction of the strength as shown in Figure 8-4(b). At the balanced point, the slopes of the R_Δ and R_P curves starts to decrease implying that the effectiveness of the partially bonded system is decreased since the ultimate load is decreased and the rate of the deflection increase is reduced. Therefore, it is recommended that the partially bonded system should be applied with the unbonded length less than the balanced unbonded length to maximize the effectiveness of the partially bonded system.

8.4.2 Parametric study for various configurations of the beams

The parametric study was performed using the analytical model to study the effect of the main variables on the performance of the partially bonded system. Ultimately, the design recommendations for partially bonded beam have been proposed based on the results of the parametric study. The main variables are the area of steel reinforcement, A_s, the area of FRP reinforcement, A_f, the concrete strength, f'_c, and the effective prestress in the FRP, f_{pe}. The study was conducted for the basic beam configuration presented in Section 3.2.5, and the main variables were changed one at a time. For the area of steel reinforcement and FRP reinforcement, half of the area, 1.5 times and 2 times of the area were investigated. For the concrete strength, 30MPa, 40MPa, 52.5MPa, and 60MPa were used. The level of the prestressing force of FRP was also changed from 0% to 60% of the ultimate tensile strength. The unbonded length was varied for each beam (L_{ub}) with value of 0.1L, 0.2L, 0.3L, 0.4L, and L_{ubb}. A total of 78 different beam configurations were investigated for the loading condition of L_p = 0.05L, including the fully bonded beam. In addition, different loading conditions (L_p = 0.025L, 0.05L, 0.10L, 0.15L, and 0.20L) were investigated to derive the design recommendations discussed in the following section. Therefore, a total of 390 different beam configurations were investigated in this study.

Figure 8-5 shows the R_Δ and R_P curves of each beam configuration for the loading condition of L_p = 0.05L. As the steel reinforcement area was increased, the balanced unbonded length was decreased

and the improvement of the deflection ratio (R_Δ) at balanced condition was decreased as shown in Figure 8-5(a). Same results were observed for the case of the FRP reinforcement area as shown in Figure 8-5(b). On the other hand, the deflection ratio and the balanced unbonded length were increased when the concrete compressive strength and the level of the prestressing force were increased, as illustrated in Figure 8-5(c) and (d).

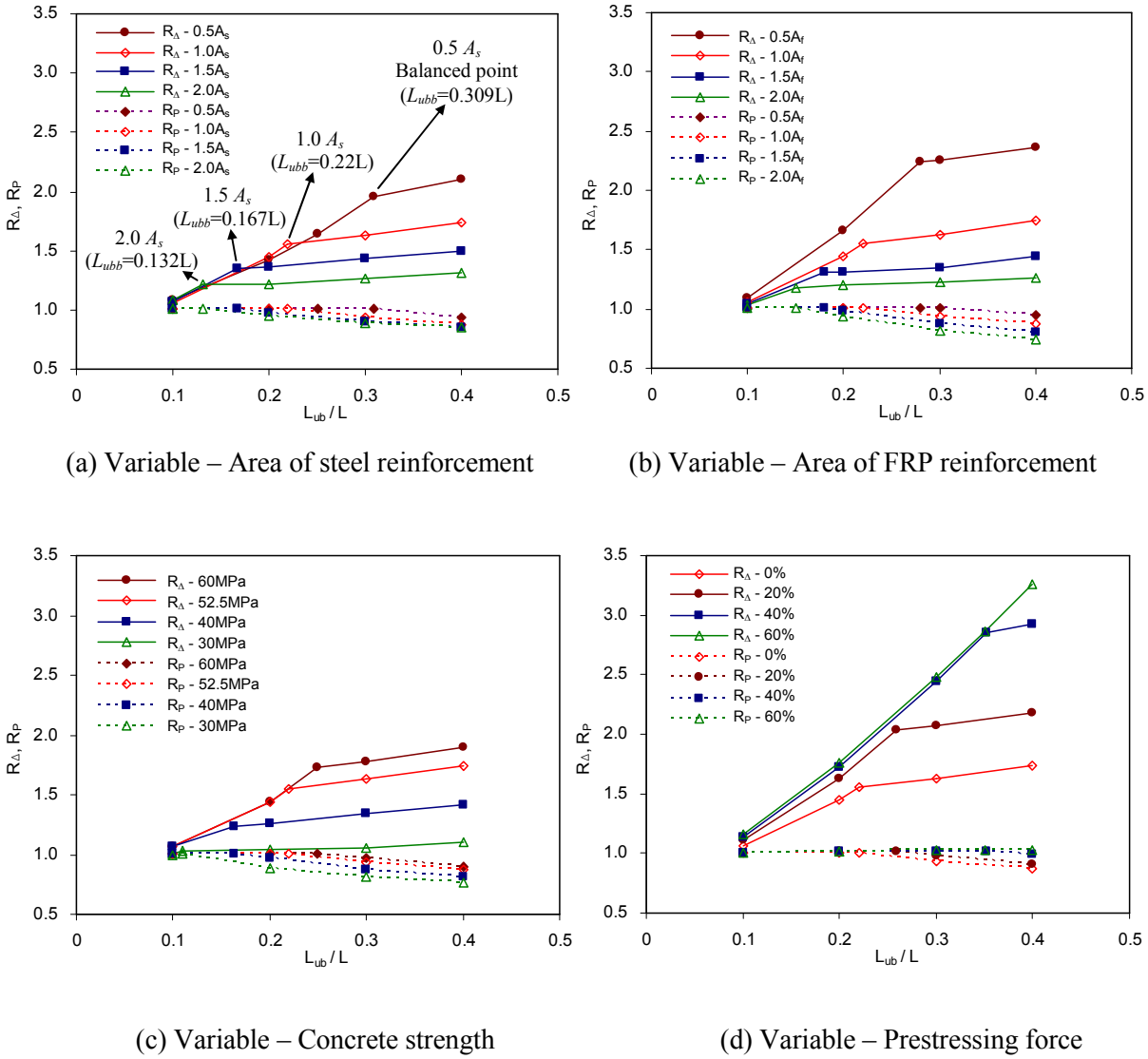

(a) Variable – Area of steel reinforcement

(b) Variable – Area of FRP reinforcement

(c) Variable – Concrete strength

(d) Variable – Prestressing force

Figure 8-5 Effect of the partial unbonding on the strength and the deflection with changing the main variables (L_p = 0.05L)

These observations are related to the balanced FRP area ($A_{f,b}$) for each beam relative to the area of the FRP used (A_f). Specifically, if $A_{f,b}$ of the given beam configuration is much greater than A_f, then the beam has high potential to increase the deflection ratio and the balanced unbonded length in comparison to the beam where $A_{f,b}$ is just slightly higher than A_f. This observation and the results of the parametric study can be explained further by examining the effect of the variables on $A_{f,b}$, as given by the equation in Figure 8-3(a). That is, $A_{f,b}$ can be increased by increasing the concrete strength (f'_c) and the prestressing force (c_b is increased because ε_{fu} is reduced due to prestressing force), and by decreasing the area of the steel reinforcement (A_s). The observations presented above were found to be independent of the different loading conditions (defined by L_p) investigated in the parametric study.

The effect of the main variable on the ultimate response of an under-strengthened beam is shown schematically in Figure 8-6. The large solid circle represents the ultimate response of the current configuration in the fully bonded condition of the under-strengthened beam. This solid circle moves along a solid arrow when a certain variable (A_s, A_f, f'_c, or f_{pe}) is increased. The small solid circle represents the ultimate response of the fully bonded beam with a changed variable. Once the unbonded length is increased, each small solid circle moves along the dotted arrow until the unbonded length reaches the balanced unbonded length. The solid square is the ultimate response of the partially bonded beam with the balanced unbonded length. For example, if the area of the steel reinforcement is increased from a certain configuration in the fully bonded condition (large solid circle), the ultimate load increases while the ultimate deflection has almost no change (small solid circle). If the unbonded length is increased at this state, the ultimate deflection is increased up to the balanced point without change of the ultimate load (solid square). If the unbonded length is increased beyond the balanced unbonded length, the strength is decreased although the deflection is slightly increased.

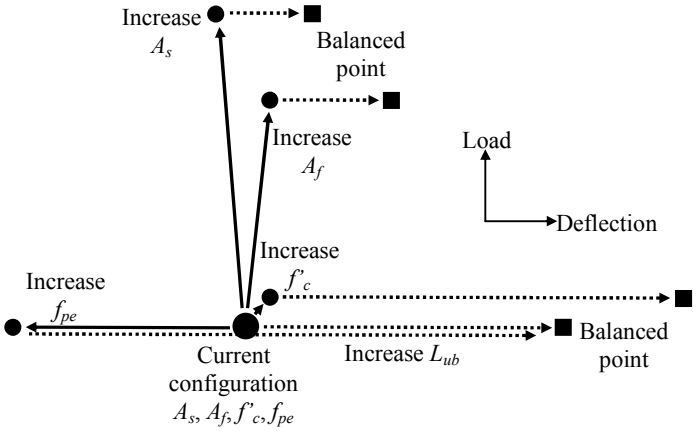

Figure 8-6 Ultimate response with changing the main variables and the unbonded length

8.4.3 Design recommendations

As investigated in the preceding sections, if the beam is under-strengthened the deformability can be increased without a reduction of the strength by increasing the unbonded length up to the balanced unbonded length. On the other hand, if the beam is an over-strengthened beam, then the partial unbonding can increase the deflection but the ultimate strength of the beam will be reduced. Therefore, it is recommended that the partially bonded system should be applied to under-strengthened beams with an unbonded length up to the balanced unbonded length.

All of the ultimate responses from the parametric study with L_{ub} up to the balanced point were plotted in one graph as shown in Figure 8-7. There was a strong relationship between the unbonding ratio (L_{ub}/L) and the deflection ratio (R_Δ) as shown in Figure 8-7 at each loading condition. The deflection ratio increased nonlinearly with increasing values of unbonding ratio, and this nonlinearity was more prominent as the loading distance decreased. Specifically, the increase of the deflection ratio was reduced as the loading distance increased as shown in Figure 8-7. For example, if the unbonding ratio (L_{ub}/L) is 0.3, the deflection ratios are 1.2, 1.4, 1.7, 2.3, and 3.2 for the beams with L_p/L = 0.2, 0.15, 0.1, 0.05, and 0.025, respectively. This indicates that the ultimate deflection can be improved by 3.2 times in the beam with the unbonded length (L_{ub}) of 0.3L and the loading distance

(L_p) of 0.025L, while the improvement is only 1.2 if the loading distance (L_p) is 0.2L with the same unbonded length (L_{ub} =0.3L).

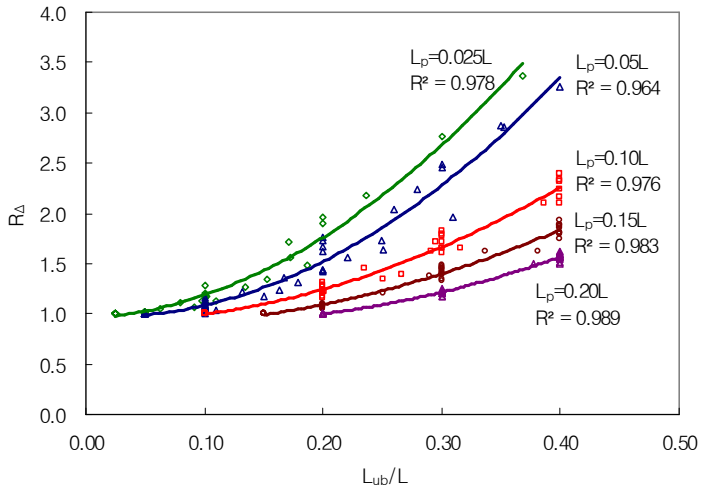

Figure 8-7 Relationship between deflection ratio (R_Δ) and partial unbonding ratio (L_{ub}/L)

To utilize the chart of Figure 8-7, the balanced unbonded length, L_{ubb}, for each configuration must be known since the curves in Figure 8-7 were derived based on the beam responses up to the balanced condition. Figure 8-3(b) shows the balanced condition in the partially bonded beam. The difference in the equations of the balanced FRP area between fully and partially bonded beams ($A_{f,b}$ and $A'_{f,b}$) is the use of ε'_f instead of ε_{fu} (c_b' instead of c_b). ε'_f can be calculated based on the overall strain compatibility, as shown in Figure 8-8 (slightly modified from Figure 3-1 in Section 3.2) by letting area A_1 equal area A_2; however, the calculation is very complicated and it needs to be simplified for design purposes.

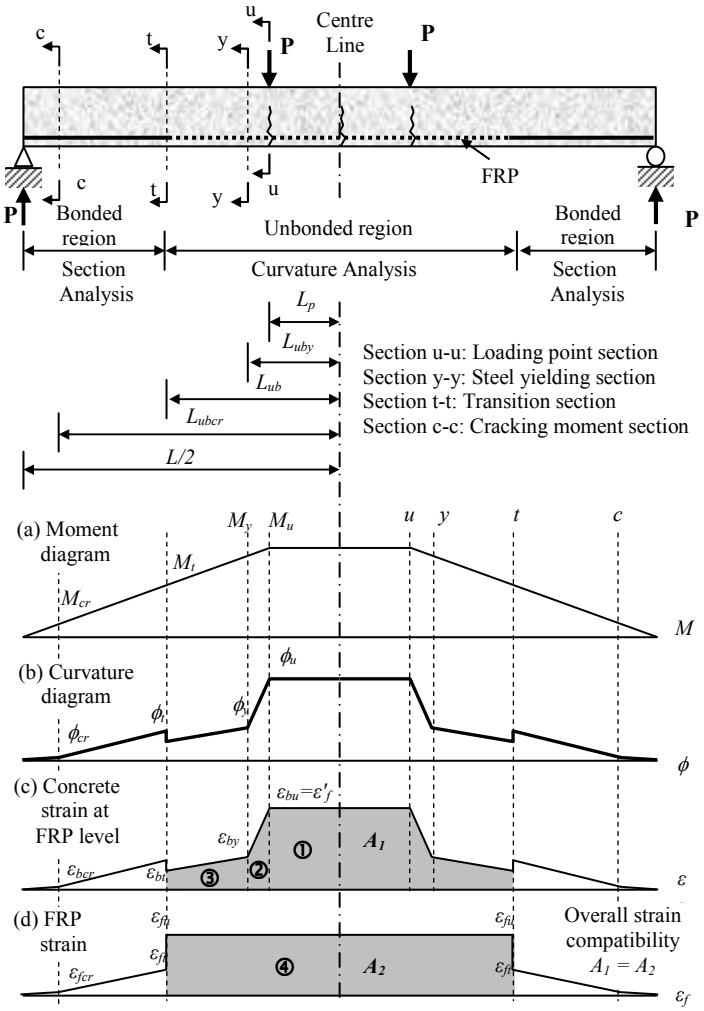

Figure 8-8 Basic concept for the analysis of the partially bonded FRP strengthened beams at ultimate

At ultimate, ε'_f is much greater than ε_{by} and ε_{bt} in Figure 8-8(c), and therefore if the areas ② and ③ are neglected for simplicity, then the overall strain compatibility can be calculated by letting the area ① equal to area ④, which gives $\varepsilon'_f \times L_p = \varepsilon_{fu} \times L_{ub}$. Therefore, $A'_{f,b}$ and c'_b on the equation in Figure 8-3(b) can be written as follows.

$$A'_{f,b} = \frac{\alpha f'_c b c'_b - A_s f_{sy}}{E_f \varepsilon_{frpu}} \text{ where } c'_b = \frac{\varepsilon_{cu}}{\frac{L_{ub}}{L_p} \cdot \varepsilon_{fu} + \varepsilon_{bi} + \varepsilon_{cu}} \cdot d_f \quad (8\text{-}1)$$

When $A'_{f,b}$ equals A_f, then L_{ub} becomes L_{ubb}. Therefore, if $A'_{f,b}$ and L_{ub} in Eq. (8-1) are replaced with A_f and L_{ubb}^*, respectively, and ε_{bi} is assumed to be zero, then Eq. (8-1) can be rearranged as shown in Eq. (8-2), where, L_{ubb}^* represents the balanced unbonded length calculated based on the simplification above.

$$\frac{L_{ubb}^*}{L_p} = \frac{\varepsilon_{cu}}{\varepsilon_{fu}} \left(\frac{\alpha f'_c b d_f}{A_f E_f \varepsilon_{frpu} + A_s f_{sy}} - 1 \right) \quad (8\text{-}2)$$

Eq. (8-2) is derived based on the rectangular section without compression steel reinforcement. Therefore, if the sectional and geometric properties are different, an appropriate equation should be derived. Figure 8-9(a) shows the relationship between L_{ubb} calculated by the model and L_{ubb}^* calculated using Eq. (8-2) for the various beam configurations used in the parametric study. L_{ubb} is always greater than L_{ubb}^* because the areas ② and ③ in Figure 8-8 were neglected when calculating L_{ubb}^*. The difference between them is greater when the loading distance (L_p) is smaller since the portion of areas ② and ③ is decreased compared to the portion of the area ① as the loading distance increases. Figure 8-9(b) shows the correction factor with the loading distance derived from the results of the regression shown in Figure 8-9(a). Once L_{ubb}^* is calculated using Eq. (8-2), the final L_{ubb} can be predicted by multiplying L_{ubb}^* by the correction factor in Figure 8-9(b) for a certain loading condition. For cases where L_p is greater than 0.15L, the balanced unbonded lengths of most beams were greater than 0.4L.

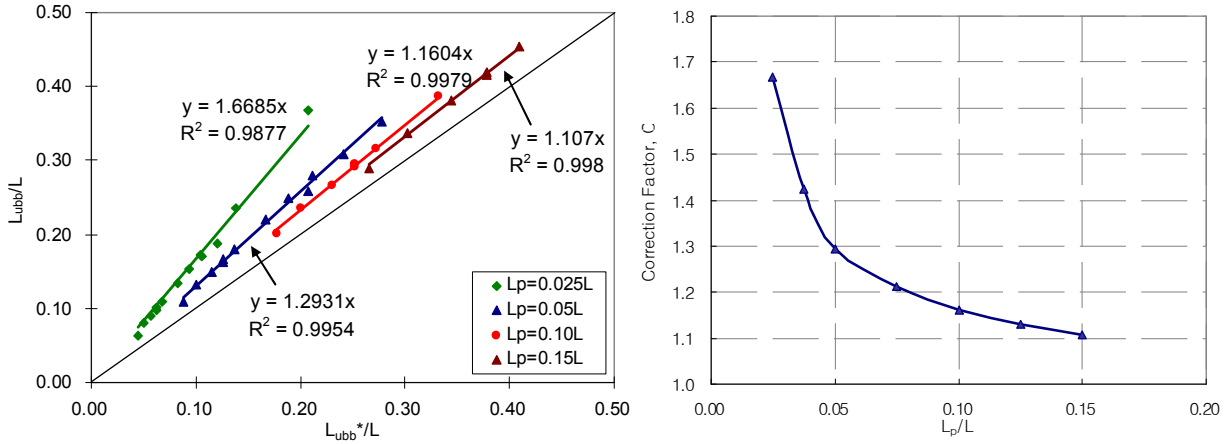

(a) Estimation of L_{ubb} from L_{ubb}^{*} (b) correction factor with L_p/L

Figure 8-9 Design charts for the use of the partially bonded FRP strengthening system

The general procedure to apply the partially bonded system for the design of flexural strengthening utilizing the charts in Figure 8-7 and Figure 8-9 is proposed as follows.

1. Calculate the required area of FRP, A_f, based on the strength limit state for the fully bonded condition.
2. Check $A_{f,b} > A_f$. $A_{f,b}$ can be calculated by the equation in Figure 8-3(a). If $A_{f,b}$ is less than A_f the beam is over-strengthened and the use of partially bonded system is not recommended since the ultimate strength can be decreased.
3. Calculate L_{ubb}^{*} using Eq. (8-2) and find L_{ubb} by multiplying L_{ubb}^{*} by the correction factor in Figure 8-9(b) for a given loading condition.
4. Determine the final L_{ub} which should be less than or equal to L_{ubb}, assuring the required anchorage length to prevent debonding failure.
5. Find R_Δ using Figure 8-7 to determine the improvement of the ultimate deflection compared to a fully bonded beam when applying the partially bonded length, L_{ub}, to the beam.

6. If the partially bonded system is applicable and advantageous, detailed calculation can be done using the analytical model developed in Section 3.2 to confirm the predicted load-deflection behaviour.

Note that the charts in the Figure 8-7 and Figure 8-9 were developed considering many possible variations of the main variables of the beam; therefore they can be used for the general design purpose. However, more configurations should be investigated and more experimental verification should be accompanied in the future.

8.5 Summary

An overall evaluation of the test results and the analytical model was performed. A parametric study was conducted for the partially bonded fibre-reinforced-polymer (FRP) strengthening system and a design procedure for the use of this system was proposed. The following conclusions are made:

1. The test results of the partially bonded beams showed improved ultimate deformation while sustaining a high load carrying capacity without a change of the serviceability compared to the fully bonded beams.
2. An analytical model predicted the behaviour of the beams near failure well.
3. A parametric study was performed and showed that the FRP strengthened beam that has an FRP area (A_f) less than the balanced FRP area ($A_{f,b}$) for the section has high potential to improve the deformability as the unbonded length increases. The balanced FRP area is increased as the concrete strength and the FRP prestressing force are increased, or as the areas of the steel reinforcement decreases.
4. A simplied design procedure and design charts were proposed for the partially bonded system to provide the improved deformability for a given unbonded length compared to the fully bonded beam.

Chapter 9
Conclusions and Future Work

9.1 Conclusions

A comprehensive investigation on the effect of partial unbonding for various FRP strengthening systems was conducted with the specific objective of increasing the deformability of CFRP flexural strengthened concrete T-beams. A new analytical model was developed and an extensive experimental program was conducted. Finally, design recommendations and procedures were proposed for the effective use of the partially bonded FRP strengthening system. The specific conclusions drawn from this study are provided in the following sections.

9.1.1 Development of analytical model

- An analytical model was developed based on the curvature approach for the analysis of partially bonded beams. This model uses the simplified curvature and strain variations that change linearly between several critical sections of interest along the beam length. Strains and curvatures at critical sections are calculated based on the applied load (moment of the section) while addressing the overall strain compatibility of the partially bonded system.
- An equivalent 4-point loading was proposed for the analysis of partially bonded beams subjected to uniform loading based on the equivalent deflection and moment of the beam.
- The developed model predicted the general behaviour of the partially bonded beams well with various unbonded lengths. The model also showed that a balanced condition and a balanced unbonded length exist in under-strengthened beams, where the deformability of the beam was maximized without loss of the flexural strength.

- The analytical model showed that the partially bonded FRP strengthening system has a high potential to improve the beam deformability while sustaining high load carrying capacity in comparison to the fully bonded system.

9.1.2 Externally bonded (EB) FRP strengthening system

- A typical flexural crack induced debonding failure was observed in the fully bonded beam, while this type of debonding failure was avoided in the partially bonded beams due to intentional unbonding at mid-span. However, debonding failure was initiated at the transition point in the partially bonded beams. The partially bonded beams exhibited the increase of the ultimate load carrying capacity and ultimate deflection compared to the fully bonded beam.
- Among partially bonded beams, the ultimate response (load and deflection) was decreased as the unbonded length was increased. The bond strength at the FRP-concrete interface may decrease as the unbonded length increases because the anchorage (bonded) length at both ends is decreased.
- The predicted load-deflection behaviour and the strain distribution matched the experimental results well except that the ultimate response at failure was over-predicted due to early debonding failure that occurred in the tested beams.
- Three-dimensional nonlinear finite element (FE) analysis was performed utilizing interfacial elements and contact modeling, and showed that the maximum bond stress in the fully bonded beam was approximately 8MPa; the effect of U-wraps at transition point was significant to improve the flexural capacity; and the maximum bond strength in the partially bonded beams was decreased as the unbonded length increased. FE analysis also showed that the bond stress in the fully bonded beam was high near loading point at the crack location, inducing a debonding failure at that location. High bond stress occurred at the transition point where the debonding was initiated in the partially bonded beams.

9.1.3 Near surface mounted (NSM) FRP strengthening system

- Prominent stiffness reduction at the post-yielding stage was observed in the load-deflection diagrams as the unbonded length was increased in the NSM strengthened beams. This stiffness reduction induced the increased the deformability of the partially bonded beams for a given applied load in comparison to the fully bonded beam.
- The ultimate deflection in the partially bonded beams at failure showed only a slight increase (4.4% ~ 32.4%) compared to the fully bonded beam due to the complex behaviour of the strengthened beams including FRP slip and concrete gradual failure. The ultimate load carrying capacity was slightly decreased (10.0% ~ 15.7%) as the unbonded length increased because the failure mode was changed from FRP rupture to concrete crushing.
- An advanced model was proposed to demonstrate the effect of concrete gradual failure and FRP reinforcement slip using the idealized section model and slip model. This model represented the nonlinear behaviour in both the fully bonded and the partially bonded beams well.
- The NSM beams were much more effective than the EB beams (with similar axial stiffness of the FRP reinforcement) for the improvement of ultimate flexural capacity due to the apparent higher bond strength at the interface. The ultimate load carrying capacity of NSM beams was improved by 47.9%, 14.2%, 22.6%, and 27.4% in the fully bonded beam and partially bonded beams with the unbonded length of 2×650mm, 2×850mm, and 2×1050mm respectively compared to the EB beams. The ultimate deflections of the NSM beams were also greater by 205.1%, 60.5%, 135.6%, and 193.9% compared to EB beams in the same order. However, the serviceability, such as crack distributions and deflections at the service load was almost identical between the two systems.

9.1.4 Prestressed NSM FRP strengthening system

- Prestressed CFRP strengthened beams were very effective to improve the cracking load, to decrease the deflection at service load, and to increase ultimate load without regard to the bond

condition in comparison to the unstrengthened beam. The improvement was greater as the prestressing force increased, while the ultimate deflection was decreased.

- Partially bonded prestressed beams showed a significant improvement of deformability (12.1% ~ 77.5%) compared to the fully bonded beams without a significant loss of ultimate load carrying capacity (3.1% ~6.7%) and without significantly affecting serviceability. The improvement provided by partial unbonding was more effective at higher levels of prestressing force.
- The development length of the 40% prestressed FRP strengthened beams was approximately 700mm.
- The prestressed NSM strengthening system is much more effective to improve the ultimate load carrying capacity and the serviceability in comparison to the non-prestressed NSM beams. However, the deformability of the prestressed beams was decreased compared to the non-prestressed beams.

9.1.5 Design recommendations and procedures

- A parametric study was performed using an analytical model for 390 different beam configurations. The study showed that the FRP strengthened beam that has an FRP area (A_f) less than the balanced FRP area ($A_{f,b}$) for the section has high potential to improve the deformability as the unbonded length increases. The balanced FRP area is increased as the concrete strength and the FRP prestressing force are increased, or as the area of the steel reinforcement decreases.
- A design procedure and design charts were proposed for the design of the partially bonded system to provide the improved deformability for a given FRP reinforcement area and an unbonded length compared to the fully bonded beam.

9.2 Future Work

To apply the developed partially bonded system to real structures, further research and investigations considering field conditions are required.

For the prestressed strengthening system, the development of prestressing assembly suitable for field conditions is required because there is no access to the end of most beams or girders in buildings and bridges. Figure 9-1 shows the possible prestressing setup for the field application. The prestressing assembly is firmly attached to the bottom of structures using anchor bolts and the bar alignment might be slightly bent for the prestressing work as shown in Figure 9-1. For this case, the effect of the deviators on the tensile strength of the FRP bars should also be considered.

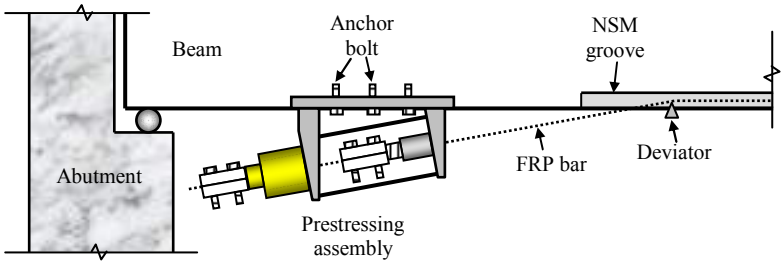

Figure 9-1 Prestressing assembly for the field application of the prestressed NSM system

In addition, more study on the bond properties of the strengthening systems is also needed, since the bond strength depends on many factors as described in Section 2.4.2. Particularly, the study on the bond property in the prestressed NSM system is very limited. For the effective use of the partially bonded prestressing system, a development length and a transfer length depending on the materials and geometric properties should be determined, so that an appropriate anchorage length can be applied to real structures. Figure 9-2 shows the partially bonded prestressed NSM beam with the bond stress distribution along the FRP bar. An appropriate anchorage length (bonded length at the end of FRP reinforcement) that is greater than the development length should be determined to prevent premature debonding failure.

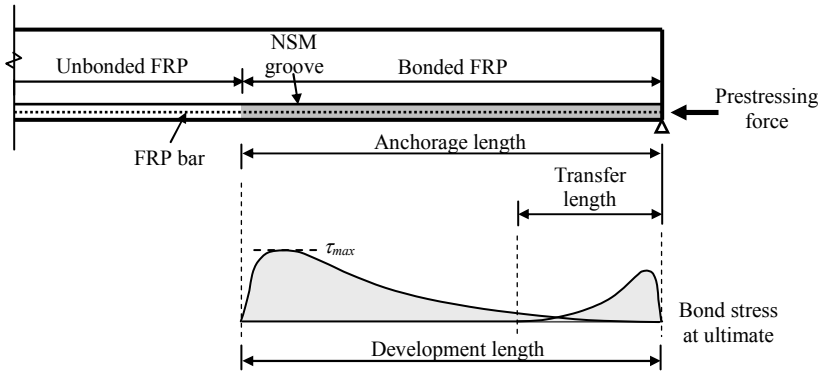

Figure 9-2 Anchorage length of partially bonded prestressed strengthened beam

For EB system beams, a quantitative approach that considers the effect of mechanical anchorage is required, so that the EB strengthening system can be effectively applied. Most bond stress-slip relationships have been derived based on the simple shear test for the specimens with no mechanical anchors (Dai et al. 2005, Nakaba et al. 2001), and only a qualitative approach has been performed for the effect of mechanical anchors including U-wraps (Teng et al. 2002b, Hollaway and Mays 1999). More research in this area is needed.

Appendix A
Flowcharts for Analytical Model

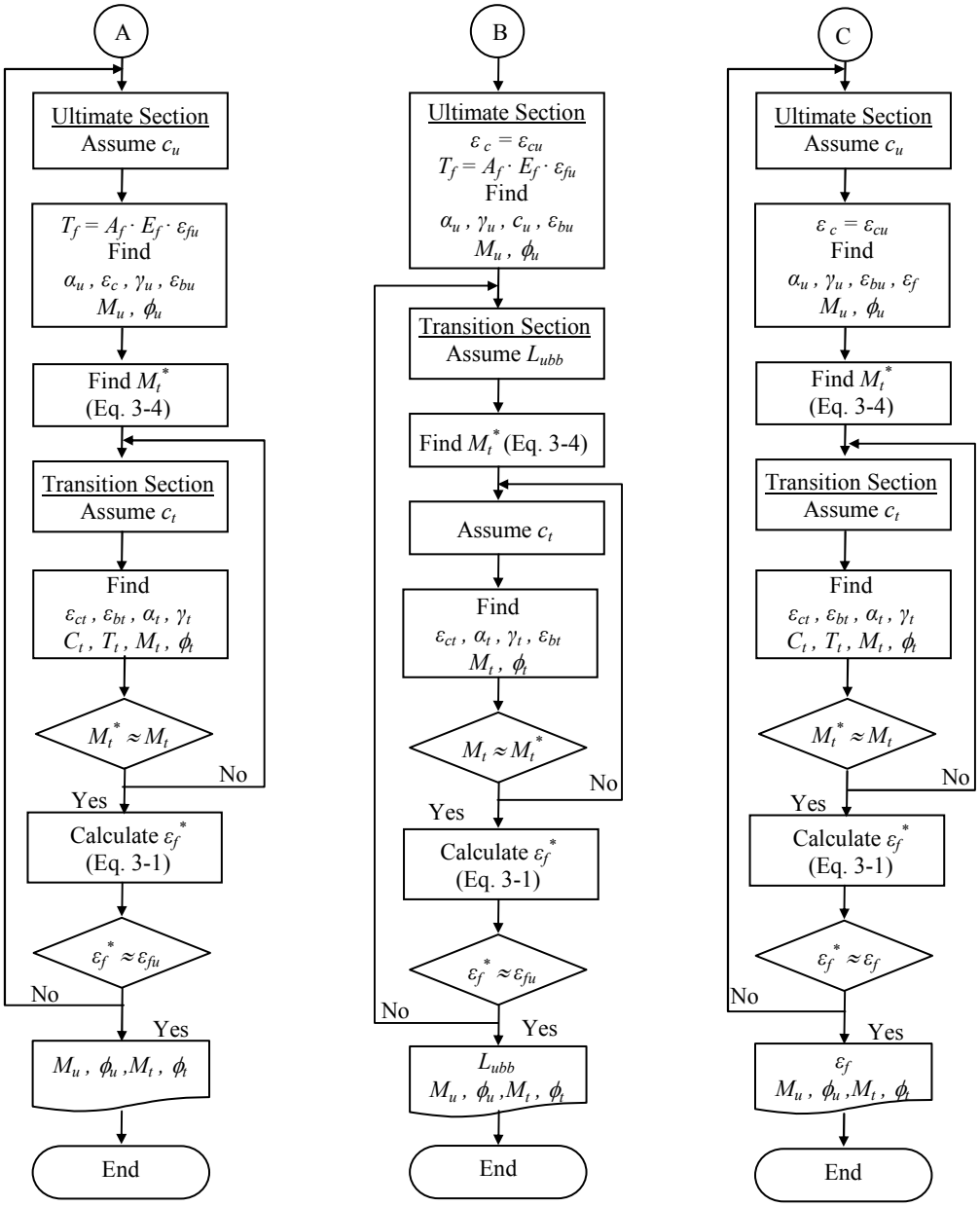

Figure A-1 Flowcharts for subroutines A to J

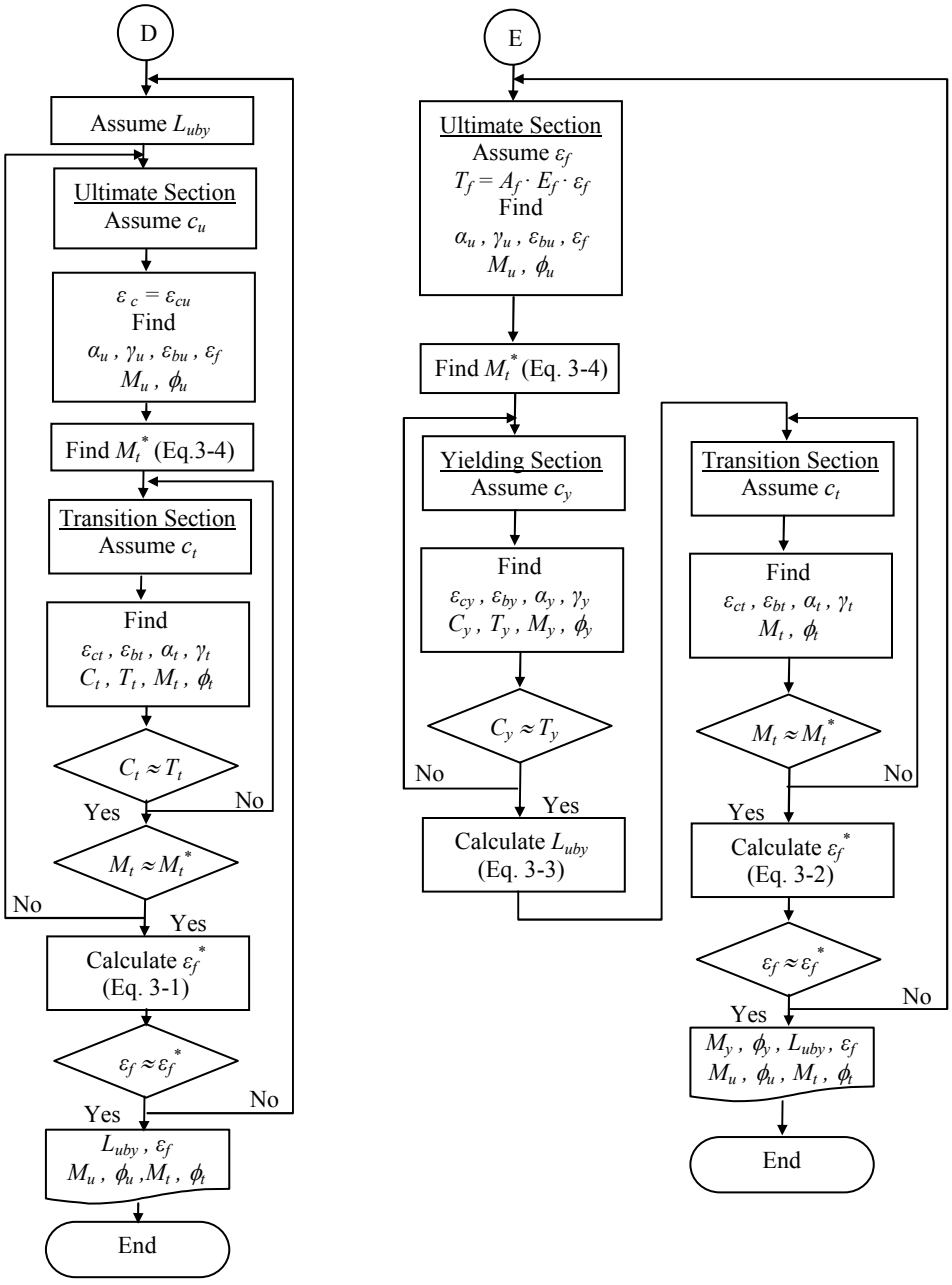

Figure A-1 Flowcharts for subroutines A to J (continued)

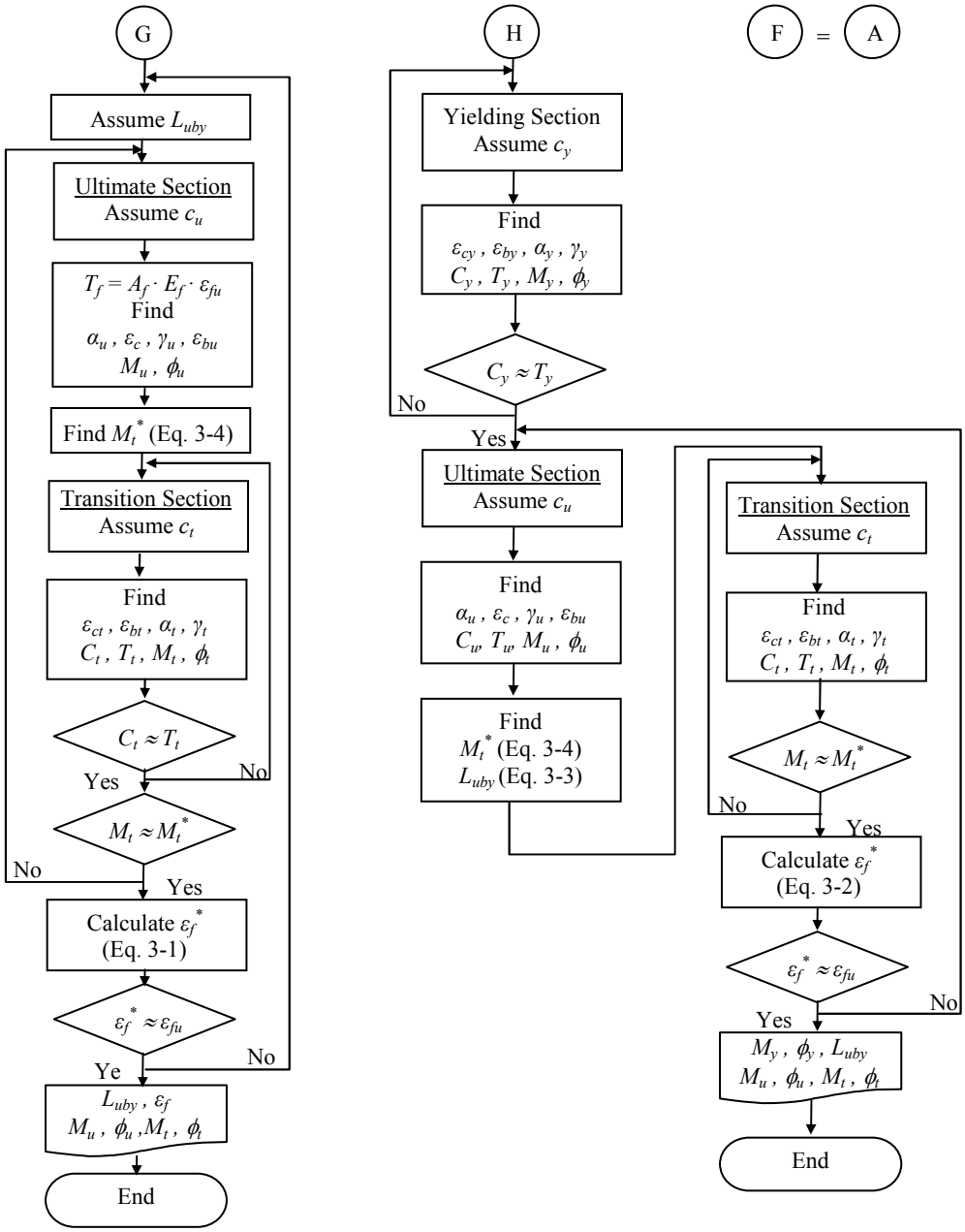

Figure A-1 Flowcharts for subroutines A to J (continued)

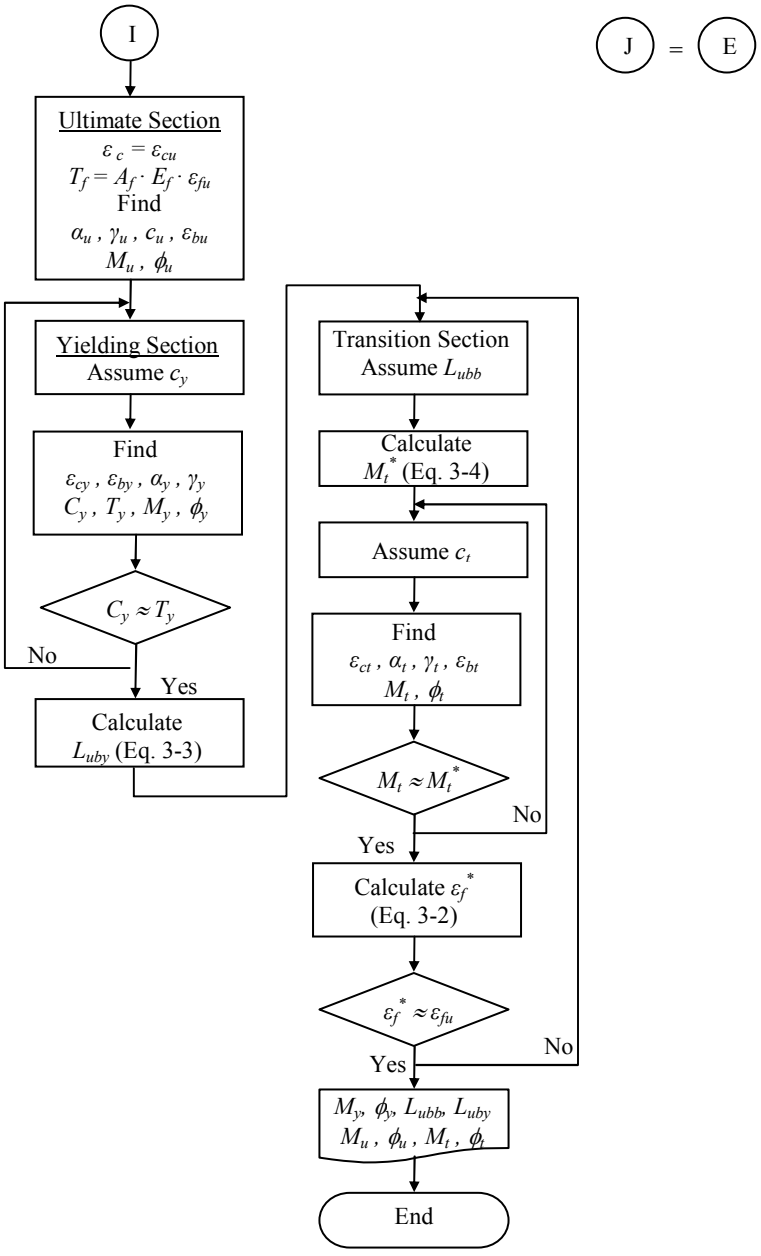

Figure A-1 Flowcharts for subroutines A to J (continued)

Appendix B

Prestressing Loss with Time during Curing of Adhesive

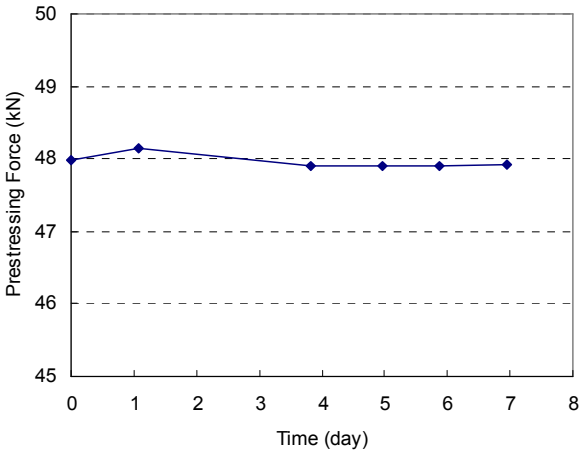

(a) Beam PBFB

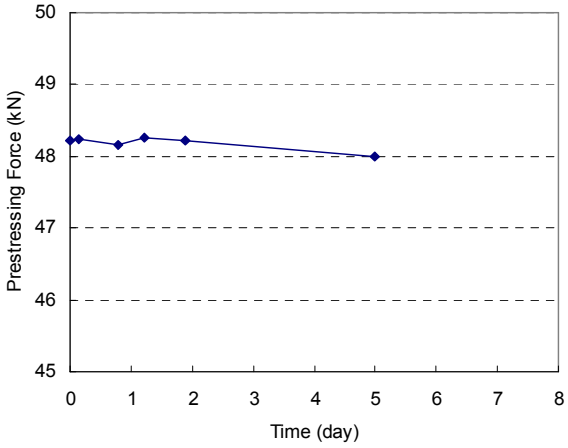

(b) Beam PBPB2

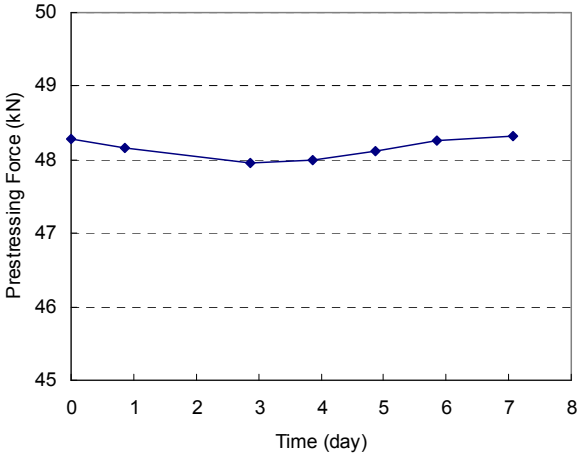

(c) Beam PBPB3

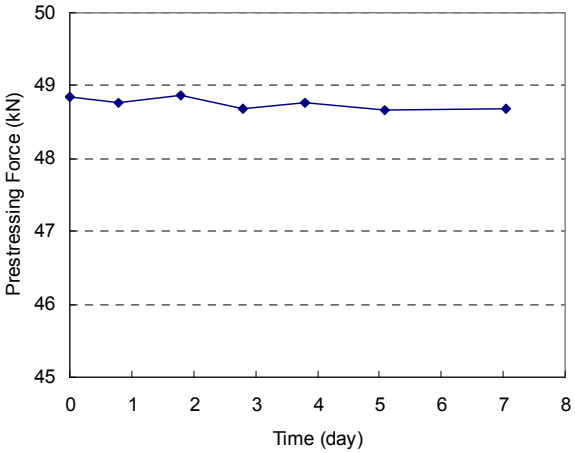

(d) Beam PBPB4

Figure B-1 Prestressing loss of prestressed CFRP strengthened beams with time

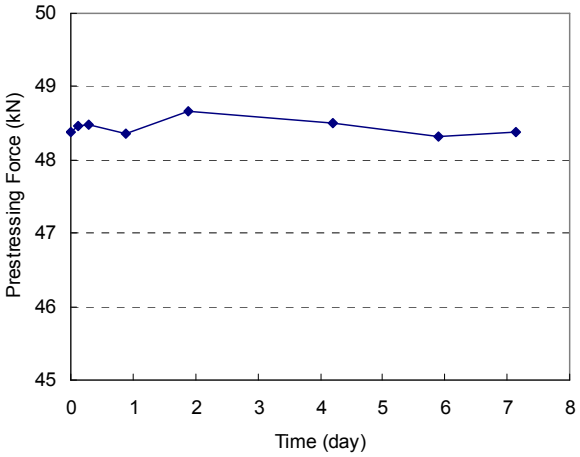

(e) Beam PBPB5

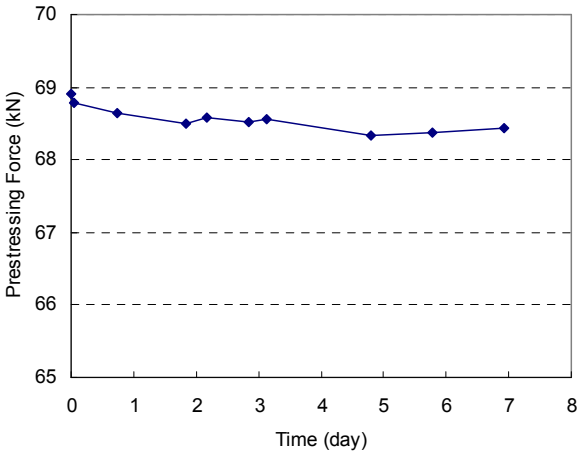

(f) Beam PBFB-60

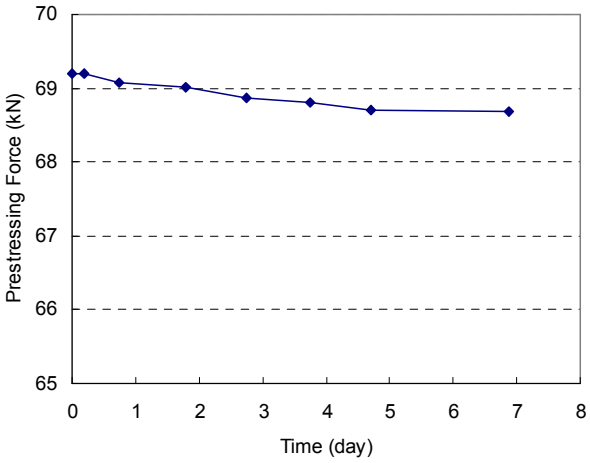

(g) Beam PBPB4-60

Figure B-1 Prestressing loss of prestressed CFRP strengthened beams with time (continued)

Appendix C

Failure Modes of Strengthened Beams

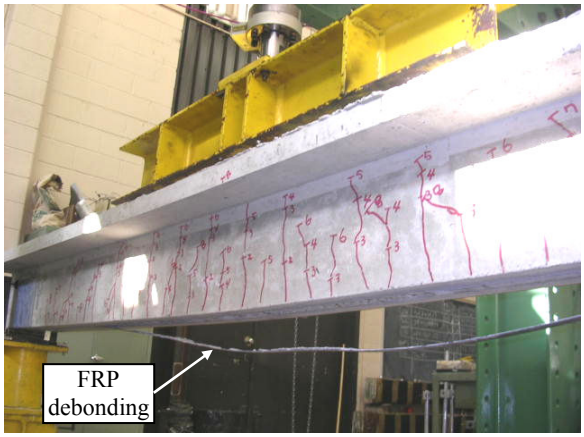

(a) Beam NPFB

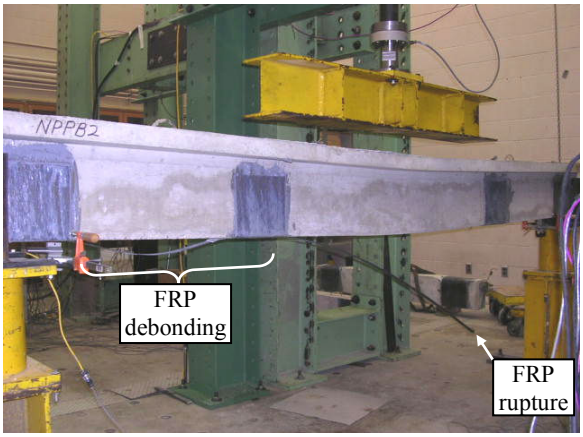

(b) Beam NPPB2

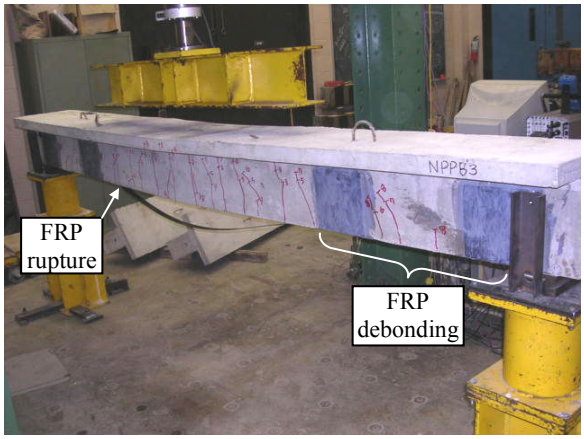

(c) Beam NPPB3

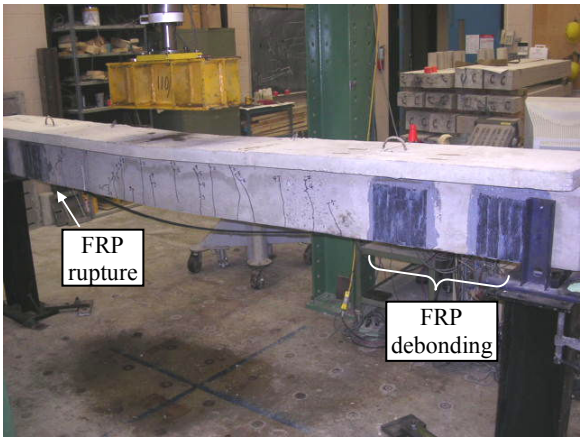

(d) Beam NPPB4

Figure C-1 Failure modes of EB strengthened beams (Group I)

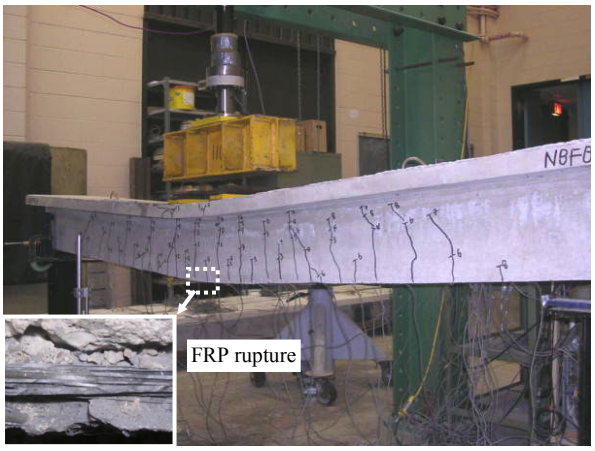

(a) Beam NBFB

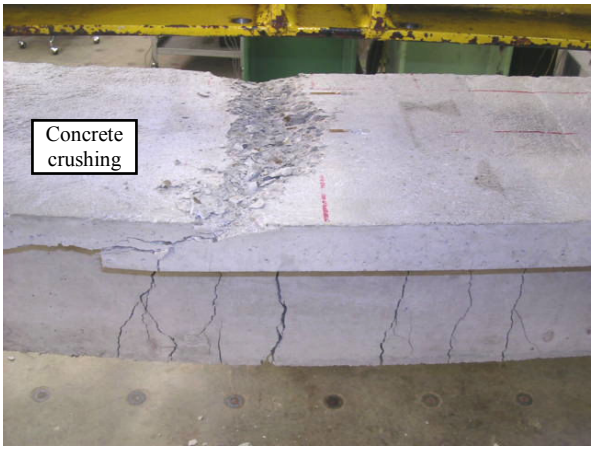

(b) Beam NBPB2

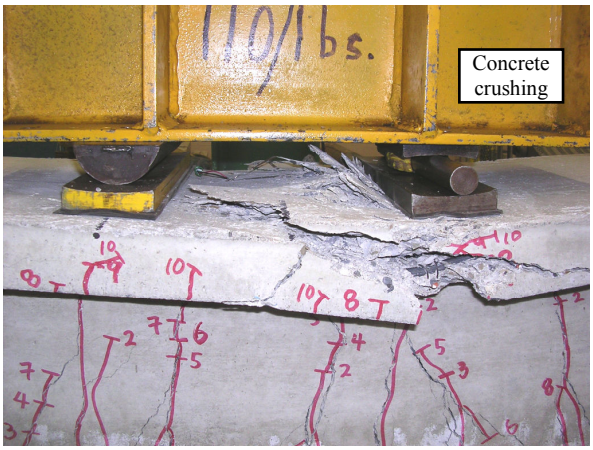

(c) Beam NBPB2.5

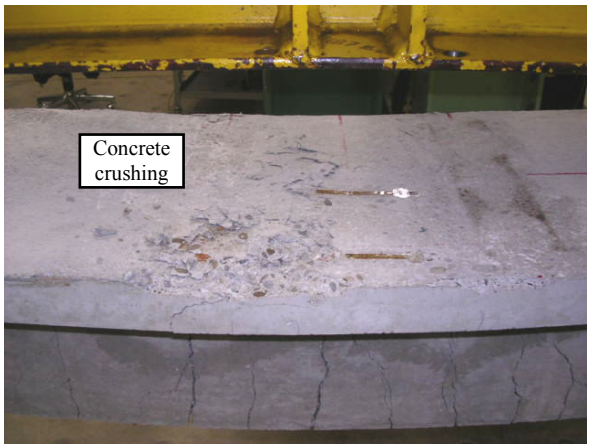

(d) Beam NBPB3

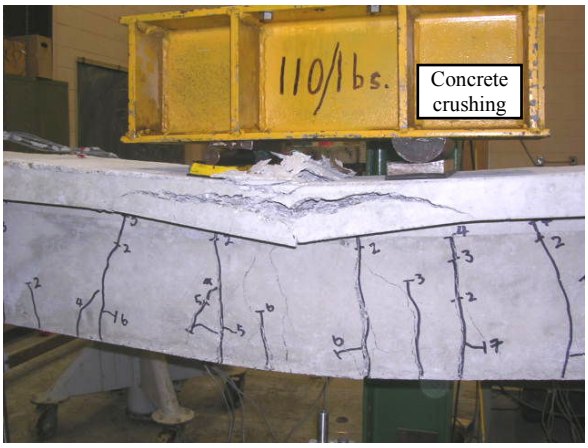

(e) Beam NBPB4

Figure C-2 Failure modes of NSM strengthened beams (Group II)

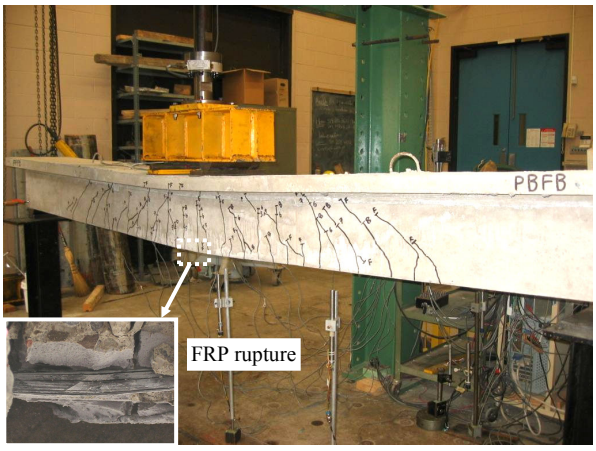

(a) Beam PBFB

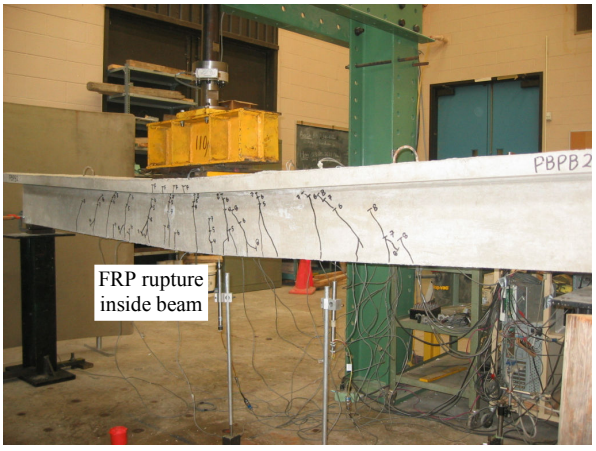

(b) Beam PBPB2

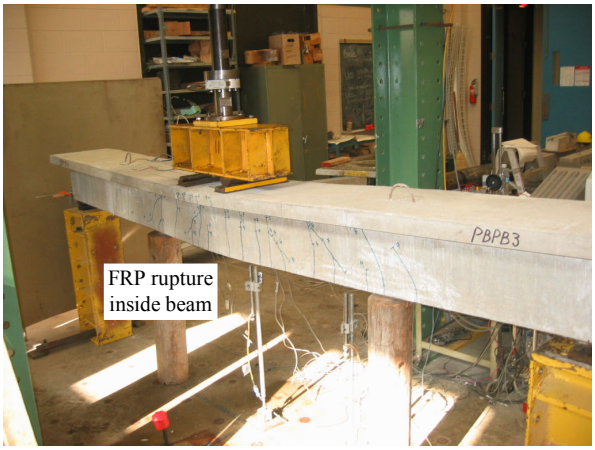

(c) Beam PBPB3

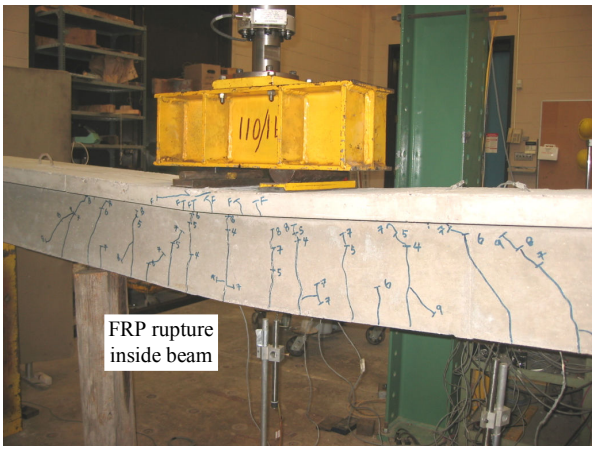

(d) Beam PBPB4

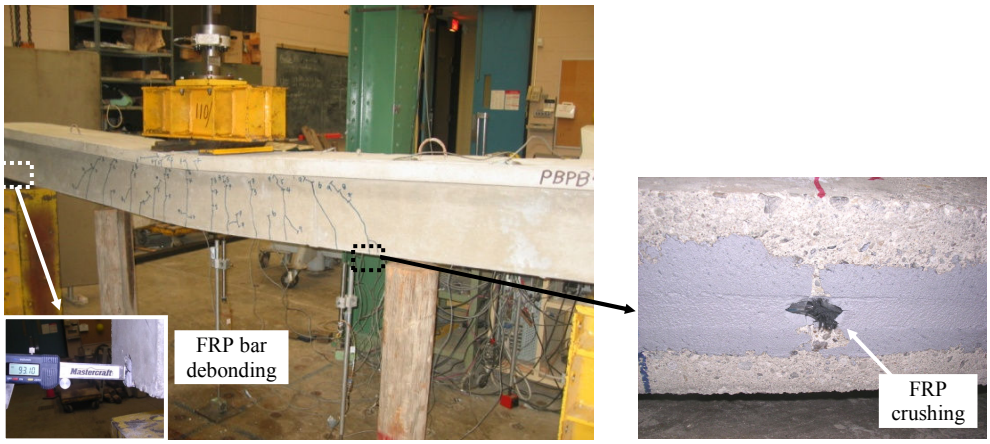

(e) Beam PBPB5

Figure C-3 Failure modes of prestressed NSM (40%) strengthened beams (Group III)

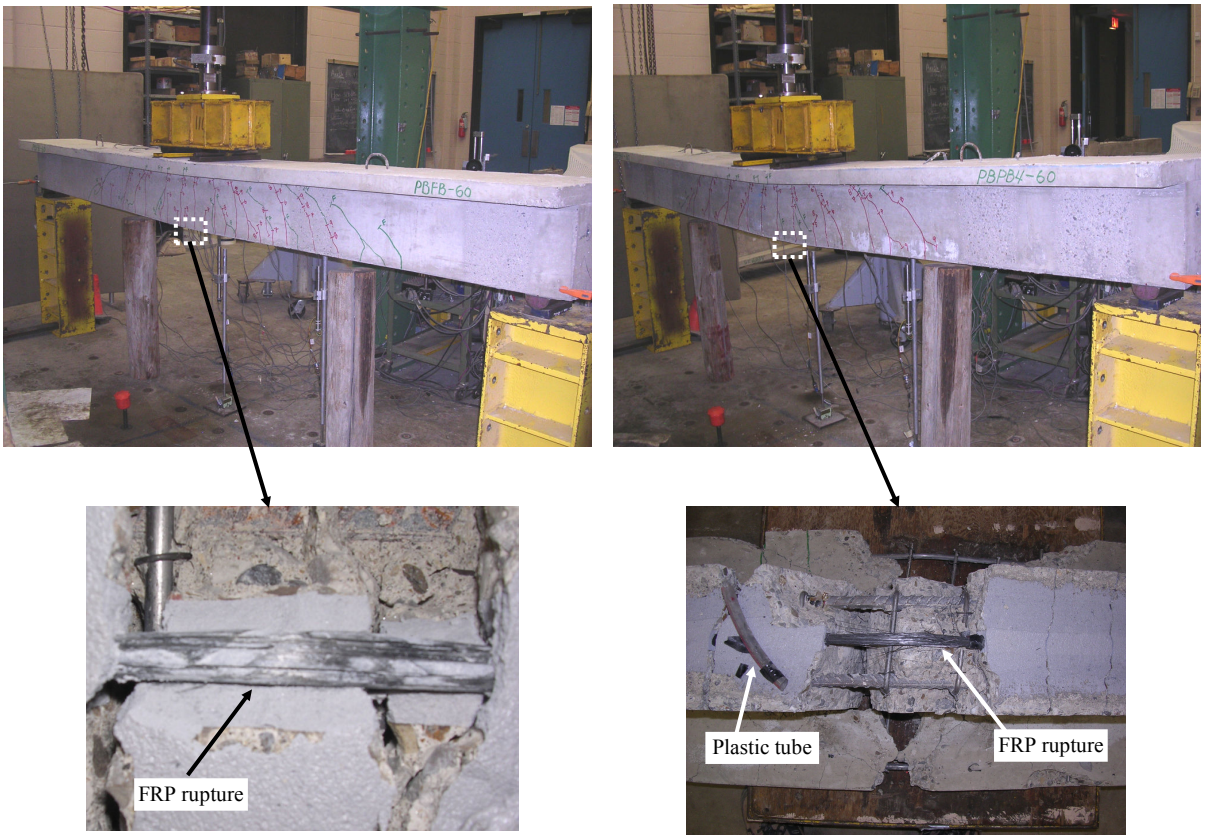

(a) Beam PBFB-60 (b) Beam PBPB4-60

Figure C-4 Failure modes of prestressed NSM (60%) strengthened beams (Group IV)

Appendix D

Variation of Measured Strains with Applied Load

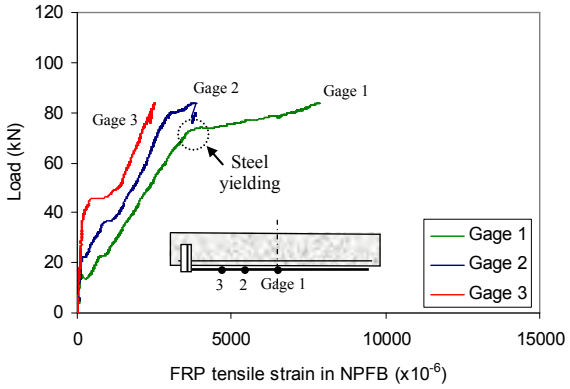

(a) Beam NPFB

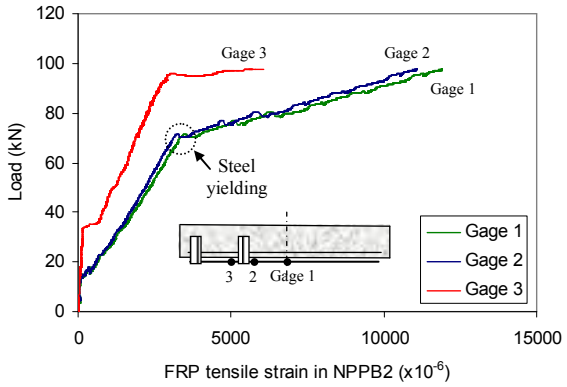

(b) Beam NPPB2

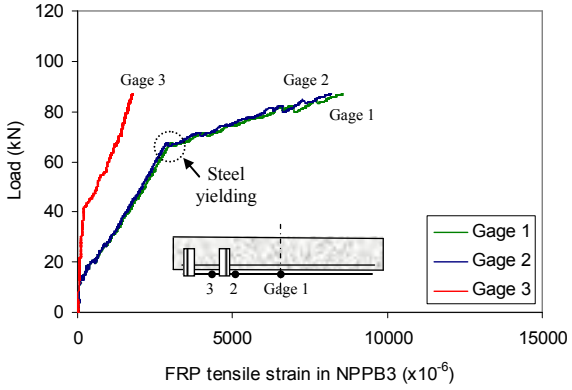

(c) Beam NPPB3

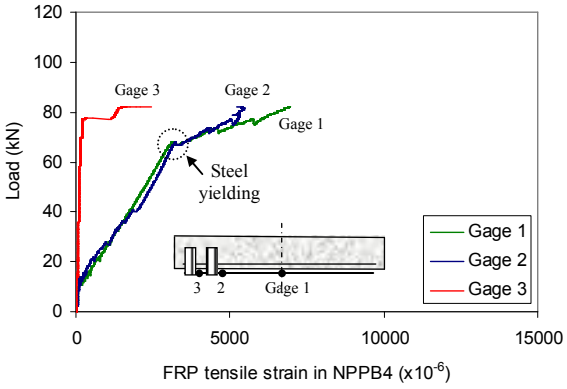

(d) Beam NPPB4

Figure D-1 Variation of FRP strains with applied load (Group I beams)

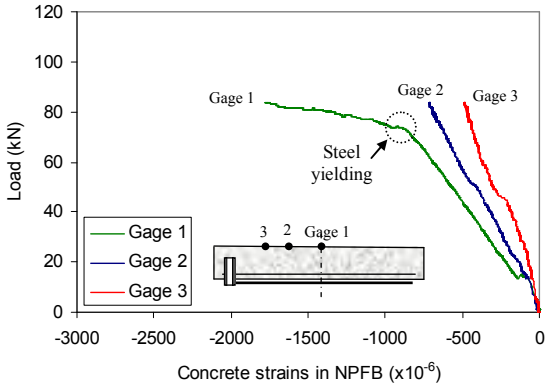

(a) Beam NPFB

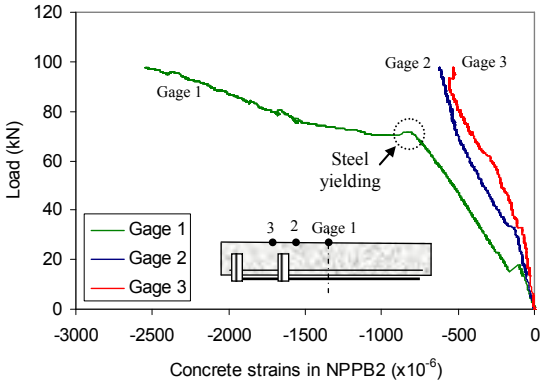

(b) Beam NPPB2

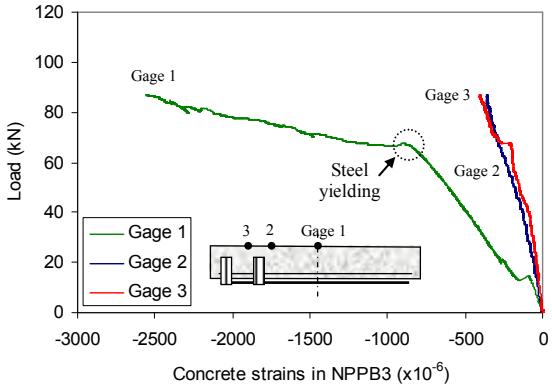

(c) Beam NPPB3

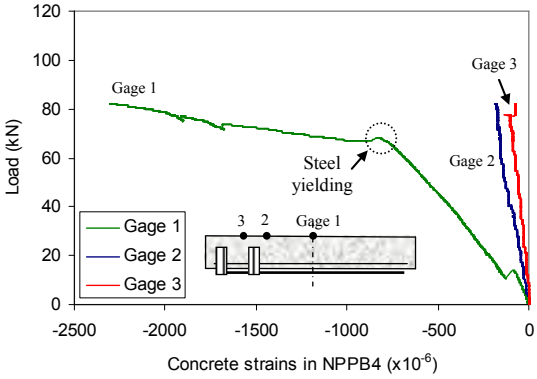

(d) Beam NPPB4

Figure D-2 Variation of concrete strains at top fibre with applied load (Group I beams)

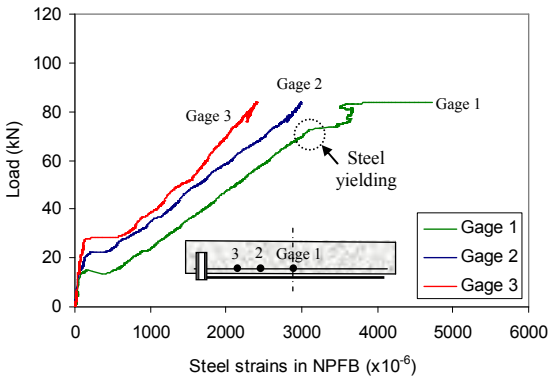

(a) Beam NPFB

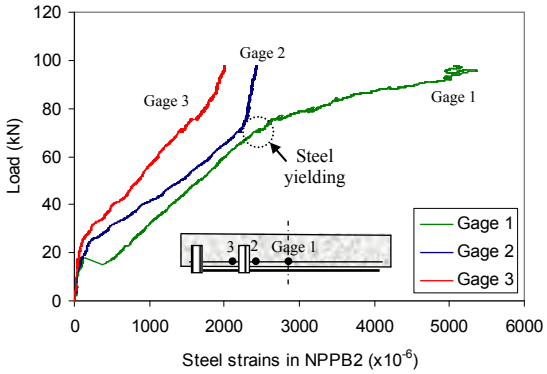

(b) Beam NPPB2

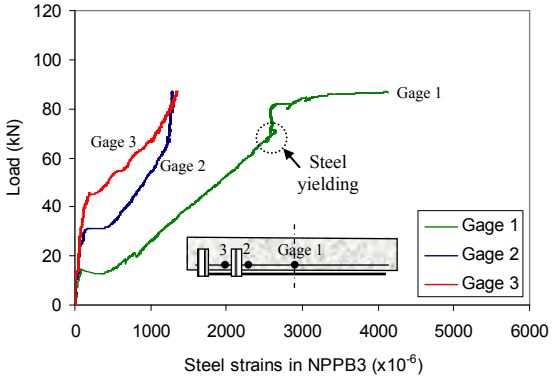

(c) Beam NPPB3

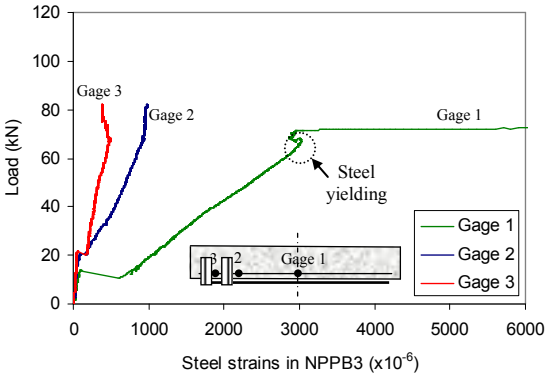

(d) Beam NPPB4

Figure D-3 Variation of steel reinforcement strains with applied load (Group I beams)

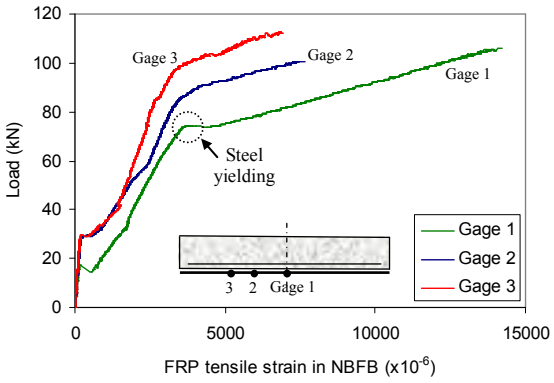

(a) Beam NBFB

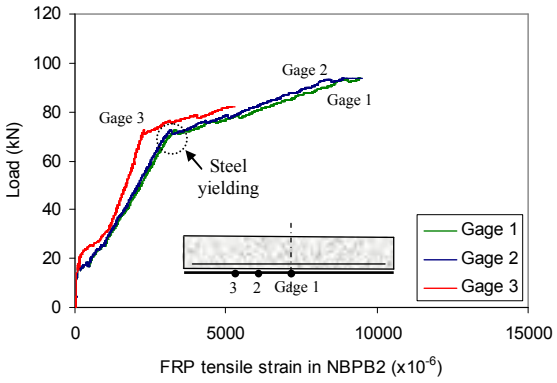

(b) Beam NBPB2

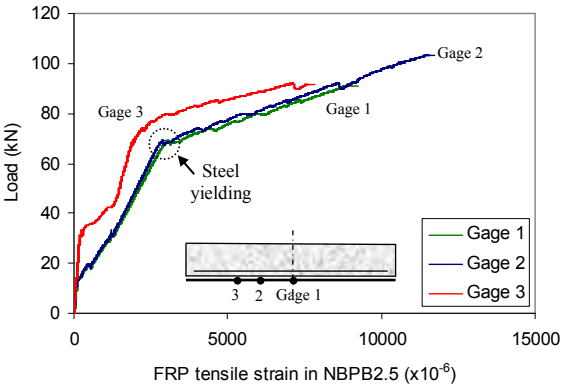

(c) Beam NBPB2.5

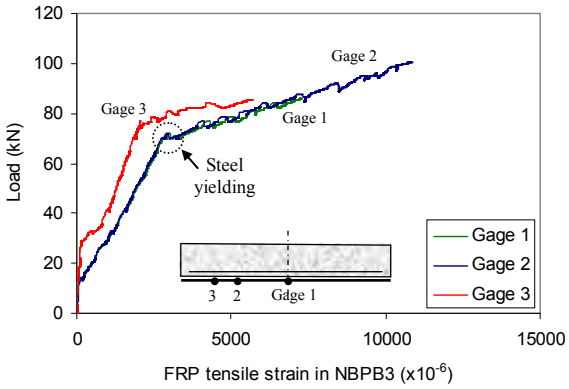

(d) Beam NBPB3

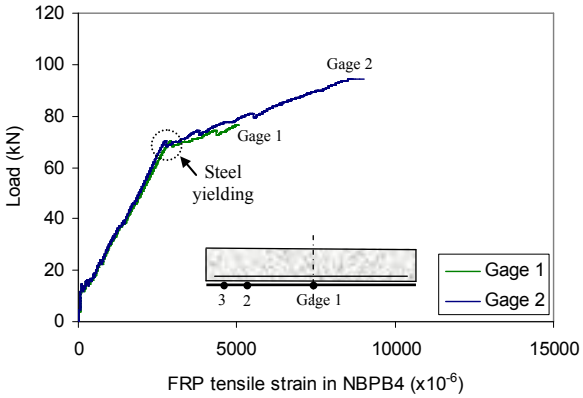

(e) Beam NBPB4

Figure D-4 Variation of FRP strains with applied load (Group II beams)

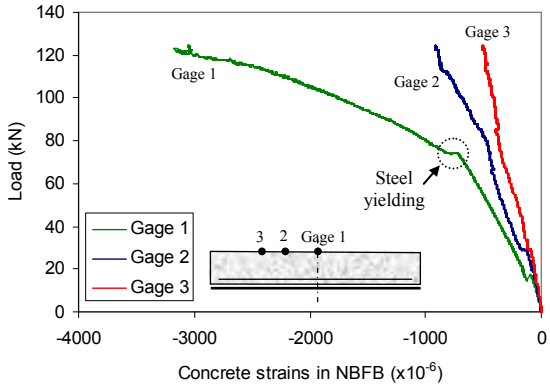

(a) Beam NBFB

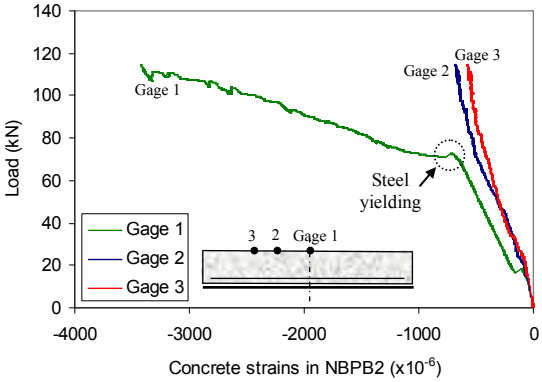

(b) Beam NBPB2

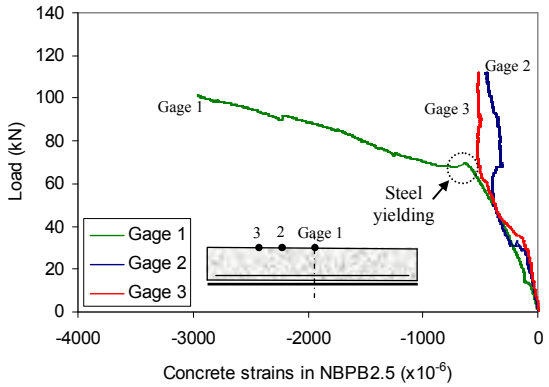

(c) Beam NBPB2.5

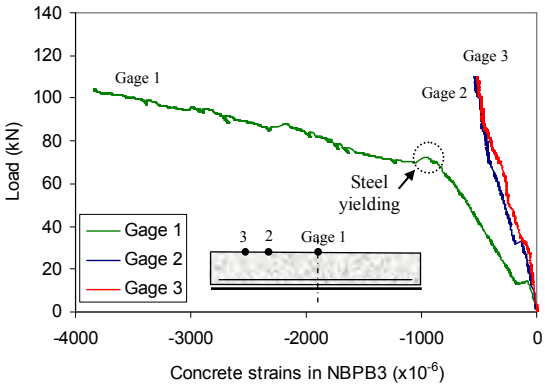

(d) Beam NBPB3

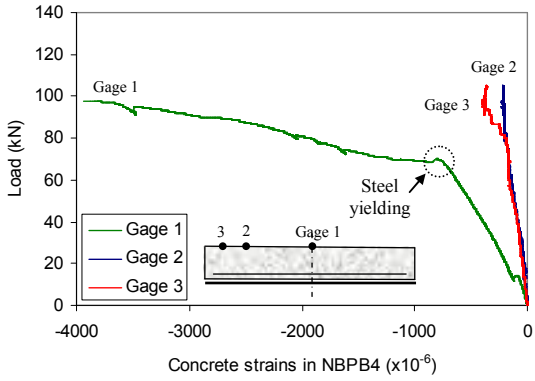

(e) Beam NBPB4

Figure D-5 Variation of Concrete strains with applied load (Group II beams)

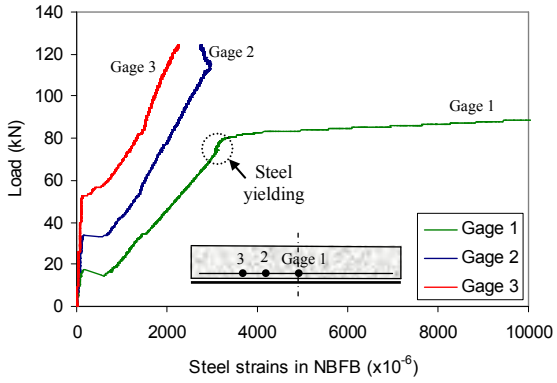

(a) Beam NBFB

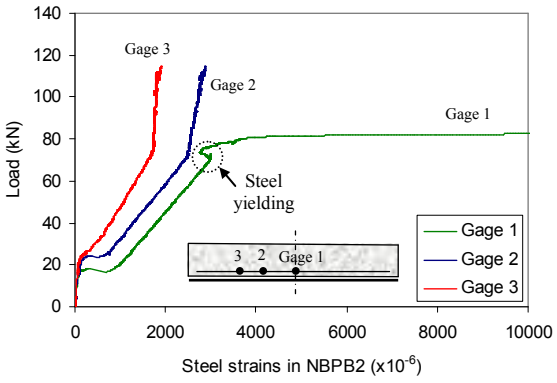

(b) Beam NBPB2

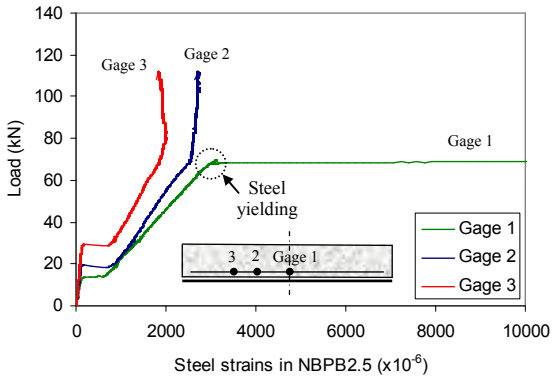

(c) Beam NBPB2.5

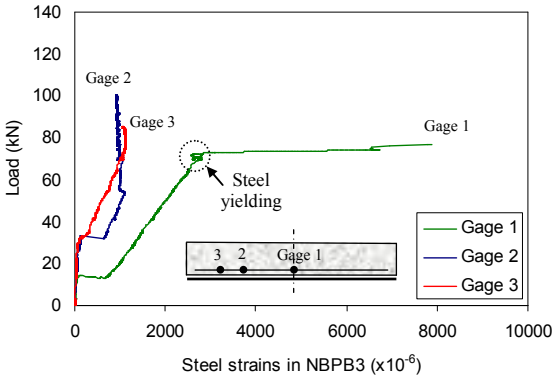

(d) Beam NBPB3

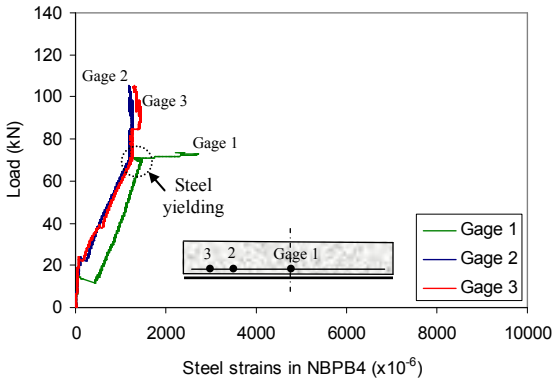

(e) Beam NBPB4

Figure D-6 Variation of steel reinforcement strains with applied load (Group II beams)

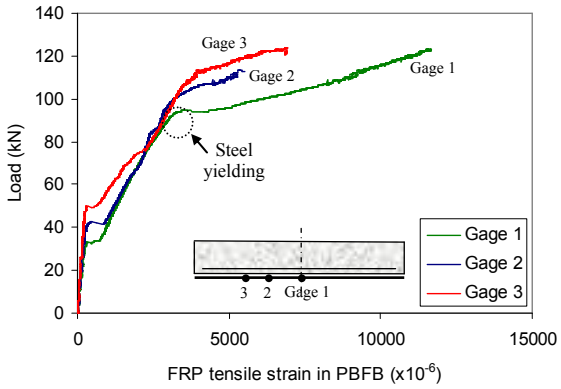

(a) Beam PBFB

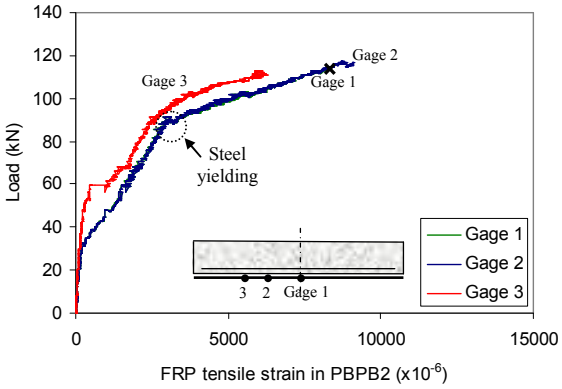

(b) Beam PBPB2

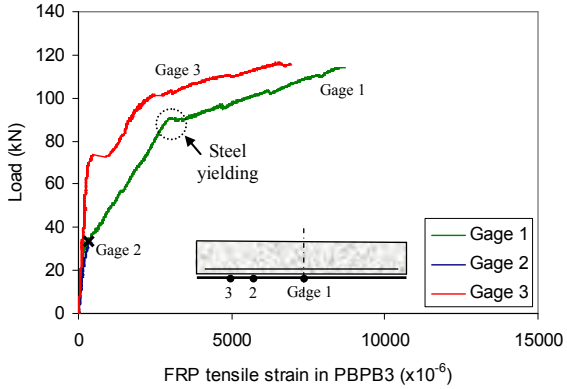

(c) Beam PBPB3

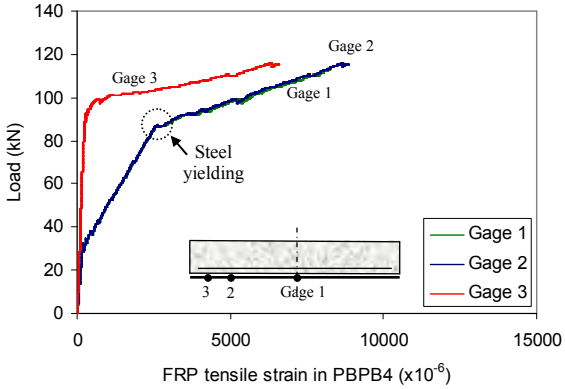

(d) Beam PBPB4

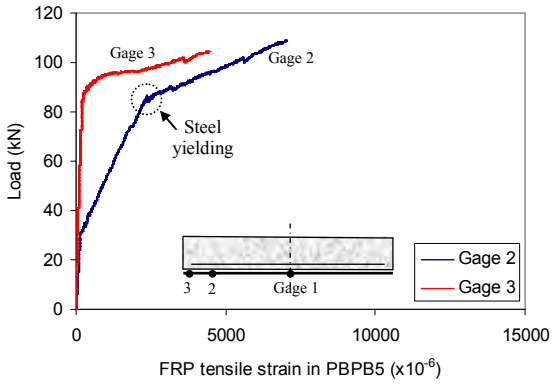

(e) Beam PBPB5

Figure D-7 Variation of FRP strains with applied load (Group III beams)

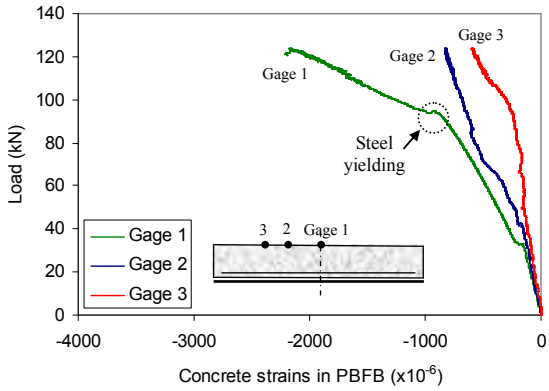

(a) Beam PBFB

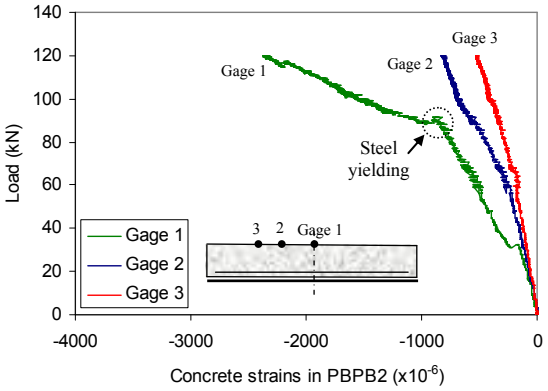

(b) Beam PBPB2

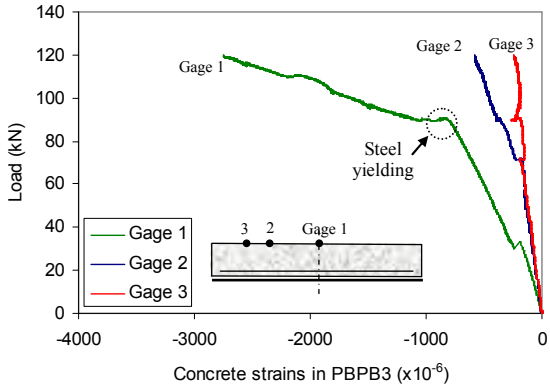

(c) Beam PBPB3

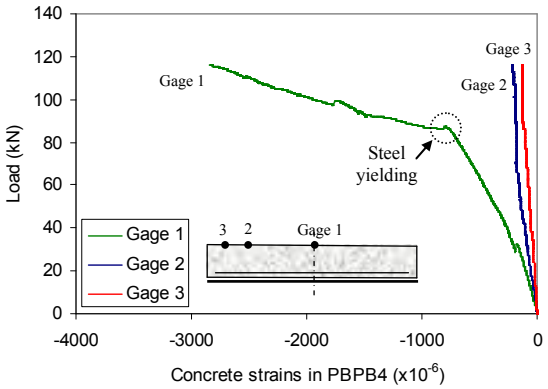

(d) Beam PBPB4

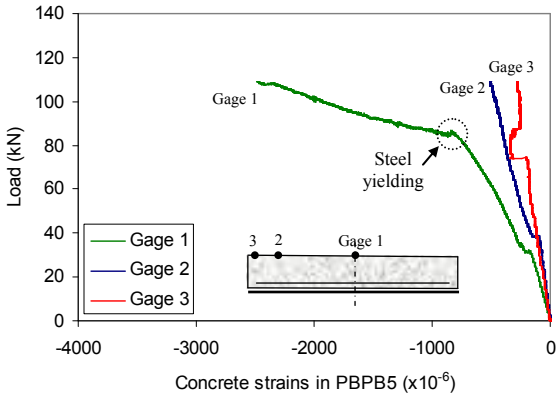

(e) Beam PBPB5

Figure D-8 Variation of concrete strains with applied load (Group III beams)

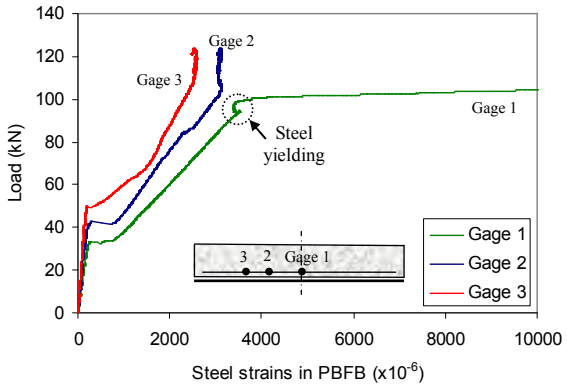

(a) Beam PBFB

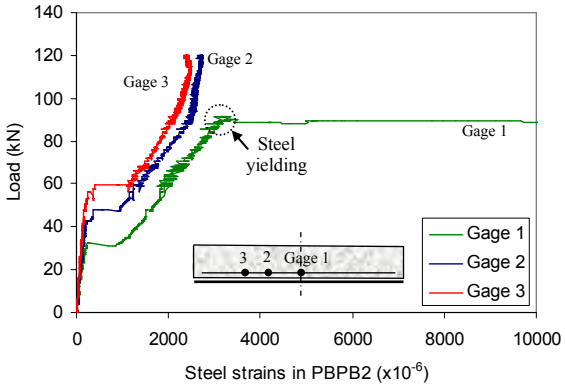

(b) Beam PBPB2

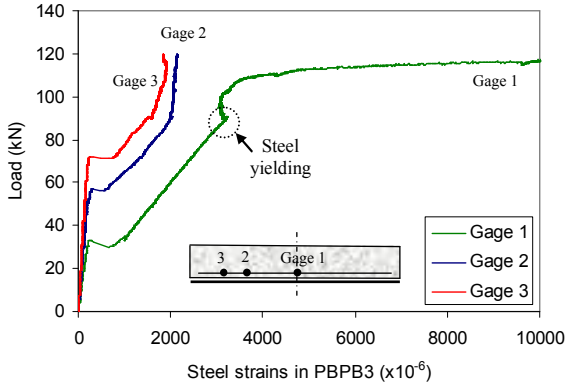

(c) Beam PBPB3

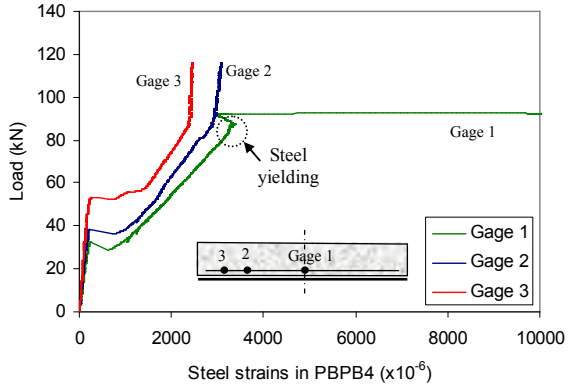

(d) Beam PBPB4

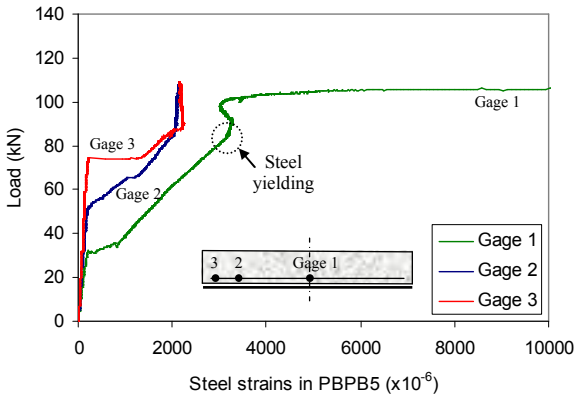

(e) Beam PBPB5

Figure D-9 Variation of steel reinforcement strains with applied load (Group III beams)

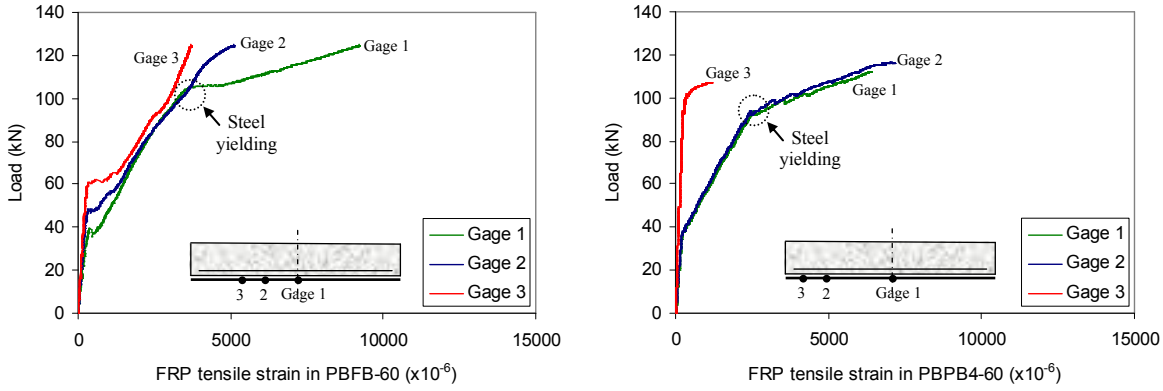

(a) Beam PBFB-60 (b) Beam PBPB4-60

Figure D-10 Variation of FRP strains with applied load (Group IV beams)

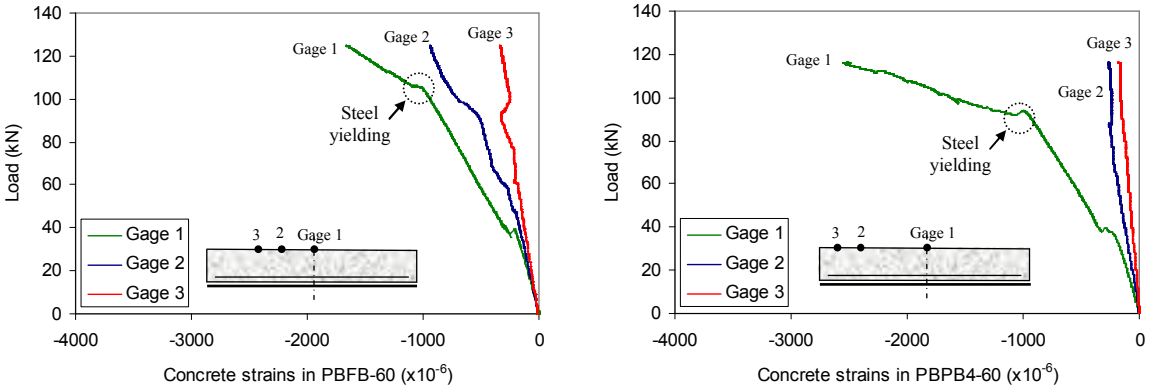

(a) Beam PBFB-60 (b) Beam PBPB4-60

Figure D-11 Variation of concrete strains with applied load (Group IV beams)

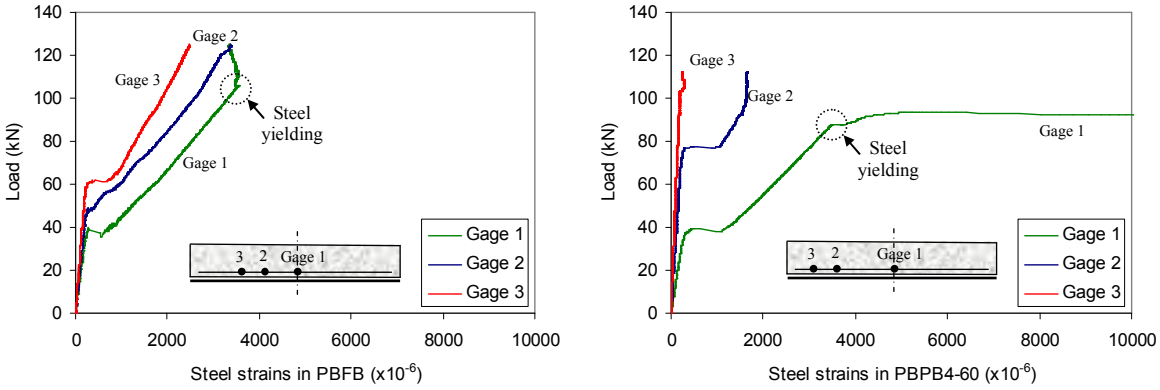

(a) Beam PBFB-60 (b) Beam PBPB4-60

Figure D-12 Variation of steel reinforcement strains with applied load (Group IV beams)

Appendix E

Crack Patterns at Failure and at Service Load

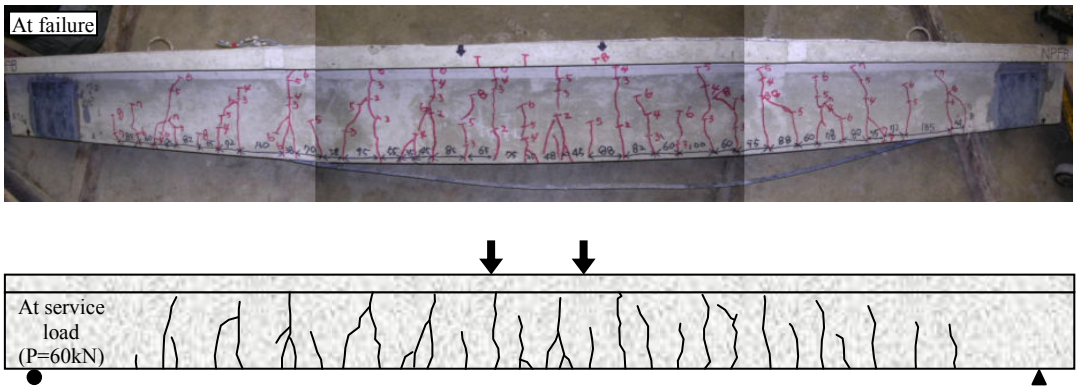

(a) Beam NPFB (EB CFRP plate)

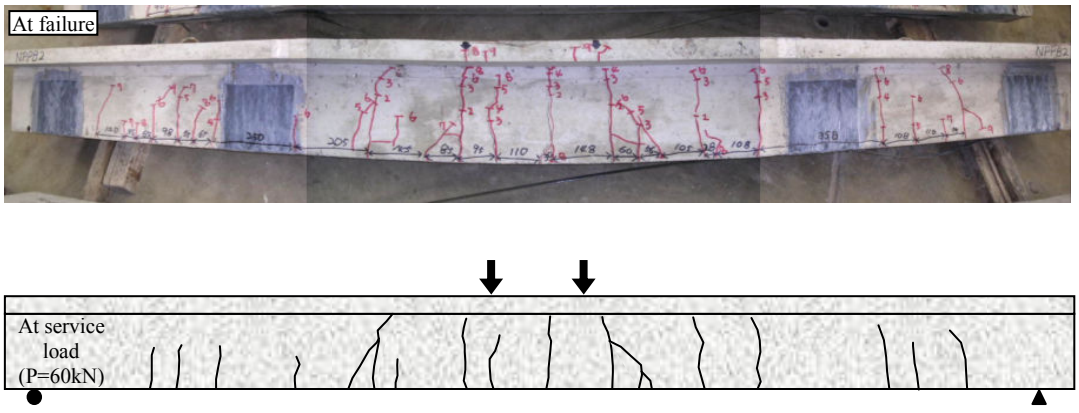

(b) Beam NPPB2 (EB CFRP plate)

Figure E-1 Crack patterns of Group I beams at failure and at service load (P = 60kN)

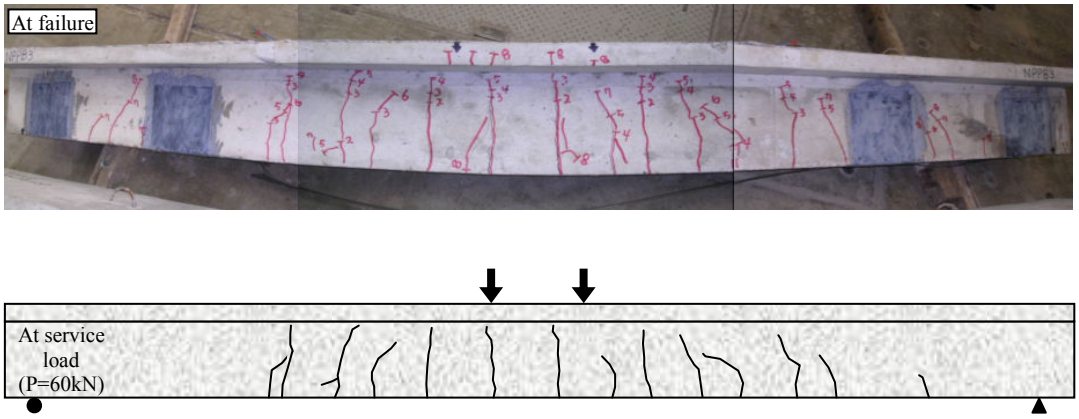

(c) Beam NPPB3 (EB CFRP plate)

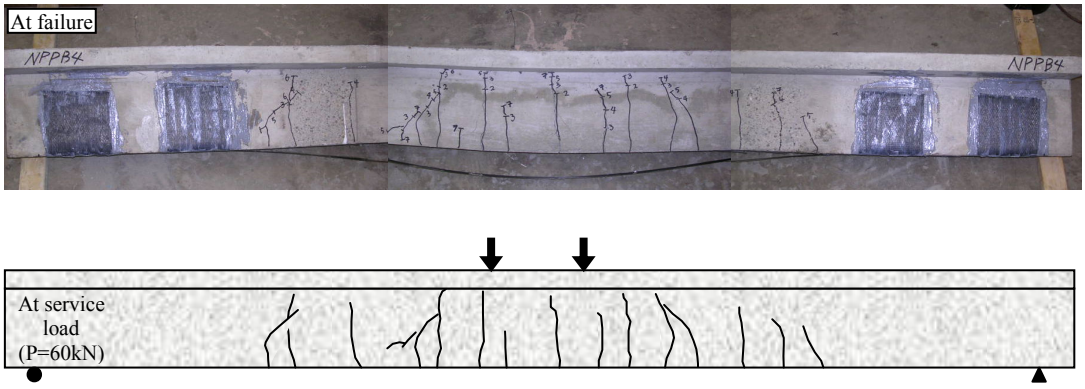

(d) Beam NPPB4 (EB CFRP plate)

Figure E-1 Crack patterns of Group I beams at failure and at service load (P = 60kN) (continued)

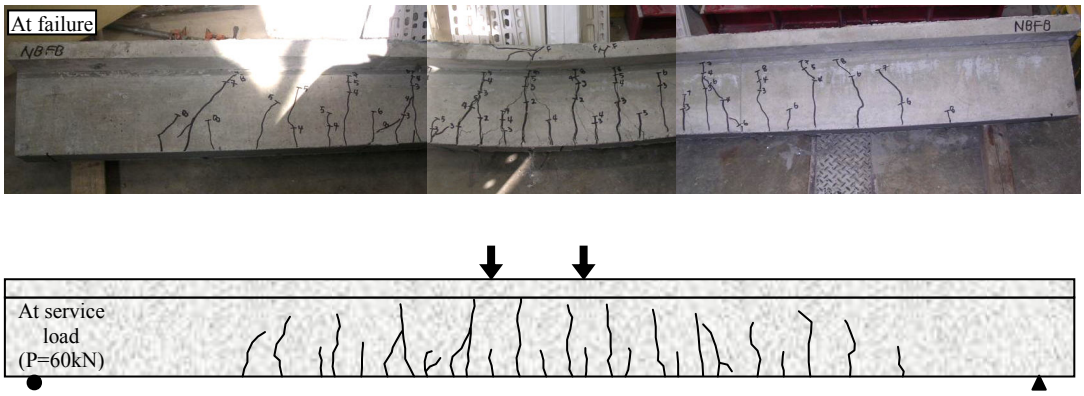

(a) Beam NBFB (NSM CFRP bar)

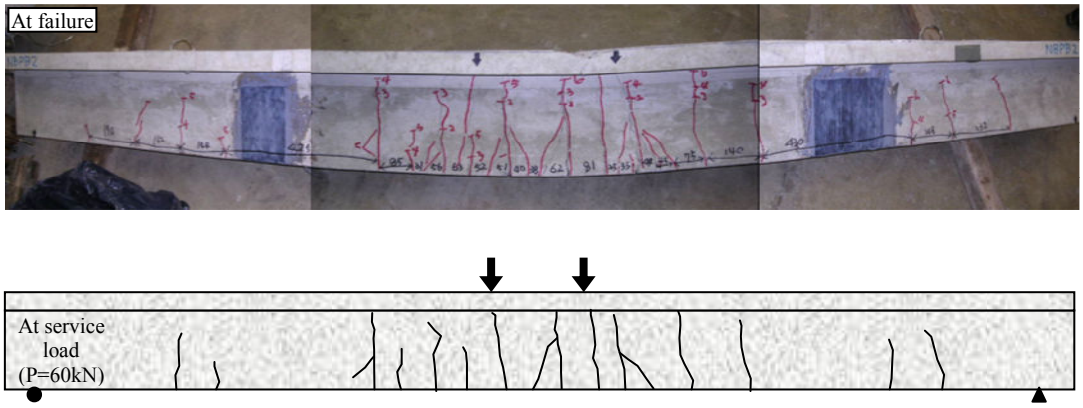

(b) Beam NBPB2 (NSM CFRP bar)

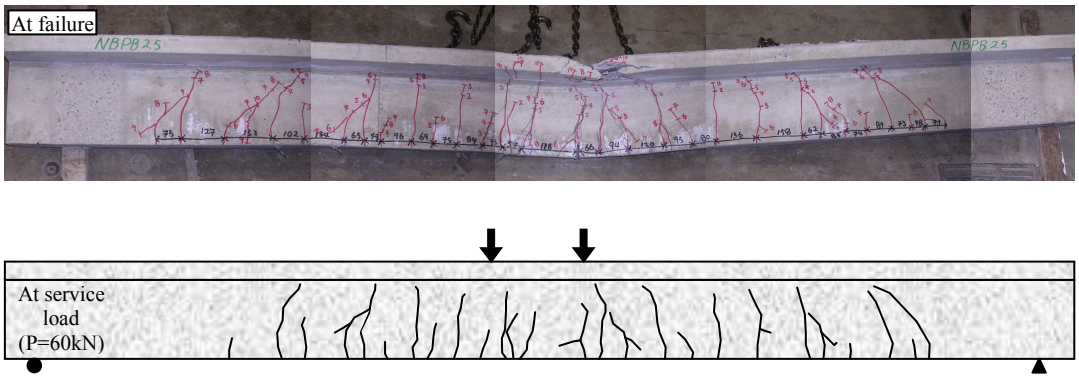

(c) Beam NBPB2.5 (NSM CFRP bar)

Figure E-2 Crack patterns of Group II beams at failure and at service load (P = 60kN)

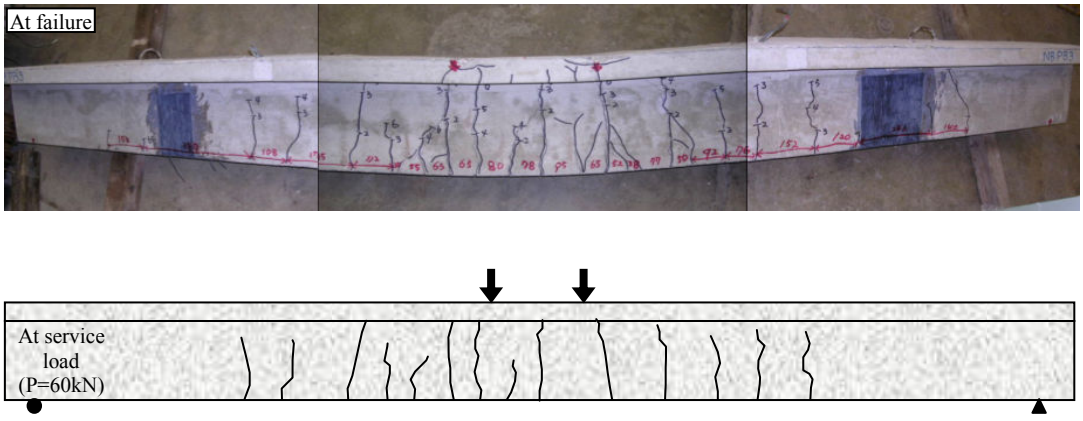

(d) Beam NBPB3 (NSM CFRP bar)

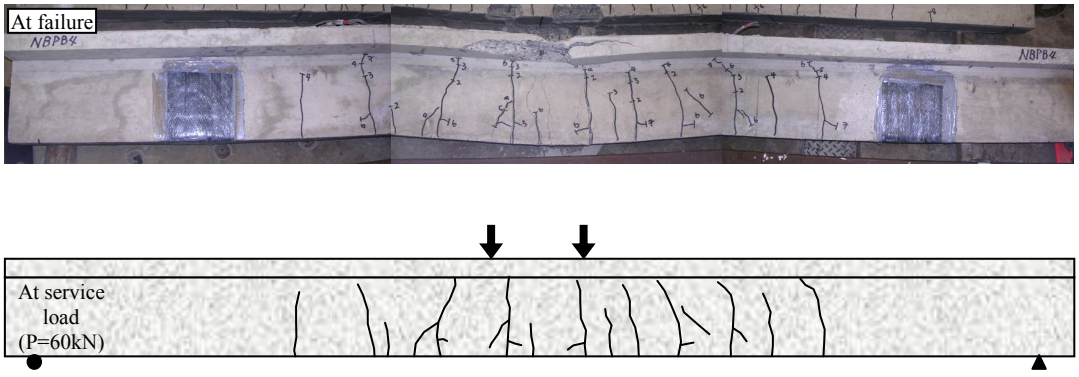

(e) Beam NBPB4 (NSM CFRP bar)

Figure E-2 Crack patterns of Group II beams at failure and at service load (P = 60kN) (continued)

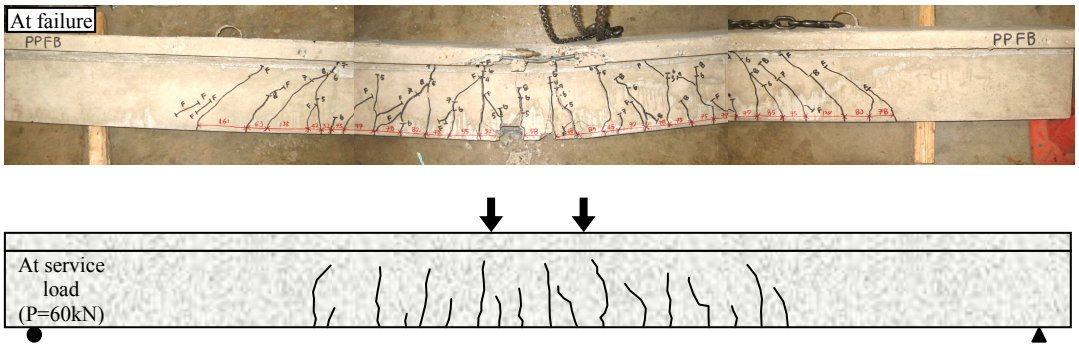

(a) Beam PBFB (40% prestressing force)

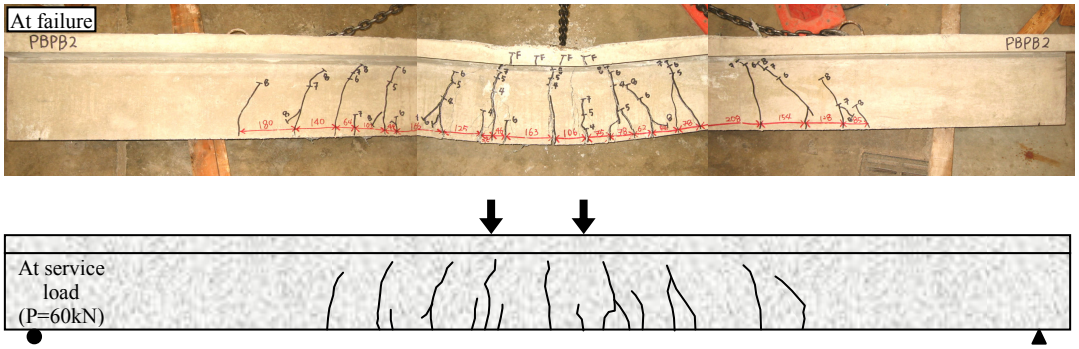

(b) Beam PBPB2 (40% prestressing force)

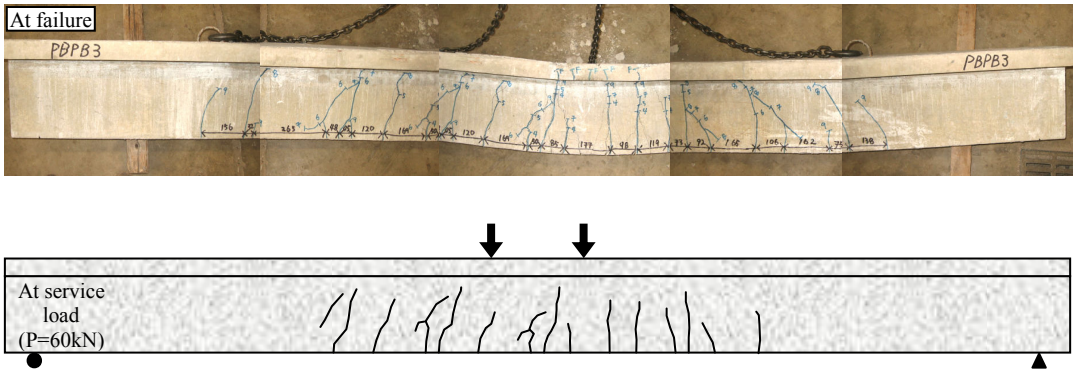

(c) Beam PBPB3 (40% prestressing force)

Figure E-3 Crack patterns of Group III beams at failure and at service load (P = 60kN)

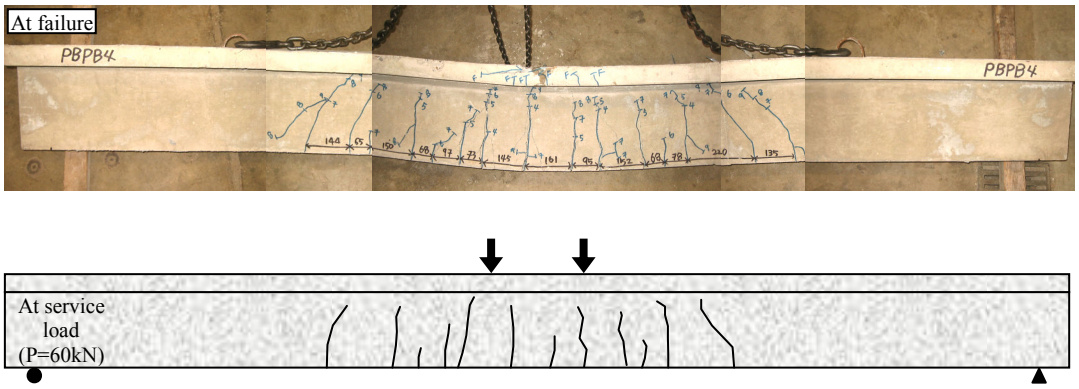

(d) Beam PBPB4 (40% prestressing force)

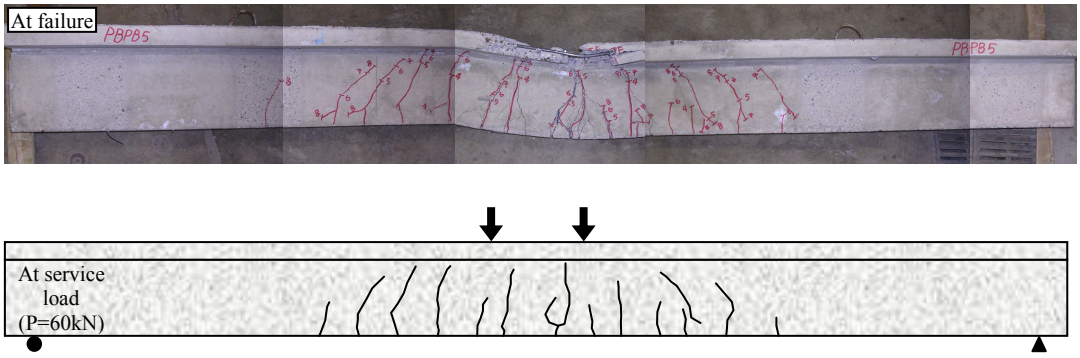

(e) Beam PBPB5 (40% prestressing force)

Figure E-3 Crack patterns of Group III beams at failure and at service load (P = 60kN) (continued)

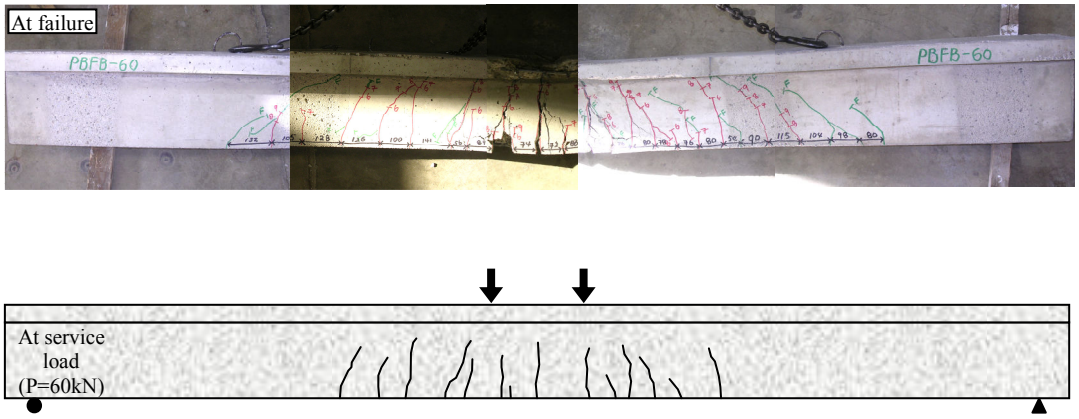

(a) Beam PBFB-60 (60% prestressing force)

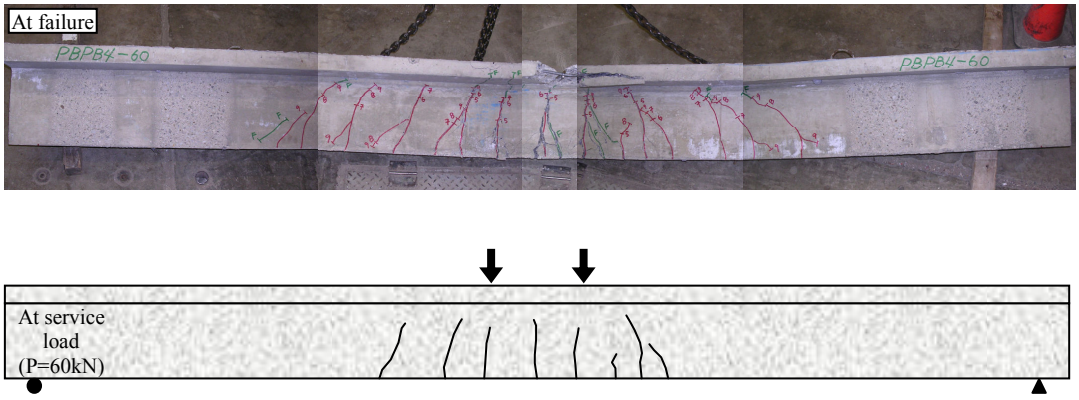

(b) Beam PBPB4-60 (60% prestressing force)

Figure E-4 Crack patterns of Group IV beams at failure and at service load (P = 60kN)

Bibliograhpy

ACI 440.1R-06, (2006). "Guide for the Design and Construction of Structural Concrete Reinforced with FRP Bars," ACI Committee 440, American Concrete Institute, Farmington Hills, MI, 44pp.

ACI 440.2R-08, (2008). "Guide for the Design and Construction of Externally Bonded FRP Systems for Strengthening Concrete Structures," ACI Committee 440, American Concrete Institute, Farmington Hills, MI, 45pp.

ACI 440.4R-04, (2004). "Prestressing Concrete Structures with FRP Tendons," ACI Committee 440, American Concrete Institute, Farmington Hills, MI, 35pp.

ACI 440R-07, (2007). "Report on Fiber-Reinforced Polymer (FRP) Reinforcement for Concrete Structures," ACI Committee 440, American Concrete Institute, Farmington Hills, MI, 104pp.

Aidoo, J., Harries, K. A., and Petrou, M. F., (2006). "Full-Scale Experimental Investigation of Repair of Reinforced Concrete Interstate Bridge Using CFRP Materials," Journal of Bridge Engineering, V. 11, No. 3, pp. 350-358.

Al-Mayah, A., (2004). "Interfacial Behaviour of CFRP-Metal Couples for Wedge Anchor Systems," PhD Thesis, University of Waterloo, Waterloo, Ontario, Canada.

Arduini, M., Tommaso, A. D., and Nanni, A., (1997). "Brittle Failure in FRP Plate and Sheet Bonded Beams," ACI Structural Journal, V. 94, No. 4, pp. 363-370.

ASCE, (2005). Report Card for America's Infrastructures, http://www.asce.org/reportcard/2005 (retrieved June 2, 2008)

ASTM A370, (2007). "Standard Test Methods and Definitions for Mechanical Testing of Steel Products," American Standards for Test and Materials, West Conshohocken, PA.

Badawi, M., (2007). Monotonic and Fatigue Flexural Behaviour of RC Beams Strengthened with Prestressed NSM CFRP Rods, PhD thesis, University of Waterloo, Waterloo, Ontario, Canada.

Badawi, M., and Soudki, K. A., (2006). "Strengthening of RC Beams with Prestressed Near Surface Mounted CFRP Rods," Proceedings of the 3rd International Conference on FRP Composites in Civil Engineering, Miami, FL, USA.

Bank, L. C., (2006). Composites for Construction: Structural Design with FRP Materials, John Wiley & Sons, Inc., New York, NY, 560pp.

Bazant, Z. P., (1976). "Instability, Ductility and Size Effect in Strain-Softening Concrete," Journal of Engineering Mechanics Division, V. 102, No. EM2, pp. 331-344.

Bizindavyi, L., and Neale, K. W., (1999). "Transfer Lengths and Bond Strengths for Composites Bonded to Concrete." Journal of Composites for Construction, V. 3, No. 4, pp. 153-160.

Burgoyune, C. J., (1993). "Should FRP be Bonded to Concrete?" Fiber Reinforced Plastic Reinforcedment for Concrete Structures International Symposium, SP-138, ACI, Farmington Hills, MI, pp. 367-380.

Chahrour, A., and Soudki, K., (2005). "Flexural Response of Reinforced Concrete Beams Strengthened with End-Anchored Partially Bonded Carbon Fiber-Reinforced Polymer Strips," Journal of Composites for Construction, V. 9, No. 2, pp. 170-177.

Chansawat, K., Yim, S. C. S., and Miller, T. H., (2006). "Nonlinear Finite Element Analysis of a FRP-Strengthened Reinforced Concrete Bridge," Journal of Bridge Engineering, V. 11, No. 1, pp. 21-32.

Chajes, M. J., Finch, W. W., Januszka, T. F., and Thomson, T. A., (1996). "Bond and Force Transfer of Composite Material Plates Bonded to Concrete," ACI Structural Journal, V. 93, No. 2, pp. 208-217.

Chen, W., (1982). Plasticity in Reinforced Concrete, McGraw-Hill, Inc., 474pp.

Chen, J. F., and Teng, J. G., (2001). "Anchorage Length Models for FRP and Steel Plates Bonded to Concrete," Journal of Structural Engineering, V. 127, No. 7, pp. 784-791.

Choi, H. T., West, J. S., and Soudki, K. A., (2007). "An Experimental Study on the Flexural Response of Partially Bonded FRP Strengthened Concrete Beams," Proceedings of the 8th International Symposium on FRP Reinforcement for Concrete Structures in Patras, Greece, 8-6.

Choi, H. T., West, J. S., and Soudki, K. A., (2008a). "Analysis of the Flexural Behavior of Partially Bonded FRP Strengthened Concrete Beams," Journal of Composites for Construction, V. 12, No. 4, pp. 375-386.

Choi, H. T., West, J. S., and Soudki, K. A., (2008b). "Effect of Partial Unbondig on Prestressed Near-Surface-Mounted CFRP Strengthened Concrete T-beams," Journal of Composites for Construction, under review.

Choi, H. T., West, J. S., and Soudki, K. A., (2008c). "Ultimate Flexural Behavior of Concrete T-Beams Strengthened with Partially Bonded Near-Surface-Mounted CFRP," Construction and Building Materials, under review.

Choi, H. T., West, J. S., and Soudki, K. A., (2008d). "Nonlinear Finite Element Analysis of Partially Bonded FRP Strengthened Concrete Beams," Proceedings of the 2nd Canadian Conference on Sustainability of Civil Engineering Structures in Hamilton, Canada.

Choi, H. T., West, J. S., and Soudki, K. A., (2008e). "Flexural Behaviour of Partially Bonded Near-Surface-Mounted Carbon Fibre-Reinforced-Polymer Strengthened Concrete T-Beams," Proceedings of the 5th International Conference on Advanced Composite Materials in Bridges and Structures in Winnipeg, Canada.

Collins, M. P., and Mitchell, D., (1987). Prestressed Concrete Basics, Canadian Prestressed Concrete Institute (CPCI), Ottawa, 614pp.

Comité Euro-International du Béton (CEB), (1991). CEB-FIP Model Code 1990, Thomas Thlford, London, 437pp.

Concrete Society, (2004). Design Guidance for Strengthening Concrete Structures Using Fibre Composite, 2nd Edition, TR55, Concrete Society, 128pp.

Coronado, C. A. and Lopez, M. L., (2005). "Sensitivity Analysis of Reinforced Concrete Beams Strengthened with FRP Laminates." Cement Concrete Composites, V. 28, No. 1, pp. 102-114.

CSA A23.2, (2004). "Concrete Materials and Methods of Concrete Construction/Methods of Test and Standard," Canadian Standards Association (CSA), Rexdale, Ontario, Canada.

CSA A23.3, (2004). "Design of Concrete Structures," Canadian Standards Association (CSA), Rexdale, Ontario, Canada.

CSA S6, (2006). "Canadian Highway Bridge Design Code," Canadian Standards Association (CSA), Rexdale, Ontario, Canada.

CSA S806, (2007). "Design and Construction of Building Components with Fibre-Reinforced Polymers," Canadian Standards Association (CSA), Rexdale, Ontario, Canada.

CSCE, (2003). Civil Infrastructures Systems: Technology Road Map, http://www.csce.ca/TRM/index.htm (retrieved June 2, 2008)

Czaderski, C. and Motavalli, M., (2007). "40-Year-Old Full-Scale Concrete Bridge Girder Strengthened with Prestressed CFRP Plates Anchored Using Gradient Method," Composite Part B: Engineering, V. 38, No. 7-8, pp. 878-886.

Dai, J., Ueda, T., and Sato Y., (2005). "Development of the Nonlinear Bond Stress-Slip Model of Fiber Reinforced Plastics Sheet-Concrete Interfaces with a Simple Method," Journal of Composites for Construction, V. 9, No. 1, pp. 52-62.

Dodds, R. H., Darwin, D., and Leibengood, L. D., (1984). "Stress Controlled Smeared Cracking in R/C beams," Journal of Structural Engineering, V. 110, No. 9, pp. 1959-1976.

El-Hacha, R., Filho, D. S., Melo, G. S., and Rizkalla, S. H., (2004a). "Effective of Near Surface Mounted FRP Reinforcement for Flexural Strengthening of Reinforced Concrete Beams," Proceedings of International Conference on Advanced Composite Materials in Bridges and Structures, ACMBS-IV, Calgary, Ontario, Canada.

El-Hacha, R., Green, M. F., and Wight, R. G., (2003). "Innovative System for Prestressing FRP Sheets," ACI Structural Journal, V. 100, No. 3, pp. 239-252.

El-Hacha, R., Green, M. F., and Wight, R. G., (2004b). "Flexural Behaviour of Concrete Beams Strengthened with Prestressed Carbon Fibre Reinforced Polymer Sheets Subjected to Sustained Loading and Low Temperature," Canadian Journal of Civil Engineering, V. 31, pp. 239-252.

El-Hacha, R. and Rizkalla, S. H., (2004). "Near-Surface-Mounted Fiber-Reinforced Polymer Reinforcements for Flexural Strengthening of Concrete Structures," ACI Structural Journal, V. 101, No. 5, pp. 717-726.

El Refai, A., (2007). Monotonic and fatigue flexural performance of RC beams strengthened with externally post-tensioned CFRP tendons, PhD thesis, University of Waterloo, Waterloo, Ontario, Canada.

Eshwar, N., Nanni, A., and Ibell, T. J., (2008). "Performance of Two Anchor Systems of Externally Bonded Fiber-Reinforced Polymer Laminates," ACI Material Journal, V. 105, No. 1, pp. 72-80.

Gaafar, M. A., and El-Hacha, R., (2007). "Prestressing concrete beams using NSM FRP technique," Proceedings of International Symposium on Fiber-Reinforced Polymer Reinforcement in Concrete Structures, FRPRCS-8, Partas, Greece, 8-11.

GangaRao, H. V. S., and Vijay, P. V., (1998). "Bending Behavior of Concrete Beams Wrapped with Carbon Fabric," Journal of Structural Engineering, V. 124, No. 1, pp. 3-10.

Garden, H. N. and Mays, G. C., (1999). "Structural Strengthening of Concrete Beams Using Prestressed Plates," Strengthening of Reinforced Concrete Structures Using Externally-Bonded FRP Composites in Structural and Civil Engineering, edited by L.C. Hollaway and M.B. Leeming, Woodhead Publishing, Cambridge, UK, 327pp.

Grace, N. F., Abdel-Sayed, G., and Ragheb, W. F., (2002). "Strengthening of Concrete Beams Using Innovative Ductile Fiber-Reinforced Polymer Fabric," ACI Structural Journal, V. 99, No. 5, pp. 692-700.

Gopalaratnam V. S. and Shah S. P., (1985). "Softening Response of Plain Concrete in Direct Tension," Journal of American Concrete Institute, V. 82, No. 3, pp. 310-323.

Harris, H. G., and Somboonsong, W., (1998). "New Ductile Hybrid FRP Reinforcing Bar for Concrete Structures," Journal of Composites for Construction, V. 2, No. 1, pp. 28-37.

Hassan, T. and Rizkalla, S. H., (2002). "Flexural Strengthening of Prestressed Bridge Slabs with FRP Systems," PCI Journal, V. 47, No. 1, pp. 76-93.

Hassan, T. K. and Rizkalla, S. H., (2004). "Bond Mechanism of Near-Surface-Mounted Fiber-Reinforced Polymer Bars for Flexural Strengthening of Concrete Structures," ACI Structural Journal, V. 101, No. 6, pp. 830-839.

Hibbitt, Karlsson, and Sorensen, Inc. (HKS), (1997). ABAQUS/Explicit Theory Manual and User's Manual, Version 5.7, Pawtucket, RI.

Hillerborg A., Modéer M., and Petersson P. E., (1976). "Analysis of Crack Formation and Crack Growth in Concrete by means of Fracture Mechanics and Finite Elements," Cement and Concrete Research, V. 6, No. 6, pp. 773-781.

Hollaway, L. C. and Mays, G. C., (1999). "Structural Strengthening of Concrete Beams Using Unstressed Composite Plate," Strengthening of Reinforced Concrete Structures Using Externally-

Bonded FRP Composites in Structural and Civil Engineering, edited by L.C. Hollaway and M.B. Leeming, Woodhead Publishing, Cambridge, UK, 327pp.

Hu, H. T., Lin, F. M., and Jan, Y. Y., (2003). "Nonlinear Finite Element Analysis of Reinforced Concrete Beams Strengthened by Fiber-Reinforced Plastics," Composite Structures, V. 63 No. 3-4, pp. 271-281.

ISIS Canada Network of Excellence, (2007). Reinforcing Concrete Structures with Fibre Reinforced Polymers, Design Manual, No. 3, ISIS Canada Corporation, Winnipeg, Manitoba, Canada.

ISIS Canada Network of Excellence, (2008). FRP Rehabilitation of Reinforced Concrete Structures, Design Manual, No. 4., ISIS Canada Corporation, Winnipeg, Manitoba, Canada.

ISIS Canada Network of Excellence, (2008). Prestressing Concrete Structures with Fibre-Reinforced ;olymers, Design Manual, No. 5., ISIS Canada Corporation, Winnipeg, Manitoba, Canada.

Jung, W. T., Park, H. Y., Park, J. S., Kang J. Y., and Yoo, Y. J., (2005). "Experimental Investigation on Flexural Behavior of RC Beams Strengthened by NSM CFRP Reinforcement," Proceedings of International Symposium on Fiber-Reinforced (FRP) Polymer Reinforcement for Concrete Structures, ACI Symposium Publication, SP-230-46, pp. 795-806.

Jung, W. T., Park, J. S., and Park, Y. H., (2007). "A study on the Flexural Behavior of Reinforced Concrete Beams Strengthened with NSM Prestressed CFRP Reinforcement," Proceedings of International Symposium on Fiber-Reinforced Polymer Reinforcement in Concrete Structures, FRPRCS-8, Partas, Greece, 8-10.

Kishi, N., Zhang, G., and Mikami, H., (2005). "Numerical Cracking and Debonding Analysis of RC Beams Reinforced with FRP Sheet." Journal of Composites for Construction, V. 9, No. 6, pp. 507-514.

Lee, Y. J., Boothby, T. E., Bakis, C. E., and Nanni, A., (1999). "Slip Modulus of FRP Sheets Bonded to Concrete," Journal of Composites for Construction, V. 3, No. 4, pp. 161-167.

Lee, J., and Fenves, G. L., (1998). "Plastic-Damage Model for Cyclic Loading of Concrete Structures," Journal of Engineering Mechanics, V. 124, No. 8, pp. 892-900.

Lees, J. M., and Burgoyne, C. J., (1999). "Experimental Study of Influence of Bond on Flexural Behavior of Concrete Beams Pretensioned with Aramid Fiber Reinforced Plastics," ACI Structural Journal, V. 96, No. 3, pp. 377-385.

Lees, J. M., and Burgoyne, C. J., (2000). "Analysis of Concrete Beams with Partially Bonded Composite Reinforcement," ACI Structural Journal, V. 97, No. 2, pp. 252-260.

Lorenzis, L., (2004). "Anchorage Length of Near-Surface Mounted Fiber-Reinforced Polymer Rods for Concrete Strengthening – Analytical Modeling," ACI Structural Journal, V. 101, No. 3, pp. 375-386.

Lorenzis, L., Miller, B., and Nanni, A., (2001). "Bond of Fiber-Reinforced Polymer Laminates to Concrete," ACI Materials Journal, V. 98, No. 3, pp. 256-264.

Lorenzis, L., Lundgren, K., and Rizzo, A., (2004). "Anchorage Length of Near-Surface Mounted Fiber-Reinforced Polymer Bars for Concrete Strengthening - Experimental Investigation and Numerical Modeling," ACI Structural Journal, V. 101, No. 2, pp. 269-278.

Lorenzis, L., and Nanni, A., (2002). "Bond between Near-Surface Mounted Fiber-Reinforced Polymer Rods and Concrete in Structural Strengthening," ACI Structural Journal, V. 99, No. 2, pp. 123-132.

Lubliner, J., Oliver, J., Oller, S., and Onate, E., (1989). "A Plastic-Damage Model for Concrete," International Journal of Solids Structures, V. 25, No. 3, pp. 299-326.

MacGregor, J. G. and Bartlett, F. M., (2000). Reinforced Concrete Mechanics and Design: 1st Canadian Ed., Prentice Hall Canada Inc., Toronto, ON, 1042pp.

Malek, A. M., Saadatmanesh, H., and Ehsani, M. R., (1998). "Prediction of Failure Load of R/C Beams Strengthened with FRP Plate due to Stress Concentration at the Plate End," ACI Structural Journal, V. 95, No. 2, pp. 142-152.

Malvar, L. J., (1998). "Review of Static and Dynamic Properties of Steel Reinforcing Bars," ACI Structural Journal, V. 95, No. 5, pp. 609-616.

Meier, U., Deuring, M., Meier, H., and Schegler, G., (1992). "Strengthening of Structures with CFRP Laminates: Research and Applications in Switzerland," Proceedings of International Conference on Advanced Composite Materials in Bridges and Structures, ACMBS-I, Sherbrooke, Quebec, Canada, pp. 243-251.

Millar, D., Scott, P., and Clenin, R., (2004). "Bridge Strengthening with Prestressed CFRP Plate System," Proceedings of the second international conference on FRP composites in civil engineering, Adelaide, Australia, pp. 463-469.

Mufti, A. A., Newhook, J. P., and Tadros, J., (1996). "Deformability versus Ductility in Concrete Beams with FRP Reinforcement," Proceedings of the 2nd international conference on advanced composite materials in bridges and structures, CSCE, pp. 189-199.

Naaman, A. E., and Alkhairi, F. M., (1991a). "Stress at Ultimate in Unbonded Post-Tensioning Tendons: Part 1 – Evaluation of the State-of-the-Art," ACI Structural Journal, V. 88, No. 5, pp. 641-651.

Naaman, A. E., and Alkhairi, F. M., (1991b). "Stress at Ultimate in Unbonded Post-Tensioning Tendons: Part 2 – Proposed Methodology," ACI Structural Journal, V. 88, No. 6, pp. 683-692.

Naaman, A. E., Burns, N., French, C., Gamble, W. L., and Mattock, A. H., (2002). "Stresses in Unbonded Prestressing Tendons at Ultimate: Recommendation," ACI Structural Journal, V. 99, No. 4, pp. 518-529.

Naaman, A. E. and Jeong, S. E., (1995). "Structural Ductility of Concrete Beams Prestressed with FRP Tendons," Non-Metallic (FRP) Reinforcement for Concrete Structures, Proceedings of the 1995 2nd International RILEM Symposium, FRPRCS-2, pp. 379-386.

Nakaba, K., Kanakuto, T., Furuta, T., and Yoshizawa, H., (2001). "Bond Behavior between Fiber-reinforced Polymer Laminates and Concrete," ACI Structural Journal, V. 98, No. 3, pp. 359-367.

Nanni, A., (2003). "North American Design Guidelines for Concrete Reinforcement and Strengthening Using FRP: Principles, Applications, and Unsolved Issues," Journal of Construction and Building Materials, Vol. 17, No. 6-7, pp. 439-446.

Nanni, A., Bakis, C. E., and Boothby, T. E., (1995). "Test method for FRP-concrete systems subjected to mechanical loads: stage of the art review," Journal of reinforced plastics and composites, Vol. 14, No. 6, pp. 524-558.

Ngo, D., and Scordelis, A. C., (1967). "Finite Element Analysis of Reinforced Concrete Beams," Journal of American Concrete Institute, V. 64, No. 3, pp. 152-163.

Nilson, A. H., (1968). "Nonlinear Analysis of Reinforced Concrete by Finite Element Method," Journal of American Concrete Institute, V. 65, No. 9, pp. 757-766.

Nordin, H., (2005). "Strengthening Structures with Externally Prestressed Tendons – Literature Review," Technical Report, Luleå University of Technology, Luleå, Sweden.

Nordin, H., and Taljsten, B., (2004). "Prestressed Near Surface Mounted Reinforcement (NSMR) for Strengthening Concrete Beams," Proceedings of the second international conference on FRP composites in civil engineering, Adelaide, Australia, pp. 447-454.

Nordin, H., and Täljsten, B., (2006). "Concrete beams strengthened with prestressed near surface mounted CFRP," Journal of Composites for Construction, V. 10, No. 1, pp. 60-68.

Park, R., and Paulay, T., (1975). Reinforced Concrete Structures, John Wiley & Sons, New York, 769pp.

Pham, H. and Al-Mahaidi, R., (2004). "Assessment of Available Prediction Models for the Strength of FRP Retrofitted RC Beams," Composite Structures, V. 66, No. 1-4, pp. 601-610.

Pham, H. B., and Al-Mahaidi, R., (2005). "Finite Element Modeling of RC Beams Retrofitted with CFRP Fabrics," Fiber-Reinforced (FRP) Polymer Reinforcement for Concrete Structures, SP-230. Shield C. K., Busel, J. P., Walkup, S. L., and Gremel, D. D. eds., American Concrete Institute, Farmington Hills, MI, pp. 499-513.

Rashid, Y. R., (1968). "Ultimate Strength Analysis of Prestressed Concrete Pressure Vessels," Nuclear Engineering and Design, V.7, pp. 334-344.

Rots, J. G., and Blaauwendaad, J., (1989). "Crack Models for Concrete: Discrete or Smeared? Fixed, Multi-directional or Rotating," HERON, V. 34, No. 1, pp. 1-59.

Shin, H. M., (2000). Prestressed Concrete, Dongmyoungsa, Seoul, Korea, 458pp. (Korean)

Sika Canada Inc., (2008). http://www.sikacanada.com/con/con-prod/con-prod-appl-ss.htm (retrieved June 2, 2008)

Stocklin and Meier, U., (2001). "Strengthening of Concrete Structures with Prestressed and Gradually Anchored CFRP strips," Proceedings of the fifth international conference on fibre-reinforced plastics for reinforced concrete structures, Cambridge, UK, pp. 291-296.

Taljsten, B., (1997). "Strengthening of Beams by Plate Bonding," Journal of Materials in Civil Engineering, V. 9, No. 4, pp. 206-211.

Tann, D. B., Davies, P. and Delpak, R., (2003). "A Review of Ductility Determination of FRP Strengthened Flexural RC Elements," Proceedings of the sixth international symposium on FRP reinforcement for concrete structures, FRPRCS-6, V. 1, pp. 347-356.

Teng, J. G., Chen, J. F., Smith, S. T., and Lam, L., (2002a). FRP Strengthened RC Structures, John Wiley & Sons, LTD, NY, 245pp.

Teng, J. G., Zhang, J. W., and Smith, S. T., (2002b). "Interfacial Stresses in Reinforced Concrete Beams Bonded with a Soffit Plate: a Finite Element Study," Construction and Building Maerials, V. 16, No. 1, pp. 1-14.

Wight, R. G., Green, M. F., and Erki, M. -A., (2001). "Prestressed FRP Sheets for Poststrengthening Reinforced Concrete Beams," Journal of Composites for Construction, V. 5, No. 4, pp. 214-220.

Wong, R. S. Y. and Vecchio, F. J., (2003). "Towards Modeling of Reinforced Concrete Members with Externally Bonded Fiber-Reinforced Polymer Composites," ACI Structural Journal, V. 100, No. 1, pp. 47-55.

Yuan, H., Teng, J. G., Seracino, R., Wu, Z. S., and Yao, J., (2004). "Full-Range Behavior of FRP-to-Concrete Bonded Joints," Engineering Structures, V. 26, No. 5, pp. 553-565.